Synthesis, Characterisation and Olefin Oligomerization over Nickel, Cobalt and Zinc Substituted Synthetic Mica Montmorillonite

By

Alex Philip Vogel

(BSc. Chem. Eng., Hons)

Submitted to the University of Cape Town in fulfilment of the requirements for the degree of

DOCTOR OF PHILOSOPHY

Department of Chemical Engineering
University of Cape Town
Rondebosch
Cape Town
Republic of South Africa

August 1996

ACKNOWLEDGEMENTS

The assistance of my supervisor, Prof Cyril O'Connor, and that of Dr Jack Fletcher, Dr Masami Kojima, Prof Mark Dry, Dr Eric van Steen and Dr Klaus Moller is acknowledged in the completion of this thesis.

My research colleagues, Bo Andersen, Stefan Schwarz, Radley Hartford and Miles van Niekerk are thanked for the academic interactions and social occasions enjoyed with them.

The assistance of the research staff, Leslie Petrick, Connie Wishart and Pam Linck, mechanical personnel, Tony Barker and Rob Senekal, and electrical personnel, Bill Randall and Granville de la Cruz, is appreciated.

The financial support of the following institutions is acknowledged:

- Foundation for Research and Development, CSIR
- SASOL
- AECI Ltd

I would also like to thank my parents, Philip and Sonja, for their continued support and encouragement and Angela for her help and unending patience.

SUMMARY

Nickel, cobalt and zinc were substituted for structural octahedral aluminium in SMM. X-ray diffraction, together with elemental analysis, confirmed that a 2:1 layered aluminosilicate had been formed. The inclusion of these metals facilitated the crystallisation of the SMM structure in the synthesis process as was shown by their more well-defined X-ray diffraction patterns over unsubstituted SMM synthesized in this work. The 2:1 layer spacings increased at nickel contents of 16 and 34wt%, indicating a more montmorillonite-like structure. Cobalt levels at 33wt% were seen to disrupt the basal spacing. The opposite effect was seen with zinc, where increased zinc loadings caused the 2:1 layers to be drawn closer together. This was indicative of a more mica-like structure.

The packing density of the metals as given by the corrected intensities of the 06 (trioctahedral) X-ray diffraction peak, showed an increase in the order, nickel < cobalt < zinc. This effect was due to the ionic radii of the divalent metal cations which increase similarly. Higher levels of extra-framework cobalt than nickel (0.73 compared with 0.15mmol H_2 consumed/g at >30wt% metal) were identified by the size of the low temperature peak found in temperature programmed reduction (TPR). The greater accessibility of nickel was shown by the decrease in the position of the high temperature TPR peak from 650°C to 623°C as the nickel loading was increased from 10 to 34wt%. No zinc was reduced in the TPR experiments due to the low standard reduction potential of Zn^{2+}.

Incorporation of 1wt% nickel increased the SMM surface area from 141 to 195m^2/g. As the nickel content was increased to 10wt%, surface area increased further to 219m^2/g. This effect was still present when the surface areas were normalised to area per unit cell to accommodate the increase in unit cell density as more nickel replaced aluminium. It was postulated that the increase in surface area was as a result of smaller platelets crystallising out, thus increasing the contribution of platelet edge area. The nickel in the SMM structure was given as possible sites of SMM crystal growth termination, causing the smaller platelets and greater nickel accessibility at the platelet edges.

The acidity of the catalysts was measured by temperature programmed ammonia desorption (NH_3-TPD) and infrared (IR) pyridine adsorption. Although there were discrepancies between

the acidity values obtained from the two analytical techniques and results reported previously, it was seen by IR pyridine adsorption that acidity increased from 0.643 to 0.756mmol pyridine adsorbed/g with nickel content increasing from 1 to 34wt%. This increased acidity was shown by IR pyridine adsorption to be as a result of an increase in Lewis acidity. This increase was due to weak Lewis acidity at the higher nickel loadings. The weak Lewis acidity was proposed to be present at the octahedral nickel acid sites exposed at platelet edges. The acidity could generally be said to decrease with metal type, NiSMM > CoSMM > ZnSMM.

Combined TG-DTA thermoanalysis was shown to be a useful technique for comparing olefin adsorption levels and the low pressure oligomerization activity of acid catalysts. It was found that both adsorbed iso-butene and iso-butene in the gas stream were necessary for low pressure oligomerization to occur.

The product selectivity of propene oligomerization at 5MPa and 130°C was found to be consistent with a series/parallel reaction mechanism in that heavier products were formed at increased conversion levels. Increasing nickel content from 1 to 34wt% increased the level of propene conversion from 11.6 to 39.4% (@ 1hr runtime). The product selectivity as measured at a constant conversion level of 17.5% by the C_{12+} content of the product was shifted from 12.1 to 35.7% as nickel content increased from 7 to 34wt%. This was indicative of lighter products being formed with increased nickel incorporation and was attributed to the effect of weak Lewis acidity at the higher nickel contents. A linear correlation was able to be made between nickel content, Lewis acidity and propene oligomerization activity. The propene oligomerization activity decreased with metal type, NiSMM > CoSMM > ZnSMM.

Kinetic studies of 1-butene oligomerization at 5MPa and 130°C were unable to differentiate between Langmiur-Hinshelwood and Langmuir-Rideal reaction mechanisms. It was therefore not possible to verify a Langmuir-Rideal reaction mechanism which had been suggested by the thermogravimetric study.

TABLE OF CONTENTS

LIST OF FIGURES

LIST OF TABLES

LIST OF PUBLICATIONS

Vogel, A.P., O'Connor, C.T., and Kojima, M., "Thermogravimetric Analysis of the Iso-butene Oligomerization Activity of Various Forms of Synthetic Mica Montmorillonite", Clay Minerals, **25**, 355-362 (1990)

Chapter 1

Introduction

INTRODUCTION

1.1 Natural Clays

Clays were first used 25000 years ago by the primitive people in Europe and Asia to make clay figures, pottery and ceramics (Hulthéin, 1986). Today clay is an important industrial raw material, used in ceramics, the paper, iron ore and metal industries, oil drilling and pet feeding. In agriculture the clay-humus and clayoxide complexes determine the structure, texture, water retention and the inorganic and organic fertilizer composition of the soils.

Clay minerals have been widely used as catalysts for several hydrocarbon reactions. The first commercial cracking processes employed acid treated clays (montmorillonite and halloysite) as catalysts (Benesi and Winquist, 1978; Voge, 1958). Other reactions included polymerization and isomerization (Davidtz, 1976; Swartzen-Allen and Matijevic, 1974). They are also used as starting materials in catalyst manufacture and as ion-exchange supports and catalyst supports. Because of their layered structure and ability to swell, clay minerals can absorb bulky and long chain molecules and are used for the purification of hydrocarbons by removing definic compounds and colouring materials which are polar compounds (Jasra and Bhat, 1985; Odom, 1984; Jepson, 1984). These minerals are believed to have had a role in natural petroleum formation due to their acidic properties (Johns and Shimoyama, 1972).

1.1.1 Structure

Clay minerals are phyllosilicates: layered (or two-dimensional) silicates. The basic building blocks are the Si $(O, OH)_4$ tetrahedra and the M $(O, OH)_6$ octahedra with M = Al^{3+}, Mg^{2+} or $Fe^{2+, 3+}$. This type of structure is shown in Figure 1.1.

The condensation of a monolayer of tetrahedra with a layer of octahedra gives the 1:1 or TO minerals known as kaolinites (M = Al^{3+}) and serpentines (M = Mg^{2+}). They are respectively called dioctahedral and trioctahedral 1:1 minerals. The structure of

kaolinite is given in Figure 1.2. The unit layer is composed of one sheet of silicon oxide and a sheet of aluminium oxide building blocks.

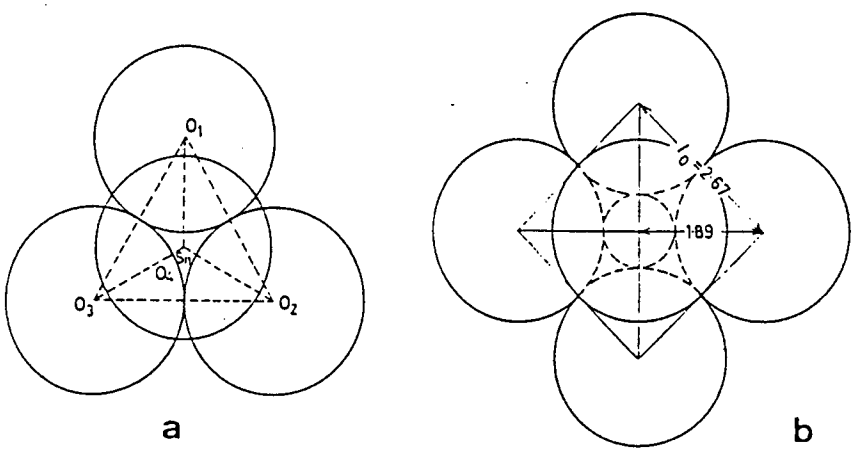

Figure 1.1 Phyllosilicate building blocks (a) The SiO_4 tetrahedron; O_1, O_2 and O_3 are the basal oxygens; O_4 is the apical oxygen. (b) The AlO_6 octahedron. Distances are in Angstroms.

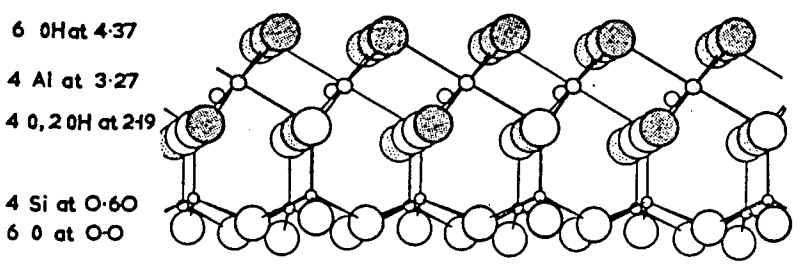

Figure 1.2 The structure of kaolinite

When a monolayer of Al-octahedra is sandwiched between two monolayers of Si-tetrahedra, a 2:1 type of clay is obtained. They are dioctahedral in the case of Al-octahedra and trioctahedral for Mg-octahedra. In the former case two out of three octahedral sites are occupied and in the latter case all three sites are occupied. The parent mineral of the 2:1 layered group is pyrophyllite (Figure 1.3).

It can be seen from Figure 1.3 that there are three distinct sheets in which the cations are found. The inner sheet, consisting of octahedrally co-ordinated aluminium ions, shares two-thirds of its oxygen with the outer tetrahedrally co-ordinated silicon sheets. The remaining oxygens of this layer form hydroxyl groups. It is this layered structure from which the term 2:1 layer lattice or triphormic is derived (Farmer and Russel, 1964). Kaolinite is thus a diphormic mineral. The layered structure extends in two dimensions and the layers stack on top of one another to form the bulk mineral. These layers are held together by van der Waals forces. The silicate sheets, seen from above, show hexagonal symmetry, with the oxygen atom of the structural hydroxyl groups of the octahedral sheet projecting into the hexagonal hole (Farmer and Russel, 1964).

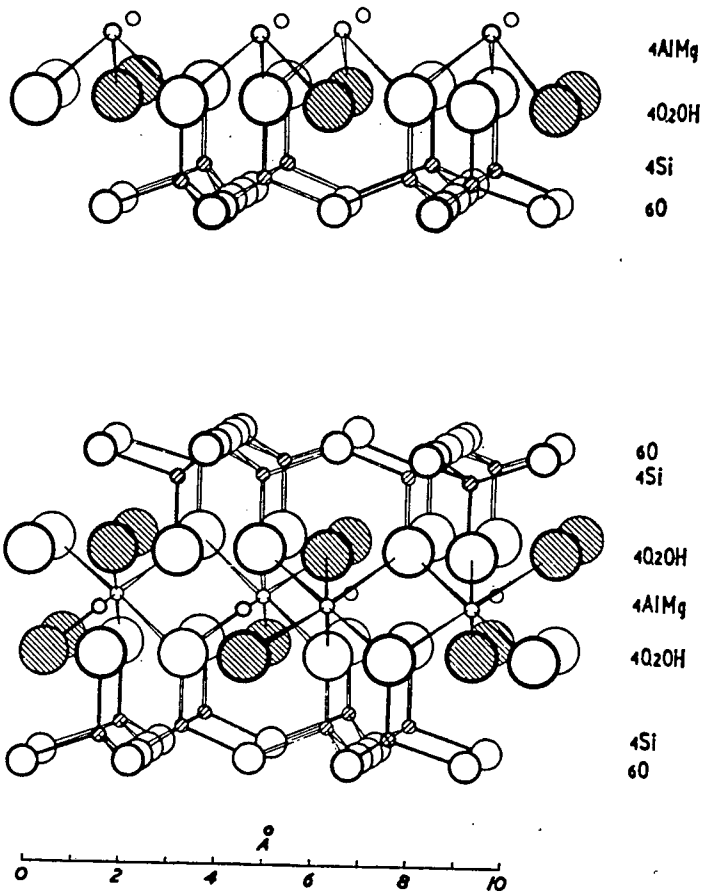

Figure 1.3 The structure of pyrophyllite

The 2:1 layered clays are classified according to their layer charge as shown in Table 1.1 (Brindley, 1964).

Table 1.1 Classification of 2:1 clay minerals

Charge/Formula	Group	Subgroup	Name
0	pyrophyllite talc	dioctrahedral trioctahedral	pyrophyllite talc
0.25-0.6	smectite	dioctahedral trioctahedral	montmorillonite beiddelite saponite hectorite
0.6-0.9	vermiculite	dioctahedral trioctahedral	vermiculite vermiculite
1	mica	dioctahedral trioctahedral	muscovite biotite

The general formula representation is

$$(Si_{8-x}\,M_x)^{IV}(Al_{4-y}\,M^{I}_{y})^{VI}(OH)_4O_{20}M^{II\,n+}_{(x+y)/n}\,mH_2O$$

for dioctahedral clays or

$$(Si_{8-x}\,M_x)^{IV}(Mg_{6-y}\,M^{I}_{y})^{VI}(OH)_4O_{20}M^{II\,n+}_{(x+y)/n}\,mH_2O$$

for trioctaheral clays.

The subscripts IV and VI refer to the tetrahedral and octahedral layers respectively. M and M^{I} have one unit of charge less than the cation that they replace and M^{II} is the exchangeable cation with valency n.

The electroneutral structures are pyrophyllite and talc. The other 2:1 layers of lamellae of structural clays carry a net negative charge due to isomorphous substitution of lower valence cations for higher valence cations within the structure (Van Olphen, 1963; Grim, 1968; Farmer and Russel, 1964; Davidtz, 1976). Lattice imperfections, broken bonds at the edges of particles and exposed hydroxyl groups can also contribute towards the lattice charge (Grim, 1968). In mica and montmorillonite, respectively, cations substituting for Si^{4+} in the tetrahedral sheet (eg., Al^{3+}, Fe^{3+}) and for Al^{3+} in the octahedral sheet (eg., Fe^{2+}, Mg^{2+}) give rise to a negative layer charge. Members of the smectite family are distinguished by the type and location of the substituting cations within the structural lattice.

The charge deficit is balanced by exchangeable cations (eg., Mg^{2+}, NH_4^+) situated between the layers. The extent of isomorphous substitution therefore determines the cation exchange capacity (CEC) of the clay.

Figure 1.3 also shows that only two of the three possible octahedral positions (per unit cell) are occupied. This mineral type is termed dioctahedral. Triphormic minerals in which all the octahedral positions are occupied (eg., talc with Mg^{2+} insteal of Al^{3+}) are called trioctahedral clays.

The smectite group is divided into saponites, which are trioctahedral, and montmorillonites, which are dioctahedral. The most common example of the subgroup of saponites is saponite, which has the ideal formula:

$$M_x^+ (Si_{8-x} Al_x)^{IV} (Mg_4)^{VI} O_{20} (OH)_4$$

in which M^+ is the exchangeable charge balancing cation and x is the layer charge. Hectorite is also a member of this subgroup, but has its substitution (Li or Mg) in the octahedral layer.

Dioctahedral smectites are montmorillonites, which include a wide range of minerals within this subgroup. Its two extremes are represented by compositions in which the

charge is completely tetrahedral in origin, or completely octahedral. The former is beidellite:

$$M_x^+ (Si_{8-x}\ Al_x)^{IV}\ (Al_4)^{VI}\ O_{20}\ (OH)_4$$

An average value of x for beidellite is 0.7 (Brown, 1972). The octahedral species carries the same name as the subgroup, i.e., montmorillonite:

$$M_x^+ (Si_8)^{IV}\ (Al_{4x}\ Mg_x)^{VI}\ O_{20}\ (OH)_4$$

An important property of smectites is their ability to swell by intercalation of water or alcohols (Farmer and Russel, 1964; Barrer and Macleod, 1950; Cariati, *et al*, 1983; Barrer and Reay, 1958). The extent of the swelling depends upon the layer charge, the interlayer cation, and the nature of the swelling agent (Mortland, 1968). Where a high degree of substitution occurs, with a layer charge of about 2, little or no water is associated with the outer layer cations and these minerals, viz. micas, do not swell in the presence of water due to the strong electronic charge holding the 2:1 layers together.

The dimensions of the surface of the smectite unit cell are approximately 5.2 x 8.9Å (Brown, 1972). Ignoring the very small contribution from the area of the edges of the lamellae, the surface area is estimated to be 750m²/g. Hongdu (1981) reported a BET surface area of 51m²/g for a naturally occurring montmorillonite sample, while Brindley and Sempels (1977) reported a BET surface area of 73m²/g for a naturally occurring beidellite sample. These low surface areas occur as a result of the extensive face to face layer stacking in the two clays. The BET nitrogen method involves initial degassing, and this pulls the lamellae together such that they are not subsequently intercalated by N_2.

1.1.2 Acidic properties of smectites

Clays have been shown to be able to protonate bases like pyridine and ammonia (Horvath *et al*, 1982; Barrer and Reay, 1958; Mortland and Raman, 1968) even though

the outerlayer cation is not a proton. The mechanism whereby clays which contain charge balancing cations (other than hydrogen ions) protonate bases is thought to be due to the ability of the cation to polarize the water molecules forming its hydration sphere (Mortland and Raman, 1968; Frenkel, 1974). Farmer and Mortland (1966) and Mortland and Raman (1968) substantiated this claim by reporting that the acidity of magnesium and calcium montmorillonite increased as the clay was progressively dehydrated. It is argued that the removal of some of this water increases the degree of polarization in the remaining molecules thereby making their protons more liable. The acidity of montmorillonite has been shown by Mortland and Raman (1968) and Frenkel (1974) to be strongly influenced by the polarizing power of the cation. The acid strength and amount decreased in the order Al^{3+}, Mg^{2+}, Na^{+}.

This may be represented as:

$$[M(H_2O)_x]^{n+} \xleftrightarrow{k_1} [M(H_2O)_{x-1}(OH)]^{(n-1)+} + H^{+} \quad \text{..... (1)}$$

$$[M(H_2O)_x\ (H_2O)y]^{n+} \xleftrightarrow{k_2} [M(H_2O)_{x-1}(OH)\ (H_2O)y]^{(n-1)+} + H^{+} \quad \text{..... (2)}$$

where M is the exchangeable ion, x the amount of inner sphere co-ordinated water, y the amount of outer sphere co-ordinated water, and k_1, k_2 the ionization constants for the two systems.

Equation (1) represents the drier system with directly co-ordinated water, while equation (2) represents a moist system. It has been shown that k_1 is greater than k_2, indicating that the drier system is the more efficient proton donor (Mortland and Raman, 1968). NMR studies (Frenkel, 1974; Benesi and Winquist, 1978) have revealed that the water absorbed on montmorillonite is between 10^4 and 10^7 times as dissociated as in the liquid state.

The clay catalysts employed in early catalytic cracking processes were acid treated and thought to contain protons. Hydrogen exchanged clays have been obtained by washing clays with dilute mineral acids (Coleman and Harward, 1953), and ammonium

exchange followed by electrodialysis (Davidtz, 1976) or thermal decomposition (Russel and White, 1966). If the protons released to the lattice by these methods form typical acid sites, H-clays can be expected to be active for hydrocarbon reactions. The catalytic activity of acid treated montmorillonite towards Bronsted acid catalysed reactions has been shown to be highly dependent on the degree of acid treatment of the clay (Rhodes and Brown, 1994). It has, however, been shown that acid treated clays contain appreciable quantities of aluminium acting as the charge balancing cation (Coleman and Harward, 1953; Coleman and McAuliffe, 1954; Mathers *et al.* 1954). In this manner the strong acid sites expected in H-clays may be lost. The loss of framework aluminium to exchange positions is accelerated by heating and may occur when NH_4^+ clays are converted to the hydrogen form by thermal decomposition of the ammonium ions.

In his study of the decompositon of t-butyl alcohol by H-clays, Davidtz (1976) found that the acidic activity of the H-clays was directly proportional to the tetrahedral exchange capacity. He proposed that protonic centres in the octahedral sheet are unstable and combine with structural hydroxyls to be lost as water. Furthermore, Mathers *et al.* (1954) found that octahedral aluminium and presumably other octahedral cations are more easily leached from the lattice than tetrahedral aluminium.

Solomon (1968) has found that clays catalyze the polymerization of unsaturated compounds. He reported that kaolinite was more active than montmorillonite followed by pyrophyllite. Talc (Mg^{2+} in the octahedral layer only) was not active. The results indicated that the presence of aluminium in the octahedral sheet is important and that the crystal edges are involved in the hydrocarbon reactions. Solomon and Rosser (1965) suggested that the catalytic activity was related to aluminium in octahedral co-ordination at the crystal edges.

The proton donating ability of structural hydroxyl groups on clay minerals has been reported by Hall (1985) and Davidtz (1976). Min-Yuan *et al.* (1988) used a montmorillonite sample for ammonia adsorption and infrared examination. They found that there was a strong correlation between the number of hydroxyl groups present and Bronsted acidity.

Figure 1.4 shows a proposed structural model for the location of acid sites on tetrahedrally substituted (beidellite) and octahedrally substituted (montmorillonite) smectites (Ming-Yuan *et al.*, 1988). The designations Al (VI) and Al (IV) are for octahedral and tetrahedral aluminium, respectively. Al (CUS) indicates co-ordinatively unsaturated Al located at the terminal site on the octahedral sheet.

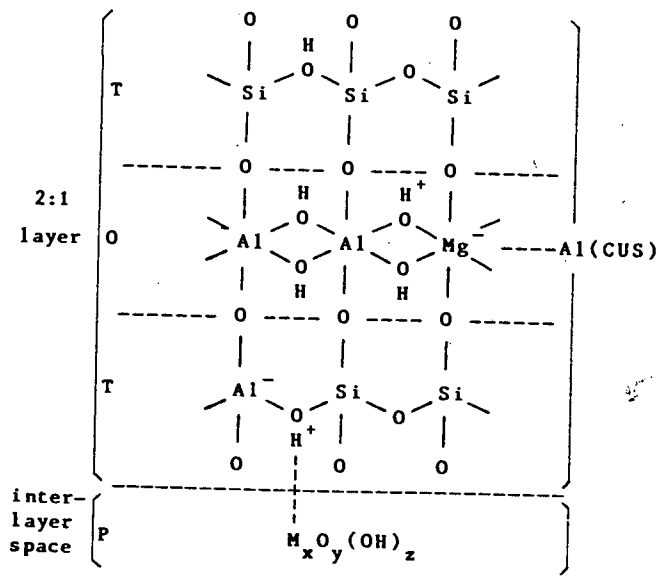

Figure 1.4 Proposed structural model for the location of acid sites on smectite minerals.

Octahedral Sheet

Hall (1985) and Davidtz (1976) pointed out that the Al (CUS)-O- linkage, or octahedrally co-ordinated aluminium exposed at crystal edges, may become either Bronsted or Lewis acid sites. However, their contributions are limited by site density. Al (VI)-O- Al (VI) and Al (VI)-O-Mg, linkages comprise most of the structural OH groups present on the clay.

A rough estimate of the amount of structural OH groups based on the idealized stoichoiometric composition of montmorillonite $(Al_{4-x}Mg_x)Si_8O_{20}(OH)_4$, gives a number of 3.4×10^{21} OH/g. Only a small proportion of these structural hydroxyl groups can become Bronsted acid sites during adsorption of chemical species. The Al (VI)-O-

Mg linkage, in Figure 1.4, compared with the Al (VI)-O- Al (VI), seems more probable to donate H^+ by transferring negative charge to Mg atoms which are located in the dioctahedral sheet. In order to verify this assumption, Yeuhua (1985) chose two montmorillonite samples with different Mg contents to study the possible contribution of octahedral Mg to Bronsted acidity. It was found that the montmorillonite sample with the higher Mg content had about twice the number of Bronsted acid sites than the other sample.

Ocelli and Tindura (1983) showed that a montmorillonite sample displayed both Bronsted and Lewis acidity. At a temperature of 400°C the acidity was mostly of the Lewis type. It seems likely that the Al (VI)-O-Mg linkage would constitute the main source of Lewis acidity in the octahedral layer.

Tetrahedral Sheet

Matsumoto (1984) demonstrated that tetrahedral aluminium atoms in 2:1 layered clays are active sites for adsorption. Figure 1.5 shows how a proton in an H^+ exchanged smectite interacts with the Si-O-Al (IV) linkage to form a Bronsted acid site and how the Si-O-Al (IV) linkage is converted to a Lewis acid site as a result of dehydroxylation.

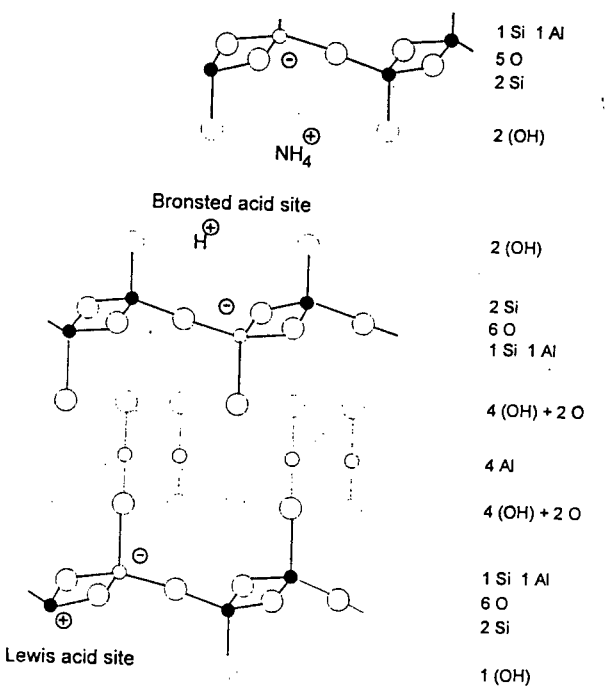

Figure 1.5 Acid sites on tetrahedrally substituted smectites

1.1.3 Natural clays as catalysts

Clay minerals are known to catalyze numerous organic reactions. Clays were used as petroleum cracking catalysts (Voge, 1958), where reaction temperatures are in the range of 400-500°C, and for the isomerization of hydrocarbons.

Montmorillonite was used extensively for making hydrocracking catalysts (Thomas, 1970). In the 1930's ESSO and ICI Ltd. of England developed various catalysts based on HF treated montmorillonite and I.G. Farbenindustrie A-G. developed a tungsten sulphide on montmorillonite catalyst by. By the late 1930's the ICI catalyst, which was iron supported on HF-treated montmorillonite, was used for hydrocracking middle oils (boiling range 230-485°C) in a two stage process. This catalytic process played an important role in supplying aviation gasoline during World War II. ESSO developed a second-stage hydrocracking catalyst consisting of nickel supported on HF-treated montmorillonite.

Acid clays have been used to catalyze sucrose inversion and ester hydrolysis (Coleman and McAulifffe, 1954), and ethanol oxidation (Grim, 1968). The dehydration of organic molecules can be achieved using a clay surface (Davidtz, 1976). Acid treated clays catalyze alkylation of aromatic rings by alcohols alkyl chlorides and alkyl ethers (Zuech, 1974; Swartzen-Allen and Matijevic, 1974). Alkylation of aromatics with olefins is enhanced by acidified clays. Acid treated clays have the ability of polymerize olefins (Soloman, 1968; Davidson, *et al.*, 1943).

1.1.4 Pillared Clays

The properties of clay minerals, as described in the previous sections, make these materials suitable for use as acid catalysts. Clays such as montmorillonite and beidellite have an extensive face to face layered structure with individual sheets separated by an interlayer space. These minerals readily expand, and numerous organic reactions can take place within the interlamellar space. On calcination, collapse of the layer structure

occurs and the interlayer spaces is virtually eliminated. Any catalysts, therefore, loses much of its activity after calcination or reaction at elevated temperatures.

In the preceding two decades, a new class of two-dimensional sieves has been synthesized from certain types of aluminosilicate clay minerals. The general procedure is to incorporate large cations between the clay layers to prop them open. The removal of water from such "pillared" clays on heat treatment would then not result in the collapse of the interlayer spaces, provided the pillars are thermally stable. It has long been known that various organic molecules such as amines and alkyl-ammonium ions readily intercalate between clay layers and form pillared structures (Barrer, 1978). In general, these organically pillared structures suffer from the instability of the organic component, although relatively stable compounds have been formed with cage-like amines (Shabtai *et al.*, 1976; Mortland and Berkheiser, 1976; Bailey, 1980).

The problem of thermal stability was tackled using large polymeric oxy-hydroxy cationic species (Vaughan and Lussier, 1980). These polycationic species are set in position within the clay as a result of ion exchange with the existing charge balancing cations on the interlayer spaces. Due to the size of these pillaring species, the ion exchange process leading to pillaring can take place only in clays with a swellable property.

Calcination of clays exchanged with these pillaring species results in the formation of permanent oxide-hydroxide props which hold the layers apart and so generate a large proportion of microporous space (Vaughan and Lussier, 1980). Such pillared clays are defined by expanded lattice basal spacings. An atomic force microscope has been used to investigate surface features of Ca and Na-bentonite (a montmorillonite) pillared with alumina clusters (Ocelli *et al.*, 1993). Atomic scale resolution images of the clay surface consisted of hexagonal arrays of bright spots, showing resolution below the scale of the unit cell. The "nearest neighbour" distance was found to be consistently greater after pillaring, suggesting that the bulky Al_{13} clusters stretched the clay's silicate layers. Molecular scale resolution images of the cross-sectional area of extrudates formed using pillared bentonite powder showed platelets about 9.0Å apart, in agreement with X-ray diffraction results.

Jones (1988) reported that certain factors had an important influence on the interlayer spacing and "pore width" in pillared clays. These included the molecular dimensions of the pillaring cation, the charge on the cation, which was dependant on the degree of hydrolysis, the orientation of the pillaring cation between the clay layers, and the charge density and distribution of the clay layers.

1.2 Synthetic Clays

The natural clays used for the cracking of petroleum feedstocks were made from acid-treated montmorillonites. This type of clay contained lattice iron (Fe^{3+}) which was activated by feed sulphur resulting in the formation of coke deposits. It was also found that this catalyst was not stable at the higher regeneration temperatures required for catalytic cracking (Swift, 1977). Synthetic silica-alumina cracking catalysts were developed (Ashley and Innes, 1952) that were iron free and more stable at higher regeneration temperatures. These catalysts gave better product quality than acid-treated montmorillonite. In the early 1960's zeolite containing catalysts were developed that resulted in significant improvement in the activity and selectivity to desired products.

In recent years there has been renewed interest in synthetic clay-like materials for catalytic applications. These synthetic materials are semi-crystalline aluminosilicates that are ordered in two dimensions. One of the routes to enhanced catalytic performance is the isomorphous substitution of various ions in the structure. A wide variety of ions can be substituted for aluminium and/or silicon atoms, which can result in substantial enhancement in catalytic properties. The resulting clays are thermally very stable and can be synthesized directly in the ammonium form. Subsequent heating results in deammoniation generating the acid form of the clay.

1.2.1 Synthetic Mica Montmorillonite

Mica montmorillonite is a dioctahedral clay. It is simlar in structure to muscovite in that both have substitution of tetrahedral Si by Al. Mica montmorillonite has a lower

substitution value than muscovite and the charge balancing species is NH_4^+ as oppsed to K^+ for muscovite. The synthesis of synthetic mica montmorillonite (SMM) was first disclosed in a patent by Granquist (1966) of the Baroid Division of N.L. Industries. Work was continued on the structure and thermal modification of the clay (Wright *et al.*, 1972). SMM was also found to exhibit cracking activity and its use as a support for hydrogenation metals was widely patented.

1.2.1.1 Synthesis

Most methods of silicate mineral synthesis fall into two broad groups: melting processes and hydrothermal processes. High temperatures are required in the former case as the mineral is crystallized from a melt. In hydrothermal synthesis, crystallisation takes place in the presence of excess water, with the required amounts of silica, alumina, alkali metal oxide and fluoride or hydroxide. Synthesis is undertaken in a pressure vessel in which the water will remain in the liquid state by autoclave action.

The mixture is maintained at the selected temperature for long enough for the mineral to form. The synthesis mixture is typically kept at 285°C for 48hr with a autogeneous pressure of 1000psia. The autoclave is cooled, the product washed in distilled water and dried.

The hydrothermal synthesis of SMM was first reported in a patent by Granquist (1966). This was followed by a publication by Granquist and Pollack (1967) which dealt with the structure and small-scale synthesis of fluoride-free SMM. These methods first resulted in the formation of the sodium form of SMM.

Improvements were later made in this synthesis procedure such that the ammonium form of SMM was crystallized directly (Granquist *et al*, 1972).

1.2.1.2 Structure

SMM is a 2:1 layered aluminosilicate consisting of randomly interstratified expandable and non-expandable dioctahedral layers. Wright *et al.*, (1972) showed that the infrared spectra of SMM and the natural clay muscovite are very similar. The small differences were attributed to the lower lattic aluminium content of SMM, the greater Si, Al ordering in muscovite, and the higher fluoride/hydroxyl substitution in SMM.

X-ray diffraction studies of SMM (Wright *et al.*, 1972) revealed a non-integral 001 sequence and irregularly shaped peaks which are indicative of mixed layering. The basal spacings of 10.4Å and 12.5Å occurred in the proportion 2:1. They also found that upon hydration the 10.4Å spacings persisted at 100% humidity indicating the mica-like nature of these layers. The 12.5Å spacing swelled to 17.3Å upon addition of ethylene glycol and collapsed to 10.8Å in dry air, thus exhibiting montmorillonite-like behaviours. Similar to mica there is no octahedral substitution and layer charge is derived solely from Al^{3+} substituting for Si^{4+} in the tetrahedral layer. This charge is balanced by the presence of cations in the interlayer space and it is suspected that aluminium (in the form of its partial hydroxides) fulfils part of this charge-balancing role (Wright *et al.*,1972). The unit cell may be presented as follows:

$$[(Al_4)^{octa}\,(Si_{\,8-x}\,Al_x)^{tetra}\,O_{20}\,(OH,F)_4]^{x-x/n}\,M^{n+}$$

where x is the number of tetrahedrally coordinated aluminium ions and thus represents the net negative charge on the unit cell, and M represents the charge-balancing cation. Wright *et al.* (1972) have determined the value of x to be approximatley 1.5. Due to the uncertainty regarding the nature of the charge balancing hydroxy-aluminium species the cation M^{n+} is represented as:

$$M^{n+} = wNH_4^+ + y\,[Al\,(OH)_{3+z}]^{z+}$$

where the primary charge-balancing ion is given as NH_4^+. Uncalcined SMM has a F/Si ratio of 0.1 and contains 175 meq NH_4^+/100g.

The proposed structure of the SMM lamellae is presented in Figures 1.6 and 1.7. It can be seen that two out of the three octahedral positions are filled and SMM is thus a dioctahedral clay.

Electron microscopy studies (Wright *et al.*,1972) have shown the bulk material to have a plate-like structure, consisting of platelets of an average diameter of 1000 Å. Based on a BET surface area of $160m^2/g$ and a density of $2.55g/cm^3$ (from X-ray unit cell measurements), the average number of layers per platelet-to-platelet sub-unit is calculated to be about 5. This gives an approximate platelet thickness of 50 Å (as shown in Figure 1.6).

The BET surface area of SMM was found to be a smooth monotomically decreasing function of the outgassing temperature up to 950°C at which point recrystallisation of new phases occurs. Outgassing at 650°C caused the surface area dropped from $160m^2/g$ to $135m^2/g$ which is ascribed to greater platelet-to-platelet association, since neither infrared nor X-ray diffraction data suggest the formation of a new high temperature, low surface area phase in this range (Wright *et al.*, 1972).

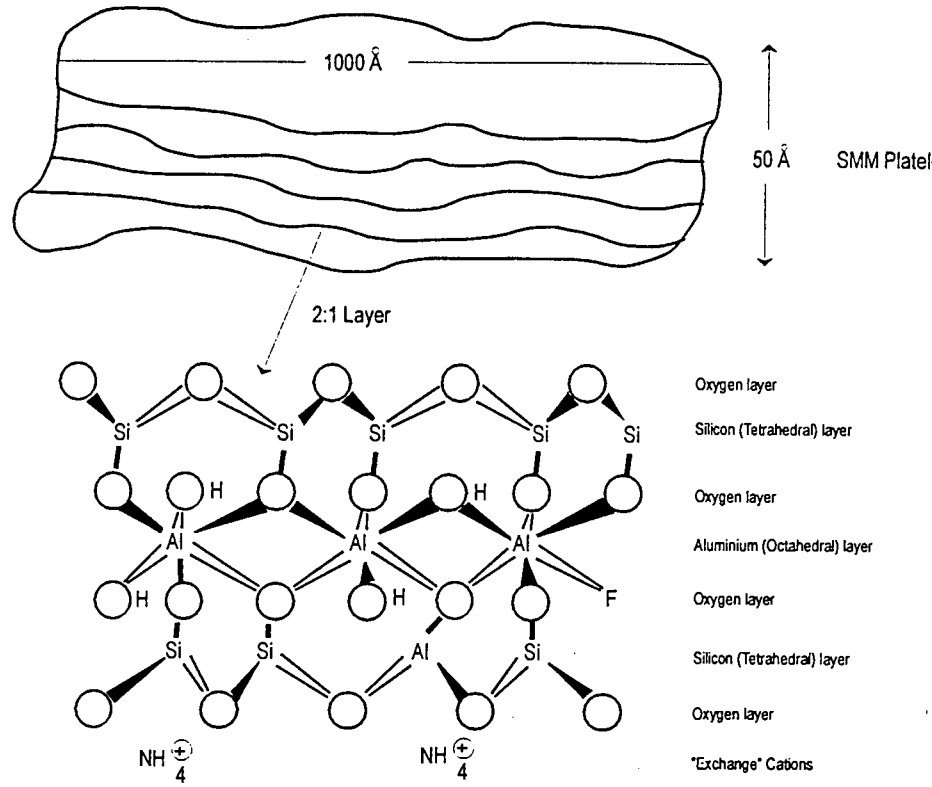

Figure 1.6 Structure of SMM lamellae (Swift, 1977)

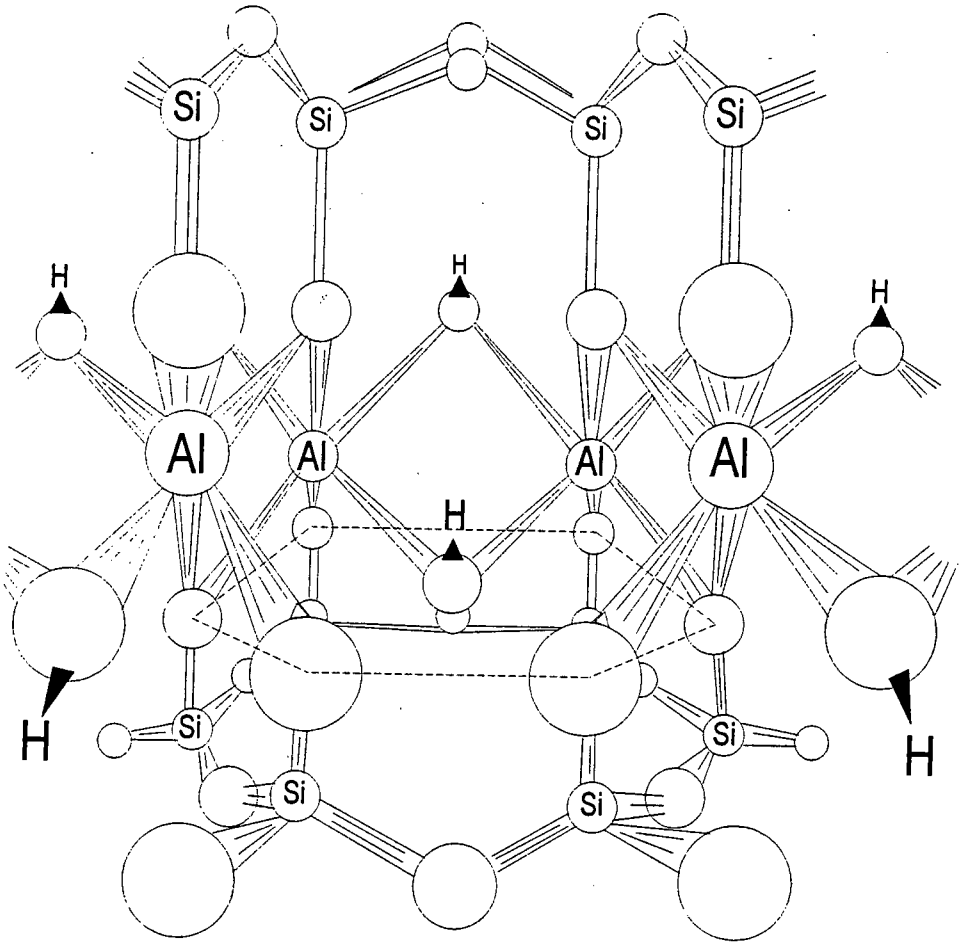

Figure 1.7 Connection of dioctahedral layer to tetrahedral layer in SMM (Swift, 1977)

The state of SMM after thermal treatment is of considerable importance for catalytic applications as this results in the active species. Mild calcination results in deammoniation and converts the material to the Bronsted acid form. More severe heat treatment (above about 500°C) yields both Lewis and Bronsted acid sites.

Wright *et al.*. (1972) showed that deammoniation and dehydroxylation occurred simultaneously although final deammoniation preceded final dehydroxylation. A similar result was found by Kojima *et al.*. (1986) who showed that Bronsted acidity disappeared at about 430°C while Lewis acidity was strongly present even at 680°C.

Wright *et al.*. (1972) suggested a structure for dehydroxylated SMM which caused a minimum disruption of the unit cell since the infrared spectrum of SMM changed slightly upon activation.

The overall equilibrium process was represented as:

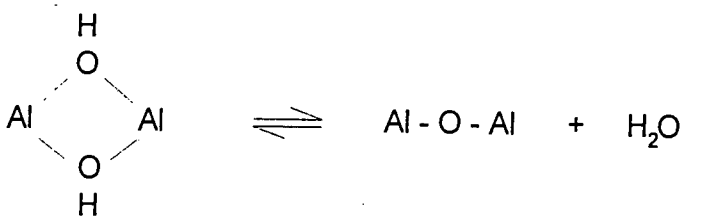

They suggested that the protons resulting from deammoniation enter sites within the lattice, such that some of the protons may be lost according to

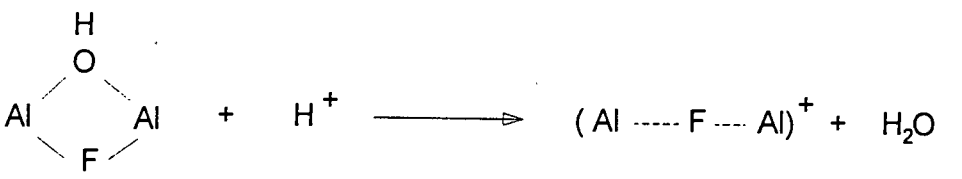

where (Al ....F .....Al)$^+$ assume the charge balancing role. The protons could react with the tetrahedral aluminosilicate lattice by a mechanism similar to that proposed by Uytterhoeven *et al.* (1965).

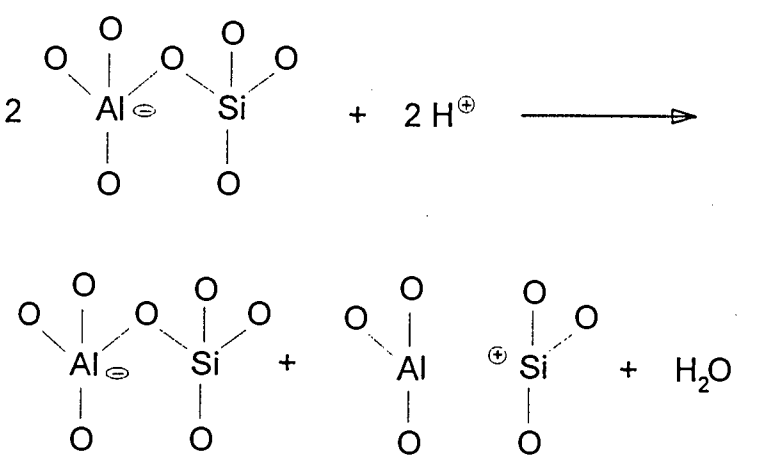

Russel and White (1966) reported that upon deammoniation and dehydroxylation a band developed at 3470cm^{-1} in the infrared spectrum. This observation was in agreement with that of Wright *et al.* (1972) who found the 3470cm^{-1} band to be stronger in fluoride-free SMM at high temperatures. Kojima *et al.* (1986) reported that a band at 3460cm^{-1} grew in intensity and then started to drop at about 227°C. The above workers believe the 3470cm^{-1} band to be a result of an interaction between the protons from deammoniation and the oxygen of the structural hydroxyl. Russel and White (1966) referred to this species as a proton perturbed lattice hydroxyl group. The electron withdrawing proton near the oxygen of the hydroxyl group weakened the O-H band and therefore lowered its frequency. The addition of ammonia cause the disappearance of the 3470cm^{-1} band thereby confirming the above proposal. The postulate made by the above workers is that the protons drop into the empty tetrahedra adjacent to the (OH, OH) or (OH, F) pairs in the octahedral layers. Wright *et al.* (1972) suggested that the dehydroxylation is proton catalyzed. Granquist and Kennedy (1967) have found that SMM has the ability to sorb appreciable quantities of water at elevated temperatures (490°C, 24 torr vapour pressure) and shown that this sorption occurs more efficiently in samples containing fluoride ions.

1.2.1.3 Acidity

The nature of acid sites present on SMM has been investigated by solid state infrared studies (Kojima *et al.* 1986; Wright *et al.* 1972) and temperature programmed desorption studies (Kojima *et al.* 1986) using pyridine as the probe molecule. Wright *et al.* (1972) reported values of 2.5meq Bronsted and 1.5meq Lewis-bound pyridine per 100g of calcined NH_4^+ - SMM giving a total acidity of 4meq per 100g. Kojima *et al.* (1986) found that the amount of Bronsted acidity decreased as the calcination temperature increased. At a calcination temperature of 500°C there was no longer evidence of Bronsted acidity. Upon addition of water to dehydroxylated SMM, Lewis sites were observed to convert to Bronsted sites. Quantitative measurements suggested a reversible one to one interconversion of these acid sites. Using the integrated absorbance coefficients of Hughes and White (1967), Kojima *et al.* (1986) computed the number of Lewis sites per gram of SMM after calcination at 500°C to be 2.4 x 10^{29} sites/g. This was the exact number obtained by Wright et at., (1972) under the same

conditions. Kojima *et al.* (1986) found that calcination at 650°C resulted in the generation of only Lewis acid sites which existed at particle edges and faces. Wright *et al.* (1972) attributed the Lewis acidity to trigonal aluminium at the edge of the tetrahedral layers. The actual amount of Lewis acidity versus the theoretical amount (approximately 20meq/100g) indicated that only a fraction of the aluminium ions have trigonal configuration or are detectable by pyridine. The conversion of Lewis to Bronsted acidity by the addition of water is represented as:

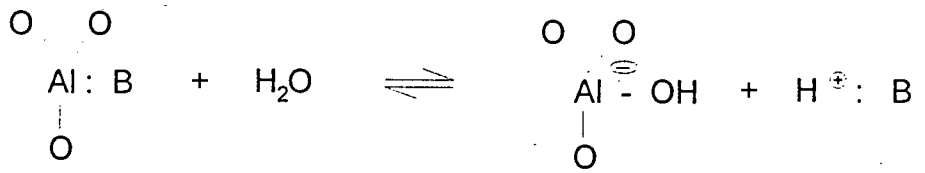

where B is a base.

At the edges of the crystals the sheet structure is broken and the crystal is terminated by OH-groups. At high pH they deprotonate, the edges become negatively charged and have a cation exchange capacity (CEC). At low pH they absorb protons and become positively charged. As a consequence, in the experimentally determined CEC is a pH-dependant part. Maes *et al.* (1976) proposed the following equations for the pH dependence of the CEC in the pH range 3.9 - 5.8 for clays saturated with monovalent and divalent cations respectively.

$$\text{CEC (meq/100g)} = 79.9 + 5.04\ \text{pH}$$

$$\text{CEC (meq/100g)} = 96.1 + 3.93\ \text{pH}$$

The crystal terminating groups of dioctahedral smectites with and without isomorphous substitution are shown in Figure 1.8. For a pH of 6.5 White and Zelazny (1988) calculated a negative charge density of 5.32mmole/m^2. If a clay particle in the form of a cube of 2mm square and 1mm thick, and a density of 2.3g/cm^3 is assumed, it corresponds to 4.63mmole/g or 0.46% of the CEC. For particles of 100nm thick,

92.6mmol/g or 9.26% of the CEC is obtained. The contribution of the edge sites to the total CEC is thus not negligible and will depend on the experimental conditions which determine crystal size and shape, type of exchangeable cation and pH.

Temperature programmed desorption (TPD) of pyridine was carried out to investigate the acid strength and distribution on SMM (Kojima *et al.* 1986). At a low calcination temperature of 250°C the acidity was mainly due to polarized water and ammonium ions. As the calcination temperature was increased there was a shift to a higher peak desorption temperature. The TPD peak resulting from calcination at 650°C yielded a Lewis acid site concentration of 1.7 x 10^{19} sites/g. This compared well with the equivalent value of 1.8 x 10^{19} sites/g determined in their infrared study.

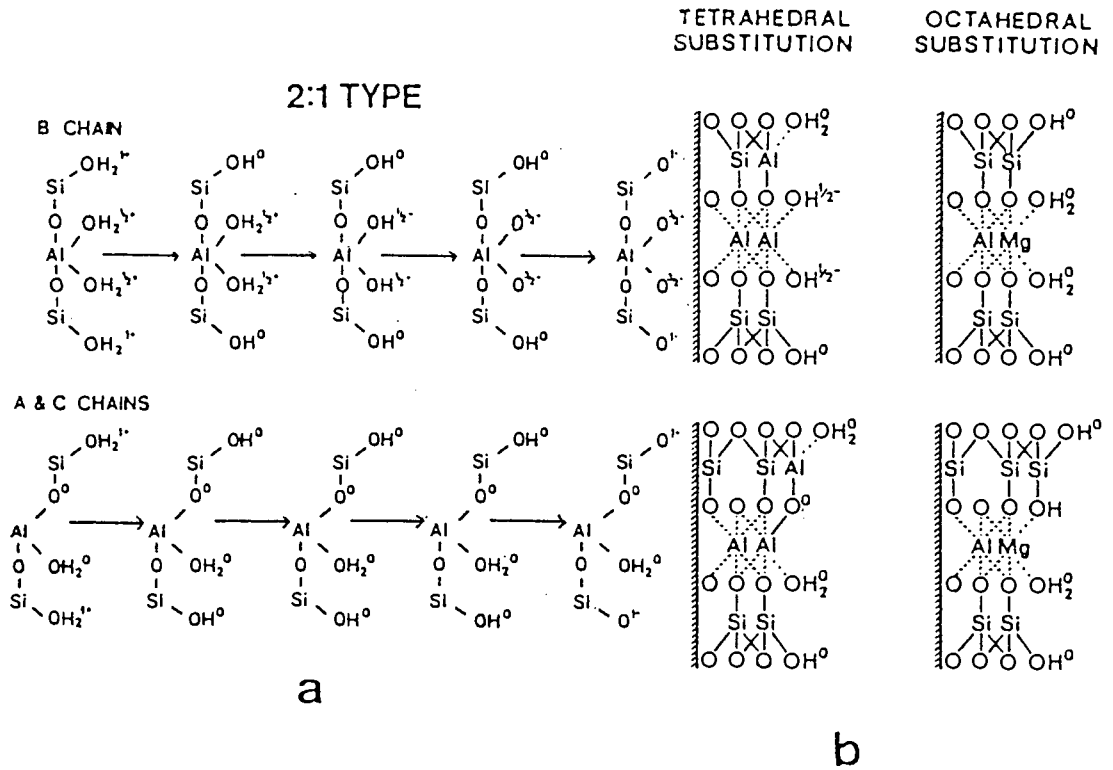

Figure 1.8 (a) Effectof pH on the edge charges of smectite layers without isomporphous substitution. The pH increases from left to right. (b) Effect of octahedral and tetrahedral substitution on the edge charges at pH = 6.5

A & C chains have a single terminal H_2O on the octahedral Al, B chains have two terminal H_2O groups.

(White and Zelazny ,1988)

1.2.1.4 Catalytic activity

Although SMM has a much lower acid site density than zeolitic catalysts, it has comparable catalytic activity. This is possibly due to the platelike nature of SMM. The measured acidity is representative of accessible acidity, whereas due to diffusional limitations, only a fraction of the measured acidity of zeolites is actually catalytically active under dynamic conditions (Thomas and Barmby, 1968).

The catalytic activity of SMM for cracking was first reported by Capell and Granquist (1966). The catalyst had an exchange capacity of 1.97meq/g and was converted to its active form by exchanging with ammonium ions followed by deammoniation at 500°C. The catalytic activity was compared to that of a synthetic alumina cracking catalyst, a sulphur resistant natural halloysite and a steam / H_2S treated commercial halloysite. SMM was observed to be twice as active as the sulphur-resistant clay and 1.5 times more active than the synthetic alumina catalyst. SMM also displayed a better product selectivity. SMM has also been shown to have similar activity to zeolite cracking catalysts by workers at the Baroid Division of N.L. Industries (Swift, 1977).

Hoffman and Granquist (1974) found that by coating kaolinite particles with a layer of SMM, a catalyst with high cracking activity and improved mechanical strength resulted. Hattori *et al.* (1973) reported that with SMM there was a higher degree of H^+ ion exchange with hydrocarbon molecules during isomerization than with silica alumina. This high degree of exchangeability of the H atoms in SMM accounts for their acting as primary sites rather than inducing activity in secondary type sites provided by the carbonaceous residue which was found on silica alumina and not on SMM. The higher cracking activity of SMM compared to amorphous silica alumina may be accounted for by this exchangeability.

The use of SMM as a support for hydrogenation metals has been patented extensively (Csicsery, 1971 a,b,c,d; Csicsery and Kittrell, 1972; Jaffe, 1972 a,b,c,d; Jaffe and Kittrell, 1972; Kittrell, 1972 a,b; Kittrell *et al.* 1972; Malasky, 1972). Catalyst made

by using an SMM carrier was shown to be more active than catalyst containing a commercial zeolite carrier, but had a lower aging stability.

Csicsery and Kittrell (1972) showed that the introduction of low concentrations of other metal ions (Mn, Cr, Fe, Cu, Zn, Co) into Pd SMM affected its catalytic performance for hydrocracking. The addition of 0.5wt% Fe resulted in a dramatic decrease in the deactivation rate of the catalyst. It was also found that there was a beneficial effect on catalyst aging by adding water, methanol or a water-producing molecule during hydrocracking. This resulted in hydration which restored the Bronsted acid sites lost during catalyst preparation and/or hydrocracking in dry hydrogen. Fletcher *et al.* (1986) investigated the activity of SMM for propene oligomerization. They reported that the presence of Lewis acidity gave high activity and long catalyst lifetime. The catalyst deactivated rapidly in the presence of water and this was attributed to a temperature runaway promoting the formation of coke precursors. Calcining at low temperatures (250°C), which resulting in the formation of mainly Bronsted acid sites showed poor catalyst lifetime. The optimum condition for propene oligomerization at 61atm was found to be a calcination temperature of 500°C and a reaction temperature of 147-187°C.

The activity and selectivity for propene oligomerization over SMM, as well as nickel cobalt and zinc ion-exchanged SMM, have been studied by O'Connor *et al.* (1988). Zinc ion-exchanged SMM had a greater activity than nickel ion-exchanged SMM. Cobalt ion-exchanged SMM was initially more active than either but deactivated rapidly. The selectivity was essentially the same for all catalysts of the study and the products were predominantly trimers and tetramers.

1.2.2 Metal Substituted SMM

1.2.2.1 Synthesis

The charge requirement of the octahedral position in SMM may be met by six divalent ions such as Ni^{2+}, Zn^{2+}, Co^{2+} and Mg^{2+}. Because of their size and charge, these ions are able to substitute for Al^{3+} in the octahedral position. When all the six octahedral positions are filled the resultant material is called a trioctahedral clay. A mixed dioctahedral-trioctahedral clay may be formed which is directly related to the concentration of divalent ions during synthesis.

The synthesis of metal substituted SMM is similar to that of SMM with the exception that the reaction mixture of the hydrothermal synthesis inlcudes a source of the divalent metal cation. Acetate, fluoride and nitrate salts are suitable and the metal salt is introduced to the synthesis mixture as an aqueous solution. The amount added determines the degree of metal substitution. Black *et al.* (1976) noted that the inclusion of soluble nickel salts in the reaction mixture tends to cause the nickel to occur predominantly in the trioctahedral phase, while relatively insoluble nickel compounds promote its occurrence in the dioctahedral phase for NiSMM. The preparation and characterization of these metal substituted 2:1 layered aluminosilicates has been described by Granquist (1974), (1976), Black *et al.* (1976); Heinerman *et al.* (1983) and Gaaf and Van Santen (1983).

The silica source is SiO_2 or a polysilicic acid solution prepared by passing a sodium silicate solution over a hydrogen exchange resin such as Amberlite IR 120-H. Hydrated alumina is generally used for alumina addition, an exception being Heinerman et al's (1983) use of aluminium isopropoxide. Ammonium fluoride or ammonium dihydrogen fluoride are added directly to the mixture to obtain partial fluoride substitution for the hydroxyl groups. Ammonium hydroxide is used to raise the pH of the solution and additional water added to break up gel formation.

The mixture is charged to the autoclave and maintained at 300°C for 3hr at a hydrothermal pressure of 1250 psig (86 atm). This differs from the SMM synthesis procedure which uses 285°C for 48 hr. After synthesis the mixture is cooled, washed and dried. The ammonium form is synthesized directly.

Palladium or any of the platinum group metals are added to the final catalyst product as a hydrogenation agent by impregnation. The catalyst is stirred for about 16hr in a Pd $(NH_3)_4$ Cl_4 solution before again being washed and dried. The hydrogenation promoting metal is usually added in concentrations of 0.1 to 1.0 wt% of the final catalyst.

1.2.2.2 Structure

A simplified formula for minerals containing varying degrees of metal substitution in both sixfold (vi) and fourfold (iv) co-ordination sites was given in a patent by Granquist (1974):

$$[(GY)^{octa}\ (QR)^{tetra}\ O(OH, F)]\ M^{+}$$

where G is trivalent ion with a maximum ionic radius of 0.75 Å, which includes Al, Cr, Mn, Fe, Co, Ga, Rh and Sc. Y is a divalent ion with a maximum ionic radius of 0.75Å, which includes Be, Fe, Mg, Ni, Co, Cu and Zn. Q is a tetravelent ion with a maximum ionic radious of 0.64 Å that includes Si and Ge. R is selected from a group of divalent ions having 0.64 Å maximum radius, including ions such as Al, Cr, Mn, Fe , Co and Ga. As with SMM, M^+ is an exchangeable cation.

A mixed dioctahedral-trioctahedral phase is formed from mixtures of the metal oxide, alumina and silica that contain less than the required amount of the metal for complete substitution into the octahedral layer (6 divalent metal atoms per unit cell). Black *et al.* (1976) found that for nickel the maximum weight percentage that could be incorporated into SMM is 36 wt%. Swift (1977) observed that formation of the mixed phases is readily detectable by X-ray diffraction as shown in figure 1.8. The trioctahedral (06)

(>1.500 Å) reflection increased while the dioctahedral (06) (<1.500 Å) reflection decreased as the nickel atoms per unit cell increased.

Black *et al.* (1976) developed a linear correlation relating the intensity of the trioctahedral reflection and the average nickel per unit cell. Basal spacings were observed to vary between 10 and 13.5 Å showing the variable mixed layered native of the clay. Generally, as the Ni atoms/unit cell increased the interlayer spacing increased. The structural characterization of NiSMM from 0 to 6 nickels per unit cell by X-ray diffraction has been extensively reported by Black *et al.* (1976).

Swift and Black (1974) reported that the incorporation of nickel into the SMM lattice via synthesis resulted in a significant increase in the stable surface area as shown in Table 1.2. A loss in surface area was observed in catalyst I (made by impregnating catalyst A (SMM) with nickel nitrate). Swift (1977) stated that the surface area decreased as Zn is included in the matrix, although a more crystalline structure is formed.

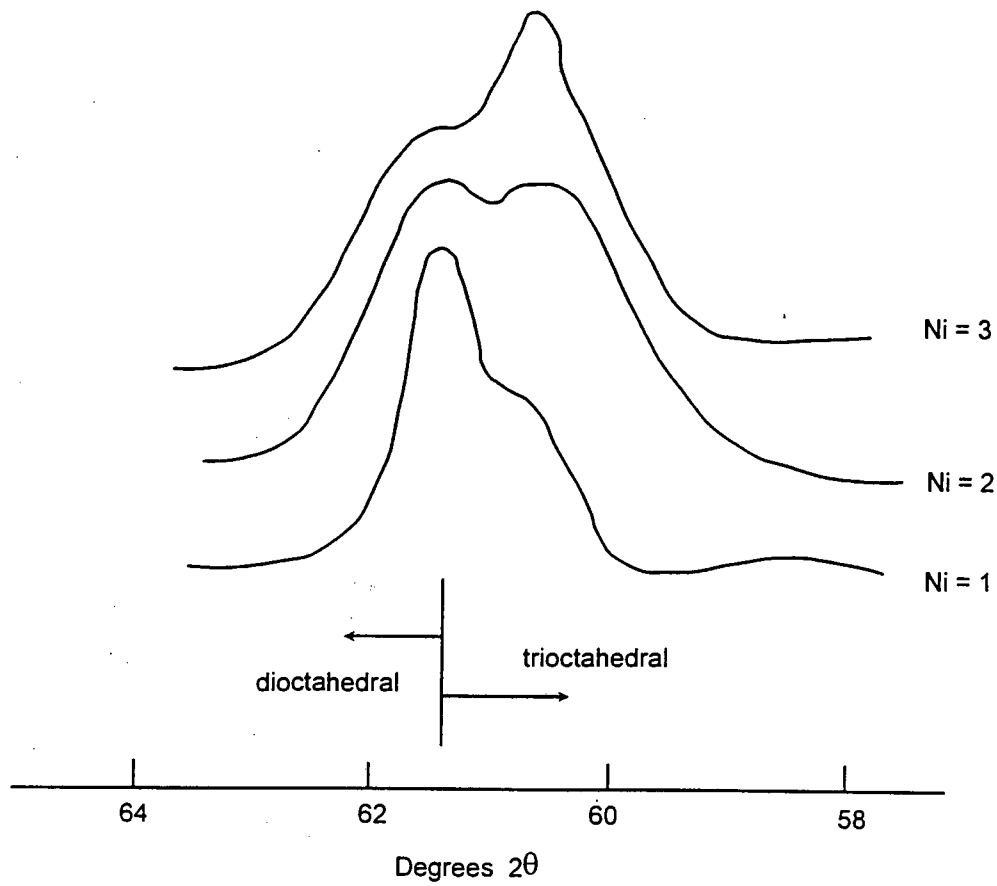

Figure 1.9 Increase of the trioctahedral (06) (>1.500 Å) X-ray diffraction reflections as the nickel atoms per unit cell increase for NiSMM

Table 1.2 Physical Properties of NiSMM Catalysts [a]

Catalyst	Approximate Ni atoms/unit cell	Wt % Ni	Wt % F	Surface Area m^2/g
A	0	0	1.21	145
B	1	6.75	0.50	199
C	2	14.3	0.61	230
D	2	150.0	1.01	244
E	3	21.6	0.73	302
F	4	26.4	0.53	254
G	5	30.5	0.28	258
H	6	35.7	0.37	332
I[b]		15.0	1.01	94
Pd-rare earth-Y zeolite[c]				467
1% Pd-H-mordenite[c]				406

[a]All samples calcined at 538°C before analyses and contain approximately 0.7%Pd. [b]Catalyst made by impregnating SMM base (A) with nickel nitrate to incipient wetness, oven dried at 121°C for 16 hr and then calcined at 538°C for 10 hr. [c]Surface areas obtained on formed materials after being calcined at 538°C for 10hr.

1.2.2.3 Nickel reducibility in NiSMM

It has been reported that upon the reduction of NiSMM in flowing hydrogen at elevated temperatures, a highly active catalyst for hydroisomerization and hydrocracking is formed (Heinerman *et al.* 1983; Robschlager *et al.* 1984). During the reduction process, the Ni^{2+} ion in the octrahedral layer is converted to its metallic form. Swift (1977) postulated that the metallic nickel atoms formed are expelled from the lattice due to ionic radius expansion (Ni^{2+}, radius = 0.69Å is reduced to metallic nickel atoms of radius 1.25Å?). The metallic nickel atoms combine on the surface of the catalysts to form nickel crystallites of varying diameters.

Swift (1977) stated that the rate of nickel reduction does not become appreciable until 425°C. Heinerman et al. (1983) investigated the reduction of NiSMM using temperature programmed reduction (TPR) and found that nickel crystallites were formed at a reduction temperature of 450°C. Introducing Pt or Pd lowered this temperature to 380°C. The lower reduction temperature for Pt or Pd impregnated NiSMM was expected since Pt and Pd are known to catalyze the reduction of nickel (Swift and Black, 1974). It was also found that the degree of reduction increased with increasing reduction temperature (Heinerman *et al.* 1983).

The basic NiSMM structure remained unaffected when samples contained an appreciable amount of octahedral aluminium. Heinerman *et al.* (1983) found that upon the reduction of 22% NiSMM (3 Ni/unit cell), the structure was partly destroyed.

In their infraread study Heinerman *et al.* (1983) found that upon the reduction of 20% NiSMM the number of Bronsted sites increased four times while the Lewis sites decreased by a quarter. This was confirmed by Robschlager *et al.* (1984) who studied the thermal desorption of pyridine from Pd-NiSMM. Their results showed a five-fold increase in Bronsted acidity upon reduction. These results suggest that the newly formed acidic sites were responsible for the increased acidity of reduced NiSMM compared with SMM. The reduction process may be represented as:

$$Ni^{2+} + H_2 \longrightarrow \underset{\text{metallic nickel}}{Ni^0} + \underset{\text{Bronsted sites}}{2H^+}$$

O'Connor *et al.* (1988) found that removal of the reduced nickel by carbon monoxide increased the propene oligomerization activity of the catalyst.

1.2.2.4 Catalytic activity

NiSMM and CoSMM have been reported to catalyze hydrocarbon reactions including hydroisomerization and hydrocracking (Swift and Black, 1974), oligomerization of olefins (Bercik *et al.* 1978) and hydrotreating (Swift and Vogel, 1979).

Swift and Black (1974) evaluated hexane hydroisomerization activity of Pd-SMM, Pd-NiSMM and Pd-H-mordenite. The catalysts were reduced at 350°C. Pd-NiSMM was observed to be 20 times more active than Pd-SMM and 1.7 times more active than Pd-

H-mordenite. This demonstrated the importance of nickel incorporation in the SMM structure. The maximum activity was obtained using a catalyst containing 5 Ni atoms/unit cell. Robschlager *et al.* (1984) and Heinerman *et al.* (1983) provided evidence that hydroisomerization may be described by a dual function mechanism in which the metal sites (nickel and/or palladium) were responsible for (de)hydrogenation and acid sites for the isomerization of the hydrocarbon.

Black *et al.* (1976) reported that, for hydrocracking of hexane and raffinate, presulphiding the catalyst improved its activity and selectivity. Pd-NiSMM with 2 Ni atoms per unit cell gave the best results, yielding LPG (liquid petroleum gas which consists mainly of propane and butane) with a minimum of undesired products. Swift and Black (1974) also studied the effect of cobalt and zinc in the SMM lattice. They found that there was an increase in hexane hydroisomerization activity with increasing cobalt content. However, the increase in activity was not as marked as the catalyst with a corresponding amount of nickel. ZnSMM exhibited low activities for hydrocracking.

The sulphur sensitivity and its effect on the long-term stability of a Pd-NiSMM catalyst was studied by Fisher and Giannetti (1975) for hydrocracking of a commercial raffinate. Sulphur was found to be essential for increased LPG yield and reduced the amounts of C_1 and C_2 hydrocarbons produced. A level of 100-200ppm of sulphur in the feed was critical to obtain good catalyst stability. When the sulphur level was increased to 500 ppm, pronounced aging occurred.

NiSMM has been shown by Bercik *et al.* (1978) to be an active catalyst for the oligomerization of C_3-C_4 olefins. It was found that with proper sulphiding of the catalyst, product quality could be improved and a sulphur-containing feed could be used without affecting the catalyst lifetime. Sulphided NiSMM yielded a dimer and trimer product with a research octane number (RON) of 98. The degree of catalyst sulphiding controlled the yield of gasoline, kerosene and heavier products. O'Connor *et al.* (1988) reported that a 7% NiSMM was twice as active for high pressure propene oligomerization than unsubstituted SMM. The product selectivities of the two clays were similar.

1.3 Thermal Analysis of Catalysts

Thermal methods are widely used alone and in combination with other techniques for study of the strucutre and function of catalysts. The thermal methods used for catalyst characterization include differential scanning calorimetry (DSC), differential thermal analysis (DTA), thermogravimetric analysis (TGA), temperature programmed desorption (TPD), temperature programmed oxidation (TPO), and temperature programmed reduction (TPR). Use of thermal analytical methods can give information on catalyst/support interaction, dispersion of catalyst on a support, the oxidation state of the metal, role of promoters, number and strength of binding sites, catalyst activity, and reaction mechanisms. A comprehensive review of the experimental work undertaken using these thermal methods has been presented by Austermann (1987). This section discusses the analytical techniques relevant to this work.

1.3.1 Thermogravimetric Analysis

TGA adsorption data for ethylene and water were combined with infrared (IR) and nuclear magnetic resonance (NMR) spectroscopic results to obtain information on the role played by the acidic Bronsted sites in H-ZSM-5 in the adsorption and activation of ethylene (Bolis and Vedrine, 1980). Water and ethylene were seen to compete for such sites in various ways which depend on the pretreatment of the zeolite. Physisorbed water prevented the adsorption of ethylene. They showed that ethylene was readily activated and reacted on the Bronsted acidic sites, even at room temperature. Evidence for the formation of carbenium-type intermediates was also shown.

A comparative study of the formation and stability of coke deposits on ZSM-5, offretite and mordenite during the conversion of methanol to hydrocarbons has also been reported (Dejaifre *et al.* 1981). The deposition of carbonaceous residues differed according to the size and shape of the interconnecting channels of the materials. For zeolite ZSM-5, it was observed that the coke were primarily formed on the outer surface of the crystallites, resulting only in slight modification of its molecular shape-selective properties and produced a high resistance to aging. The channels in offretite and mordenite were large enough to accommodate carbonaceous residues, which lead to a drastic loss of catalytic activity and a very fast aging. In a similar study Kubelkova *et*

al. (1985) obtained kinetic measurements of surface species formation in the reaction of ethylene on ZSM-5 and Zeolite Y as a function of acidity and pore size.

Thermogravimetry together with temperature programmed desorption (TG-TPD) was used to study the low-temperature reaction of olefins on ZSM-5 (Kofke and Gorte, 1989). Propene reacted readily inside the zeolite at 22°C to from large oligomer chains, while the zeolite had to be heated to above 97°C for ethylene oligomerization to occur. In both cases reaction did not stop until more than 50% of the zeolite pore volume was filled. This suggested that reaction stoped only when blocking prevented the reactants from reaching the acid sites.

The adsorption of 2-propanol and propene on ZSM-5 has been characterized using TG-TPD by Grady and Gorte (1985). The propene reacted to form hexenes and nonenes, with the number of product moles formed equalling the number of hydrogen cations in the zeolite, indicating that reaction occurs at the site of the cations.

1.3.2 Differential thermal analysis

Precursors of unsupported cobalt-molybdenum hydrodesulfurization catalysts were studied by DTA under reduction/desulfurization conditions with subsequent oxidation of the sulphide samples. It was found that the presence of cobalt markedly affected the reduction/desulfide (Wu *et al.*, 1984).

Results from DTA have been correlated with catalytic activity. The DTA behaviour of sodium molybdate and sodium tungstate adsorbed on zeolite 3A have been correlated with their catalytic behaviour (Agrawal and Banerjee, 1985). DTA has also been used to screen Fischer-Tropsch catalysts to determine their degree of activity, the appropriate reactor operating range, and their product slate (Van Wagner *et al.* 1984). DTA combined with gas chromatography (DTA-GC) has been used for the evaluation of hydrodealkylation catalysts (Zhou and Zhang, 1985) and together with mass spectroscopy (DTA-MS) for the study of reaction intermediates of methanol conversion on ZSM-5 (Rogers and Parker, 1989).

1.3.3 Combined thermogravimetric and differential thermal analysis

Simultaneous TG-DTA has the ability to obtain comparative information on the adsorption and reaction of probe molecules on acid-catalysts. This analytical technique was used by Gabelica *et al.* (1984) to study crystallisation, pore structure and catalytic activity of synthetic zeolites.

Quantitative information was obtained on the dehydration and decomposition of organic guest molecules that interact with intermediate phases that were obtained during hydrothermal transformation of amorphous aluminosilicate gels into crystalline zeolites. In particular, weight losses (TGA) and heat effects (DTA) due to the oxidative decomposition of tetrapropylammonium ions occluded in an intermediate phase were related to the amount of zeolite ZSM-5 present. Isothermal adsorption of small hydrocarbon molecules (n-hexane, 3-methyl-pentane) were used to probe the intracrystalline pore volume of ZSM-5. The total hydrogen uptake (TGA) and the shape of the corresponding DTA peak were sensitive to steric modifications of the ZSM-5 channel system.

The competitive isothermal adsorption of nitrogen, water and ethylene on ZSM-5 was studied by the above authors to obtain information on the behaviour of ethylene in the MTG process. It was seen that ethylene did not replace water which had previously saturated the catalyst's acidic sites, whereas it was strongly adsorbed on a 'clean' zeolite surface. In comparison water was able to displace pre-adsorbed ethylene. After isothermal adsorption of water and/or ethylene, the mass change and temperature effects of surface alkylation, oligomerization and eventual coking were seen during temperature programming of the catalyst sample.

A thermal study of n-butylamine (nBA) and ammonia absorbed on mordenites was also undertaken using TG-DTA by Ghosh and Curthoys (1984). Two DTA peaks were seen for nBA, the first was as a result of desorption of nBA from acid sites and the second was due to decomposition of nBA into alkanes. Only one DTA peak was present when NH_3 was the base and NH_3 was desorbed completely at lower temperature than nBA. The number of acid sites was determined from the TGA curves. The results showed a higher acidity (2 to 3 times) than theoretical values.

1.4 General Routes to Liquid Fuels

In South Africa the production of liquid fuels from coal is currently undertaken by the South African Coal, Oil and Gas Corporation Limited (SASOL) and from natutal gas by Mossgas. The history of SASOL which was formed in 1950, and its process have previously been described by Hoogendoorn (1982). It was reported in 1923 by Franz Fischer and Hans Tropsch that CO and H_2 could be converted to a variety of hydrocarbon products using an iron catalyst (Dry, 1981). The first four Fischer-Tropsch (F-T) plants were in operation in Germany in 1936 producing 200 000te hydrocarbons per year. Production was severly cut back due to plant damage and the prohibition of start up after World War II (Frohning *et al.* 1982). Diminished interest in F-T processes resulted from the discovery of large crude oil and natural gas resources in the Middle East during the 1950's (Jager, 1978).

The absence of oil and the country's specific strategic requirements for a reliable fuel source led to the consideration of a F-T process as early at 1927 in South Africa (Hoogendoorn, 1974). SASOL I, the first South African F-T plant was commissioned in 1955. Though the original plant flowsheet has been changed (Hoogendoorn, 1974) the plant has been instrumental in supporting the development of South African chemical process industries. In 1973 the OPEC oil crisis resulted in the rise of crude oil prices and two larger plants, SASOL 2 and 3, were built to concentrate mainly on gasoline production (Public relations department, SASOL, 1980).

Figure 1.10 shows the general layout of the Secunda plants (Dry, 1981). The primary products produced are ethene, gasoline and diesel (Dry, 1982a). This flow scheme allows for a large degree of flexibility as regards product work-up by changing the mode of plant operation. The overall gasoline to diesel ratio can be varied from about 10:1 to 1:1 according to demand (Dry, 1981).

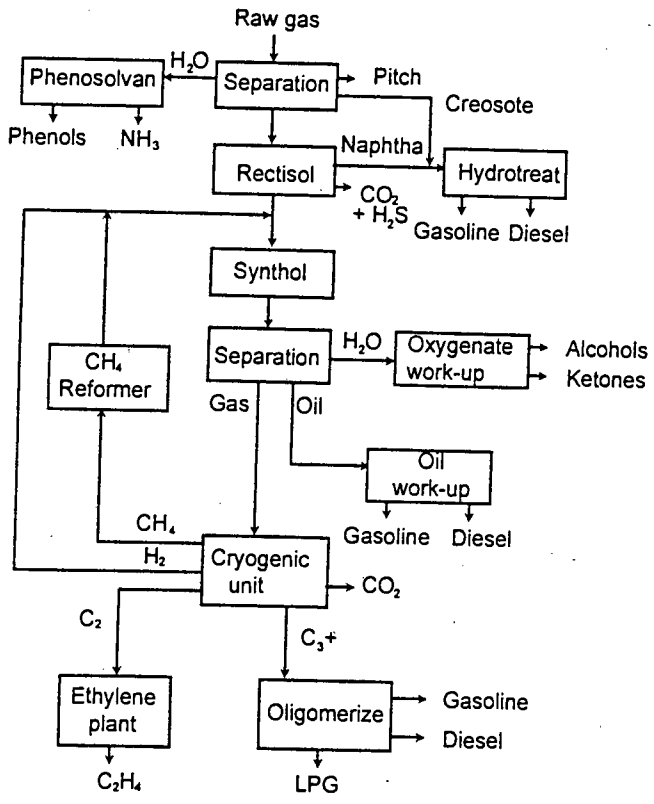

Figure 1.10 Flow Diagram of the Secunda SASOL Plant

Tables 1.3 and 1.4 show that the synthol reactors produce significant quantities of alkenes and that less than 50% of the products fall in the gasoline and diesel range. the remaining products are converted by reforming, cracking and oligomerization of methane, wax and C_3-C_4 alkenes respectively. Approximately one third of the total gasoline and diesel output is produced by alkene oligomerization over solid phosphoric acid in the CATPOLY process.

The gasoline from synthol reactors is upgraded by isomerization of the C_5 and C_6 alkenes and platforming of the C_7-C_{11} fraction. This fuel is subsequently blended with the gasoline derived from C_3 and C_4 oligomerization to yield a final leaded product with RON = 93 (Brink and Swart, 1982). The diesel fuel produced by oligomerization is light, but is hydrogenated, yielding a cetane number of 33-35. Blended with the synthol diesel it is marketed with a cetane number of 46 (Brink and Swart, 1982). Although this diesel fuel conforms to the South African standards it is considered to have poorer density and viscosity than desired.

Table 1.3 Products from SASOL Fixed Bed and Synthol Reactors

Product	Composition/% Carbon atom	
	Fixed Bed at 220°C	Synthol at 325°C
CH_4	2.0	10
C_2H_4	0.1	4
C_2H_6	1.8	4
C_3H_6	2.7	12
C_3H_8	1.7	2
C_4H_8	3.1	9
C_4H_{10}	1.9	2
C_5 to C_{11} (gasoline)	18.0	40
C_{12} to C_{18} (diesel)	14.0	7
C_{19} to C_{23}	7.0	4
C_{19} to C_{23} (medium wax)	20.0	4
$> C_{35}$ (hard wax)	25.0	4
Water soluble non-acid chemicals	3.0	5
Water soluble acids	0.2	1

SASOL has utilised fixed fluidised bed technology to develop their advanced synthol reactor which has higher throughputs and improved conversion for lower capital and operating costs. Conitinuous catalyst addition to their synthol reactors now allows for uninterrupted operation for a year. Considering the need for environmentally clean distillates for "city fuels", a plant is being constructioned to produce the first unleaded petrol in February 1996 (Annual Report, SASOL, 1995).

Table 1.4 Properties of Products from SASOL Reactors

Product Cut	Property	Fixed Bed[a]	Synthol[a]
Gasoline C_5 - C_{11}	Olefins	32%	65%
	Paraffins	60%	14%
	Aromatics	0%	7%
	Alcohols	7%	6%
	Ketones	0.6%	6%
	Acids	0.4%	2%
	n-Paraffins	95%[b]	55%[b]
	RON (Pb free)	35	88
Diesel C_{12} - C_{35}	Olefins	25%	75%
	Paraffins	65%	10%
	Aromatics	0%	10%
	Alcohols	6%	4%
	Ketones	<1%	2%
	Acids	0.05%	1%
	n-Paraffins	93%[b]	60%[b]
	Cetane No.	75	55
Medium Wax C_{24} - C_{35}	Olefins	10%	-

[a] wt% of cut except for RON and Cetane No.

[b] % of the paraffins which are straight chained

Alternative routes to fuels in the distillate range are in great demand. Three of these routes are outlined in the next section.

1.4.1 Low Temperature F-T Processing

Fixed Bed Arge reactors have been shown in Tables 1.3 and 1.4 to yield better diesel fuel than synthol reactors. The final product spectrum of such a plant, including diesel derived from hydrocracking of waxes produced, could yield a volumetric diesel to gasoline ratio of between 3:1 and 6:1 with a cetane number of approximately 65 (Dry, 1982b).

1.4.2 Methanol Conversion

The production of high quality gasoline uses methanol as an important feedstock. ZSM-5, discovered at Mobil (Arguaer and Landolt, 1972), is a highly successful catalyst for the conversion of methanol to olefins, gasoline and diesel.

The reaction path for converting methanol to hydrocarbons is shown in Figure 1.11

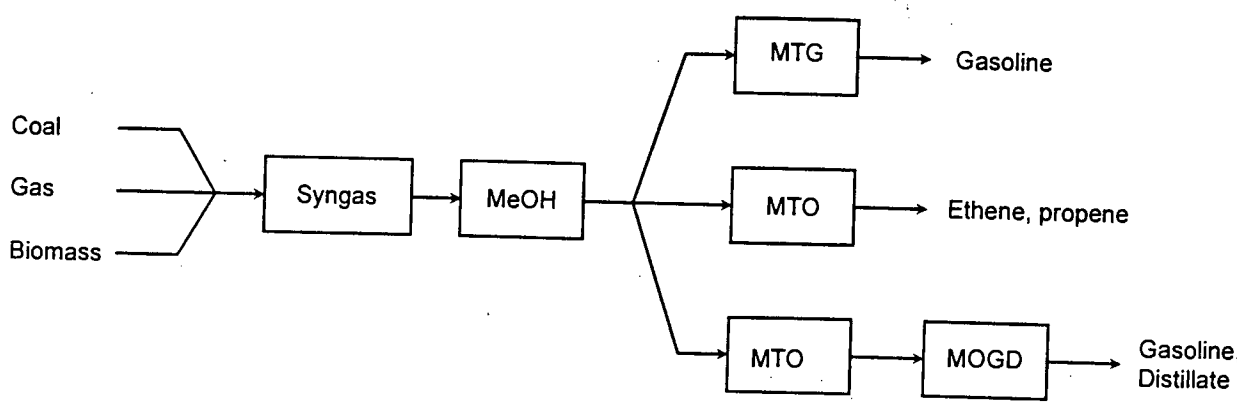

Figure 1.11 Production of fuels and chemicals from methanol

The methanol-to-gasoline (MTG), methanol-to-olefins (MTO) and the Mobil olefin to gasoline and distillate (MOGD) processes are discussed in the following sections.

1.4.2.1 Methanol-to-gasoline (MTG)

This process has been used commercially in New Zealand (Maiden, 1988). Crude methanol containing about 17% water is converted to hydrocarbons and water. The conversion reaction is highly exothermic and a product gas recycle stream is used to limit the temperature rise. The recycle also ensures that the gasoline product is both highly aromatic and highly alkylated, resulting in gasoline of high octane number (Meisel *et al.* 1976). The major products are gasoline (85%) and LPG (13-14%). Unlike the Fischer-Tropsch process it contains only 1-2% undesired methanol (Dry, 1981). An unusual byproduct of the process is durene (1,2,4,5 - tetramethylbenzene). This necessitates that the raw gasoline be distilled and the heavy fraction treated to reduce the durene content to a satisfactory level.

1.4.2.2 Methanol-to-olefins (MTO)

In this process methanol is converted at high temperatures (470-515°C) which results in the heavy hydrocarbons formed at these conditions being cracked to lighter products, mainly propene and butene. The ethane content in the product is low. The process operates at almost complete conversion and hence no recycle stream is necessary. The process produces about 56% light olefins ($C_2^=$ to $C_4^=$) and about 36% gasoline (C_5 to C_{11}). Table 1.5 shows a comparison of MTO and F-T product yields (Dry, 1981).

Table 1.5 Comparison of MTO and F-T Product Yields

	MTO* Product	F-T Product
C_1	1.4	10.0
C_2	0.3	4.0
C_3	2.3	2.0
C_4	3.9	2.0
$C_2^=$	5.0	4.0
$C_3^=$	31.8	12.0
$C_4^=$	19.6	9.0
Gasoline C_5-C_{11}	35.7	40.0
Diesel C_{12}-C_{18}	-	7.0
Heavy Products	-	4.0
Water Soluble Oxygenate	0.3	6.0
	100.0	100.0
Total Light Saturates (C_1 - C_3)	4.0	16.0
Total Light Olefins ($C_2^=$ - $C_4^=$)	56.3	25.0

* 482°C, 102 kPa methanol partial pressure.

1.4.2.3 Mobil Olefin to gasoline and distillate (MOGD)

In the MOGD process light olefins are reacted to produce gasoline and diesel products (Owen *et al.* 1984). ZSM-5 is used as the catalyst with an alumina binder for industrial application. Two modes of operation are used depending on the product requirements. Distillate mode has typical fixed bed reactor operating conditions of 190-310°C and 4-10MPa. In this mode 82wt% of the product may be diesel with a cetane number of >55 after hydrogenation. Gasoline mode operates at higher temperatures and lower pressures (285-375°C, 0.4 - 3MPa) and produces a gasoline with a research octane number of 92. The gasoline and diesel yield from both types of operation are shown in Table 1.6.

Table 1.6 MOGD Process Yields

	Distillate Mode	Gasoline Mode
C_1 - C_3	1	4
C_4	2	5
C_5 - 165°C Gasoline	15	-
165°C$^+$ Diesel	82	-
C_5 - 200°C Gasoline	-	84
200°C$^+$ Diesel	-	7

The paraffinic MOGD diesel fuel has a low density but its low pour point and extremely low sulphur content make it a good blending stock (Tabak and Yurchak, 1990). The MOGD process also produces high quality jet fuels due to the isoparaffinic structure of the products and low aromatics content. A MOGD plant has the flexibility to produce both gasoline and diesel to accommodate fluctuations in the demand for liquid product

1.4.3 Alkene Oligomerization

The supply of diesel produced by the F-T process is supplemented in South Africa by olefin oligomerization. The CATPOLY process is used at SASOL to react propene and butenes with a phosphoric acid/bieselguhr catalyst. This catalyst produces about 75% diesel. The diesel obtained has a low molecular weight with a low viscosity (1.8cs at 40°C, Dry 1990) and is highly branched. The process produces good quality gasoline but the cetane number of the diesel produced is low. High quality diesel fuels have been reported (Tabak *et al.* 1986) to be produced by the MOGD using the Zeolite ZSM-5 as a catalyst and has superior properties to CATPOLY diesel. Alkene oligomerization is discussed more fully in the following section.

1.5 Alkene Oligomerization

Oligomerization is the synthesis of molecules consisting of a small number of monomer units whereas polymerization is the production of high molecular weight products. Alkene oligomerization is an important industrial route for the production of motor fuels, additvies, resins, dyes, detergents, plasticizers and lubricants. In South Africa its use for fuel production is of substantial importance. It is also the source of aromatic-free fuel which makes it environmentally attractive. There are a number of sources of alkenes for such a process, viz. off-gases from the SASOL Fischer-Tropsch process, from crude oil cracking and olefins from the MTO process.

Alkene oligomerization may be carried out via both heterogenous and homogeneous catalysts, such as clay minerals and zeolites, have been used as dimerizing catalysts. Some of the different catalytic routes for alkene oligomerization are discussed below.

1.5.1 Heterogeneous Routes

1.5.1.1 Non Zeolites

Phosphoric Acid

One of the most widespread applications of non-zeolite acid catalysts in alkene oligomerization uses phosphoric acid supported on kieselguhr. This catalyst is used in the CATPOLY process to convert lower alkenes into gasoline (Ipatieff, 1935; McClean, 1988). As the concentration of the acid is varied from 92 to 109% the conversion of propene to oligomers increased from 93 to 97% with the average molecular weight of the product increasing from 139 to 151, the major product shifting from trimer to tetramer (Bethea and Karchmer, 1956). Reaction typically takes place at 200°C and 3MPa. The catalyst is, however, corrosive and produces poor quality distillate fuels.

Cation exchange resins

Using a sulfonated styrene divinylbenzene copolymer, Haag (1967) has shown for 89% isobutene oligomerization, at 160°C, 1 MPa and LHSV = 180, the product distribution was 33% dimer, 57% trimer and 10% tetramer. In the oligomerization of butenes over a range of sulfonated styrene-divinyl-benzene copolymers, at least 50% of the product was dimer with Amberlyst 15 being most effective for gasoline production (O'Connor *et al.* 1985). The RON of the gasoline was 99 and the diesel fraction cetane number was 35. There are limitations in using these catalysts due to their poor thermal stability above 130°C. This may be overcome by attaching trimethoxybenzyl silane to previously activated silica and by subsequent sulfonation (Saus and Schmidl, 1985).

Loss of sulfonic groups and deactivation of others by esterification result in a 50% decrease in activity over 120hr at 130°C.

SMM and NiSMM

As shown previously in Sections 1.2.1.4 and 1.2.2.4 both these acidic clays are good propene oligomerization catalysts. Since almost 65% of the products are in the diesel range both SMM and NiSMM should be better catalysts for diesel production than phosphoric acid or resins.

Silica alumina and nickel silica alumina

As with the SMM catalysts, nickel silica alumina was more active than silica alumina (Harms *et al.* 1989). Nickel silica alumina produced a lighter product, shifting the tetramer+ fraction at 200°C and 4.1MPa from 48 wt% to 25 wt%. Silica alumina is a potential catalyst for diesel production as it did not deactivate after 20hrs on stream with a catalyst utilization value (CUV) of 50g liquid/g catalyst. Nickel silica alumina, however, with a RON of 90.4 is better for gasoline production (Hogan *et al.* 1955).

1.5.1.2 Zeolites

An industrial route for the oligomerizing of light alkenes into liquid fuels is the MOGD process pioneered by Mobil (Garwood *et al.* 1972; Garwood and Lee, 1980; Tabak, 1984). This process uses ZSM-5 discovered by Mobil (Argauer and Landolt, 1972) and produces excellent quality diesel or gasoline fuels from light alkenes. A production plant has been operating successfully at Mossgas (South Africa) for several years using a ZSM-5 type catalyst developed by Süd-Chemie. When operated in the distillate mode (fixed bed, 190-310°C, 4-10MPa, WHSV-0.5-1) as much as 80% mass of the product can be distillate fuels with a cetane number after hydrogenation of over 55. In the gasoline mode (285-375°C and 0.4-3 MPa) distillate production can be kept very low and C_{5+} olefinic gasoline with a RON = 92 is formed in good yield. The commercial plant at Mossgas has shown that the reduction in pressure may not be necessary for operation in the gasoline mode.

ZSM-12 with a silica alumina ratio >80 is active for alkene oligomerization between 40 and 150°C when contacted with a liquid feed (Tabak, 1981). At 40-50°C and 4.1MPa, HZSM-12 is more active for propene oligomerization than HZSM-5. Under these conditions and at WHSV = 0.6 the product of propene reaction over HZSM-12 is mainly trimer and tetramer.

The optimum conditions for converting light olefins to gasoline, distillate and lubricant range hydrocarbons over HZSM-48 have been reported to be 200-260°C, 5-7MPa and WHSV = 0.3-4 (Chu and Valyocsik, 1987). Under these conditions ZSM-48 and ZSM-5 give essentially the same boiling point fractions.

Ocelli *et al.* (1985) compare the activity of HZSM-5, boralite, offretite, HY, H-mordenite and omega for high pressure propene oligomerization. At 4.8 MPa and 1.0 WHSV their HZSM-5 was unusually unreactive and showed little activity below 300°C. Under similar conditions boralite was more active, achieving complete conversion at 300°C. Omega and offretite were active between 200 and 350°C and between 150 and 250°C, respectively. HY was active at 40°C while H-mordenite converted little propene

below 250°C. The degree of branching of the liquid product, as calculated from ^{1}H and ^{13}C NMR spectra, increased in the order boralite < offretite < ZSM-5 ~ H-mordenite < HY < omega (Ocelli *et al.* 1985).

The oligomerization of butenes at 5MPa has been examined by O'Connor et al. (1986a) by varying the NH_4/Na content in NH_4 Na zeolite Y. The activity decrease with increasing Na content but the product spectrum was independent of % exchange. The effect of varying NH_4/Na content on the oligomerization of butenes over NH_4Na-mordenite at 200°C and 5MPa has also been investigated (Kojima *et al.* 1988). It was found that the product distribution was fairly dependent of % exchange.

1.5.2 Homogeneous Routes

One of the most important uses of homogenous nickel catalysts for ethene oligomerization is in the Shell Higher Olefin Process (SHOP) developed by Bauer *et al.* (1972). The SHOP process produces over 1 million tons of linear α–olefins per annum from ethene. At 80-120°C and 7-14MPa a mixture of mainly C_4-C_{20} α–olefins is formed with a Schultz-Flory distribution. The catalyst used is a non-Ziegler nickel-ligand based catalyst. The high cost of producing the α-olefins as a feedstock for detergents make them unacceptable for fuel production.

The IFP Dimersol process for the dimerization of light alkenes is another important industrial application of nickel based homogenous oligomerization (Benedek and Mauleon, 1980). This process produces high octane gasoline blending components but the nickel-aluminiumalkyl complex catalyst has a limited lifetime and requires liquid olefinic feed. Other potential catalysts are Ni^{2+} -dithio-ß-diketone phosphine complexes (Cavell, 1988) and Ni^{+}-cyclooctadiene-ß-diketonate complex (Keim *et al.* 1983) which obtain 20 and 40 wt% trimer+ from propene respectively. These catalysts, however, suffer from chemical and thermal stability and product separation from solvent and catalyst.

1.5.3 Mechanism

1.5.3.1 General Reactions

Evans and Polyani (1947) have shown from calculations of proton affinities of C-atoms in the double bond that the proton will add to the end carbon atom thus obeying Markownikoff's rule in the formation of the carbonium ion.

The above carbonium ion may then attack the double bond of another propene molecule, forming a C_6 carbonium ion. This can then either react further to form higher oligomers or form an isomer of hexene by proton loss. McMahon *et al.* (1963) have summarized the many other reactions that a carbonium ion may undergo during polymerization.

- Lose a proton to the catalyst so regenerating the acid.
- Transfer a proton to another alkene generating a new carbonium ion.
- Add a hydride ion by transfer from a hydrocarbon.
- Crack a hydrocarbon.
- Isomerize a hydrocarbon.
- Lose a hydride ion, which may result in cyclization.
- After cyclization the hydrogen thus generated may be used in saturating other alkenes.

Thus the products of polymerization reactions will be complex mixtures which can include alkanes, alkenes, aromatics and other cyclic compounds. The following terms have been proposed by Schmerling and Ipatieff (1950) to differentiate between the various reactions taking place.

True polymerization - yields products which consist of alkenes with

molecular weights which are integral multiples of the monomer alkene.

Conjunct polymerization - produces alkanes, alkenes, dienes, cyclic alkanes and alkenes and aromatics with a random carbon number distribution.

Copolymerization - inter or cross polymerization of two or more different alkenes.

In nature oligomerization is thus a combination of all the above reactions. Alkene oligomerization has been summarized by Tabak (1985) as follows:

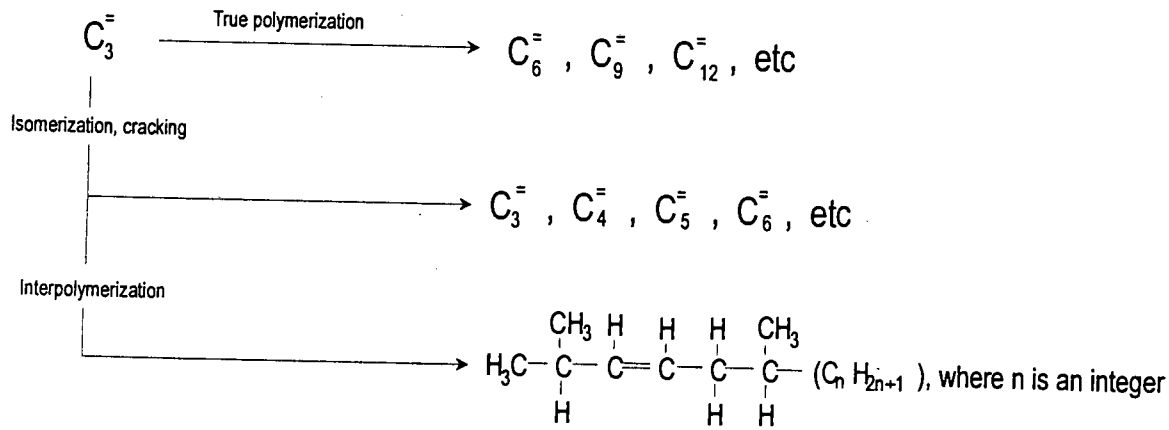

1.5.3.2 Propene Oligomerization

Trimers are more readily formed than dimers under propene oligomerization conditions. The products of propene oligomerization over phosphoric acid consist of 50% nonenes, 25% dodecanes with less than 5% hexenes (Schmerling and Ipatieff, 1950). The relative stability of the propene dimer and monomer carbonium ions explains the low yield of hexene. The dimer generates a more stable tertiary carbonium ion, existing longer before expelling a proton, than the secondary carbonium ion of the monomer.

The dimer thus has a greater chance for further monomer addition than there is for monomer dimerization.

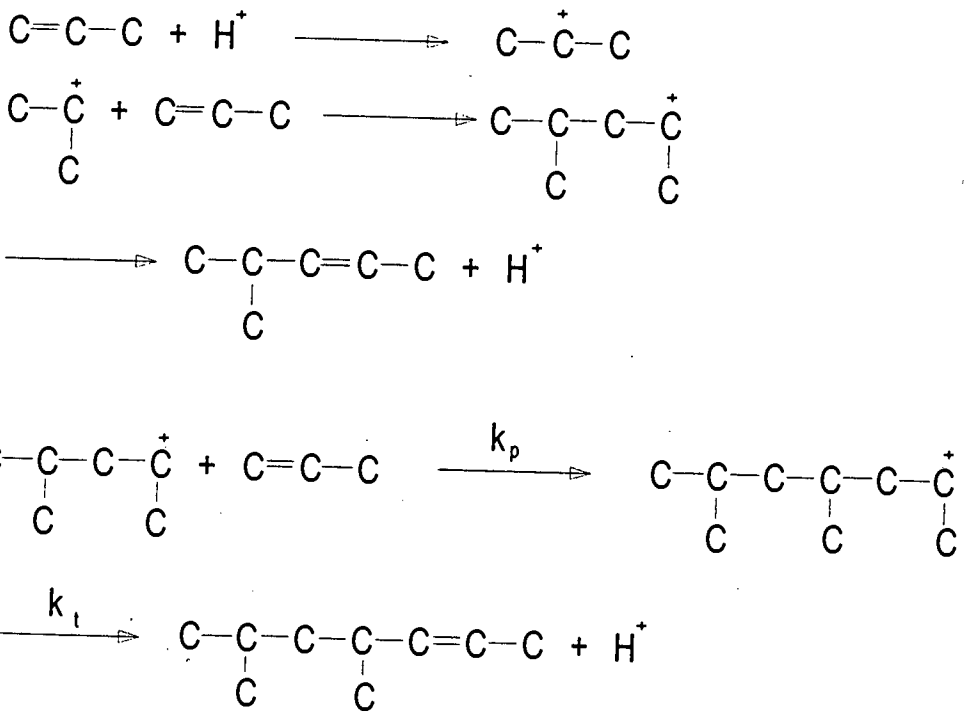

Thus $k_p/k_t >> 1$ where

k_p = rate of further alkene addition (polymerization)

k_t = rate of proton expulsion to form an alkene (termination)

The above carbonium ion mechanism is the most widely accepted for alkene polymerization in heterogeneous catalysis (Schmerling and Ipatieff, 1950; Flory, 1969).

The dimer, trimer, and tetramers of propene should have the following structures according to Germain (1969):

Dimer

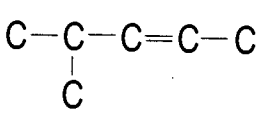

Trimer

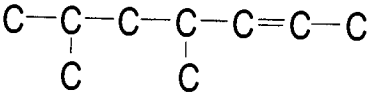

Tetramer

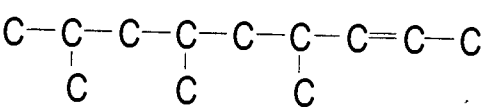

Skeletal isomers will be present and for the propene dimer (ignoring double bond position) the following possibilities exist:

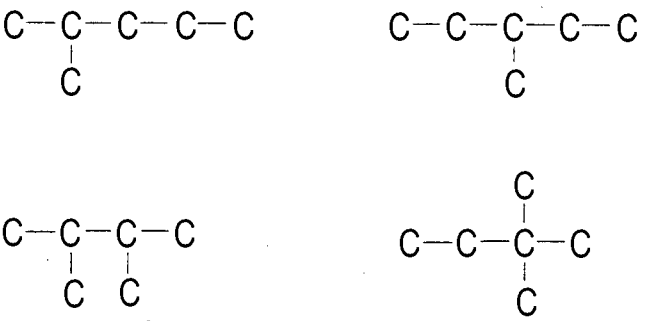

1.5.4 Thermodynamics

Reviews of the thermodynamics of oligomerization have focused mainly on dimerization of propene and butene (Oblad *et al.* 1958). Alberty (1987) has published data on individual species up to C_6H_{12} and has extended this to C_8H_{16} using the Benson group method (Alberty and Gehrig, 1985). More recently Sealy *et al.* (1994) studied the dimer of hexene isomers of propene oligomerization at 5MPa and 250°C over ZSM-5. They found that at low conversions (5%) the system achieves equilibrium with respect to double bond isomerization but not with respect to the skeletal structures.

Thermodynamically, low temperatures and high pressures favour polymerization (Aberty, 1987). This has been found to be true experimentally for alkene oligomerization over ZSM-5 by Quann *et al.* (1988) and Garwood (1983). Garwood (1983) has also shown that, over ZSM-5 at 0.1 bar and 277°C, ethene, propene, a pentene mixture, 1-hexene and 1-decene all form similar product mixtures which approach equilibrium values. Cracking, which reduces the product carbon numbers, is favoured at higher temperatures as expected from mechanistic considerations.

Alberty (1987) has therefore treated oligomerization over ZSM-5 as an equilibrium of exothermic reactions, yielding progressively fewer product molecules. The equilibrium calculations are hindered by the increasingly large number of isomers with higher carbon numbers. Researchers have been forced to make use of isomer groupings (Tabak, 1986) since Read (1976) has shown that for alkenes with carbon numbers 5,10 and 15, there are 6, 895 and 185310 isomers respectively.

1.6 Objectives of Research

The object of the research was to synthesize nickel, cobalt and zinc substituted SMM in order to determine the effect of the metal type and loading on the clay structure, acidity and olefin oligomerization activity. The full range of metal substitution from 1wt% to a fully trioctahedral SMM was prepared for the study.

Having become skilled in the synthesis procedure for 2:1 layered aluminosilicates and confirmed the clays to be such by X-ray diffraction and elemental analysis, the following questions on the effect of the metals on the SMM structure were addressed:

i) How easily are these metals incorporated into the SMM structure and what properties of the metals affect this inclusion?
ii) How is the 2:1 layer spacing affected?
iii) What impact does metal substitution have on the crystal structure of SMM with particular respect to the octahedral and tetrahedral layers?
iv) How and why is the surface area altered by metal substitution?

The acidity of the catalysts was studied with the following objectives:

i) How does the number and strength of the acid sites vary with metal type and content?
ii) Where are the different acid sites most likely to be located in the SMM structure?

Thermogravimetric analysis was used to determine the ability of this technique to differentiate between acid catalysts on low pressure olefin oligomerization and adsorption and to ascertain how much information could be obtained on the nature of the reaction and on the interaction between reactant molecules and acid sites.

Olefin, in particular propene, oligomerization was the hydrocarbon conversion reaction used to answer the following questions on the catalytic properties of the clays:

i) How well do the synthesised catalysts compare with commercially available material?

ii) Do changes in the conversion level have the classical effect on product selectivity of a series/parallel reaction of a shift to heavier products with increasing conversion levels?

iii) How does conversion and selectivity change with nickel content and what explanation are possible for the observed behaviour?

iv) In what way do cobalt and zinc in SMM behave differently from nickel?

v) What kinetic information can be obtained on the olefin oligomerization reaction?

Chapter 2

Experimental

EXPERIMENTAL

2.1 Catalysts

The catalysts used were SMM and metal substituted SMM. The metals incorporated into the SMM structure were nickel, cobalt and zinc. The details of the synthesis procedure for these clays is given in the next section. SMM and 7% NiSMM samples were supplied by the Harshaw-Filtrol Corporation, USA. These were provided comparative results for the clays synthesised for this work. ZSM-5, synthesized previously, (Swartz, 1990), was also used in the thermal analysis study.

2.1.1 Synthesis of Metal Substituted SMM Catalysts

The synthesis procedure used for the synthesis of metal substituted SMM was based on Example 4 (excluding palladium addition) of the patent by Black *et al.* (1976).

2.1.1.1 Preparation of Synthesis Mixture

The synthesis mixture was prepared in a 500ml polypropylene beaker (ammonium hydrogen difluoride etches glass). The mixture was continuously stirred on a magnetic stirrer using a teflon coated stirrer bar. 10.0g of SiO_2 (Aerosil 200, Degussa) was added to 200ml distilled water at room temperature. To this mixture 9.6g Al $(OH)_3$ (British Drug House) and 0.5g NH_4F. HF (Aldrich Chemical Co.) were added. The required amount of metal acetate for the desired loading (indicated in Table 2.1), previously dissolved in a minimum of distilled water at 80°C, was added to the silica-alumina slurry. The pH of the resulting solution was raised by the addition of 3.5ml 25% NH_4OH. If gel formation occurred, sufficient distilled water was added to break the gel so that efficient stirring could continue. Finally, solution pH was set to the desired value (usually at 8.5, see Table 2.1) by the addition of either 99.7% glacial acetic acid or the 25% NH_4OH solution, as appropriate.

The masses of nickel acetate used for the specific loadings were calculated as shown in Appendix 1. The masses of cobalt and zinc acetate added were calculated to give equivalent molar loadings to 1.0, 6.8 and 35.7 wt% nickel respectively (calculation shown in Appendix 2).

Table 2.1 Metal Acetate Additions for Required Metal Loading

Catalyst	Metal Type	Metal Loading (wt%)	Metal Acetate Mass (g)	Synthesis pH
NiSMM-1	Ni	1.0	0.75	8.5
NiSMM-7-pH7		6.8	5.4	7.0
NiSMM-7		6.8	5.4	8.5
NiSMM-7-pH10		6.8	5.4	10.0
NiSMM-10		12.0	10.1	8.5
NiSMM-16		21.6	20.4	8.5
NiSMM-34		35.7	41.2	8.5
CoSMM-1	Co	1.0	0.75	8.5
CoSMM-7		6.8	5.4	8.5
CoSMM-33		35.8	41.2	8.5
ZnSMM-1	Zn	1.1	0.66	8.5
ZnSMM-7		7.5	4.8	8.5
ZnSMM-31		38.2	36.2	8.5
SMM	-	0	0	8.5

2.1.1.2 Hydrothermal Synthesis

The autoclave used for hydrothermal synthesis is shown in Figure 2.1. The autoclave was manufactured from stainless steel and the seal was constructed from a graphite sheet. Prior to each synthesis, the autoclave was thoroughly cleaned with distilled water to remove all traces of the previous synthesis and dirt. The interior dimensions of the autoclave are 9cm (depth) x 6cm (diameter). An Autoclave Engineering Magnedrive mechanism is used to agitate the reactant mixture employing an impeller, which is a rectangular blade of dimensions 4cm x 0.7cm. The autoclave is equipped with a

temperature controller which maintained the synthesis mixture at the selected temperature under autogeneous pressure.

In all cases 200ml of the synthesis mixture was charged to the autoclave. The autoclave was sealed and the stirring mechanism started. The temperature controller was set to 340°C in order to maintain the synthesis mixture temperature at 300°C, as read by the temperature readout. The autoclave heated quickly (1½ hr) and reached a pressure of 85atm at 300°C. The synthesis mixture was held at these conditions for 3hr after which the temperature controller was switched off and the autoclave was allowed to cool overnight under continued stirring.

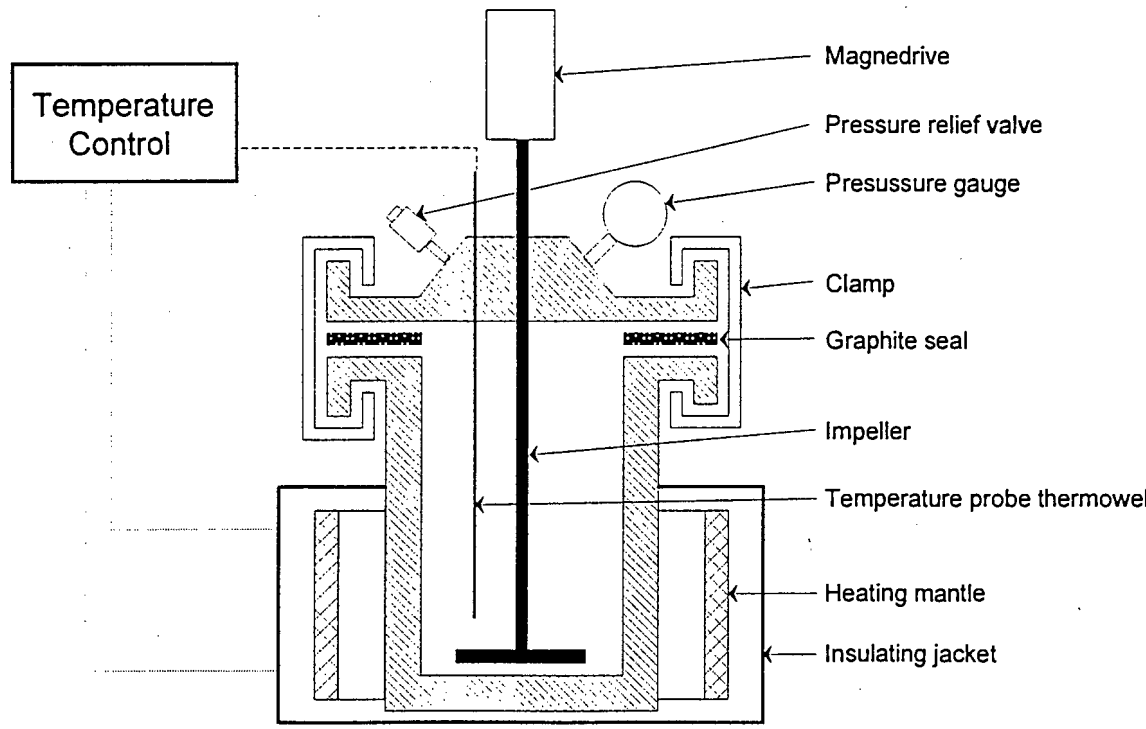

Figure 2.1 Hydrothermal synthesis autoclave

2.1.1.3 Post-Synthesis Treatment

After hydrothermal synthesis the contents of the autoclave were pressure filtered and the catalyst was washed twice by redispersion in distilled water. The final filter cake was oven dried overnight at 80°C, cooled, crushed and sieved to the required particle size. Due to the formulation of the synthesis mixture, all the catalysts were synthesized in the ammonium form and thus required no NH_4^+ ion-exchange procedure.

2.1.2 Commercial SMM and NiSMM Catalysts

The commercial SMM (SMM-F) and 7% NiSMM (NiSMM-7-F) catalysts used in this work were supplied by the Harshaw-Filtrol Corporation, USA. Their SMM was prepared using Example 7 of US Patent 3 252 757 (Granquist, 1966) with meta-kaolin being used to supply about 90% of the total alumina requirement for the synthesis. US Patent 3 852 405, Example B, was used for their NiSMM synthesis.

2.1.3 Metal Ion-Exchanged And Impregnated Catalysts

Metal ion-exchanged SMM materials were obtained by ion-exchanging the ammonium form of SMM (supplied by the Harshaw-Filtrol Corporation, USA) in aqueous nickel, cobalt or zinc nitrate solutions in well mixed glass vessels (Gallezot and Imelik, 1973; Elliot and Lunsford, 1979). In this procedure, 6g of Filtrol SMM were added to 800ml of a 0.00025N metal ion solution and stirred for 8hr at room temperature. The samples were filtered, washed and oven-dried at 80°C. According to this preparation method the catalysts contained 0.06wt% metal and are coded NiSMM-0.06-F-IX, CoSMM-0.06-F-IX and ZnSMM-0.06-F-IX, respectively. 100% Exchange would be approximately 6wt% Ni^{2+}. The target exchange was therefore only about 1%. To produce 1wt% Ni ion-exchanged and 1wt% Ni impregnated SMM samples two 0.005N nickel ion solutions were stirred for 8hr in 800ml distilled water with 6g of SMM which was produced in this work. The ion-exchanged samples were filtered, washed and oven-dried at 80°C, while the impregnated sample was only oven dried at 80°C. They were coded NiSMM-1-F-IX and NiSMM-1-F-IMP, respectively

2.1.4 ZSM-5 Catalyst

The ZSM-5 used in this work was synthesized with a Si/Al ratio of 65 according to the method of Argauer and Landolt (1972) and has been characterised by Schwarz *et al.* (1989).

2.1.5 Catalyst Nomenclature

The catalysts have been coded to indicate their origin, synthesis procedure and metal type and content. They have the general nomenclature:

ASMM-B-C-D

A - Metal type (Ni, Co or Zn)
B - Metal content (wt%)
C - Origin (F for Harshaw - Filtrol)
D - Synthesis procedure (IX - ion-exchanged,
IMP - impregnated,
pH7 or pH10 - synthesis pH)

The absence of any of the letters indicates the following:

A - no metal present (unsubstituted SMM)
B - no metal present
C - synthesized in this work
D - no ion-exchange or impregnation done, synthesized at a pH of 8.5

The ZSM-5 used was coded as ZSM-5.

2.2 Catalyst Characterisation

The following aspects of the catalysts were characterised according to the techniques indicated.

- Structural features	:	X-ray diffraction (XRD)
		Temperature programmed reduction (TPR)
- Composition	:	Atomic absorption (AA)
		X-ray fluorescence (XRF)
		Ion-sensitive electrode
- Surface area	:	N_2 BET
- Acidity	:	Temperature programmed ammonia desorption (NH_3- TPD)
		Infrared pyridine adsorption (IR)

2.2.1 X-Ray Diffraction

Diffractograms of the catalyst samples were recorded using a Philips diffractometer with Cu-K_α radiation. The instrumental settings used are given in Table 2.2:

Table 2.2 - XRD Parameters

Voltage	40kV	Divergent slit	½°
Current	30mA	Receiving slit	½°
Range	2 x 10^3 counts/s	Anti-scatter slit	1°
Time Constraint	1		
Scanning Speed	2° 2θ/min		

When examining the basal spacings (001 diffraction peaks) of clay minerals, Brown (1961) suggests that samples be prepared for analysis by drying a small amount of an aqueous solution of <2μm clay particles on a glass slide. This ensures a well ordered orientation of particles on the surface of the slide and increases the intensity of the reflections representative of first order basal spacings. As it proved difficult to obtain a <2μm size fraction from the clays, the so-called "back loading" technique was used for

sample preparation. In this method, the <75μm fraction of the clay powder was packed into a 1mm deep perspex holder and the sample surface was orientated by applying pressure with a glass slide. Samples were scanned in the range $2\theta = 3° - 66°$.

To examine the 06 reflections of the synthesized clays in detail, the signal intensity for this reflection was enhanced by widening both the divergent and receiving slits to 1°. The anti-scatter slit was removed and the recording range halved to 10^3 counts/s.

2.2.2 Temperature Programmed Reduction

2.2.2.1 Experimental Apparatus

The equipment used for the temperature programmed reduction experiments is depicted in Figure 2.2.

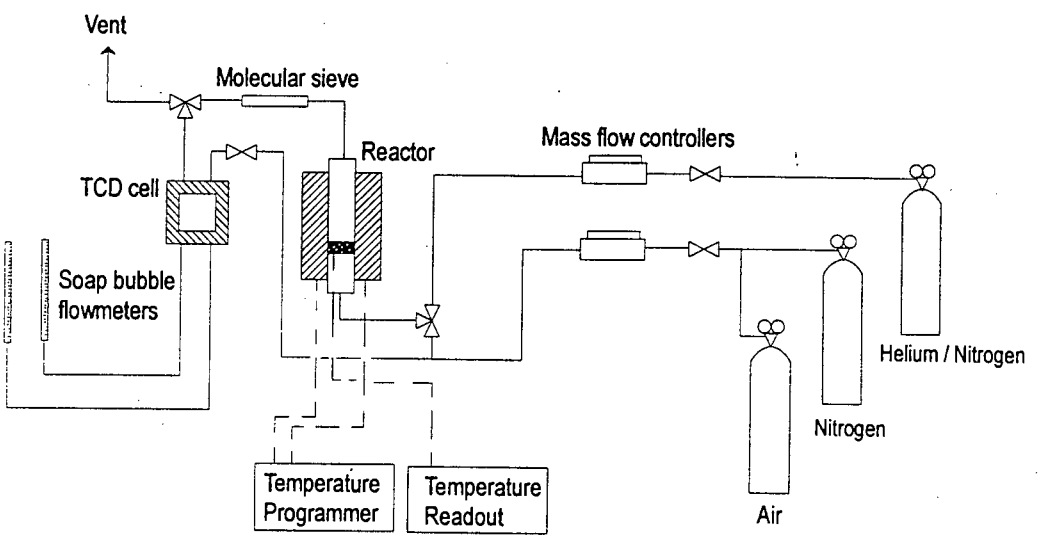

Figure 2.2 Temperature programmed reduction apparatus

2.2.2.2 Experimental Technique

An amount of approximately 0.1g of catalyst (38 - 75μm) was packed into the reactor. This was calcined in situ by increasing the temperature to 500°C at 10°C/min in flowing air (60ml/min). These conditions were maintained for 4hr. The reactor was thereafter cooled at 5°C/min to 100°C. The thermal conductivity detector (TCD) was allowed to stabilise for 6hr at 100°C. A baseline was then set for pure N_2 (60ml/min) flow over a period of 30min. The flow was then changed to 5.94% H_2 in N_2 (60ml/min) and the baseline allowed to settle (30min). The temperature was increased from 100 to 650°C at 10°C/min and held at 650°C for 45min.

2.2.3 Atomic Absorption Spectroscopy

The nickel, cobalt and zinc analyses of the catalysts were obtained by atomic absorption spectroscopy. The samples were dissolved in a mixture of HNO_3, HF and $HClO_4$ in a teflon beaker. They were fumed to near dryness and then redissolved in HNO_3 . After diluting to a fixed volume, an aliquot was taken and KNO_3 added as a deionizing agent. Measurements were taken on a Varian Model 1275 atomic absorption spectroscometer using a nitrous flame against calibration standards prepared in the same way as the catalyst samples.

2.2.4 X-Ray Fluorescence

Silica and alumina analyses were obtained using a Siemens MRS 400 X-ray fluorescence meter. The samples were fused with lithium tetraborate using lanthanum as a heavy absorber. Calibration was performed using synthetically prepared standards. Calculation of matrix correction was performed by using multiple regression analysis.

2.2.5 Ion-Sensitive Electrode

An Orion ion-sensitive electrode was used for fluoride analyses of the clays. Samples were fused in a mixture of Na_2O and Na_2CO_3 in a graphite crucible, leached in a solution of $AlCl_3$ and HCl and then diluted to volume. An aliquot was buffered to pH9

with EDTA: sulphosalicylic acid and diluted to standard volume for measurement. This was compared against standard fluoride solutions.

2.2.6 N_2 BET

The surface areas of the clay samples were estimated from the results of adsorption experiments using nitrogen as the adsorbate. Experiments were carried out using a Carbo-Erba Sorptometer. Prior to adsorption, samples were outgassed on the sorptometer at 110°C for 1hr. The volume of nitrogen adsorbed was measured at between seven and nine different relative pressures in the range 0.01-0.35. All samples used for adsoprtion had previously been calcined at 500°C for 4 hr. The samples were exposed to atmospheric conditions between calcination and outgassing.

2.2.7 Temperature Programmed Ammonia Desorption

2.2.7.1 Experimental Apparatus

The apparatus used for the temperature programmed ammonia desorption experiments is depicted in Figure 2.3

The catalyst was supported on a frit in a quartz sample cell. The quartz cell was connected to two glass blown gas inlet and outlet fittings. This was placed in a cylindrical brass heating block with four heating elements connected to a temperature programmer. Iron filings were packed around the sample cell to provide a uniform heat transfer medium.

A temperature controlling thermocouple was placed in the brass heating block and a sample temperature monitoring thermocouple inserted in the quartz cell through a thermowell. The gases flowed through the sample cell into a thermal conductivity detector (TCD). The TCD was temperature controlled at 40°C by a water bath. The helium carrying desorped NH_3 was back titrated as a check for the total amount of NH_3 desorbed during the experiment.

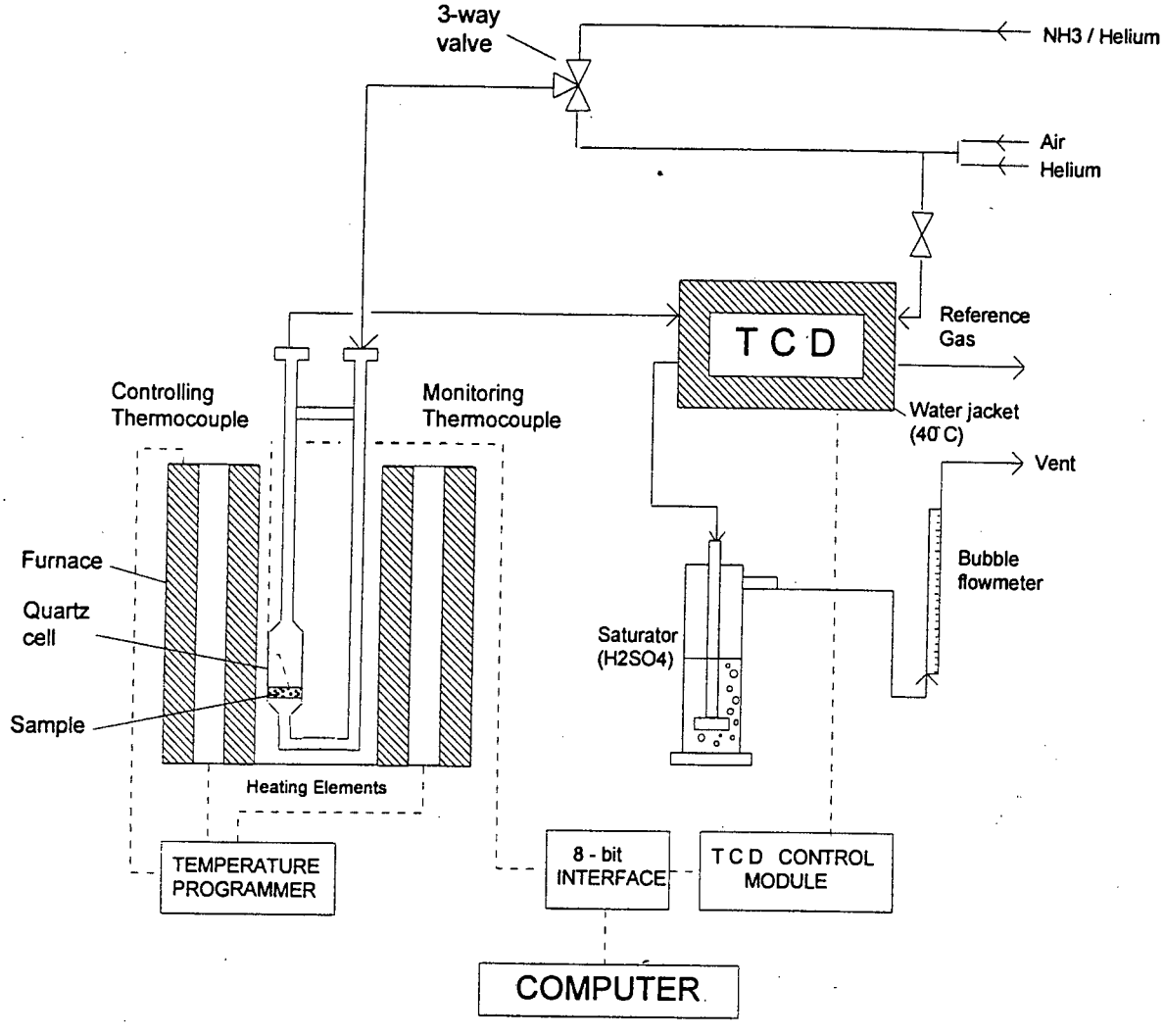

Figure 2.3 Temperature programmed ammonia desorption apparatus

The flowrates were monitored by a soap bubble flowmeter. The TCD was controlled by a TCD control module and the data collected by a computer through an 8-bit interface.

2.2.7.2 Experimental Technique

A catalyst sample (75 - 106μm) of 0.5g was calcined *in situ* in the quartz sample cell for 4hr at 500°C in air (40ml/min). NH_3 (40ml/min, 4% in He) was adsorbed for 45min at 100°C and then flushed with flowing He (40ml/min) for a further 45min while still at 100°C. The temperature programmed desorption experiments were then conducted at a heating rate of 10°C/min between 100°C and 500°C.

2.2.8 Infrared Study of Pyridine Adsorption

2.2.8.1 The Infrared Cell

The infrared system used for the pyridine adsorption study has been described by O'Connor *et al.* (1986b) and Fletcher (1984), except that in this study a Nicolet model 5 ZDX Fourier transform infrared spectrophotometer was used as opposed to a dispersion instrument used in their work. A diagram of the infrared cell and sample holder is shown in Figure 2.4.

The cell (Figure 2.4a) was constructed from Pyrex except for the heating section which was made of quartz. CaF_2 windows were attached to the ends of the housing section (A) using Silastic silicon rubber. This could be dissolved in ether if necessary, enabling the windows to be removed. A tube was blown to the wider section of the cell (B). This was connected via a Rotaflow stopcock and ball joint to the vacuum line. The middle section of the cell (C) was glass blown to a tube of Pyrex (D) followed by a section of quartz (E).

The end of section E was connected via a 24/29 ground-glass conical joint to a Pyrex tube (F). An iron-constantan thermocouple in a metal sheath was inserted via a 3/13 conical joint at G and held fast by means of Apiezon W40 wax. The end of section F incorporated a ground-glass joint which was stoppered normally but which could be used as an access point for flow experiments.

The transparent wafer had a diameter of 13mm and was housed in the stainless steel holder shown in Figure 2.4(b). This holder consists of two machined sections which interlock as shown. The holder was inserted via two prongs into the base of a stainless steel rod. The rod was rectangular in cross section with a broadened receptacle for the prongs. The wafer was removed from the beam and located in the quartz section by withdrawing the rod using an electromagnet which surrounded this end section.

The rod described above moved freely in the glass tube except for a pinch point at H and a locating rod at I. These ensured that the wafer did not change its orientation with

respect to the beam when it was withdrawn or inserted from section C. No grease was used and all joints are secured using Apiezon W40 wax.

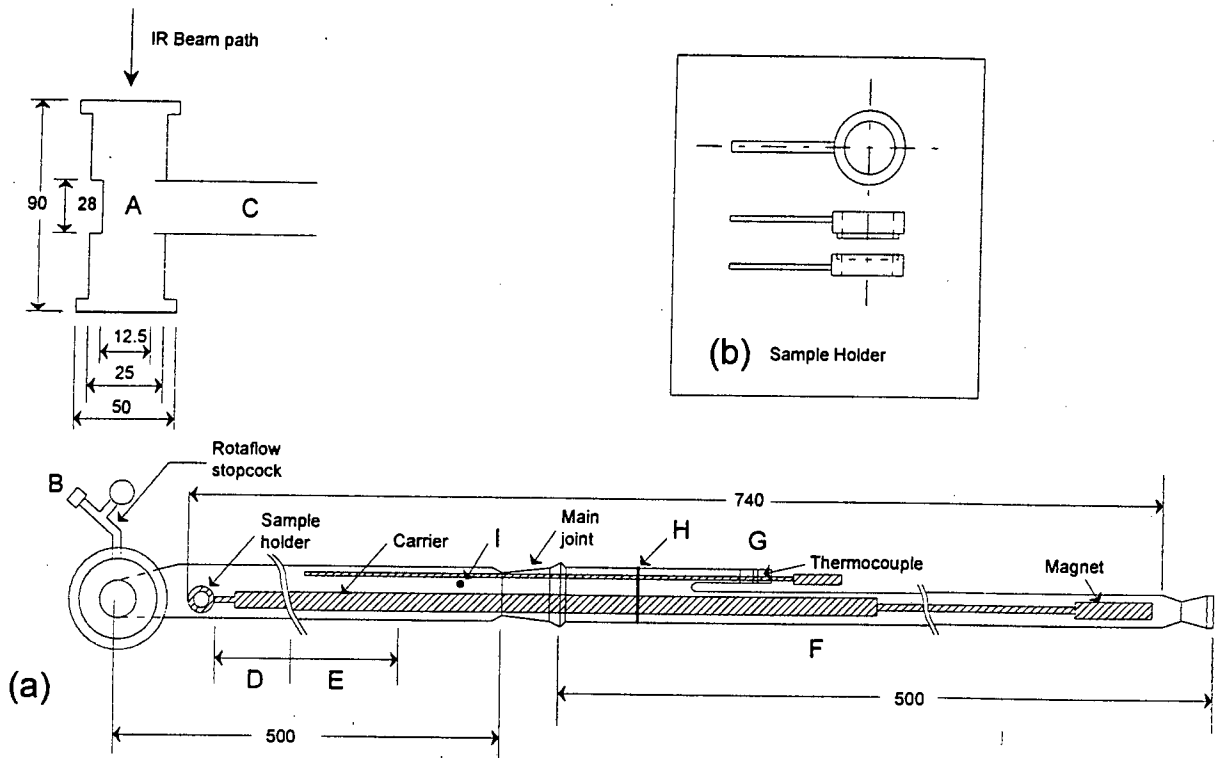

Figure 2.4(a) Infrared cell (b) Sample holder

2.2.8.2 The Complete Infrared Apparatus

The infrared system is shown schematically in Figure 2.5. Evacuation was carried out using an Edward ED-100 high speed rotary pump and a mercury diffusion pump. Both the suction and discharge lines to the mercury pump were fitted with nitrogen traps.

Pyridine was prepared and stored in a standard glass vacuum line (Figure 2.6) fitted with Rotaflow greaseless stopcocks. A Pirani gauge (LKB 3294 Autovac) was used to monitor evacuation. Twin bubbles were available for the adsorbate, one for storage of the 'crude' chemical and the second for the highly purified pyridine used.

The infrared sample cell was connected to the line via a glass tube with ground glass joints. All the joints were sealed with Apiezon W40 wax.

The temperature of the furnace was controlled by a temperature controller via a thermocouple situated in the furnace wall. The thermocouple measuring the sample temperature (Figure 2.4) was connected to a temperature readout.

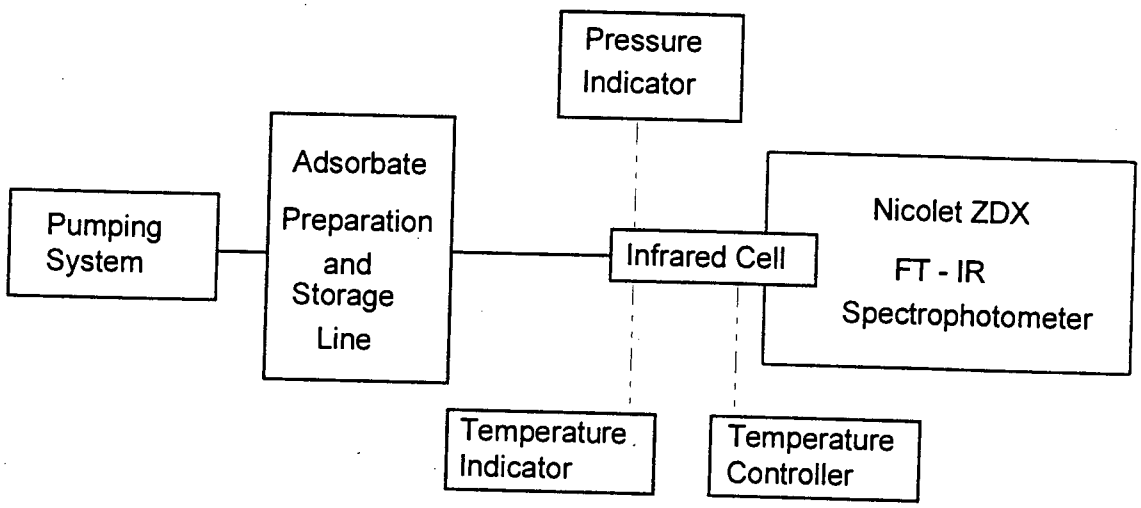

Figure 2.5 Infrared System

All spectra were recorded at room temperature using calcium fluoride windows by taking an average of 10 scans at a resolution of $4cm^{-1}$. The signal to noise ratio was less than 2% and the scanning range was $4000\text{-}400cm^{-1}$.

2.2.8.3 Pyridine Preparation

The vacuum-line used for adsorbate preparation and storage is shown in Figure 2.6. Bulb B1 was loaded with Merck 3A molecular sieves and evacuated at 350°C for 3hr and isolated from the line with stopcock S1. Merck spectroscopic grade pyridine was introduced to bulb B2 via stopcock S2 (with the teflon stopcock insert removed).

Approximately 1/3 of the pyridine was evacuated into the liquid nitrogen trap after which the line was isolated from the trap by closing S3. With bulb B1 and B2 open to the line a liquid nitrogen reservoir placed around B1 served to transfer ½ the remaining pyridine in B2 into B1. Thus, about 1/3 was of the pyridene originally charged to B2

was stored in a thoroughly outgassed condition in B1, isolated by S1. Valve S4 kept the IR cell isolated throughout the pyridine purification procedure.

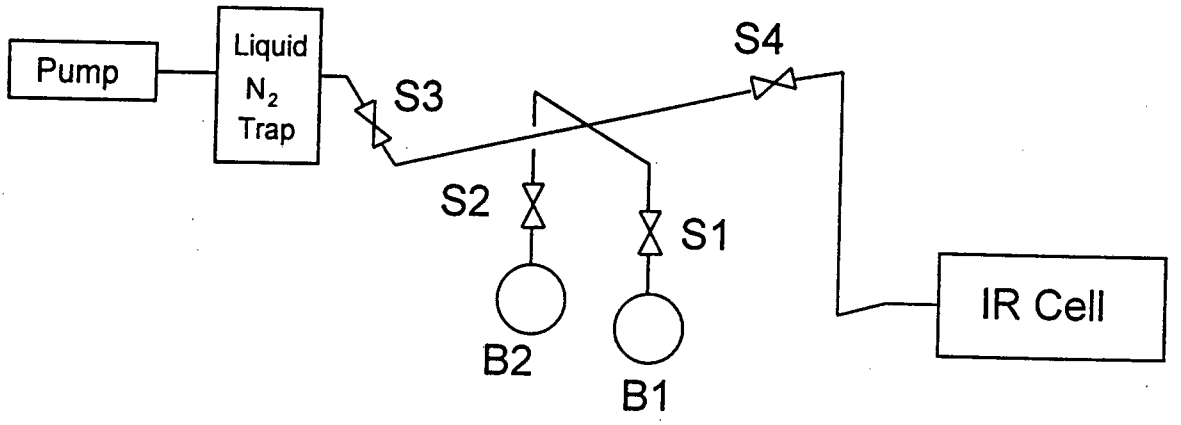

Figure 2.6 Vacuum line for pyridine preparation and storage

2.2.8.4 Experimental Procedure and Conditions

Wafers for the infrared study could not be obtained from the metal substituted SMMs by filtering a slurry onto a Millipore filter (Wright *et al.*, 1972) as had been used by Kojima *et al.* (1986) for pure SMM.

The samples were thus precalcined at 500°C for 4hr in air and self-supporting wafers were formed by pressing the catalyst under 10 tons pressure to yield a wafer with a 13mm diameter. The sample wafer was placed in the sample holder of the infrared cell. The system was then sealed and evacuated. The wafer was then recalcined at 500°C for 4hr under vacuum and allowed to cool to room temperature, followed by pyridine adsoprtion at 4torr for ½hr. After pyridine adsorption the sample was degassed at 2 x 10^{-6} torr for 16hr. These conditions for adsorption and degassing were found by Fletcher (1984) to result in samples free from physisorbed and hydrogen bonded pyridine species and were also found to be suitable for metal substituted SMM forms.

For the experiments in which the concentrations of chemisorbed pyridine species on the catalyst were determined at temperatures greater than room temperature, spectra were recorded after successively heating the sample, in 50°C intervals, from 100°C to 300°C.

The sample was left to equilibrate at the new temperature for 3hr. In all cases, spectra were recorded only after the wafer had cooled to room temperature.

2.3 Iso-Butene Adsorption and Reactivity Studies

The iso-butene adsorption and reactivity studies were undertaken using a thermogravimetric balance on a range of selected catalysts. This enabled the atmospheric adsorption and reaction of iso-butene to be studied by interpreting the combined mass and temperature effects.

2.3.1 Thermogravimetric Apparatus

A Stanton-Redcroft STA 750 thermogravimetric balance was used. This was coupled to a computer controlled flow system with digital data capture by the same computer used for the flow control. A schematic of the system is given in Figure 2.7

2.3.1.1 Gas Flow

The feed gases were air, nitrogen and iso-butene. They were stored in standard gas cylinders and introduced to the flow system by solenoid valves. Prior to each experiment the gas type and flow sequencing thereof were entered into the controlling computer together with the catalyst mass.

The gas flow rate was calculated by the controlling computer using the pressures from the transducers on the capillary columns. There were compared to the setpoints and the flow regulated accordingly through a feedback control loop to the automatically operated needle valves. The rotameters gave a visual check of the flowrates. The gases were dried by flowing over type 3A molecular sieves.

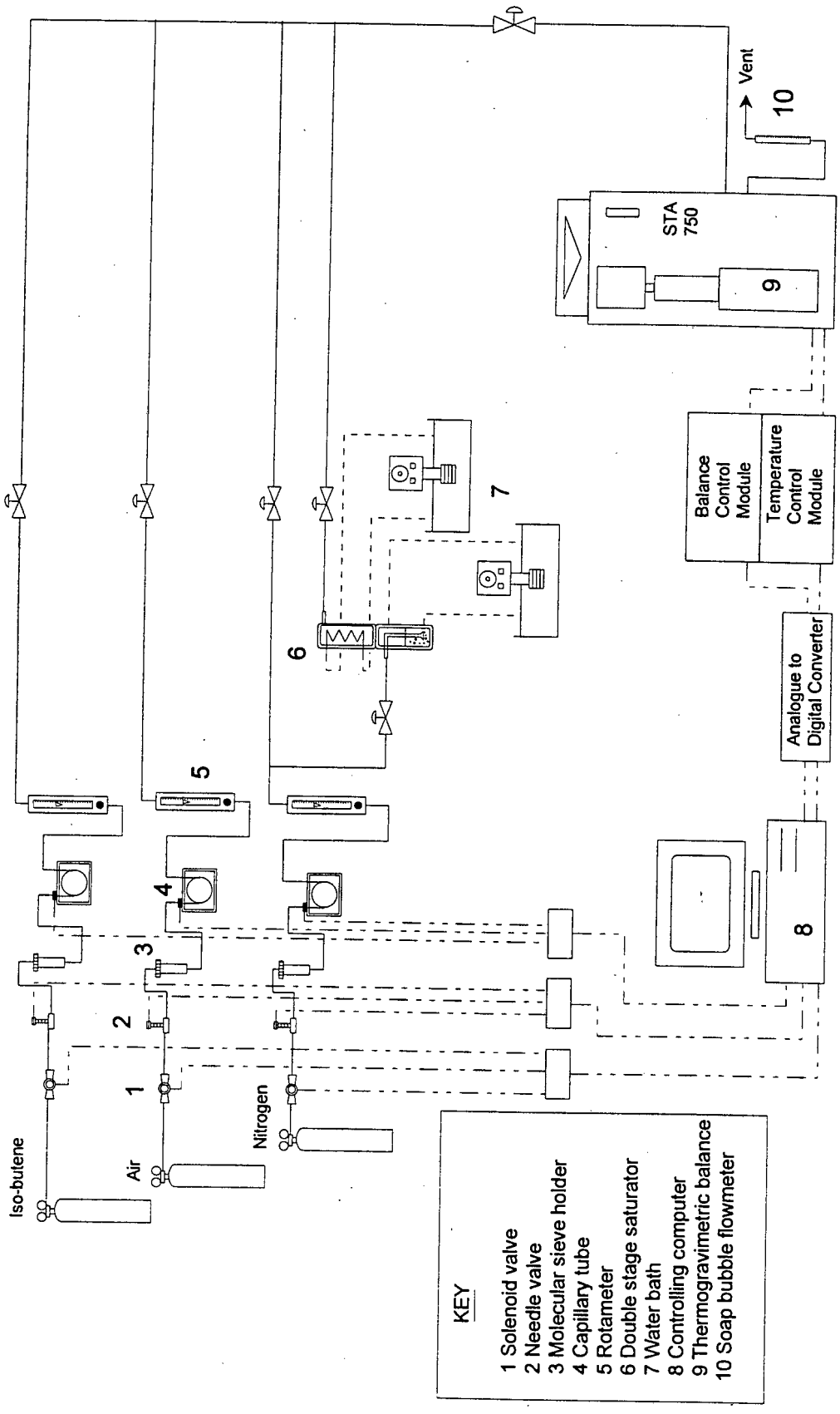

Figure 2.7 Thermogravimetric apparatus

Water was introduced into the nitrogen gas through a double stage saturator. The first stage saturating the gas at 30°C and the second stage, operating at 20°C, set the water content to 12torr. The temperature of the saturating water in the first stage and saturated gas in the second stage were controlled by two independant water baths. The exit line from the saturator to the thermogravimetric analyser was set to 25°C using temperature controlled heating tape to prevent any water from condensing out of the saturated nitrogen.

The feed gases combined and flowed into the thermogravimetric analyser through a common feed line. The exit line was vented to the atmosphere via a soap bubblemeter which monitored the total gas flow leaving the instrument.

2.3.1.2 Temperature Control

The furnace temperature and heating rate were controlled by the temperature control module of the thermogravimetric analyser. The furnace temperature was related to the sample temperature by correlating the furnace temperature to the melting point of known standards over the temperature range and heating rate used (30 to 500°C, 3°C/min). The catalyst bed temperature was found to lag behind the furnace temperature according to the relationship: $T_{bed} = 1.05\ T_{furnace} - 34°C$. This melting point calibration was done prior to the experimental programme.

2.3.1.3 Data Capture

The analogue signals of furnace temperature, differential temperature and mass change were converted to digital signals that were recorded by the computer along with the runtime. These were stored as record files which were later converted to print files. The data could then be manipulated in a standard spreadsheet for interpretation and presentation.

2.3.1.4 Experimental Procedure

Platinum crucibles were used as the containers for the reference and sample materials. These contained 15mg of sample and 15mg of quartz glass as a reference. Quartz was used since alumina, the standard reference material for thermogravimetric work, exhibited temperature effects above 330°C whereas quartz was completely inert. An unexpected adaptation of the experimental conditions was required to prevent reaction of iso-butene at the adsorption temperature. A reduction in sample size from 20mg to 15mg achieved this. This low temperature reaction has previously been reported (Derouane *et al.* 1981, 1982). ^{13}C-NMR studies showed that surface alkylation and polymerisation of ethylene occur at room temperature on a dehydrated zeolite. The particle size used was 38-75μm. The catalysts investigated were NiSMM-7-F, SMM-F, Ni-, Co-, ZnSMM-0.06-F-IX and ZSM-5. The samples were calcined for 4hr at 500°C *in situ* in 60ml/min flowing N_2 (SMM catalysts) or air (ZSM-5) and then cooled to below 30°C in the flowing calcination gas.

Iso-butene was used as the probe olefin due to its greater reactivity over lower molecular weight olefins. A comparison of the relative reactivities of ethene, propene, 1-butene and iso-butene is given in Section 3.2.1.1

After calcination, iso-butene (10ml/min), diluted in N_2 (20ml/min), was passed over the crucibles isothermally at 30°C for 1hr for the adsorption phase. The catalyst's temperature was then ramped at 3°C/min to 500°C to allow reaction to occur. The temperature was maintained at 500°C for 1hr to monitor catalyst coking. Weight changes were relative to the weight of the dry calcined catalyst.

Part of this study investigated the effect of water on both the adsorption and reaction of iso-butene on NiSMM-7-F. During the adsorption phase the catalyst was exposed to a 12torr water partial pressure N_2 stream (30ml/min) at 30°C for 1hr. This was termed a 'wet adsorption'.

This wet adsorption was followed in some cases by a dry N_2 flow (30ml/min) for 1hr to remove excess water. A catalyst prepared in this manner was termed 'hydrated'. A

similar dry N_2 flushing technique was used after iso-butene adsorption to determine iso-butene 'chemisorption' levels.

When water was required during the temperature programmed reaction phase it was added at a 12torr water vapour pressure in N_2 (20ml/min) together with the iso-butene reactant at 10ml/min. This was termed a 'wet reaction'.

2.3.1.5 Identification of Reaction Peaks

The identification or chemical characterization of the events associated with temperature excursions during the reaction phase required a separate study. This was as a result of the iso-butene conversion levels being too low for evolved gas analysis. NiSMM-7-F was packed into a micro reactor system similar to that described in Section 2.4.1 and is shown in Figure 2.8 The catalyst bed has a mass of 2g and was calcined in N_2 (60ml/min) at 500°C for 4hr, followed by cooling in flowing N_2.

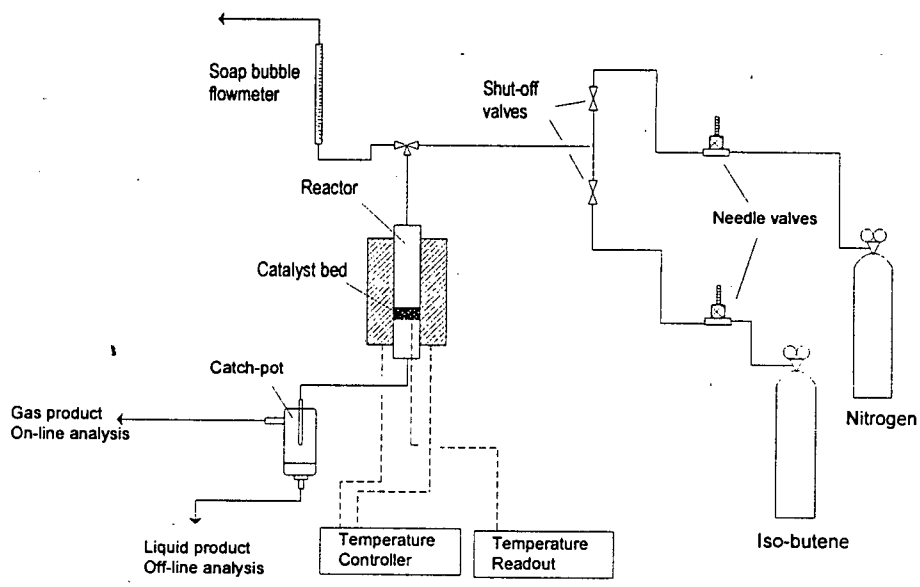

Figure 2.8 Atmospheric reactor line

The feed gases (iso-butene and N_2) were contained in standard gas cylinders as for the thermogravimetric work. Their flowrate was controlled by needles valves and checked using a soap bubblemeter. Iso-butene (40ml/min) diluted in N_2 (80ml/min) was passed through the reactor at atmospheric pressure. The bed temperature was controlled at four different temperatures, viz., 60-100°C, 130°C, 170°C, and 270°C.

The gas analysis was conducted on-line using a Varian 3700 gas chromotograph with a SP-1700 column and thermal conductivity detection. Liquid product analyses were performed off-line on a Varian 3400 gas chromatograph using a stainless steel column packed with OV 101 supported on Chromasorb WHP-SP and flame ionization detection.

2.4 Alkene Oligomerization

2.4.1 Reaction System

The high pressure oligomerization apparatus is shown in Figure 2.9. The alkene feeds were stored in inverted domestic gas cylinders. The feed cylinder was heated using temperature controlled heating tape at 30°C. This was to increase the pressure at the inlet to the feed pump. The feed was dried by flowing over 3A molecular sieves before passing through a 0.5μm physical filter.

A Lewa type FLM 1 high pressure diaphragm pump was used to pump the feed through either the bypass or the reactor. The feed inlet pressure to the pump head was cooled to 10°C by a glycol refrigeration unit. This prevented alkene vaporization in the pump head and ensured uniform pump operation. The reactor used was a stainless steel tube 20cm long with 18mm ID. It was heated by a cylindrical brass block that contained 4 cylindrical heating elements connected to a temperature controller. A moveable thermocouple, placed in an axial thermowell, monitored reaction temperature.

The reaction pressure of 5MPa was maintained by a back pressure regulator. The regulator, placed downstream of the reactor, was pressurized to 5MPa with N_2 and was heated to 50°C by a temperature controlled heating tape to prevent freezing due to the

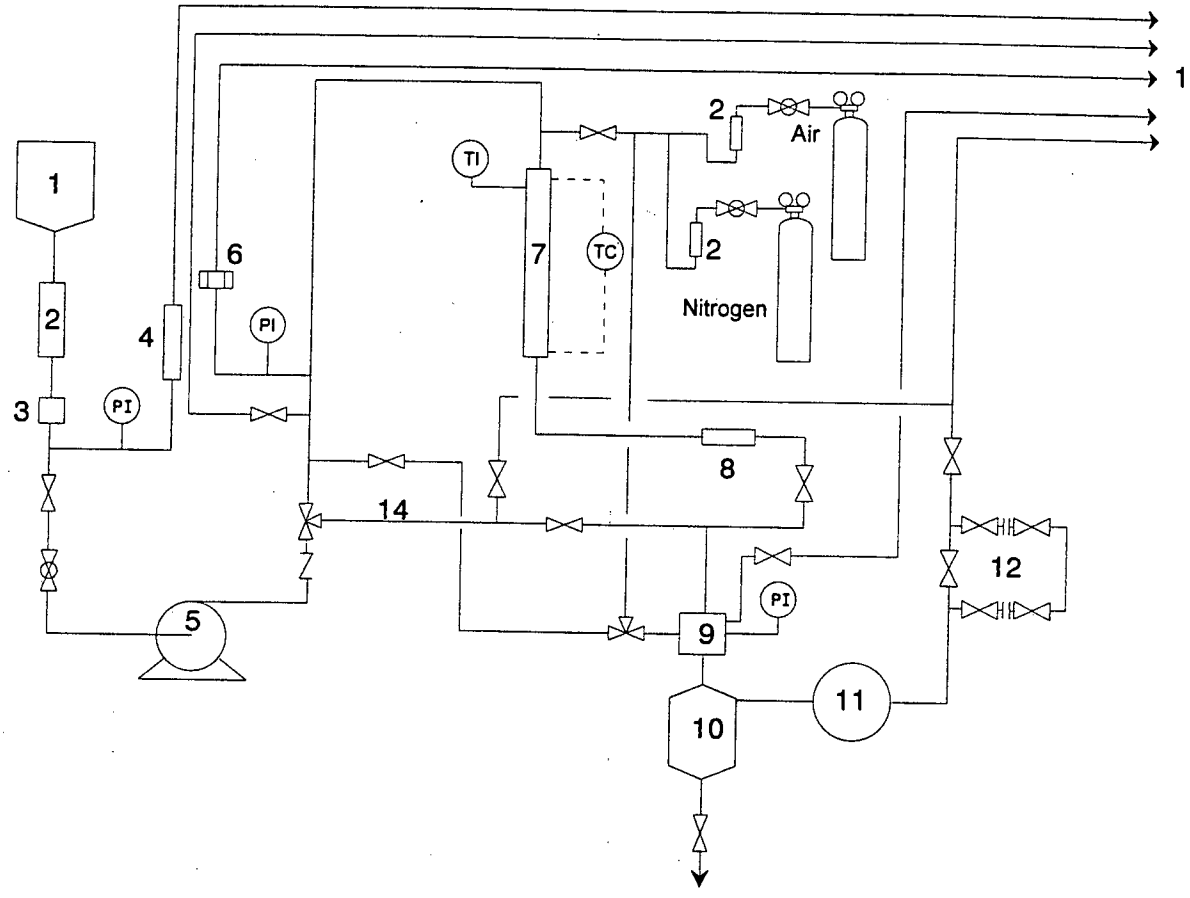

1. Feed cylinder
2. Molecular sieves (3A)
3. 0.5μm filter
4. Pressure relieve valve
5. High pressure diaphragm pump
6. Bursting disc holder
7. Reactor
8. 0.5μm filter
9. Back pressure regulator
10. Liquid catch pot
11. Wet gas flow meter
12. Gas sampling loop
13. Vent lines
14. Bypass line

Ball or plug valve

Needle valve

Non-return valve

PI Pressure gauge

TI Temperature readout

TC Temperature controller

Figure 2.9 High pressure oligomerization apparatus

vaporization of unreacted feed. A 0.5μm physical filter stopped entrained catalyst particles from fouling the back pressure regulator.

The reactor effluent, released to atmospheric pressure in the back pressure regulator, passed to a catch pot (maintained at room temperature by a water bath) from which condensed liquid product was retrieved. Gaseous product and unreacted feed flowed from the catch pot, via a wet gas flow meter, through a gas sampling loop before being vented to the atmosphere. An adjustable pressure relief valve and a bursting disc were safety features incorporated into the apparatus. Vent lines were also provided to vent the reactor line if necessary.

2.4.2 Run Procedure

2.4.2.1 Preparation

For all oligomerization runs 0.5g of catalyst (size fraction: 75-106μm) was used unless otherwise stated. The catalyst was packed into the reactor as shown in Figure 2.10.

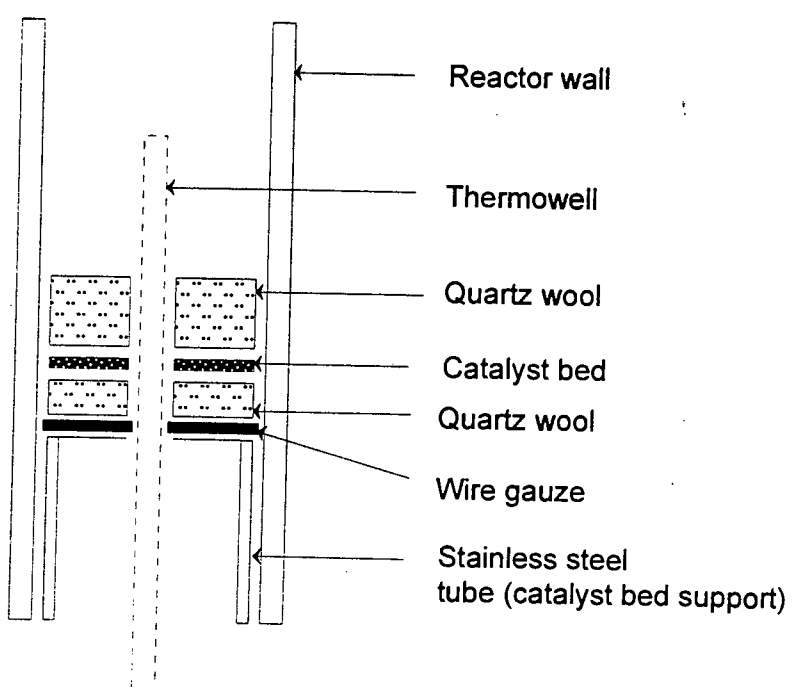

Figure 2.10 Packing of catalyst into reactor

Calcination took place *'in situ'* at 500°C for a minimum of 4 hr with a 60ml/min air flow rate. Other calcination temperatures investigated for propene oligomerization were 450 and 600°C.

To ensure that the alkene feed was dried to the same degree for each run, fresh (dried at 100°C overnight in an oven) 3A molecular sieves were installed before exposing the catalysts to alkene feed.

2.4.2.2 Startup

After calcination the reactor was allowed to cool to below 50°C under continued flowing air. While the reactor was cooling, the pump head glycol refrigeration unit, the back pressure regulator and alkene feed cylinder heaters were switched on. The back pressure regulator was pressurized to 5MPa with nitrogen. The air calcination gas flow was shut off and the reactor slowly filled with nitrogen to 5MPa. It was then isolated using shut-off valves and tested for leaks. If no leaks were detected (pressure remained constant at 5MPa for 1 hr) the desired pump stroke was set and the high pressure pump turned on.

The feed that passed over the sieves too quickly to be dried (40liter in gas state, STP) was then pumped out of the system via the bypass line over a period of 2hr. The feed was then directed to the reactor and the high pressure nitrogen was pumped out via the back pressure regulator to the atmospheric vent line. Once this had all been displaced (typically after 15min) reactor heating was started. The catalyst bed took about 1 hr to reach the reaction temperature of 130°C. The heating rate was limited to 2°C/min to prevent temperature runaways from occurring. The run log was started (time zero) when the first drop of liquid was seen in the catch pot. At this stage the catalyst bed had already reached the reaction temperature of 130°C. The feed gas cylinder was disconnected, weighed and reconnected to obtain its initial mass for the run mass balance.

2.4.2.3 Data Logging and Work-Up

The following data were collected for each time interval:

1. Actual time, used to compute runtime (t).
2. Cumulative wet gas flow meter reading (WGFM)
3. Wet gas flow meter temperature (T)
4. Liquid sample ex catch pot (mass = L)
5. Gas sample (taken halfway through each time interval)
6. Pump stroke
7. Reactor pressure.
8. Reactor temperature set point
9. Catalyst bed temperature

The mass of the catalyst packed into the reactor was recorded. This was the catalyst mass prior to calcination. The alkene feed cylinder was re-weighed at the end of the run.

The gas samples were used to calculate the average molar mass of the exit gas by computing the mole fractions of the components (Appendix 3).

The feedrate, volumetric and mass flowrates of the exit gas and conversion to liquid product were calculated from the data collected by the method given in Appendix 4.

2.4.3 Feed and Product Compositions

2.4.3.1 Gaseous Streams

A GOW-MAC 750 gas chromatograph with a 6.35mm OD, 3m long stainless steel column packed with n-octane/Porasil C was used to analyse feed and effluent gases. Detection was by flame ionization. The instrumental settings used are given:

Flowrates :	N_2 (Carrier)	40ml/min
	N_2	30ml/min
	Air	300ml/min
Temperatures:	Injector	150°C
	Detector	250°C
	Column	50°C (isothermal)

Relative Response Factors:

Ethane	1.024
Propane	1.000
Propene	0.971
Iso-butene	0.889
1-butane	1.028
1-butene	1.056

The response factors used were calculated relative to propane which was assigned a value of 1.000. The analyses were calculated on a normalised mass percentage basis.

Table 2.3 gives typical feed analyses for the propene feed and the 1-butene feed mixtures.

Table 2.3 Propene and 1-Butene feed compositions

	Composition (wt %)				
Component	**Propene**	**1-Butene Feeds**			
		20%	**40%**	**60%**	**80%**
Ethane	0.56				
Propane	11.76	0.76	0.62	0.43	0.21
Propene	86.41				
Isobutene	0.08	0.07	0.10	0.11	0.08
1-Butane	0.12	78.81	60.24	40.01	19.86
1-Butene	1.07	20.36	39.04	59.45	79.85

An example of a chromatogram from an analysis of the propane feed can be found in Appendix 3.

2.4.3.2 Liquid Streams

The liquid product was analysed on a Varian 3600 GC with a 0.351mm ID, 30m long fused silica megabore column coated with a 1.5μm film of DB-1 (100% methylpolsilane). Detection was by flame ionization.

The following instrumental settings were used:

Flowrates :	N_2 (Column)	4.5ml/min
	N_2 (Make-up)	25.5ml/min
	H_2	30ml/min
	Air	300ml/min
Temperatures:	Injector	150°C
	Detector	250°C
	Column	40°C (1min), 10°C/min, 230°C (5min)

Due to the large number of compounds produced during the oligomerization reaction the products were grouped into oligomer fractions as defined in Table 2.4. Examples of typical chromatographs for the products of propene and 1-butene oligomerization are shown in Appendix 7.

Each group of the components were quite distinctive. The retention times for each group were checked using known components to calibrate the gas chromatograph. This enabled identification of each component grouping. The product groupings were thus carried out on hydrocarbon number only. The response factors were taken to be unity.

Since the products of oligomerization form a homologous series, the errors in this assumption can be considered negligible. The composition was determined using a normalized weight percent.

Table 2.4 Oligomer Groupings

Oligomer Group	**Feed**			
	Propene		**1-Butene**	
	Designation	**Range**	**Designation**	**Range**
Monomer	C_3	C_1 - C_4	C_4	C_1 - C_5
Dimer	C_6	C_5 - C_7	C_8	C_6 - C_9
Trimer	C_9	C_8 - C_{10}	C_{12}	C_{10} - C_{13}
Tetramer	C_{12}	C_{11} - C_{13}	C_{16}	C_{14} - C_{17}
Pentamer	C_{15}	C_{14} - C_{16}	C_{20+}	C_{18+}
Hexamer	C_{18}	C_{17} - C_{19}		
Heptamer+	C_{21+}	C_{20+}		

Chapter 3

Results

RESULTS

3.1 Catalyst Characterization

3.1.1 Elemental Analysis

The analyses of the full range of catalysts for Ni, Co or Zn, Si and F content are given in Table 3.1. NiSMM-7-pH7 and -pH10 were synthesised at pH's of 7.0 and 10.0 respectively, as opposed to a pH of 8.5 used for all the other catalysts. SMM was synthesised without using any metal acetate to produce an unsubstituted SMM.

Table 3.1 Metal, Al, Si, and F analyses of the various forms of SMM

Catalyst	Metal (wt %)		Al	Si	F
	Loaded	Actual		(wt %)	
NiSMM-1	1.0	1.0	17.6	22.6	1.0
NiSMM-7	6.8	7.1	16.5	20.4	0.9
NiSMM-10	12.0	10.1	17.9	19.6	0.7
NiSMM-16	21.6	16.4	13.6	17.4	0.7
NiSMM-34	35.7	34.4	7.0	14.0	0.6
CoSMM-1	1.0	1.0	17.8	22.6	1.0
CoSMM-7	6.8	7.2	17.4	20.9	0.8
CoSMM-33	35.8	33.1	11.7	12.7	0.6
ZnSMM-1	1.1	1.2	17.1	24.8	0.9
ZnSMM-7	7.5	6.7	17.2	21.4	1.1
ZnSMM-31	38.2	31.4	12.6	13.5	0.6
NiSMM-7-pH7	6.8	7.0	16.9	20.8	0.6
NiSMM-7-pH10	6.8	7.0	16.8	21.1	0.5
SMM	-	-	16.2	26.2	0.7
SMM-F	-	-	18.3	23.2	1.3
NiSMM-7-F*	6.8	6.7	17.4	21.3	0.8

*Harshaw-Filtrol specified 6.75% Ni, analysis gave 6.7% Ni.

The actual metal wt % values measured corresponded well with the amounts loaded in the synthesis gel. Synthesis pH had no effect on Ni incorporation as seen from the comparative

elemental analyses of NiSMM-7, NiSMM-7-pH7 and -pH10. NiSMM-7 did, however, have the highest F content of the three.

The Al, Si and F contents all decreased as metal loading was increased. This was due to the normalisation inherent in calculating wt%, the Al, Si and F masses were kept constant while the amount of metal used was increased. All three elements had similar metal contents at equivalent metal loadings for the three different metal types. The only exception was NiSMM-34 which had a lower Al wt % compared to CoSMM-33 and ZnSMM-31. In all cases the final F content was about half of that charged to the synthesis gel. Al and Si showed higher levels of incorporation of 90-100% and 80-90% respectively.

3.1.2 Unit Cell Formulae

Calculations for the unit cell formulae of the catalysts analysed in Section 3.1.1 were done using their respective elemental analyses according to the method outlined by Black, *et al.* (1976). The analysis is recalculated as charge equivalents (cation equivalents x cation charge) normalised to charges per 44 charges (the negative charge per unit cell of the oxygen-hydroxyl framework of the 2:1 layer silicate) and finally expressed as cations per unit cell (e.g. the silicon charges per 44 charges divided by the charge of the silicon cation). These cations are then distributed over the tetrahedral and octahedral layers according to the types of cations found in these layers. Since no ammonium analysis was undertaken, its contribution to the 44 cation charge per unit cell was not taken into account. As the ammonium ion has been shown by Wright, *et al.* (1971) to be between 0 and 2 charges per 44 charges its contribution is small. The calculated unit cell formulae are given in Table 3.2. An example of the detailed calculation is given in Appendix 8 for NiSMM-7.

In all cases excess Al remained after the octahedral and tetrahedral positions had been filled. This remaining Al was attributed to charge balancing hydroxyaluminium species as suggested by Wright, *et al.* (1971). They have a variable charge, z+, of between 0 and 3 depending on the number of hydroxyl groups associated with the aluminium and are designated as $Al\ (OH)^{z+}_{3-z}$. The amount of $Al\ (OH)^{z+}_{3-z}$ was approximately a third of the

Table 3.2 Unit Cell Formulae for the various forms of SMM

Catalyst	Unit Cell Formula
NiSMM-1	$[(Ni_{0.14}\ Al_{3.91})^{octa}\ (Si_{6.70}\ Al_{1.30})^{tetra}\ O_{20}\ (OH)_{3.56}\ F_{0.44}].\ 0.46\ Al\ (OH)^{z+}{}_{3-z.(1.30-0.46z)}\ NH_{4+}$
NiSMM-7	$[(Ni_{1.07}\ Al_{3.29})^{octa}\ (Si_{6.43}\ Al_{1.57})^{tetra}\ O_{20}\ (OH)_{3.59}\ F_{0.41}]0.51\ Al\ (OH)^{z+}{}_{3-z.(1.57-0.51z)}NH_4^+$
NiSMM-10	$[(Ni_{1.48}\ Al_{3.01})^{octa}\ (Si_{6.00}\ Al_{2.00})^{tetra}\ O_{20}\ (OH)_{3.68}\ F_{0.32}]0.69\ Al\ (OH)^{z+}{}_{3-z.(2.00-0.69z)}NH_4^+$
NiSMM-16	$[(Ni_{2.70}\ Al_{2.20})^{octa}\ (Si_{6.00}\ Al_{2.00})^{tetra}\ O_{20}\ (OH)_{3.64}\ F_{0.36}]0.66\ Al\ (OH)^{z+}{}_{3-z.(2.00-0.66z)}NH_4^+$
NiSMM-34	$[(Ni_{6.00})^{octa}\ (Si_{5.58}\ Al_{2.42})^{tetra}\ O_{20}\ (OH)_{3.64}\ F_{0.36}]\ 0.47\ Al\ (OH)^{z+}{}_{3-z.}\ 0.55\ Ni^{2+}\ (1.32-0.47z)NH_4^+$
CoSMM-1	$[(Co_{0.15}\ Al_{3.90})^{octa}\ (Si_{6.78}\ Al_{1.22})^{tetra}\ O_{20}\ (OH)_{3.55}F_{0.45}]0.41\ Al\ (OH)^{z+}{}_{3-z.(1.22-0.41z)}NH_4^+$
CoSMM-7	$[(Co_{1.04}\ Al_{3.31})^{octa}\ (Si_{6.38}\ Al_{1.62})^{tetra}\ O_{20}\ (OH)_{3.64}F_{0.36}]0.57\ Al\ (OH)^{z+}{}_{3-z.(1.62-0.57z)}NH_4^+$
CoSMM-33	$[(Co_{5.85}Al_{0.10})^{octa}\ (Si_{4.70}Al_{3.30})^{tetra}\ O_{20}\ (OH)_{3.67}F_{0.33}]1.10\ Al\ (OH)^{z+}{}_{3-z.(3.30-1.10z)}NH_4^+$
ZnSMM-1	$[(Zn_{0.15}\ Al_{3.90})^{octa}\ (Si_{7.10}Al_{0.90})^{tetra}\ O_{20}\ (OH)_{3.62}F_{0.38}]0.30\ Al\ (OH)^{z+}{}_{3-z.(0.90-0.30z)}NH_4^+$
ZnSMM-7	$[(Zn_{0.85}\ Al_{3.43})^{octa}\ (Si_{6.50}Al_{1.50})^{tetra}\ O_{20}\ (OH)_{3.51}F_{0.49}]0.50\ Al\ (OH)^{z+}{}_{3-z.(1.50-0.50z)}NH_4^+$
ZnSMM-31	$[(Zn_{4.93}\ Al_{0.71})^{octa}\ (Si_{4.95}Al_{3.05})^{tetra}\ O_{20}\ (OH)_{3.67}F_{0.33}]1.04\ Al\ (OH)^{z+}{}_{3-z.(3.05-1.04z)}NH_4^+$
NiSMM-7-pH7	$[(Ni_{1.05}\ Al_{3.30})^{octa}\ (Si_{6.43}Al_{1.57})^{tetra}\ O_{20}\ (OH)_{3.72}F_{0.28}]0.53\ Al\ (OH)^{z+}{}_{3-z.(1.57-0.53z)}NH_4^+$
NiSMM-7-pH10	$[(Ni_{1.02}\ Al_{3.32})^{octa}\ (Si_{6.48}Al_{1.52})^{tetra}\ O_{20}\ (OH)_{3.78}F_{0.22}]0.49\ Al\ (OH)^{z+}{}_{3-z.(1.52-0.49z)}NH_4^+$
SMM	$[(Al_{4.00})^{octa}\ (Si_{7.43}Al_{0.57})^{tetra}\ O_{20}\ (OH)_{3.71}F_{0.29}]0.20\ Al\ (OH)^{z+}{}_{3-z.(0.57-0.20z)}NH_4^+$
SMM-F	$[(Al_{4.00})^{octa}\ (Si_{6.83}Al_{1.17})^{tetra}\ O_{20}\ (OH)_{3.44}F_{0.56}]0.40\ Al\ (OH)^{z+}{}_{3-z.(1.17-0.40z)}NH_4^+$
NiSMM-7-F	$[(Ni_{0.99}\ Al_{3.34})^{octa}\ (Si_{6.43}Al_{1.57})^{tetra}\ O_{20}\ (OH)_{3.65}F_{0.35}]0.52\ Al\ (OH)^{z+}{}_{3-z.(1.57-0.52z)}NH_4^+$

number of aluminium's in the tetrahedral layer for all catalysts. The rest of the negative unit cell charge arising from Al^{3+} substitution for Si^{4+} in the tetrahedral layer is balanced by NH_4^+ ions. For NiSMM-34 0.55 Ni atoms per unit cell remained after all six octahedral positions were filled. These were included as charge balancing Ni^{2+} ions.

The amount of Al in the tetrahedral layer increased with increasing metal content. This was due to more Al being available for the tetrahedral layer as increasing amounts of metal substituted for it in the octahedral positions.

3.1.3 X-ray Diffraction

3.1.3.1 Catalyst Diffractograms

The X-ray diffractograms for the range of catalysts are given in Appendix 9. Separate diagrams for NiSMM-7-pH7 and pH10 are not shown as they were the same as for NiSMM-7, pH having no effect on the SMM X-ray structure. The diffractogram for NiSMM-7 is presented below in Figure 3.1 in order to illustrate the following comments.

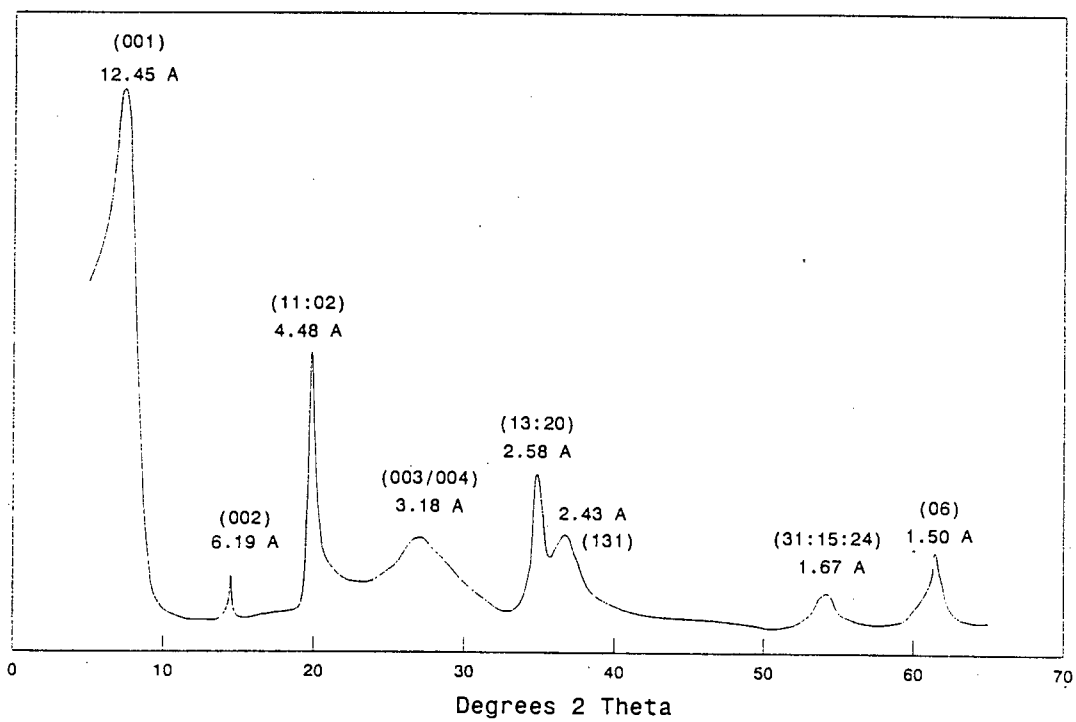

Figure 3.1 X-ray diffractogram for NiSMM-7

The indices were assigned to the peaks as given by Black, *et al.* (1976) in the X-ray discussion of their patent. The NiSMM diffractograms obtained were as described by the above authors showing that the same structures were synthesised in this work as for the patented clays.

As metal loading was increased, higher d_{001} values and less defined 001 peaks were obtained. At times the d_{001} spacing was greater than 12.5Å, which is the layer spacing for pure montmorillonite. The peak for this spacing was indiscernible from the background for CoSMM-33. This could be due to the effect of possible intercalated acetate as suggested by Black, et al (1976). The peak at circa. 3.2Å was assigned as (003/004) due to uncertainties because of the mixed layered nature of the clays. The shift in the 06 peak from 1.50 to 1.52Å with increased metal incorporation is discussed in the next section.

The diffractograms for NiSMM-7 and NiSMM-7-F compared very well, showing identical structures apart from a 0.34Å difference in layer spacing. Similar X-ray diagrams were obtained for SMM and SMM-F. A higher d_{001} value of 12.1Å compared to 11.4Å was found for SMM and the peak intensity was lower. This indicated a more montmorillonite-like structure. The percentage mica-like layers were calculated to be 12.5% (SMM) and 41.7% (SMM-F) according to the formula 100 x (12.4 - d_{001})/2.4 given by Granquist (1966). This could be due to incomplete crystallization for SMM as a synthesis time of only 3hr at 300°C was used whereas Granquist (1966) suggests an optimum synthesis time of 3 days at 280°C or 12hr at 315°C for SMM. The SMM in this work was synthesized at 300°C for 3hr as described by Black, *et al.* (1976) to enable it to be used as a baseline comparison against the metal substituted SMM's which used this synthesis procedure.

3.1.3.2 Dioctahedral/Trioctahedral 06 Reflection

A separate X-ray study was undertaken at the conditions given in Section 2.2.1 on the 06 peak. The reflections obtained for NiSMM-1 to -34, CoSMM-1 to -33 and ZnSMM-1 to 31 are given in Figure 3.2. The dioctahedral peak (1.50Å) diminishes and the trioctahedral peak (1.52Å) grows as more metal is incorporated into the structure as seen for NiSMM.

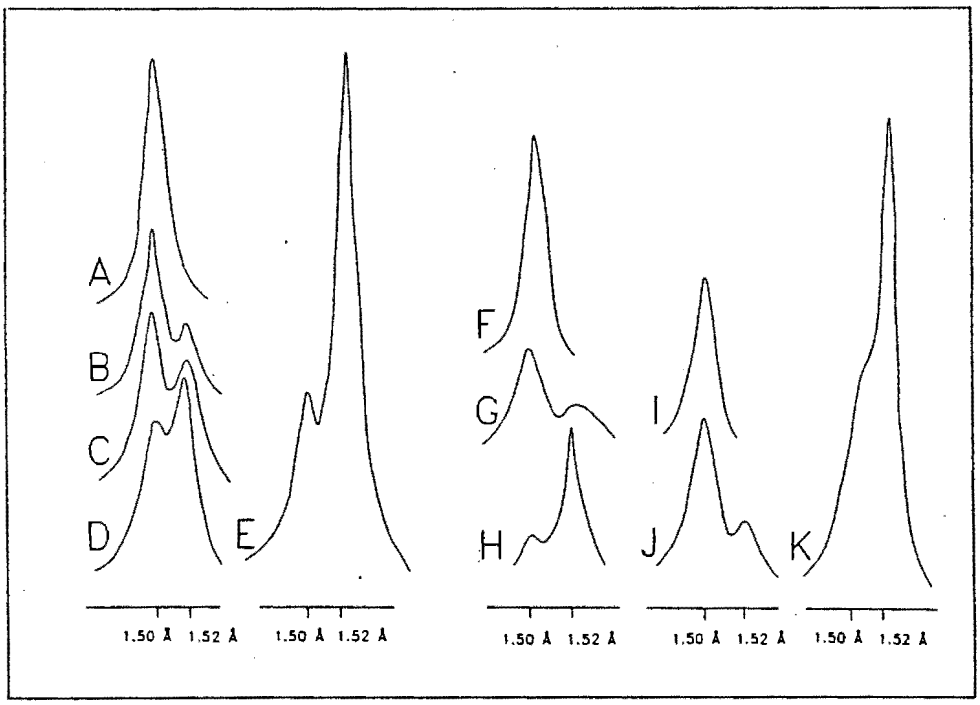

Figure 3.2 06 X-ray reflections

This confirms that three divalent metal cations substituted two trivalent aluminums in the octahedral layer to increasing extents as its weight percentage is increased. It can be seen for NiSMM-34 that even though the calculated unit cell formula gave a completely substituted octahedral layer, viz. a pure trioctahedral clay, a dioctahedral reflection at 1.50Å was still evident.

The intensity of the 06 trioctahedral reflection, corrected for changes in the mass absorption coefficient as the elemental composition of the catalysts change, can be plotted as a function of the calculated number of metal cations per unit cell (from Table 3.2) and is

shown in Figure 3.3. The calculation for correcting the reflection intensities with the mass absorption coefficients is given in Appendix 10.

The intensity of the 06 trioctahedral peak is essentially a linear function of the amount of metal per unit cell. Figure 3.3 shows that for a similar number of metals per unit cell, the 06 reflection intensities increase from Ni to Co to Zn. No peak corresponding to Ni, Co or Zn oxide was seen in the data.

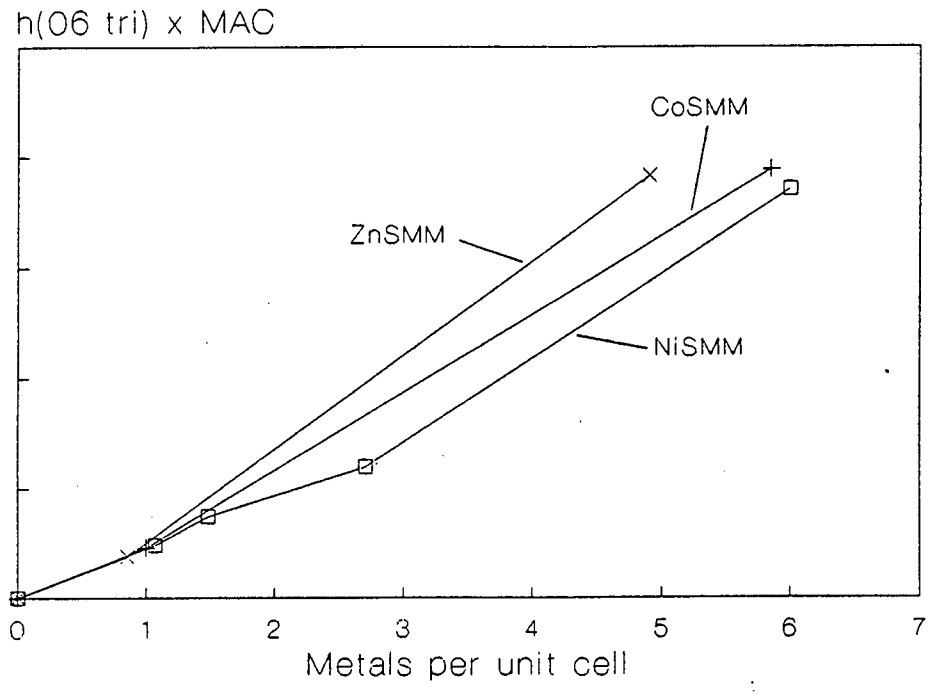

Figure 3.3 Trioctahedral 06 reflection vs metals per unit cell

3.1.4 Surface Area

The BET surface areas of the catalysts are given in Table 3.3 Results were reproducible to within 5%. The surface area values obtained by Swift and Black (1974) are included for comparative purposes. Their samples were precalcined at 538°C and contained approximately 0.7% Pd.

The increase in surface area from 141m²/g for pure SMM to 195m²/g for NiSMM by metal incorporation is thought to be due to the mineral crystallizing out in smaller platelets and thus rendering more accessible surface area after heat activation as proposed by Swift and Black (1974).

The values for NiSMM at loadings of 10% and less compare favourably to those of Swift and Black (1974). A decrease in surface area was seen for NiSMM-16 and -34 with increased metal content. This could be caused by increased platelet-to-platelet association resulting in an overall drop in area even though smaller platelets were crystallizing out. A decrease in surface area with increasing metal content was also observed by Swift and Black (1974). The surface area dropped by 15% from a Ni loading of 21.6 to 30.5%.

Table 3.3 BET Surfaces areas of Ni, Co and Zn substituted SMM

		Black and Swift (1974)		
		Ni		
Catalyst	Surface Area (m²/g)	(wt %)	(Ni/u.c.)	Surface Area (m²/g)
NiSMM-1	195	0.0	0	145
NiSMM-7	216	6.75	1	199
NiSMM-10	219	14.30	2	230
NiSMM-16	196	15.00	2	244
NiSMM-34	181	21.60	3	302
		26.40	4	254
CoSMM-1	176	30.50	5	258
CoSMM-7	178	35.70	6	332
CoSMM-33	126			
ZnSMM-1	170			
ZnSMM-7	139			
ZnSMM-31	99			
NiSMM-7-pH7	177			
NiSMM-7-pH10	209			
SMM	141			
SMM-F	145			
NiSMM-7-F	194			

Although CoSMM-1 and ZnSMM-1 showed a 25% and 21% increase in surface area respectively over the unsubstituted form, both Co and Zn showed the onset of a drop in surface area with increasing metal content, CoSMM at a metal content of 33% and ZnSMM at 7%. At similar metal loadings (Ni-, Co- and Zn SMM-7) the surface areas decreased in the order Ni > Co > Zn.

The surface areas of the three 7% NiSMM samples (NiSMM-7, NiSMM-7-F and 6.75% Black and Swift) corresponded very well, three independent sources giving similar results. NiSMM-7-pH7 synthesized at a pH of 7.0 had a lowest surface area of the three NiSMM-7 catalysts synthesised at pHs of 7.0, 8.5 and 10.0, respectively.

3.1.8 Temperature Programmed Reduction

The temperature programmed reduction (TPR) profile of hydrogen consumption with time for NiSMM-34 is shown in Figure 3.4. This profile was typical of all the metal substituted SMM catalysts.

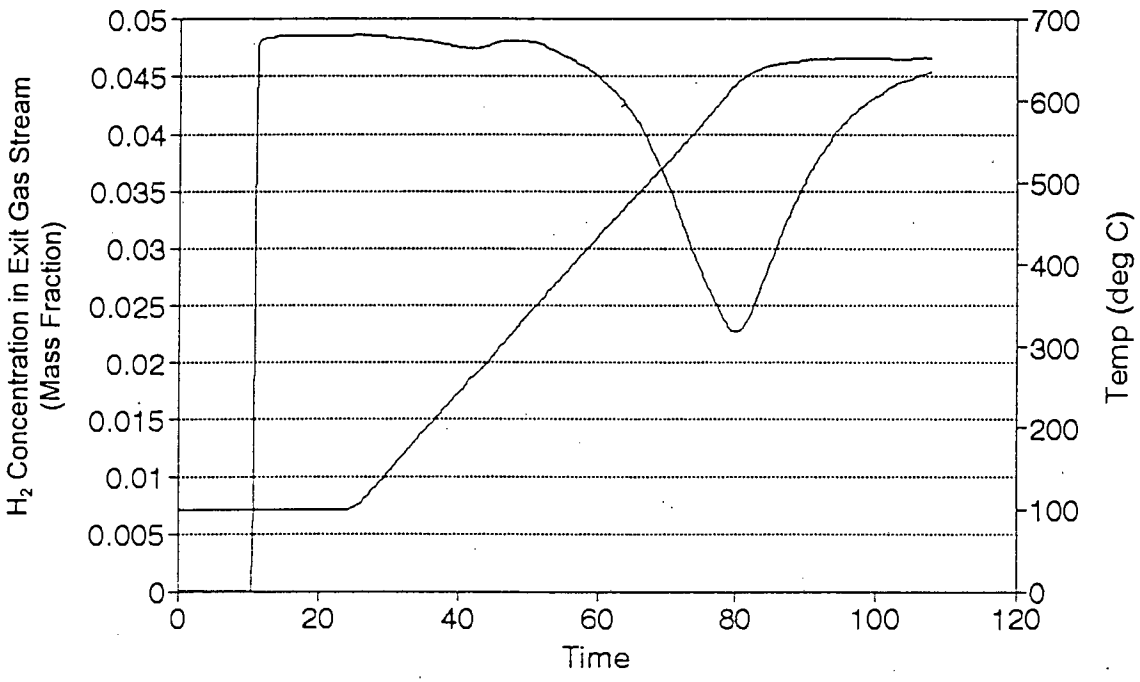

Figure 3.4 Temperature programmed reduction of NiSMM-34

Under the conditions used no metal reduction was shown for the ZnSMM catalysts. Two reduction peaks were seen for Ni and CoSMM. The first of the two peaks was at 360±3°C for CoSMM and at 260±2°C for NiSMM. The second peak was present at 650°C for CoSMM and for NiSMM-1, -7 and -10. The peak temperature was decreased to 636°C and to 623°C for NiSMM-16 and NiSMM-34, respectively. The H_2 uptake was obtained by integrating above this profile. The amount contributing towards the tail seen at the end of the experiment, was estimated by the method of triangulation. The quantities of H_2 consumed by metal substituted SMM catalysts during the reduction process are shown in Table 3.4.

The H_2 consumption peak approached but did not return to the baseline at the end of each experimental run. This area, forming part of the high temperature peak, was estimated by triangulation. The amount contributed 2 to 4% towards the total peak area. NiSMM-1 was found to be an exception in that triangulation and baseline shift adjustment accounted for 19% for the large temperature peak area. This was due to the fact that the total amount of 0.07mmol/g found for NiSMM-1 was close to the noise level of 0.02mmol/g inherent in the baseline. The values of 0.15 for NiSMM-34, 0.12 for CoSMM-7 and 0.73 for CoSMM-33, found for this peak show a form of reduction that requires less energy than the high temperature peak. TPR peaks were seen at 280 - 300°C for Co/SiO_2 by De Lange and Van Steen (1995) and at 260 and 375°C for Ni/SiO_2 by Burch and Flambard (1983). The low temperature peaks that were seen were therefore taken to be representative of metal oxide that was present outside of the catalyst's matrix structure.

The number of millimoles of metal per gram of catalyst is given in the first column of Table 3.5 to enable a comparison to be made with the total amount of hydrogen consumed. The H_2:metal ratios are shown in the last column.

For the NiSMM catalysts 89% or more of the metal was reduced. Only for NiSMM-1 was less metal reduced (53%). At the higher metal loadings (>30%) the amount of metal reduced decreased Ni > Co > Zn. For all the ZnSMM catalysts essentially none of the zinc

was reduced. The standard reduction potentials of the divalent metal ions of nickel, cobalt and zinc are -0.25, -0.28, -0.76, respectively (Purcell and Kotz, 1977). The amount of metal reduced follows the same decreasing trend as the standard reduction potentials. It is also possible that the zinc was very strongly bound in the catalyst structure, which would inhibit its tendency to be reduced.

Table 3.4 Hydrogen Consumption as a function of Peak Temperature

Catalyst		H_2 consumed		
Type	Metal Content (mmol metal/g)	Low Temperature Peak (mmol/g)	High Temperature Peak (mmol/g)	Total H_2 consumed (H_2:metal ratio)
NiSMM-1	0.17	-	0.07	0.41
NiSMM-7	1.21	-	1.06	0.88
NiSMM-10	1.72	-	1.60	0.93
NiSMM-16	2.79	-	2.63	0.94
NiSMM-34	5.86	0.15	5.69	0.99
CoSMM-1	0.17	-	-	-
CoSMM-7	1.22	0.12	0.12	0.20
CoSMM-33	5.62	0.73	3.39	0.73
ZnSMM-1	0.18	-	-	-
ZnSMM-7	1.02	-	-	-
ZnSMM-31	4.80	-	-	

3.1.6 Temperature Programmed Ammonia Desorption

The NH_3 temperature programmed desorption (NH_3-TPD) profiles were similar for all the catalysts showing a uniform acid site strength distribution and a peak maximum at 200°C (±5°C). An example of this, for CoSMM-1, is shown in Figure 3.5.

The calculated number of ammonia molecules per gram of catalyst and the corresponding projected number of acid sites (assuming one NH_3 per site) are given in Table 3.5. The results were reproducible to within 0.02 mmol NH_3/g.

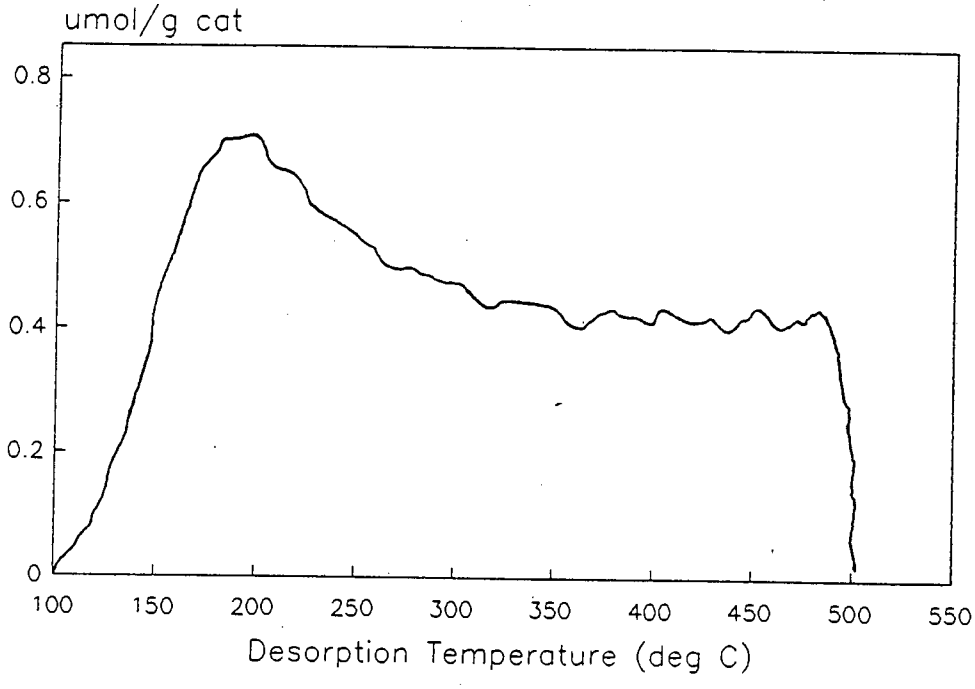

Figure 3.5 NH_3 - TPD profile for CoSMM-1

The acidity measurement for the NiSMM catalysts showed similar values for NiSMM-7, -10 and -16 but NiSMM-1 had a lower and NiSMM-34 a higher acidity. NiSMM-1 had the same acidity found for SMM. Although the acidity trend was not proportional to nickel

content, it could be said that acidity generally increased with nickel content. The acidities found for CoSMM were similar to NiSMM at equivalent metal loadings except at the high metal contents of >30%. NiSMM-34 was shown to be more acidic at 0.60mmol NH_3/g than CoSMM-33, measured at 39mmol NH_3/g. The acidities for all three ZnSMM catalysts were similar to one another and low when compared with Co and NiSMM. The acidity was more sensitive to nickel as opposed to cobalt or zinc loading. SMM-F and SMM had essentially the same acidity.

Table 3.5 Acidities measured by NH_3 TPD

Catalyst	Millimole NH_3/g	Sites/g (x 10^{-19})
NiSMM-1	0.16	9.6
NiSMM-7	0.31	18.7
NiSMM-10	0.33	19.9
NiSMM-16	0.30	18.1
NiSMM-34	0.60	36.1
CoSMM-1	0.22	13.3
CoSMM-7	0.30	18.1
CoSMM-33	0.39	23.5
ZnSMM-1	0.18	10.8
ZnSMM-7	0.14	8.4
ZnSMM-31	0.18	10.8
NiSMM-7-pH7	0.39	23.5
NiSMM-7-pH10	0.29	17.5
SMM	0.16	9.6
SMM-F	0.17	10.2
NiSMM-7-F	0.20	12.0

3.1.7 Infrared Spectroscopy of Pyridine Adsorption

Infrared absorption band assignments due to pyridine ring vibrations are given in Table 3.6. Bands are assigned to physisorbed (Py), hydrogen bonded (HPy), pyridinium ion (BPy) and coordinately bonded (LPy) species. The latter two species indicate Bronsted (BPy) and Lewis (LPy) acidity, respectively. Band assignments were based on the following synthesized standards.

Py - dilute solution of pyridine in chloroform (Parry, 1963; Bourne, *et al.*, 1970).

HPy - pyridine water interactions (Sidorov, 1960).

BPy - pyridine hydrogen chloride (Parry, 1963; Bourne, *et al.*, 1970).

LPy - pyridine aluminium chloride (Bourne, *et al.*, 1970) and pyridine borohydride (Parry, 1963).

Table 3.6 Infrared adsorption band assignments

Frequency (cm^{-1})	Absorbing Species
1637	BPy
1618	BPy, LPy
1615	LPy, HPy
1602	HPy
1582	Py
1545	BPy
1491	BPy, LPy, HPy
1468	LPy
1456	LPy
1445	LPy, HPy
1437	HPy, Py

The infrared spectrum in the range 1370 to 1693 cm^{-1} after pyridine absorption on NiSMM-1 for ½hr (A) and after desorption under vacuum (2 x 10^{-6} mm Hg) for 16hr (B) at room temperature are shown in Figure 3.6.

The peak at 1440cm^{-1} in spectrum A of Figure 3.6 was attributed to LPy, HPy, Py, a combination of the two peaks at 1437cm^{-1} and 1445cm^{-1} in Table 3.6. The LPy peaks at 1456cm^{-1} and 1468cm^{-1} were obscured by the aforementioned peak and were seen as a shoulder on it at approximately 1463cm^{-1}. Absorbence due to BPy, HPy and LPy were seen by a peak at 1490cm^{-1}. BPy alone gave rise to an absorption at 1546cm^{-1}.

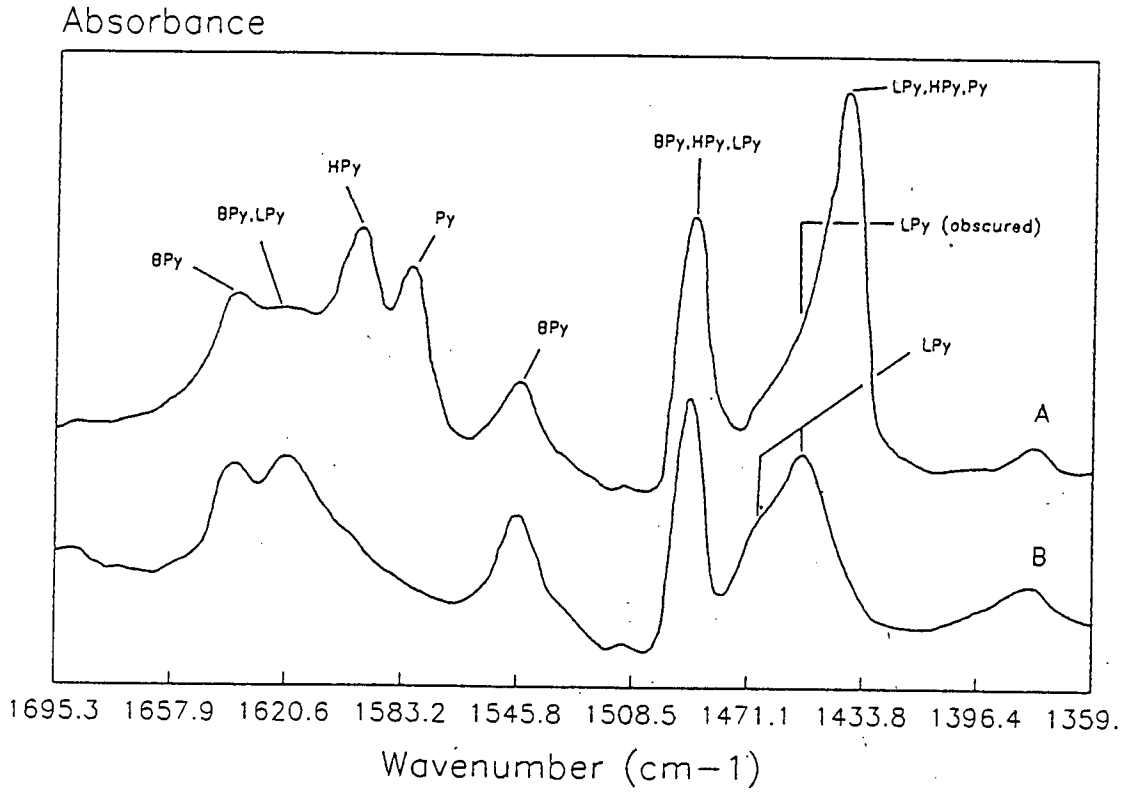

Figure 3.6 Pyridine adsorption on NiSMM-1 for ½hr (A) and vacuum desorption for 16hr (B)

Peaks were also observed at 1582cm^{-1} (Py), 1598cm^{-1} (HPy), 1520cm^{-1} (BPy, LPy) and 1637cm^{-1} (BPy). A peak corresponding to 1615cm^{-1} (LPy, HPy) was not seen.

When comparing observed peak values to those given in Table 3.6 it must be borne in mind that the scan resolution was 4cm^{-1}.

Spectrum B in Figure 3.6 was taken after 16hr of vacuum desorption. Peaks due to absorbences by physisorbed species (Py) and hydrogen bonded pyridine (HPy) all disappeared. Those that remained were at 1454cm^{-1} (LPy), a shoulder at 1468cm^{-1} (LPy), 1490cm^{-1} (BPy, HPy and LPy), 1546cm^{-1} (BPy), 1621cm^{-1} (BPy, LPy) and 1638cm^{-1} (BPy). As per a previous infrared study of pyridine absorption on SMM (Fletcher, 1984) it was found that 16hr was sufficient time to remove non-chemisorbed pyridine species.

The method used to determine site density varies between band height (Karge, 1980; Makarova *et al.*, 1995) and band area (Hughes and White, 1967; Emeis, 1993). The latter method is regarded as a better measure of concentration when the half-width of the adsorption band is not large when compared to the spectral slit width (Hughes and White, 1967) and was hence used in this work. Values for the integrated molecular extinction coefficients that are used to calculate the site density have been reported by a number of authors (Hughes and White, 1967; Stock *et al.*, 1984; Datka *et al.*, 1992; Emeis, 1993) and are shown in Table 3.7.

Table 3.7 Molecular Extinction Coefficients for Pyridine on Lewis and Bronsted Sites

Source	Catalyst	Bronsted	Lewis	Ratio
Hughes and White (1967)	Zeolite Y	1.32	1.42	0.77
Stock *et al.*, (1984)	NaX, NaY	1.2 - 1.5		
Datka *et al.* (1992)	Supported Nobium oxide	0.73	1.11	0.66
Emeis (1993)	MOR, Y, Silica-alumina	1.67	2.22	0.75
Makarova *et al.* (1995)	H-Y, H-EMT	1.1 - 1.6		

The discrepancy in extinction coefficients (20%) indicates the accuracy of the calculated concentrations. They can, however, be used to determine the relative quantities of pyridine adsorbed on the different types of acid sites. This is enhanced by the similarity of the Bronsted to Lewis extinction coefficient ratios as shown in the last column of Table 3.7. The concentrations of Bronsted and Lewis acid sites in this work were determined

according to the method of Hughes and White (1967) as were used by Kojima *et al.* (1986) in their infrared pyridine adsorption study of SMM acidity. This calculation is shown in Appendix 11.

The desorption of pyridine from NiSMM-7 at successively higher temperatures up to 300°C is shown in Figure 3.7. The two peaks pertinent to this work were those at 1454cm^{-1} (LPy) and 1546cm^{-1} (BPy) and their integrated absorbences were used to estimate the number of acid sites per gram of catalyst.

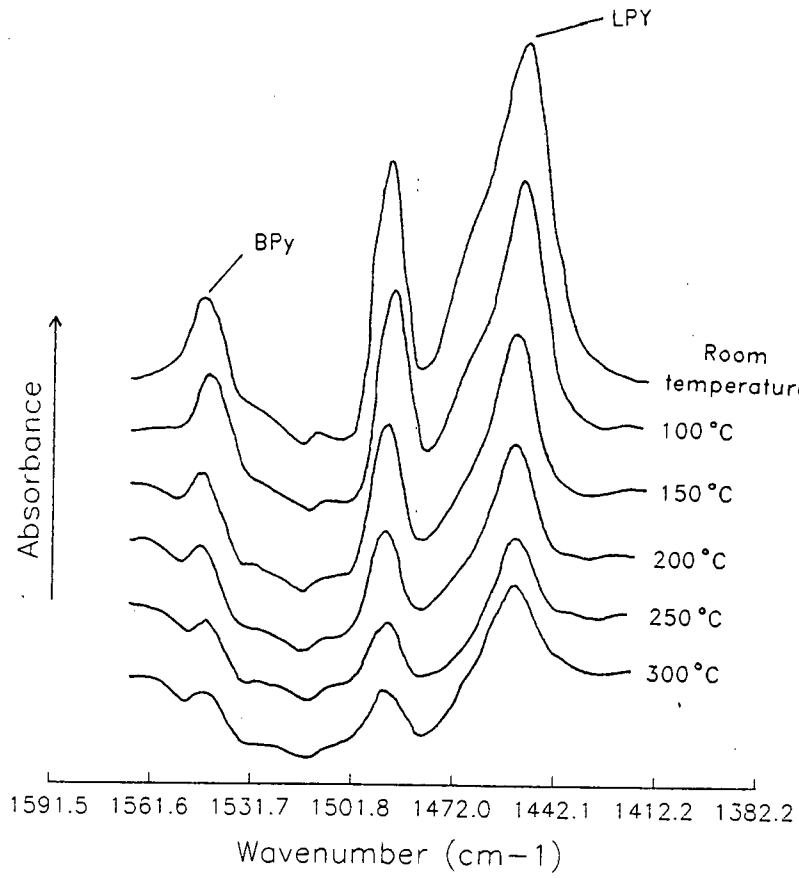

Figure 3.7 Pyridine desorption with temperature for NiSMM-7

The number of Bronsted and Lewis acid sites found at the different desorption temperatures are given in Figure 3.8 (a) for Ni, Co and ZnSMM-1 and in Figure 3.8 (b) for NiSMM-1, -7, and -34. The desorption profiles depicted were all similar and they showed most of the pyridine being lost by 150°C. The values obtained for Ni, Co and ZnSMM-1 were considered to be essentially the same. No real differences were evident between the three catalysts at this low metal content. The same could be said for NiSMM-1 and -7. An exception was seen for NiSMM-34 at room temperature (25±2°C). At this low temperature point NiSMM-34 showed a higher acidity over NiSMM-1 and -7. This was taken to be indicative of a higher level of weak acidity for NiSMM-34.

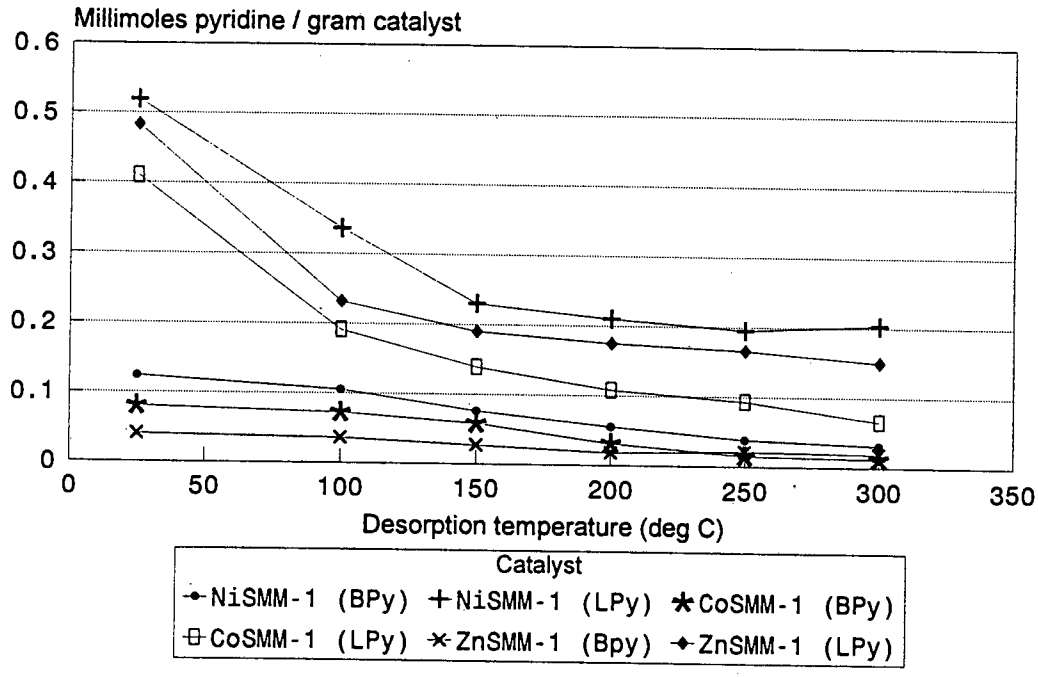

Figure 3.8 (a) Acid sites at desorption temperatures of r.t. to 300°C for NiSMM-1, CoSMM-1 and ZnSMM-1

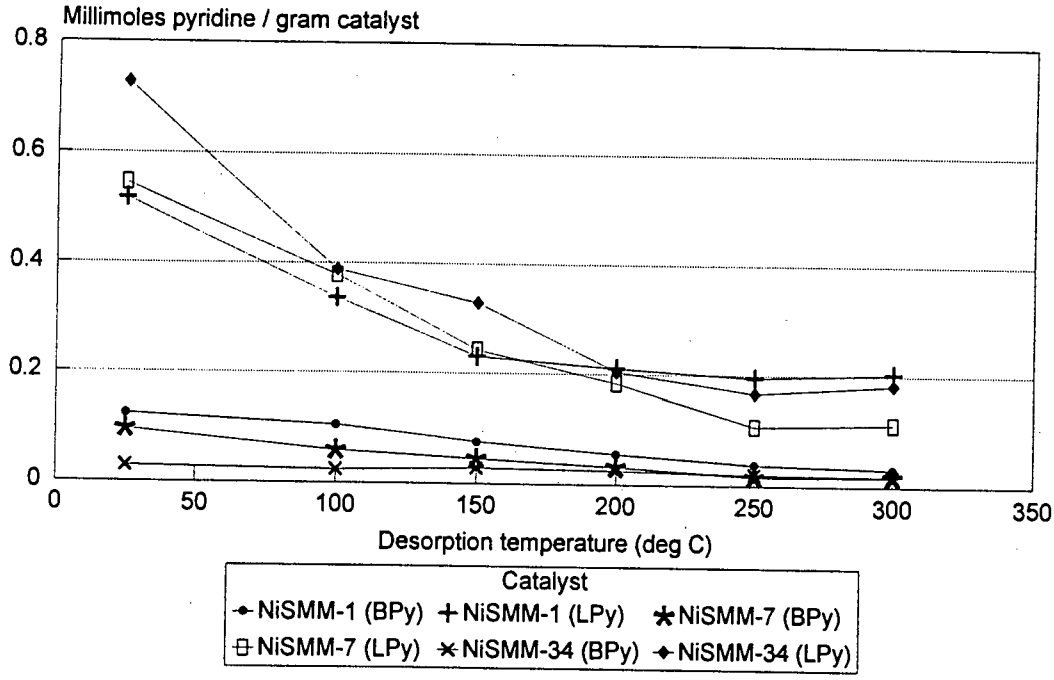

Figure 3.8 (b) Acid sites at desorption temperatures of r.t. to 300°C for NiSMM-1, -7 and -34

The acid site concentrations determined for the range of catalysts precalcined under vacuum at 500°C, are given in Table 3.8. NiSMM-0.06-F-IX and NiSMM-0.06-F-IMP samples are for 0.06 wt% nickel ion exchanged and impregnated on SMM, respectively. The values obtained were reproducible to within 7%. Pyridine was absorbed for ½hr and desorbed for 16hr under vacuum (2 x 10^{-6} mm Hg) at room temperature. The site concentrations were calculated as shown in Appendix 11, assuming one pyridine per acid site. Table 3.8 shows that ion-exchanging or impregnating SMM with 0.06% nickel resulted in a negligible change in acid site density over unmodified SMM while incorporating 1% nickel into the SMM lattice increased the total number of sites by 85%.

Table 3.8 Acid Site Concentrations as determined by Infrared Pyridine Absorption

Catalyst	BPy	LPy	Total Acidity
	(millimoles pyridine absorbed/gram catalyst)		
NiSMM-1	0.124	0.519	0.643
NiSMM-7	0.096	0.546	0.642
NiSMM-10	0.032	0.505	0.537
NiSMM-16	0.023	0.666	0.689
NiSMM-34	0.029	0.727	0.756
CoSMM-1	0.080	0.410	0.490
CoSMM-7	0.036	0.519	0.555
CoSMM-33	0.012	0.358	0.370
ZnSMM-1	0.040	0.483	0.523
ZnSMM-7	0.032	0.337	0.369
ZnSMM-31	0.009	0.372	0.381
NiSMM-7-pH7	0.043	0.456	0.499
NiSMM-7-pH10	0.049	0.421	0.470
SMM	0.070	0.277	0.347
SMM-F	0.067	0.550	0.617
NiSMM-1-IX	0.050	0.263	0.313
NiSMM-1-IMP	0.025	0.339	0.364

The SMM synthesized in this work had the same Bronsted acidity but only half the amount of Lewis acidity compared to SMM-F. As before this was attributed to incomplete

crystallization as the synthesis time used was 3hr as opposed to a recommended 12hr period in the patent for unsubstituted SMM synthesis (Granquist, 1966). It was seen that for Ni, Co and ZnSMM the Bronsted acid site density decreased with increasing metal loading. In all cases the catalysts contained predominantly Lewis acidity with the Lewis/Bronsted ratio not less than 4 and typically greater than 10. For NiSMM the total number of acid sites generally increased with increasing metal content. This trend for metal content was not observed for the Co and ZnSMM catalysts where CoSMM-33 and ZnSMM-7 and -31 showed lower acid site densities than CoSMM-7 and ZnSMM-1, respectively.

3.2 Thermogravimetric Analysis

3.2.1 Preliminary Studies

3.2.1.1 Olefin Reactivity

In order to select an olefin suitable for the olefin oligomerization study over the various SMM catalysts, the activity of ethene, propene, 1-butene and iso-butene was investigated over NiSMM-7-F. The results of this study are shown in Figure 3.9. The first hour consisted of an isothermal adsorption phase at 30°C. The temperature was then increased at 3°C /min to 500°C and then maintained at that temperature for 1hr. The catalyst bed temperature is included in the data presentation. During the course of temperature programming of the furnace, the catalyst bed temperature lagged behind the furnace temperature according to the relationship: $T_{bed} = 1.05\ T_{furnace} - 34°C$. As expected, iso-butene, the most reactive of the four olefins, was the only one to show any activity in the temperature range 30 - 120°C. This gas was therefore chosen as the reactant olefin for the TG-DTA study.

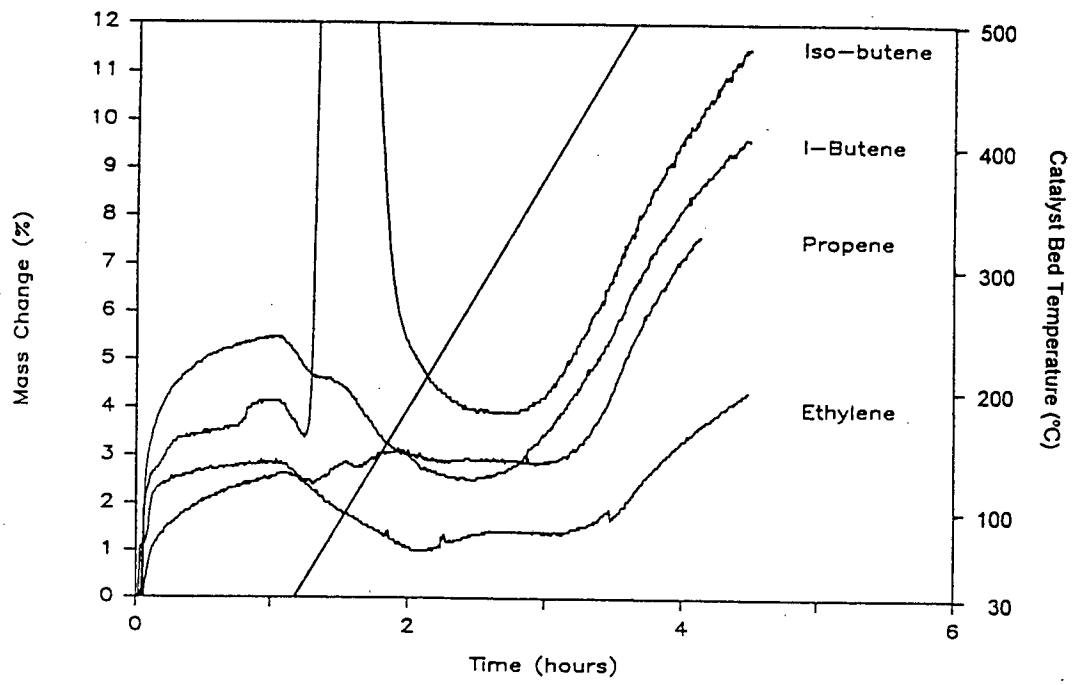

Figure 3.9 Reactivity of ethene, propene, 1-butene and iso-butene over NiSMM-7-F

3.2.1.2 Iso-butene reactivity on NiSMM-7-F

The TGA and DTA results of iso-butene reaction over NiSMM-7-F are given in Figure 3.10(a) and (b), respectively. The first hour depicts isothermal adsorption at 30°C. The maximum mass gain was attained quickly as seen by the adsorption exotherm and sharp initial mass increase. As the temperature programming began, weakly held species desorbed (DTA endotherm and TGA mass loss). The start of reaction was taken as the point at which the catalyst began to gain mass after losing weakly held species. This was 48°C for NiSMM-7-F. Upon reaching reaction temperature iso-butene oligomerization caused a sharp mass gain and a reaction exotherm.

The temperature at which the maximum reaction occurred was given by the peak temperature of the reaction exotherm, i.e. 67°C. This corresponded to the maximum rate of mass increase in the TGA. Above 89°C the reaction decreased and the product desorbed from the catalyst as represented by a mass loss and a DTA endotherm.

Both sorption and reaction contributed towards the exotherm at 67°C. As this exotherm occurs at a higher temperature than the isothermal adsorption exotherm at 30°C, the contribution of sorption to the oligomerization exotherm must be less than that of the adsorption exotherm at 30°C. The areas under the exotherm at 30°C and at 45 - 90°C were in the ratio 1:37. Hence it follows that the exotherm at 45 - 90°C is due primarily to reaction. The area under the DTA reaction peak or mass gain of the TGA peak may be used to estimate the relative extent of reaction between catalysts.

After oligomerization two exotherms occurred in the endothermic region of the DTA curve, viz. at 143°C and 184°C. The TGA curve showed a steady increase due to the build up of coke deposits.

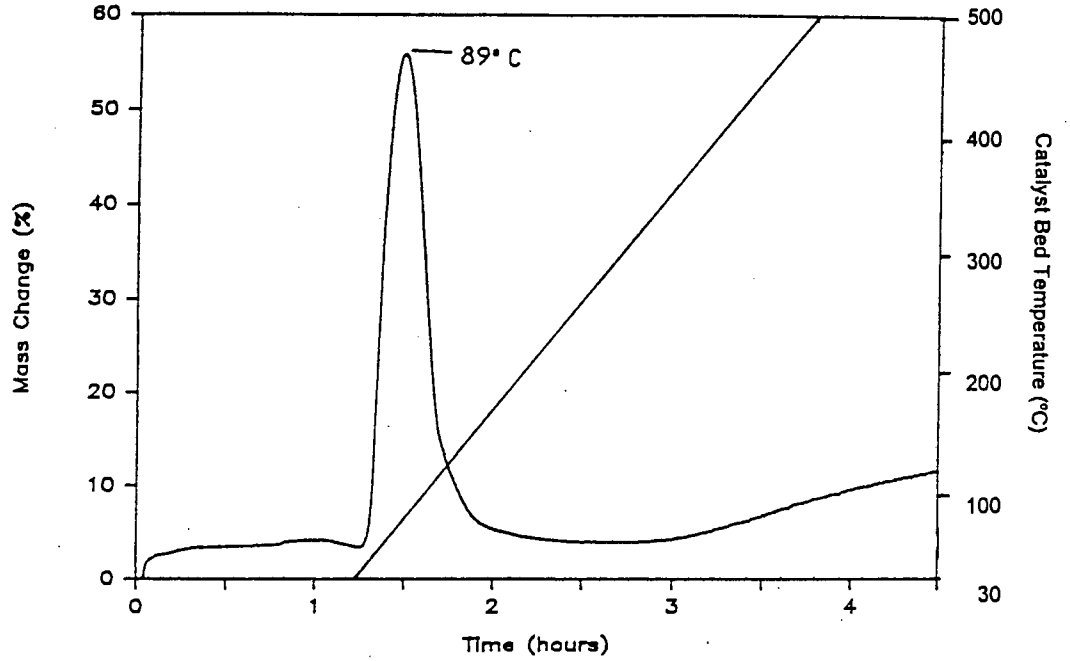

Figure 3.10 (a) TGA of iso-butene over NiSMM-7-F

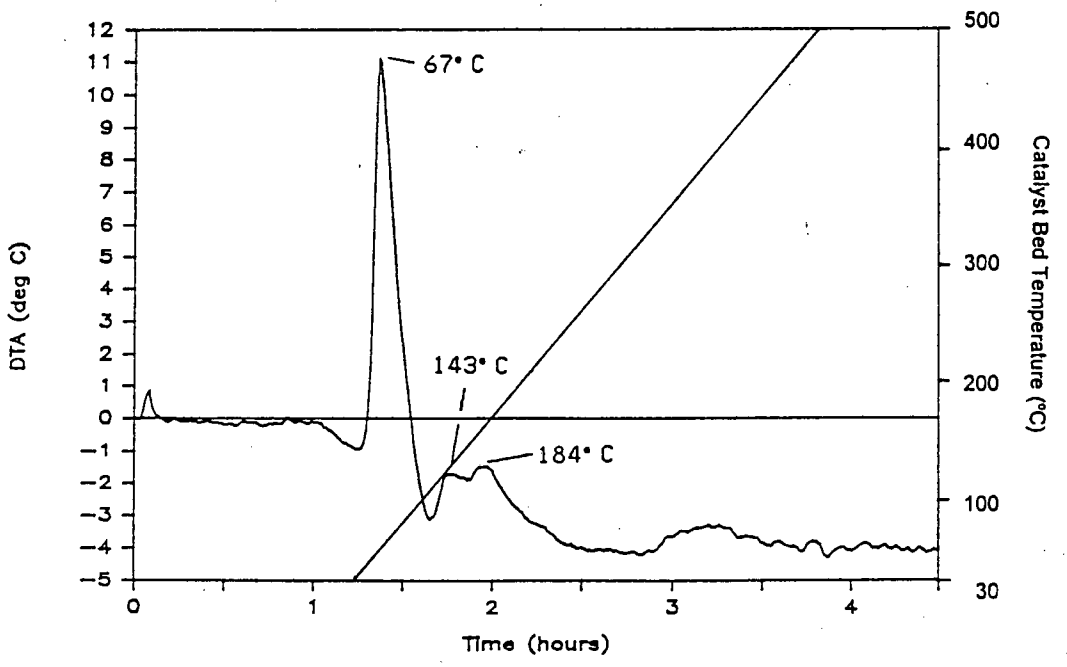

Figure 3.10 (b) DTA of iso-butene over NiSMM-7 F

In order to examine whether the iso-butene reaction was between two molecules adsorbed on adjacent acid sites or between an adsorbed molecule and one in the gas phase, the reactant gas flow was switched off after the 1hr adsorption phase at 30°C in one experiment. Dry N_2 without iso-butene was passed over the catalyst while the temperature was raised from 30°C to 500°C in the usual manner. There was no evidence of reaction in either the DTA or TGA data, as the temperature increased, the iso-butene merely desorbed from the catalyst surface.

3.2.1.3 Low Pressure Micro-reactor Study

To characterise the DTA peaks found in the iso-butene study over NiSMM-7-F product analysis was undertaken on a low pressure (operated under atmospheric pressure conditions) micro-reactor line converting iso-butene over NiSMM-7-F at four different temperatures, viz. 60-100°C, 130°C, 170°C and 270°C. The liquid product analyses are given in Table 3.9. As this study was conducted purely in an attempt to identify the temperature peaks seen in the DTA results of Section 3.2.1.2, only quantitative analyses were conducted on the post-reaction gaseous product samples. The C_4 and C_8 content of the quantitative analyses done on the liquid samples was excluded from the data presented since these oligomers would also have been present in the gas phase, making the data meaningless. The C_{18+}/C_{12} ratio was used to indicate the reaction selectivity at the different temperatures.

Table 3.9 Liquid product analysis of NiSMM-7-F low pressure micro-reactor study

Oligomer* (Mass %)	Temperature			
	60-100°C	130°C	170°C	270°C
C_{12}	65.9	48.9	35.4	32.7
C_{16}	6.7	14.6	10.0	13.6
C_{18+}	1.1	3.2	4.4	9.0
C_{18+}/C_{12}	0.017	0.065	0.12	0.28

* $C_{12} = C_{10\text{-}13}$; $C_{16} = C_{14\text{-}17}$; $C_{18+} = C_{18}$ + higher oligomers

The presence of C_{12}, C_{16} and C_{18+} oligomer groups in the 60 - 100°C temperature range indicated that the reaction peak in the DTA data at 67°C was due to oligomerization of iso-butene. The oligomerization reaction continued even up to 270°C, although significantly less liquid product was produced at temperatures above 100°C. The increase in the C_{18+}/C_{12} ratio with increased temperature showed a shift to heavier products.

A qualitative gas analysis showed an increase in the number of butene isomers as the temperature was increased from 130-270°C. The exotherms at 143°C and 184°C in the DTA results are attributed to iso-butene hydrogenation as a small iso-butane peak appearing at 130°C increases markedly at 170°C before dropping off at 270°C. The hydrogen source for the hydrogenation reactions would probably result from initial coke formation which gives rise to cyclic hydocarbons and hydrogen. Coke formation at temperatures of 143°C is not usually considered to be of any significance. The quantities of iso-butene being hydrogenated were, however, very small as indicated by the size of the hydrogenation exotherms. At 130°C and above, endothermic cracking reactions occurred, the products of which (ethane, propene, propane, hexene and hexane) were seen at these temperatures. Hence the hydrogenation exotherms appearing in the endothermic region of the DTA graph.

3.2.1.4 Reaction During Iso-Butene Adsorption

A catalyst sample size of 20mg was initially used for the NiSMM-7-F study before reducing it to 15mg. The 20mg sample size resulted in a large adsorption peak occurring during the first hour of isothermal adsorption at 30°C. The mass increase and corresponding exotherm are shown in Figure 3.11(a) and (b), respectively. This mass increase was thought to be due to water adsorbing or reaction occurring at 30°C as the sample was covered in a liquid material when examined upon removal from the TG-DTA apparatus after the 1hr adsorption phase. It was not possible to discriminate between iso-butene oligomerization product and water by differences in boiling points as the expected

predominant dimer by carbonium ion addition is 2,2,4 trimethylpentene which has a boiling point of 101.44°C.

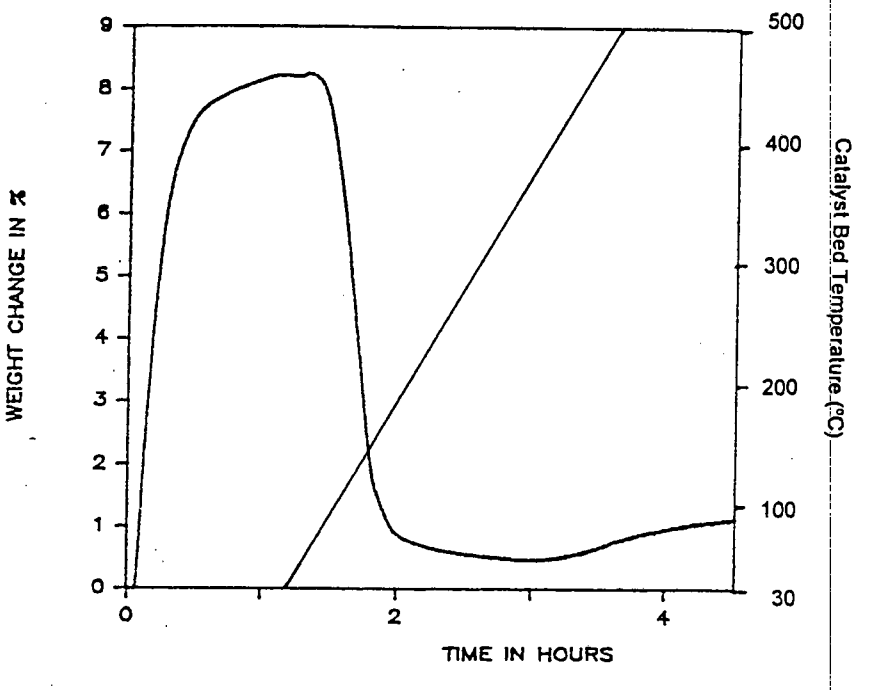

Figure 3.11(a) TGA of large adsorption peak for NiSMM-7-F

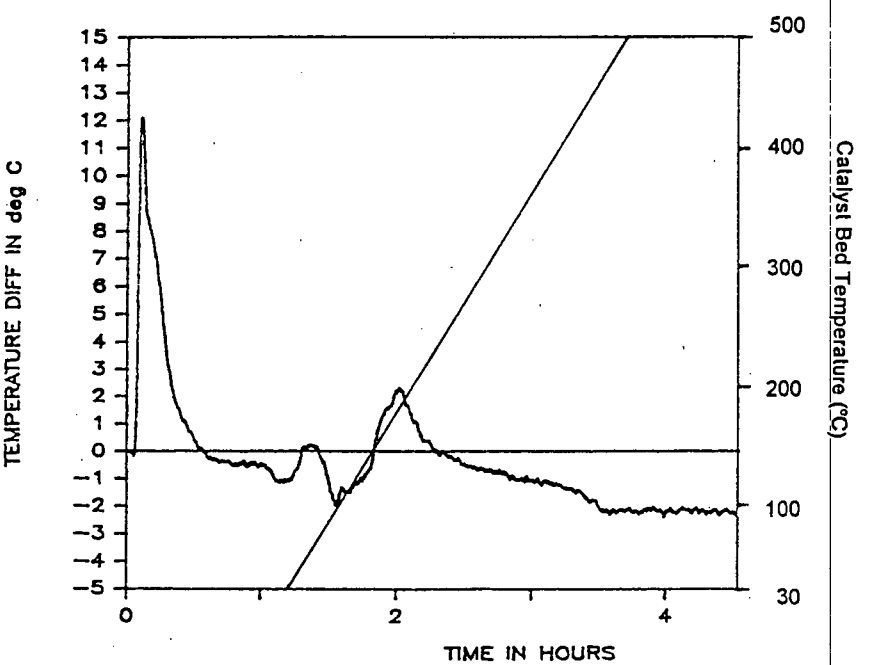

Figure 3.11 (b) DTA of large adsorption peak for NiSMM-7-F

The temperature programmed desorption DTA curve of the catalyst in N_2 after the 1hr isothermal 'large adsorption' had occurred was compared to those of NiSMM-7-F saturated

with a drop of water and another sample saturated with a drop of liquid product that was obtained from the atmospheric micro-reactor study. These curves are shown in Figure 3.12.

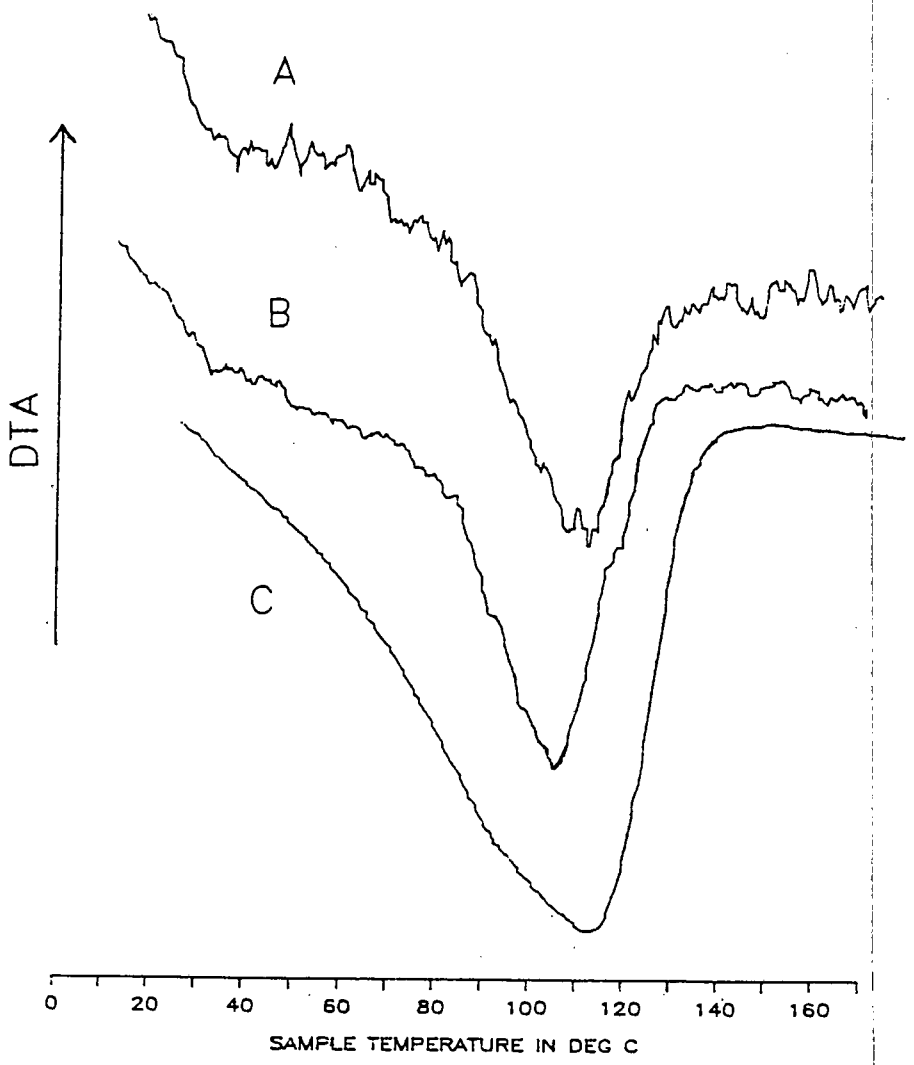

Figure 3.12 Temperature programmed desorption DTA of :
A-' Large adsorption' catalyst
B- Catalyst saturated with oligomerization liquid product,
C - catalyst saturated with water (reduced 5 times)

The profiles of (a) the 'large adsorption' catalyst and (b) oligomerization product catalyst were similar and both different from that of (c) the water saturated catalyst. The magnitudes of the peaks for (a) and (b) were also much the same and five times less than that of (c). The 'large adsorption' was thus attributed to oligomerization of iso-butene

occurring at 30°C. Iso-butene has been shown by Haag (1967) to exhibit activity at 20°C. This was, however, at a higher pressure of 150psi (1.03MPa). The DTA peak maximum of 12°C in Figure 3.11(b) when added to the adsorption temperature of 30°C is 42°C which is close to the temperature of 48°C ascribed to the start of the oligomerization reaction in Section 3.2.1.3

Lowering the iso-butene partial pressure in the feed, varying the feed flowrate and diluting the sample with glass beads were unsuccessful in eliminating oligomerization at 30°C. The large peaks were not seen when the catalyst mass was reduced from 20mg to 15mg. Catalyst masses of 5mg and 10mg also achieved this.

3.2.2 Iso-butene and Water Chemisorption on NiSMM-7-F

The chemisorption levels of iso-butene and water on NiSMM-7-F are given in Table 3.10 and are relative to dry NiSMM-7-F calcined at 500°C. NiSMM-7-F adsorbed 2.6% iso-butene compared to SMM-F which was found to adsorb 1.2%. These adsorption levels correspond to 2.8 x 10^{20} molecules/g for NiSMM and 1.3 x 10^{20} molecules/g for SMM.

Table 3.10 Iso-butene and Water Chemisorption on NiSMM-7-F

Adsorbing Species	Mass %	Molecules x 10^{-20}/g
Iso-butene	2.6	2.8
Water	1.5	5.1
Water adsorption followed by iso-butene	1.5 2.0	5.1 2.2
Iso-butene and water	2.7	Unknown
Iso-butene adsorption followed by water	2.6 0.5	2.8 1.8

Table 3.10 shows that less iso-butene (2.0%) was adsorbed when the catalyst had previously chemisorbed water (1.5%). Water adsorption levels were also reduced (0.5%) when preceded by iso-butene adsorption. During competitive adsorption, iso-butene and water co-fed, the combined level of 2.7% was slightly less than that achieved when water adsorption preceded iso-butene (3.5%) and similar to that when iso-butene was adsorbed first (3.1%), considering that error levels of 0.2% were possible in this study.

3.2.3 Comparison of SMM-F, NiSMM-7-F and ZSM-5

The thermal analysis of iso-butene on SMM-F, NiSMM-7-F and ZSM-5 are shown in Figure 3.13(a) and (b). During the isothermal adsorption at 30°C, ZSM-5 adsorbed the most iso-butene (9.3%), followed by NiSMM-7-F (4.1%) then SMM-F (2.1%). At the beginning of the temperature programming NiSMM-7-F and ZSM-5 lost 17% and 16% as weakly held species respectively, of the initial mass absorbed before reaction started. SMM-F lost only 5%.

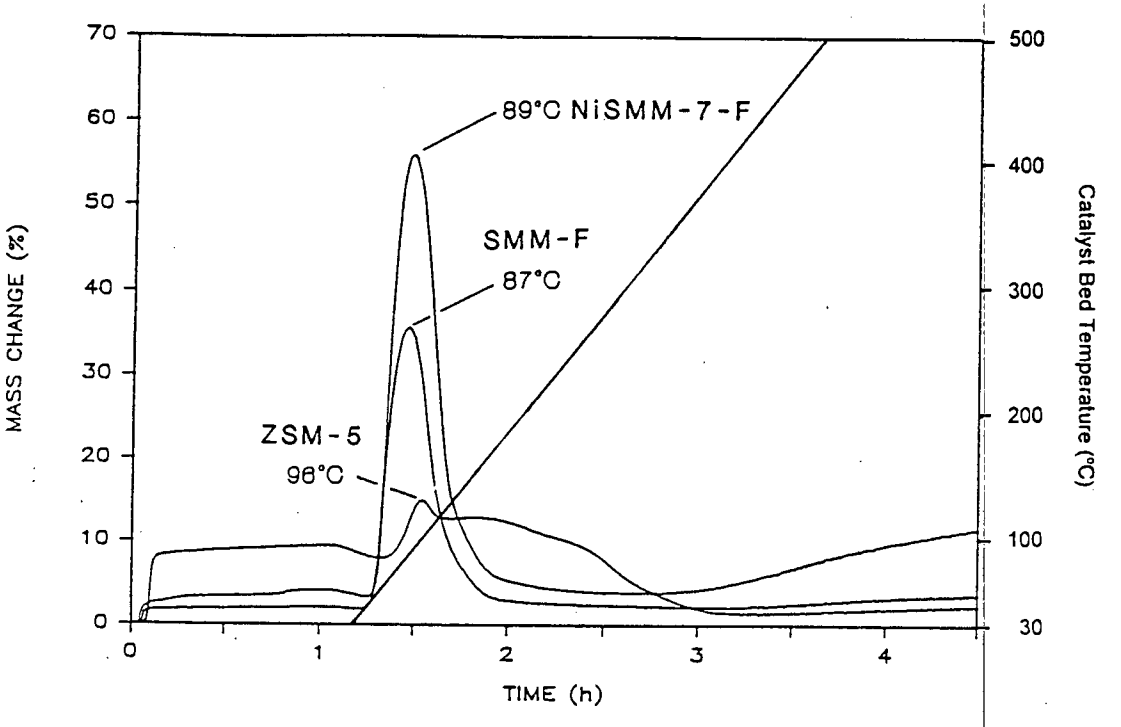

Figure 3.13(a) TGA of iso-butene over NiSMM-7-F, SMM-F and ZSM-5

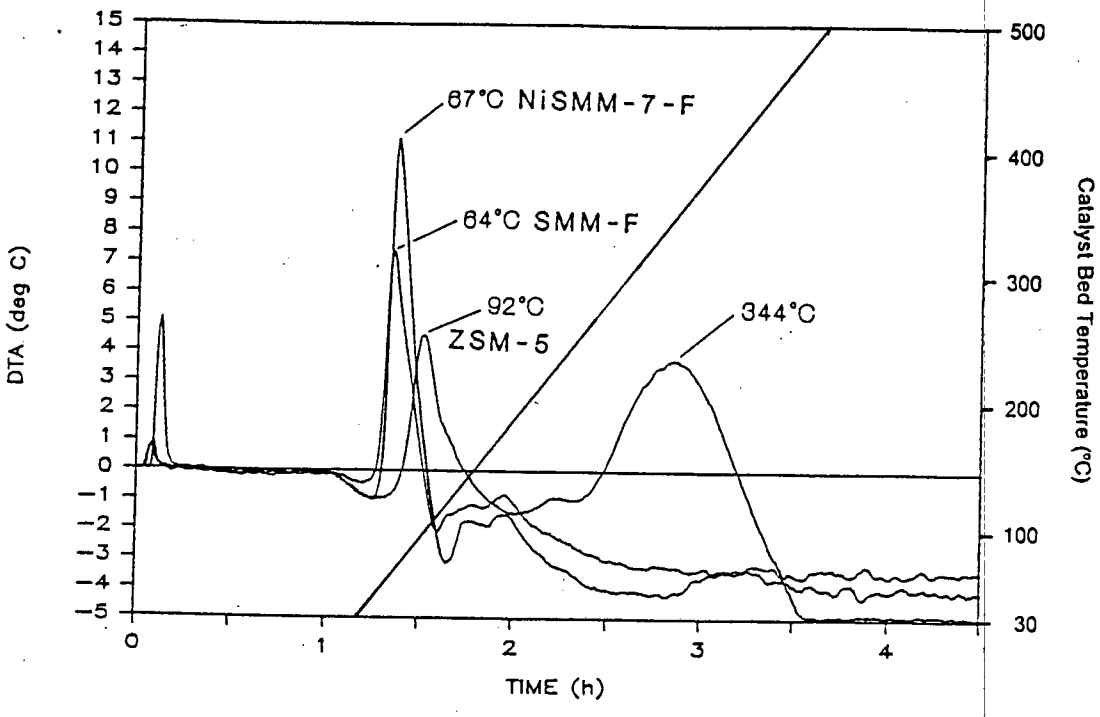

Figure 3.13 (b) DTA of iso-butene over NiSMM-7-F, SMM-F and ZSM-5

Oligomerization started first on SMM-F (44°C) followed at 48°C by NiSMM-7-F and at 60°C for ZSM-5. The maximum of the DTA exotherm followed the same trend as did the point at which reaction decreased and desorption of the products dominated the mass change. This was 87°C and 89°C for SMM-F and NiSMM-7-F and 96°C for ZSM-5. The extent of reaction as measured by the mass gain in the TGA or areas under the DTA reaction curves was greatest for NiSMM-7-F followed by SMM-F with ZSM-5 being the most unreactive of the three catalysts under these conditions. Reaction occurred over a greater temperature range for ZSM-5 as can be seen from the shoulders on the reaction peaks in Figure 3.13.

The DTA exotherms ascribed to hydrogenation occurred on both SMM-F and NiSMM-7-F and not on ZSM-5. The large exotherm at 344°C in the case of ZSM-5 was probably caused by aromatisation as suggested by Gilson (1982) who used ethene as a reactant over ZSM-5. After 3hr the TGA curves showed the onset of coke formation. Figure 3.6(a)

shows that NiSMM-7-F, the most reactive of the three catalysts, had a greater build-up of coke than SMM-F and ZSM-5.

3.2.4 Effect of Ion-exchanging SMM-F with Ni, Co and Zn

Figure 3.14 shows the effect of ion-exchanging with Ni, Co and Zn on the oligomerization of iso-butene over SMM-F. Only the reaction zone of the TGA curve is shown (1-2h, corresponding to 30-181°C). The presence of the ion-exchange metals increased the extent of reaction in all cases. Ni and Co gave identical results and are thus represented by the same curve. Zn was marginally more reactive than Ni and Co, while all three increased the TGA peak maximum by 3°C.

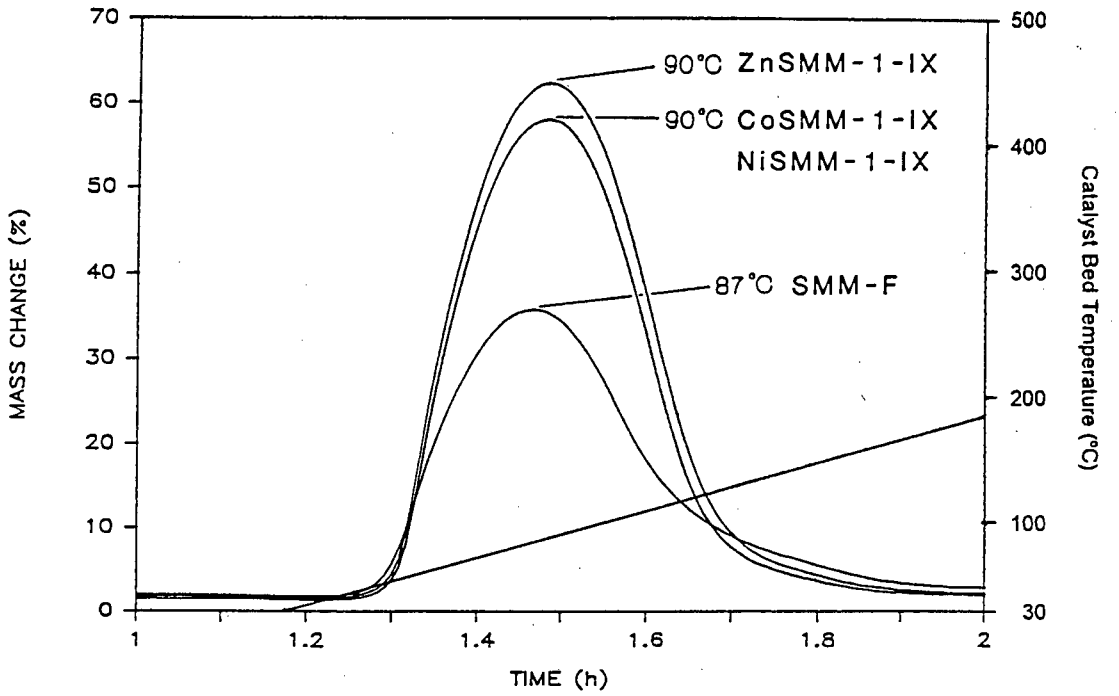

Figure 3.14 TGA of iso-butene reaction over Ni-, Co-, ZnSMM-0.06-F-IX and SMM-F

3.2.5 Effect of water on iso-butene adsorption and reaction on NiSMM-7-F.

The effect of introducing water into the feed gas is shown in Figure 3.15(a) and (b) for NiSMM-7-F. Four curves are given: (i) a completely dry run, as per Figure 3.10(a) and (b); (ii) water present only during the adsorption phase (first hour of the run); (iii) water present

throughout the run; (iv) as for (i) except that the calcined catalyst was exposed to wet N_2 feed for 1hr and then flushed with dry N_2 for 6hr, resulting in a hydrated catalyst surface.

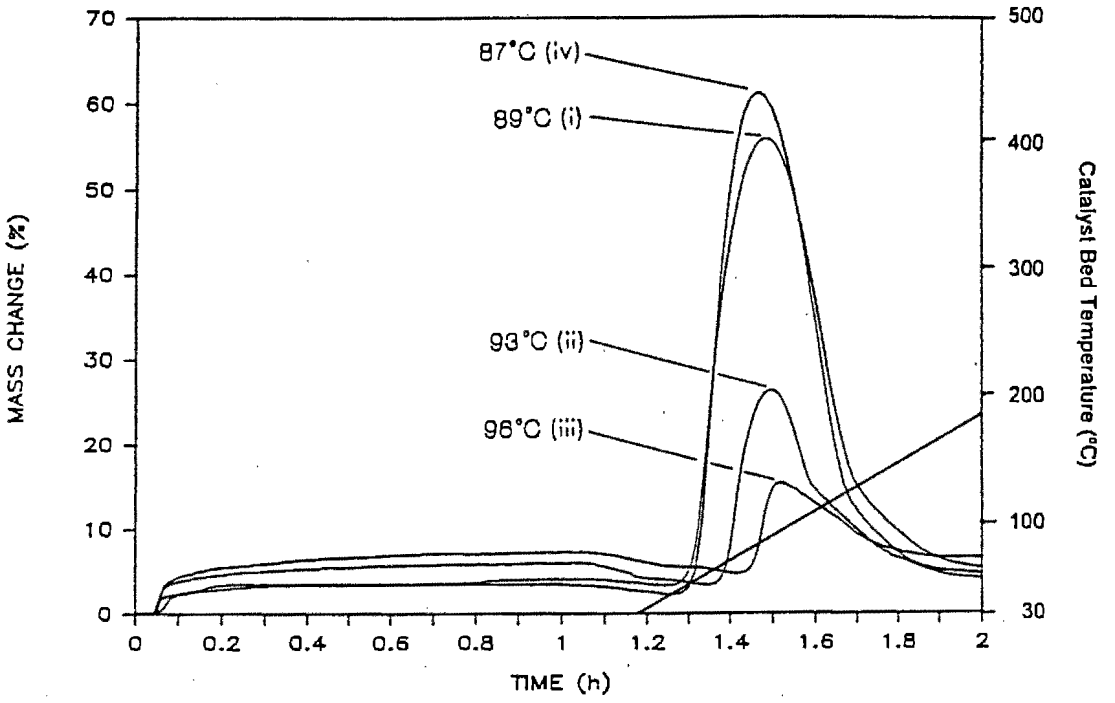

Figure 3.15 (a) TGA of the effect of water on the iso-butene adsorption and reaction over NiSMM-7-F
(i) Dry reaction (ii) Water during adsorption
(iii) Water throughout run (iv) Dry reaction on hydrated surface

The presence of water in the feed during the adsorption step caused a mass increase of 6.0-7.3% as opposed to 4.1% for the dry run Figure 3.15(a). The amount of weakly held species that desorbed, before reaction started, increased with the increase presence of water: 17% for (i), 36% for (ii) and 43% for (iii). The temperature at which oligomerization occurred also increased in the presence of water. The DTA peak maximum increased from 67°C to 82°C (ii) and 95°C (iii) (Figure 3.15(b)). The extent of reaction was also lowered and was clearly seen in the TGA curves in Figure 3.15(a) where the extent of mass gain was reduced from 56.1% (i) to 26.1% (ii) and 15.7% (iii). The mass increase due to iso-butene adsorption in (iv) was only 3.5% but the amount of weakly held species that desorbed was large (36% of the initial adsorption). The extent of reaction was slightly

higher than that in (i) (61.2% mass gain compared to 56.1%) and the DTA reaction peak occurred at a temperature 16°C higher.

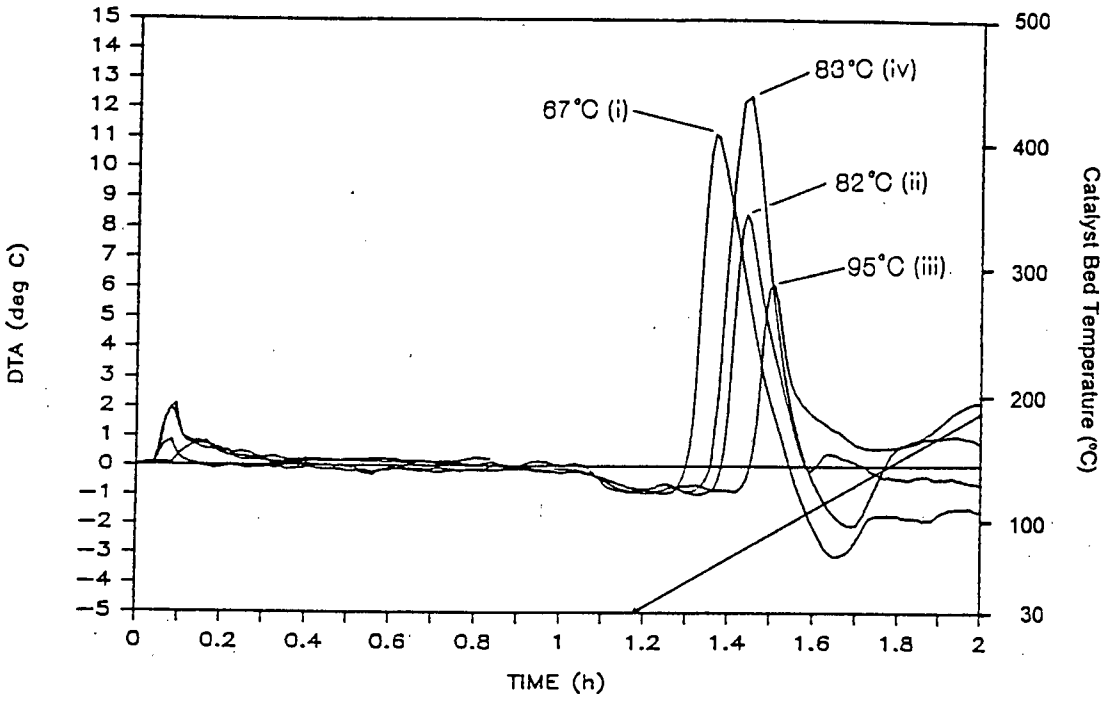

Figure 3.15 (b) DTA of the effect of water on the iso-butene adsorption and reaction over NiSMM-7-F
(i) Dry reaction (ii) Water during adsorption
(iii) Water throughout run (iv) Dry reaction on hydrated surface

3.3 Alkene Oligomerization

The high pressure oligomerization experiments conducted in this study used the propene reactant feed as described in Table 2.3. The feed was changed for the reactant partial pressure study of Section 3.3.10 in which the 1-butene/butane mixtures also described in Table 2.3 were used as feed.

In all cases a reaction temperature of 130°C and a pressure of 5MPa(g) were used. Unless otherwise indicated the catalyst size fraction was 75μm to 106μm and the calcination temperature 500°C. The high weight hourly space velocities of 90 and 50g/g.hr were employed to limit conversion levels in an attempt to approach differential reactor operation for the purpose of comparing catalyst performance. This mode of reactor operation also moderated temperature rise during reaction which has been indicated by Fletcher (1984) to be a problem. A catalyst bed size of 0.5g was consistently used except for the 1-butene partial pressure study in which the bed was 1.0g.

3.3.1 Analytical Technique

The feed and product stream compositions of the oligomerization reaction were analysed off-line, as explained in Section 2.4.3. The total gas mass flow was recorded by the wet gas flow meter. The analysis of the gaseous stream, however, did not include any C_6 and C_9 oligomers. The gas chromatograph used for the gaseous stream was not temperature programmed for the analysis but was set isothermally at 50°C. Under these conditions the C_6 and C_9 oligomers would not be detected by the gas chromatograph. As a result the gas analysis was skewed in favour of the C_3 oligomer group. The conversion of propene to oligomerization products, calculated by liquid product mass, was therefore underestimated and the product distribution favoured the heavier oligomers that were detected in the liquid product sample.

The conversion was therefore calculated using propane (C_3) as an internal standard in the pre- and post-reactor streams. The basis is that the propane that enters the reactor, is the

same amount that exits. This was considered feasible at the reaction temperature used of 130°C.

The C_3 mass flowrate in the feed was compared to the total C_3 measured in the liquid and gaseous streams. The amount of C_3 in the liquid was subtracted from the amount in the feed. This is the quantity of C_3 that should be present in the exit gaseous stream. The correction factor used to adjust this amount to equate it to the amount in the feed (minus the C_3 liquid content) was also applied to the $C_3^=$ in the exit gas stream. This adjusted $C_3^=$ quantity was then used to calculate the conversion level for that particular time period. An example of this calculation is detailed in Appendix 12. This method was used to calculate the conversion levels for all the oligomerization reactions that used off-line gas chromatograph analysis for the exit gaseous stream.

3.3.2 Reproducibility

The reproducibility of propene conversion reaction for NiSMM-1 at weight hourly space velocities (WHSV) of 90 and 50g/g.hr is shown in Figure 3.16 (a) and (b), respectively. Good reproducibility of propene conversion level was seen at both WHSV's.

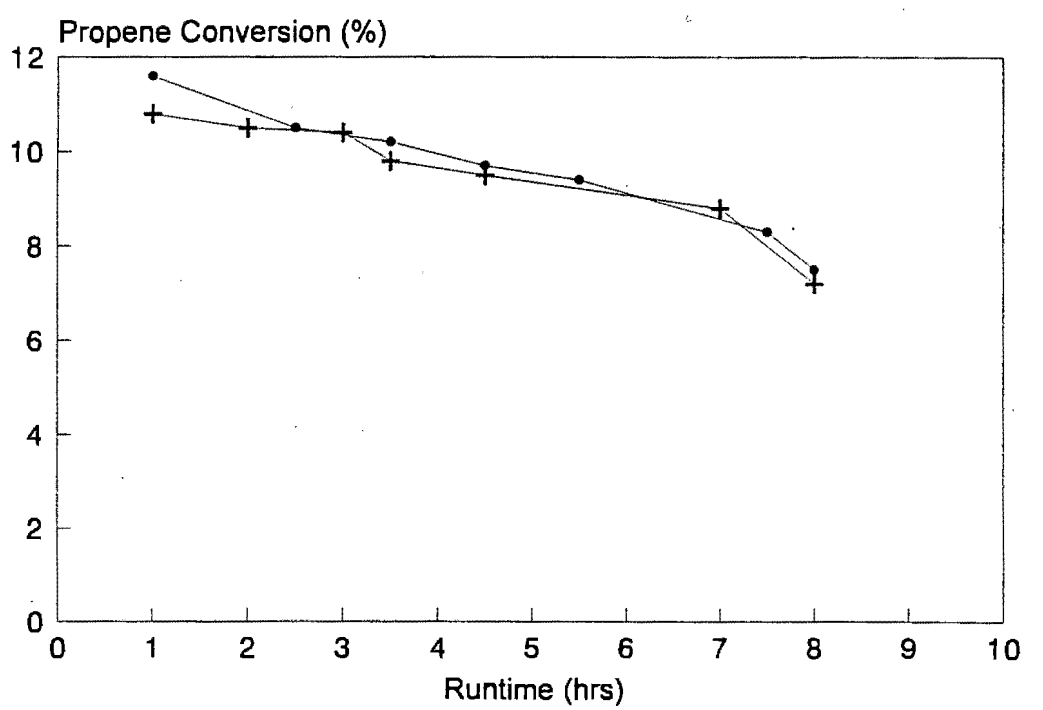

Figure 3.16 (a) Reproducibility of propene conversion over NiSMM-1 at a WHSV of 90 g/g.hr

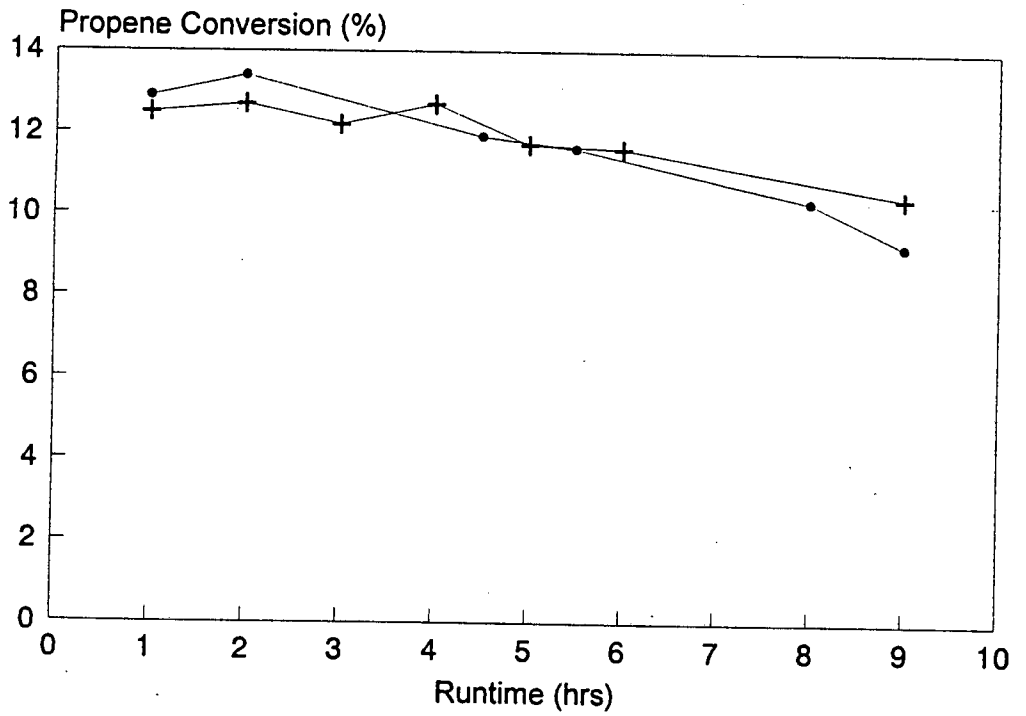

Figure 3.16 (b) Reproducibility of propene conversion over NiSMM-1 at a WHSV of 50 g/g.hr

3.3.3 Comparison between Synthesised and Commercial Catalysts

A comparison between the catalysts obtained from the Harshaw-Filtrol Corporation (SMM-F and NiSMM-7-F) and the equivalent catalysts synthesised in this work (SMM and NiSMM-7) is given in Figure 3.17 for propene conversion at a WHSV of 90g/g.hr. No result is shown for SMM as it was inactive under the conditions used. SMM-F deactivated after 4hr. NiSMM-7 realised higher conversion levels than NiSMM-7-F over the monitored run-time. At a WHSV of 8g/g.hr O'Connor, *et al.* (1988) found that the propene oligomerization performance (expressed in grams of liquid produced per gram of catalyst per hour) of NiSMM-7-F was almost three times greater than that of SMM-F. The results

shown in Figure 3.17 confirmed the enhanced activity of NiSMM-F over SMM-F as found by O'Connor *et al.* (1988).

The performance of NiSMM catalyst is therefore comparable to that of the commercial sample, NiSMM-7-F. The poor performance of the unsubstituted SMM may be due to it being synthesised according to the metal substituted SMM procedure which uses a shorter synthesis time. It was possible that the SMM was not fully crystallised.

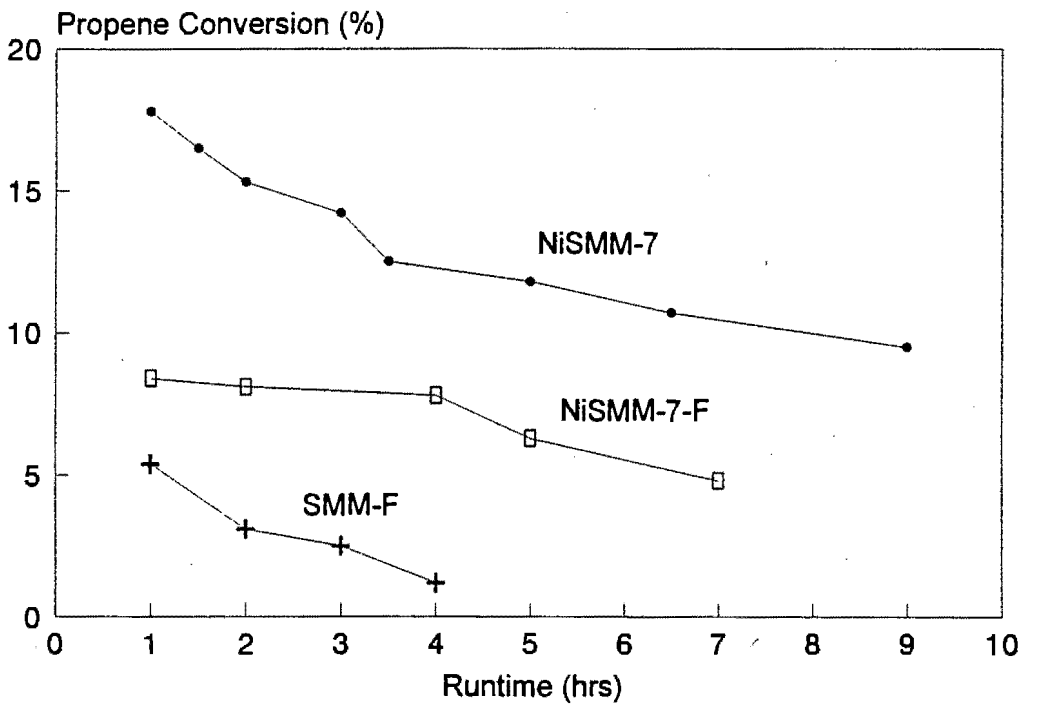

Figure 3.17 Comparison of propene conversion over SMM, NiSMM-7, SMM-F and NiSMM-7-F

3.3.4 Calcination Temperature

The effect of SMM calcination temperature on the propene oligomerization activity and lifetime was investigated by Fletcher, *et al.* (1986). They found a temperature of 500°C to be optimum. Calcination temperatures of 450, 500 and 600°C were therefore considered for propene oligomerization over NiSMM-1 at a WHSV of 50g/g.hr. The results are presented in Figure 3.18.

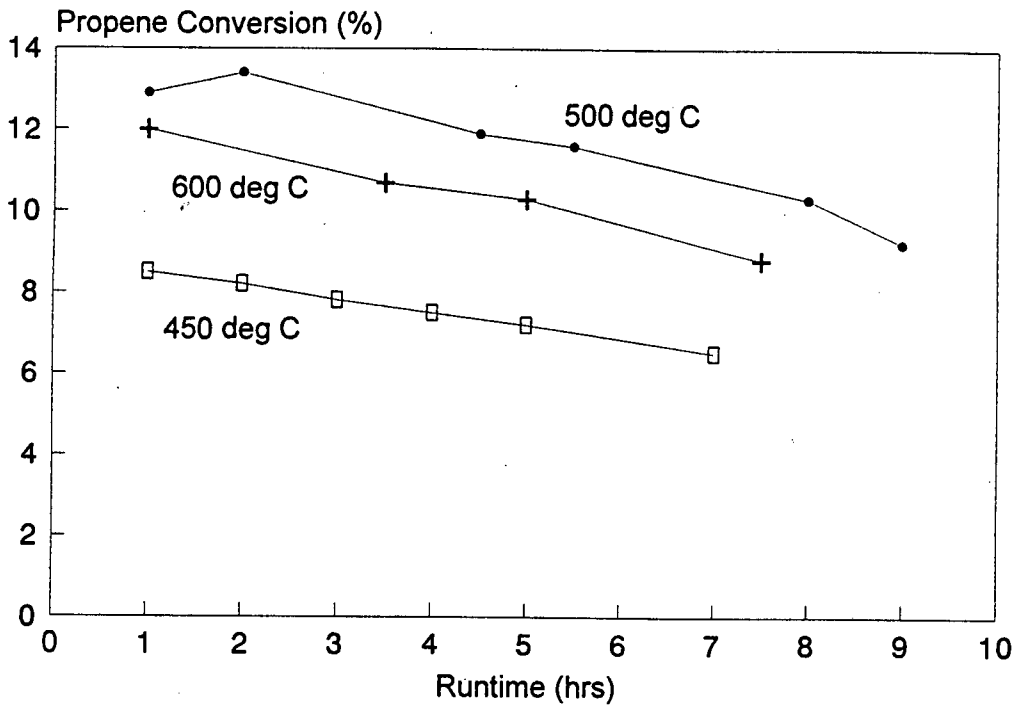

Figure 3.18 Effect of calcination temperature on propene conversion over NiSMM-1

In agreement with the findings of Kojima *et al.* (1986), a calcination temperature of 500°C resulted in the best activity of the three temperatures examined and was therefore used for all the catalysts in the alkene oligomerization study.

3.3.5 Effect of Wet Feed

It has been reported that the presence of moisture in the propene feed (wet feed) adversely affected the oligomerization performance of SMM (Fletcher *et al.*, 1986, O'Connor *et al.*, 1988). Fletcher *et al.* (1986) found that water in the feed resulted in rapid initial temperature runaway (147 to 277°C in 2min) with a corresponding increase in conversion level. This caused a reduction in catalyst lifetime. The effect of a feed that was not dried in the normal manner over 3A molecular sieves was investigated over NiSMM-7 at a WHSV of 90g/g.hr and is shown in Figure 3.19.

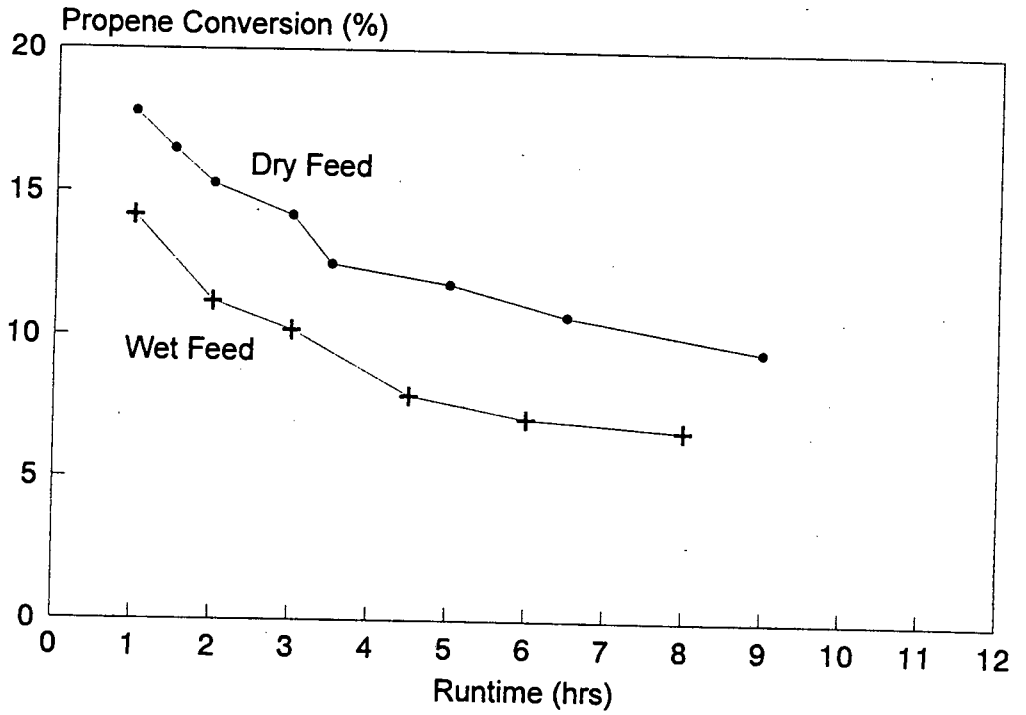

Figure 3.19 Effect of a wet feed on propene conversion over NiSMM-7

No initial increase in conversion level was seen. The conversion level in the presence of a wet feed was lower than that for a dry feed. The drastic reduction in catalyst lifetime caused by moisture, that had previously been found was not evident, even though the WHSV's used by Fletcher, *et al.* (1986) and O'Connor, *et al.* (1988) of 1.94 and 8, respectively, were lower than that of 90g/g.hr that was used in this study.

3.3.6 Effect of Synthesis pH

The propene conversion levels at a WHSV of 90g/g hr over NiSMM-7 synthesised in the pH range of 7.0 to 10.0 are given in Figure 3.20.

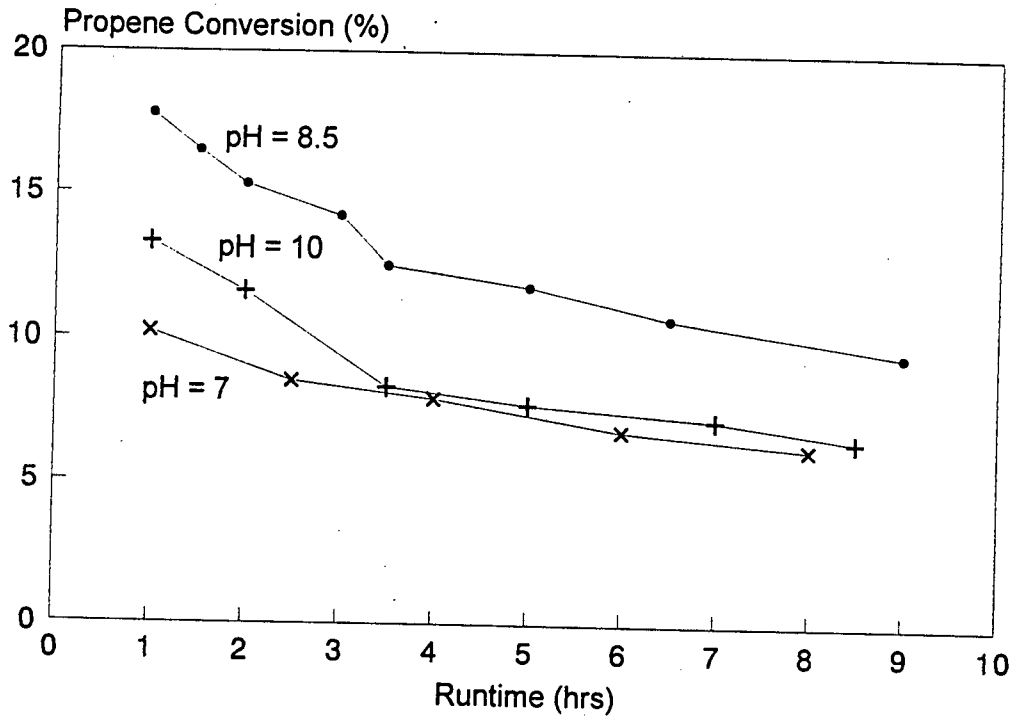

Figure 3.20 Effect of synthesis pH on propene conversion over NiSMM-7

White and Zelazny (1988) have shown that pH can affect the acidity of the particle edges of smectites. There is therefore a pH dependant component in the cation exchange capacity (CEC) of layered clays of this type. The synthesis pH of the nickel substituted SMMs was reported by Black, *et al.* (1976) to be between 8.0 and 8.5 without commenting on its effect on structure, acidity or activity.

The catalyst synthesised at a pH of 8.5 achieved a higher conversion level than the catalysts synthesised at pH's of 1.0 and 10.0, respectively. This was the pH used for the synthesis of all the other metal substituted SMM.

3.3.7 Reactant Flowrate

The effect of the propene flowrate, through the catalyst bed on the conversion level for NiSMM-1 is given in Figure 3.21. The variations in propene flow rate were used to establish product selectivity effects as a result of changes in propene conversion level to use comparatively with selectivity data generated at a later stage (Section 3.3.8) due to changes in nickel content. The propene conversion was seen to decrease with increasing propene flowrate. The conversion level increased only marginally by halving the flowrate from 90 to 50g/g.hr. The increase was more marked by flowrate reductions to 10g/g.hr and 2g/g.hr.

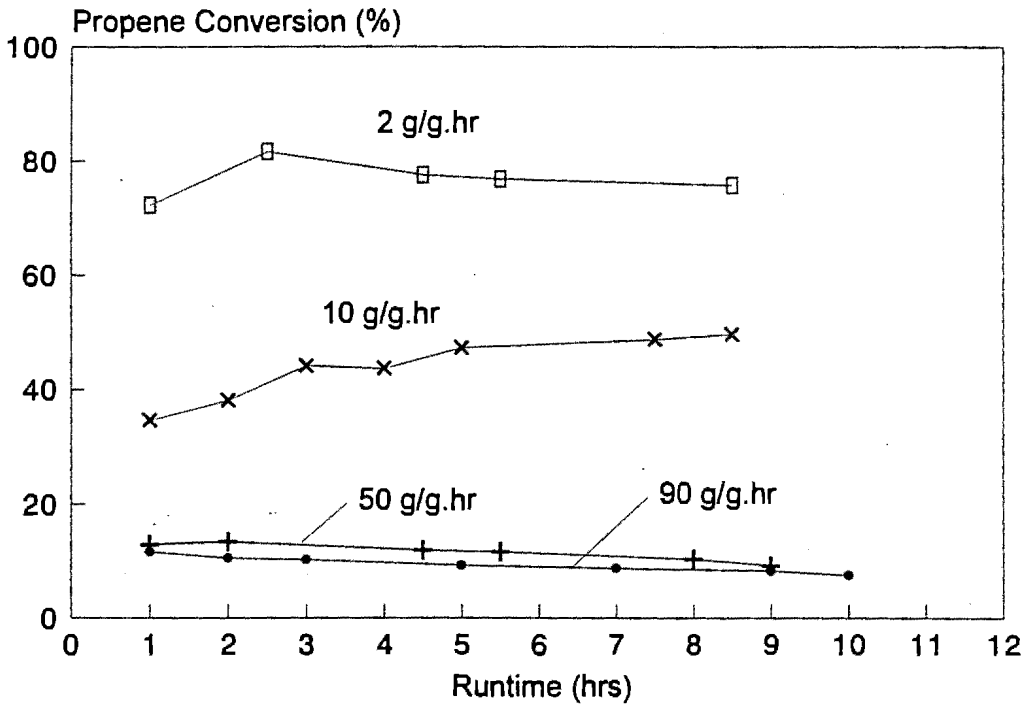

Figure 3.21 Effect of reactant flowrate on propene conversion over NiSMM-1

The data in Figure 3.21 is shown in Figure 2.22 as propene consumption at the different reactant flow rates. Unlike the propene conversion levels at 50g/g.hr and 90g/g.hr, the propene consumption rate at these flow rates did not show convergence to a particular catalyst utilisation rate. Weight hourly space velocities in excess of 90g/g.hr would be required to achieve the maximum catalyst utilisation rate. The speed of the oligomerization

reaction was seen by the fact that the maximum catalyst utilisation rate was not yet reached at high WHSVs of 90g/g.hr.

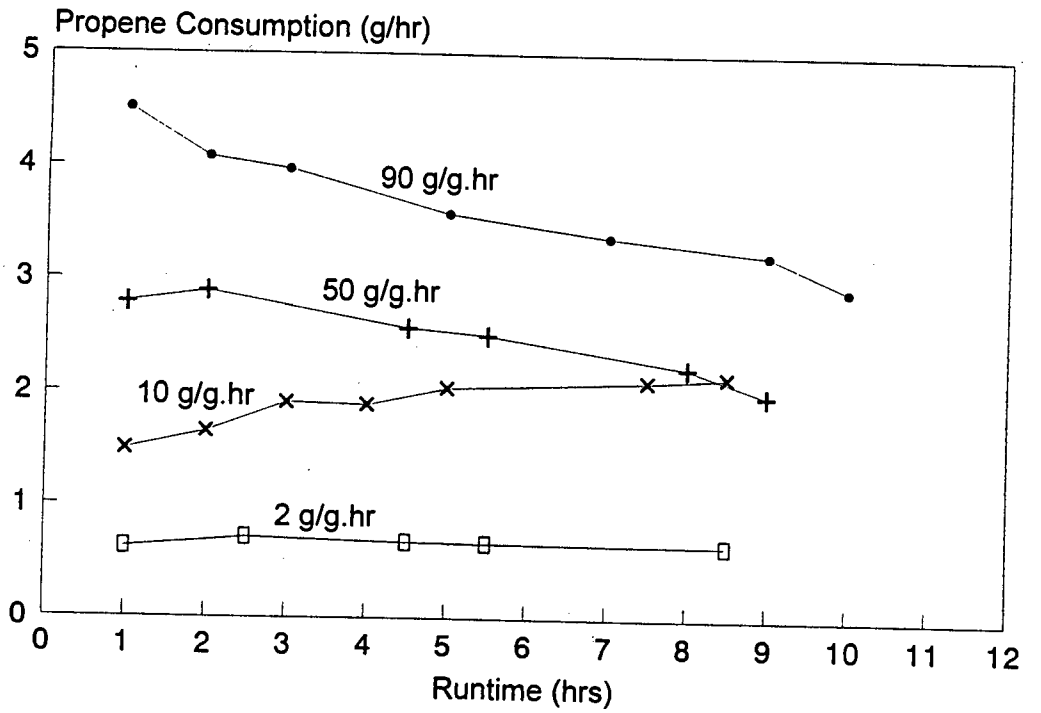

Figure 3.22 Propene consumption at varying reactant flow rates over NiSMM-1

Due to the absence of complete C_6 and C_9 oligomer analyses, the product distribution is represented by the C_{12+} oligomer grouping. Variations in this value demonstrate shifts in the weight fraction distribution of the reaction product. The C_{12+} fraction is shown as a mass percentage of the converted propene for the different reaction flow rates in Figure 3.23.

The percentage C_{12+} was seen to increase from 29% to 59% over a propene conversion range which increased from 7 to 81%. This trend was expected from a series oligomerization reaction mechanism. For the each of the WHSVs the percentage C_{12+} increased with increasing conversion.

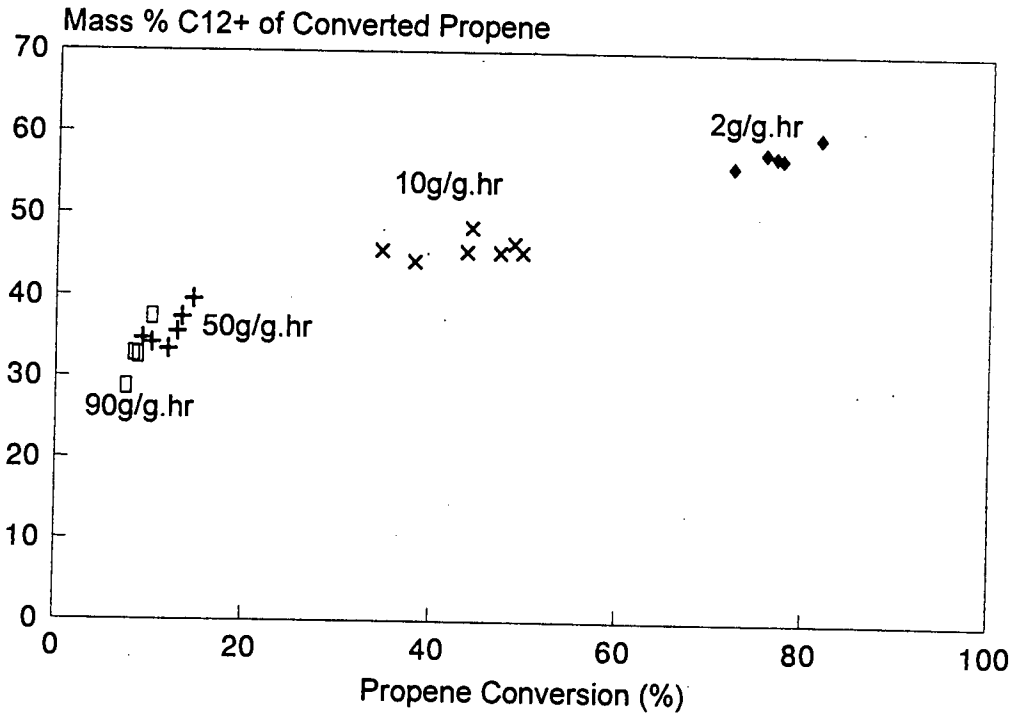

Figure 3.23 Mass % C_{12+} of converted propene at varying reactant flow rates over NiSMM-1

3.3.8 Nickel Content

The propene conversion levels at WHSV of 90g/g hr over nickel substituted SMM of varying nickel content is shown in Figure 3.24. The rate of deactivation increased with nickel loading and the initial conversion levels (1hr) were thus used for activity comparisons. The activity increased from a conversion level of 10.2% from NiSMM-1 to 39.8% for NiSMM-34. NiSMM-34, having the highest nickel content, also had the highest initial conversion level and the greatest rate of deactivation.

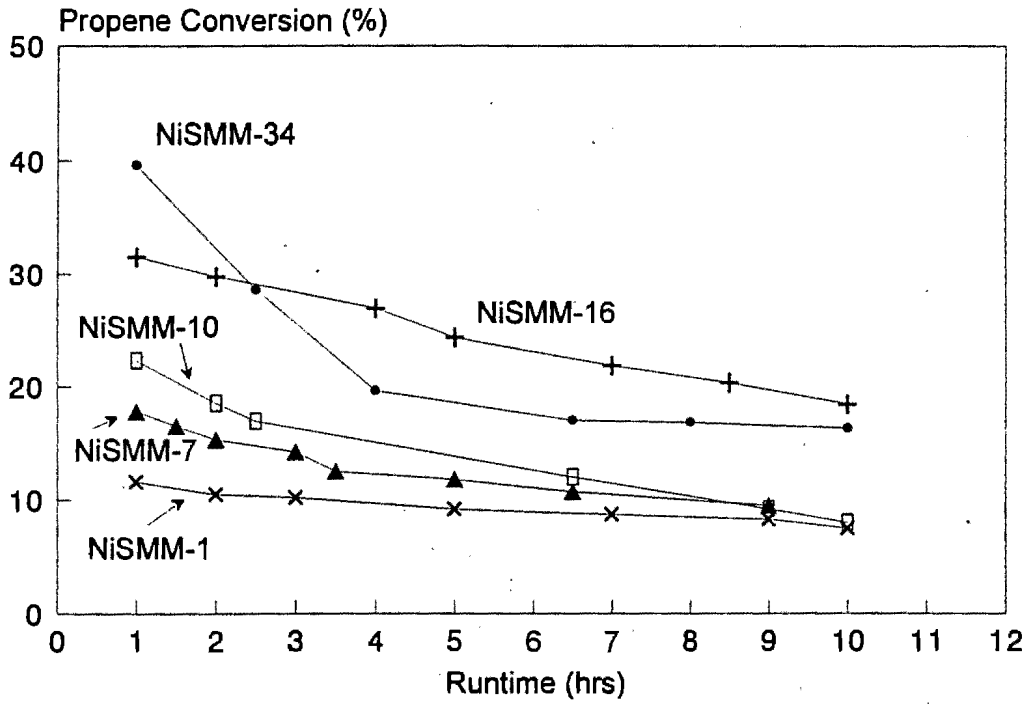

Figure 3.24 Effect of nickel content on the propene conversion over NiSMM

The percentage C_{12+} is presented as a function of conversion level in Figure 3.25. The product is seen to become heavier with increasing conversion level for each of the nickel catalyst used. This was again consistent with a series oligomerization reaction mechanism. The data when viewed collectively for all the nickel catalysts, as given by the two bordering dotted lines, appears to show a lighter product being formed as the conversion level is increased. This is contrary to the trend shown by the propene flow rate and the individual NiSMM catalyst experiments. Two factors were, however, changing in the data presented in Figure 3.25, viz. propene conversion level and nickel content. The effect of an apparent reversal in the selectivity trend with conversion that was seen in Figure 3.25 was due to the effect of nickel loading on the product distribution. This can be seen at a constant conversion level where the product was seen to become lighter with increased nickel content. This is demonstrated by the solid vertical line between 15% and 20% conversion in Figure 3.25. Nickel content had a marked effect on the product spectrum, particularly at the higher metal loadings (>10%).

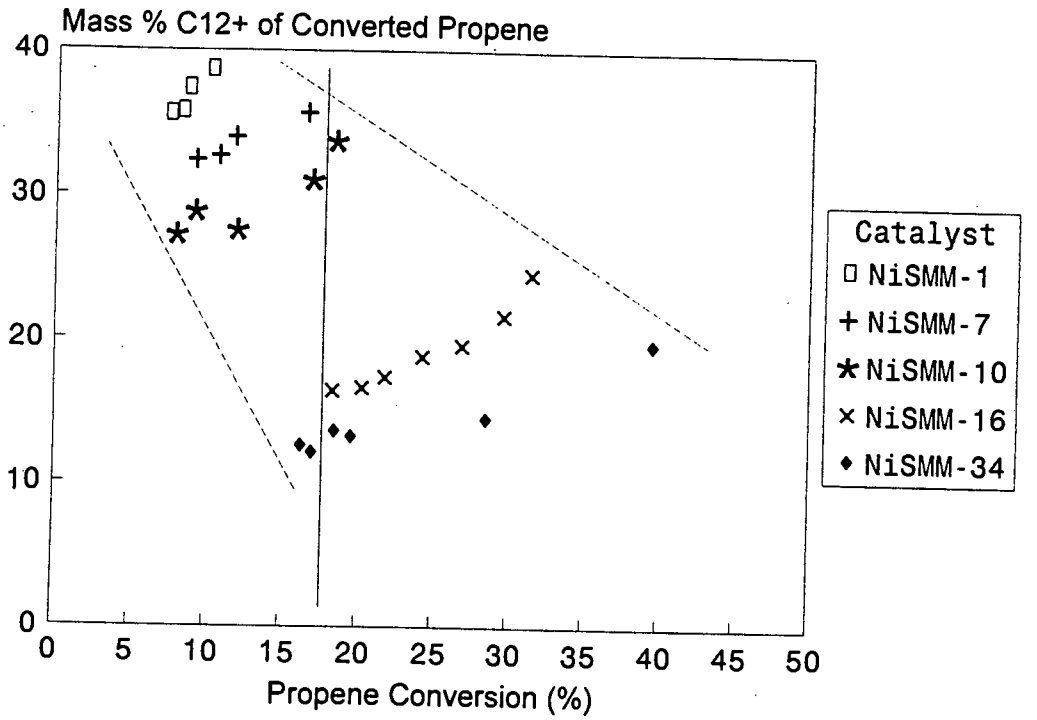

Figure 3.25 Mass % C_{12+} of converted [propene at varying nickel content in NiSMM

3.3.9 Cobalt and Zinc Content

The propene conversion levels over the cobalt and zinc substituted SMM catalysts at a WHSV of 90g/g hr are shown in Figure 3.26. NiSMM-1 has been included for comparative purposes. Under the conditions used CoSMM-33, ZnSMM-7 and ZnSMM-31 were all inactive and hence no results are observed in Figure 3.27. Unlike NiSMM which showed an increase in activity with increasing metal content, CoSMM and ZnSMM showed a decrease in activity as metal content was increased. At similar metal loadings conversion levels decrease as NiSMM > CoSMM > ZnSMM.

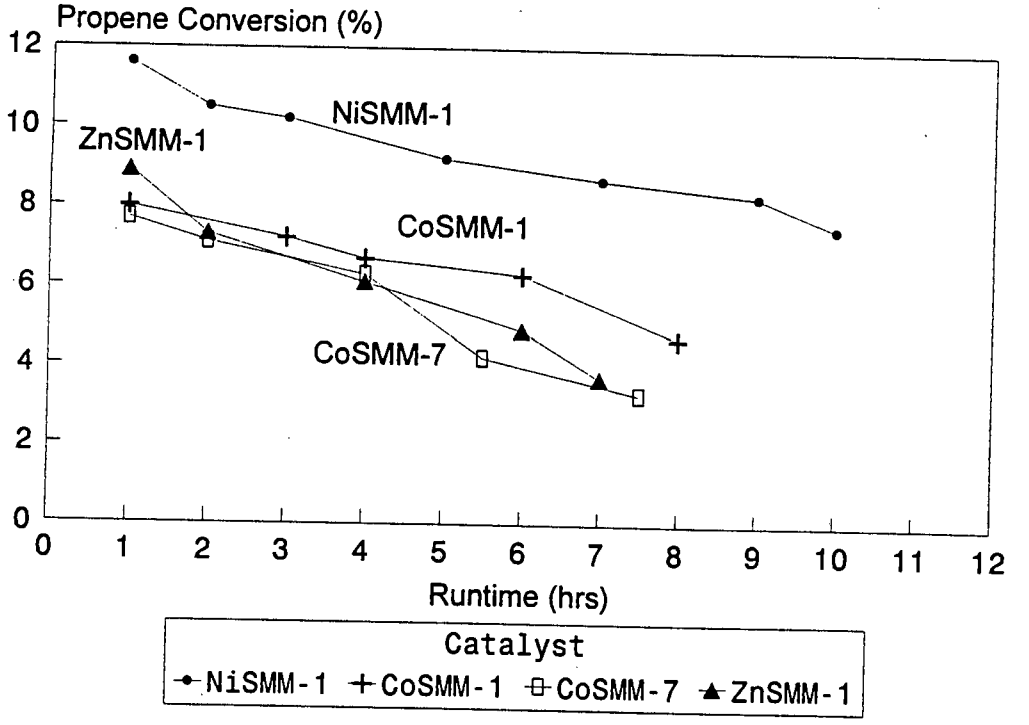

Figure 3.26 Effect of varying cobalt and zinc content on propene conversion over Co- and ZnSMM

The C_{12+} product content for these catalysts after a runtime of 1hr is given in Table 3.11 together with NiSMM-7. NiSMM and CoSMM had essentially the same product C_{12+} contents of 28 and 29%, respectively, at a 1% metal loading. This was lower, at 18.5%, for ZnSMM at the same metal content.

Table 3.11 C_{12+} content for Ni and CoSMM-1 and -7 & ZnSMM-1

Catalyst	Conversion After 1hr (%)	Mass % C_{12+} of converted propene
NiSMM-1	11.6	28
CoSMM-1	8.0	29
NiSMM-7	15.3	36
CoSMM-7	7.7	22
ZnSMM-1	8.9	19

The effect of increased nickel content decreasing the C_{12+} fraction was also seen for CoSMM. The C_{12+} content was reduced form 29% to 22% from CoSMM-1 to CoSMM-7. The effect of zinc content could not be determined due to the inactivity of the ZnSMM catalysts at loadings of 7% and higher.

3.3.10 Olefin Oligomerization Kinetics

The effect of the alkene feed partial pressure over NiSMM-1 at a WHSV of 50g/g hr is shown in Figure 3.27. For this study a 1-butene/butane mixture was used as the alkene feed since 1-butene is more reactive than propene and the WHSV was reduced from 90 to 50g/g.hr to produce meaningfully measurable conversion levels at the lowest partial pressure. Four 1-butene partial pressures; 4, 3, 2 and 1MPa were used.

The conversion levels dropped with decreasing 1-butene partial pressure. In all cases deactivation started immediately. Conversion levels were thus extrapolated from a runtime of 2hr, through 1hr to zero runtime to give initial conversion levels.

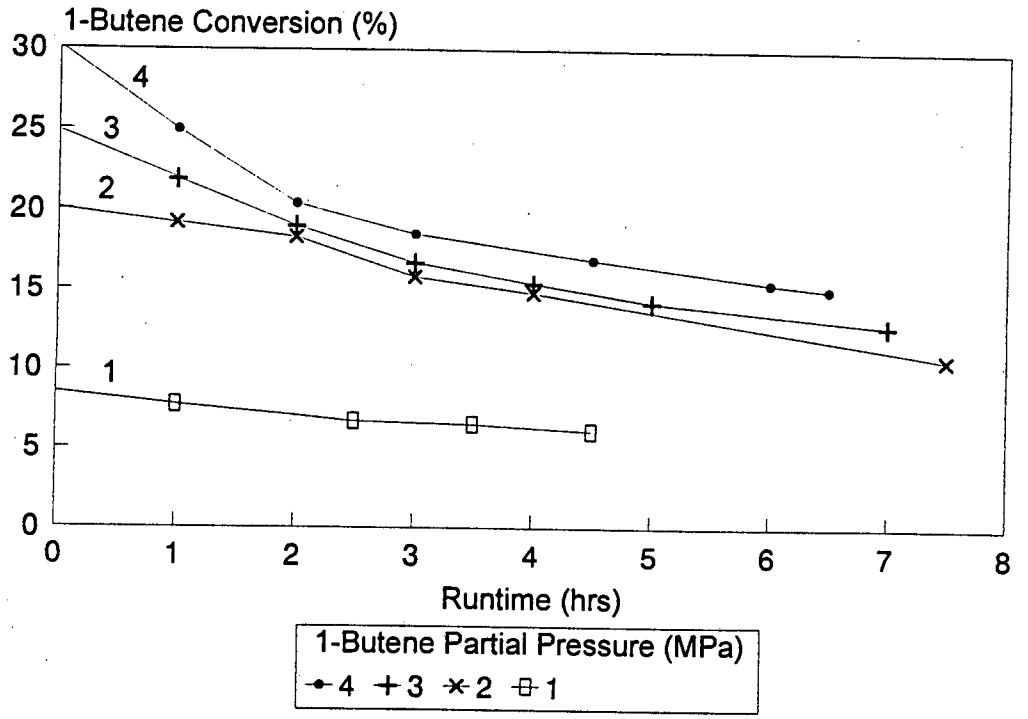

Figure 3.27 Effect of partial pressure on 1-butene conversion over NiSMM-1

A simple power law was used to model the reaction, viz.

$$-r_{C4} = k\,[C_4^=]^n \quad \ldots\ldots\ldots\ldots\ldots\ldots\ldots\ldots\ldots\ldots (1)$$

where $-r_{C4}^=$ is the rate of 1-butene consumption in g $C_4^=$ /g cat. hr, $[C_4^=]$ is the 1-butene partial pressure, n is the order of reaction and k is the rate constant.

Equation (1) can be linearised to

$$\ln(-r_{C4}) = \ln k + n \ln [C_4^=] \quad \ldots\ldots\ldots\ldots\ldots\ldots (2)$$

From a plot of $\ln(-r_{C4})$ vs $\ln [C_4^=]$ values were obtained for the reaction order, n, and the rate constant, k.

The data from Figure 3.27 that was used for the plot of equation 2 is given in Table 3.12 below.

Table 3.12 1-Butene oligomerization data work up for power law correlation

1-Butene Partial Pressure (MPa)	1Butene Concentration (mol/litre)	ln [$C_4^=$]	Initial 1-Butene Conversion (%)	1-Butene Consumption Rate (mol/g cat. hr)	ln (- $r_{C_4^=}$)
1	1.3	0.26	8.3	0.015	-4.2
2	2.7	0.99	20.0	0.071	-2.6
3	4.1	1.4	25.0	0.13	-2.0
4	5.5	1.7	30.3	0.22	-1.5

From the data in Table 3.11 a plot of ln ($-r_{C_4=}$) vs ln[$C_4^=$] was done as shown in Figure 3.28.

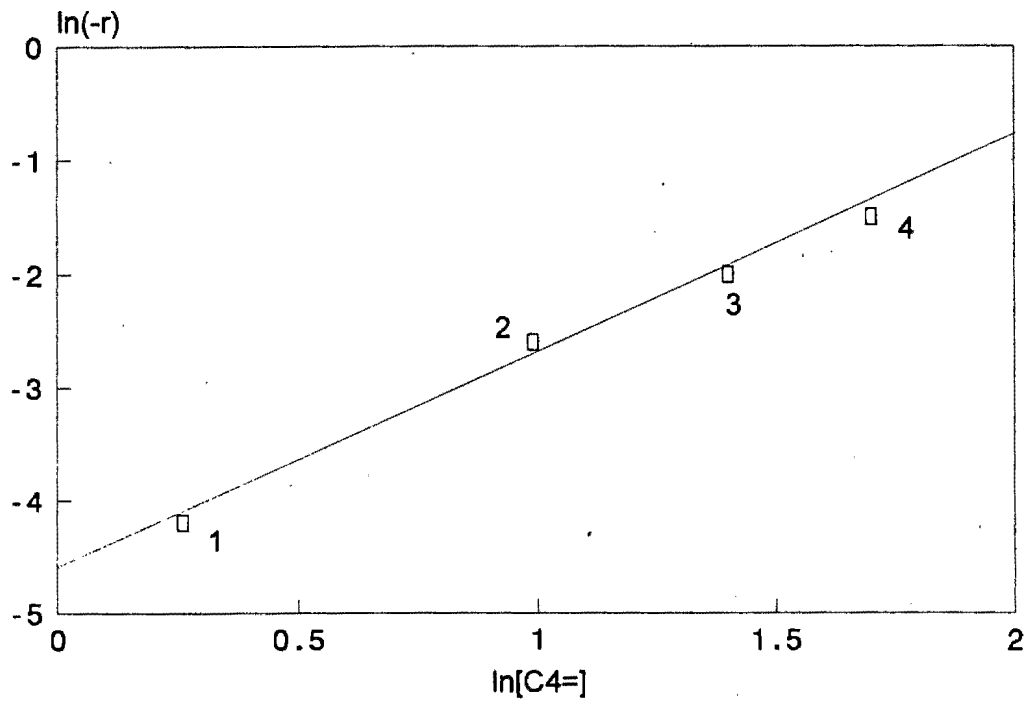

Figure 3.28 Power law plot for 1-butene conversion over NiSMM-1

A linear graph (correlation of 0.9956) was obtained which gave the following values:

$$k = 0.010 \text{ litre}^{1.87}. \text{mol}^{-0.87}. \text{g cat}^{-1}. \text{hr}^{-1}$$
$$n = 1.87$$

The value of 1.87 for n would suggest that the 1-butene oligomerization reaction is a second order process.

Chapter 4

Discussion

4 Discussion

4.1 Structure of Metal Substituted SMM

4.1.1 Chemical Composition

The synthesis and chemical composition of metal substituted SMM catalysts have been reported by various workers in the field (Swift and Black, 1974, Granquist, 1974, 1976, Black *et al.*, 1976, Heinerman *et al.*1983, Gaaf and Van Santen, 1983 and Swift, 1974). The full range of nickel substitution, from pure SMM to completely octahedrally nickel substituted SMM, has been investigated by Swift and Black (1974). This included a fluorine analysis. A full elemental analysis was not given and the structural aspects of these clays were beyond the scope of their study. A comprehensive report for determining the chemical composition of NiSMM was later given in a patent by Black *et al.*, (1976) for the full range of nickel substitution from pure SMM to a completely trioctahedral nickel substituted SMM.

Black *et al.*, (1976) showed examples where they incorporated 1.2 and 11.1% nickel into SMM from synthesis gels having 1.1 and 10.0% nickel content, respectively. The amounts of nickel cobalt and zinc loaded in the synthesis mixture were also shown in Table 3.1 to correspond well with the amounts determined by post synthesis analyses in this work. In both cases the nickel percentages were calculated on a water and acetate free basis. The increase in the trioctahedral 06 X-ray diffraction peak showed the metal incorporation into the octahedral position and hence showed the preference of the SMM structure for divalent nickel, cobalt and zinc in the octahedral position over aluminium since the amount of aluminium loaded was kept constant throughout the synthesis procedure, while the amount of metal was increased. No evidence for metal oxide species was found in the XRD data.

The aluminium displaced from the octahedral position was found in the tetrahedral position and the remainder as hydroxy aluminium species as shown in Table 3.2. Both these amounts increased, as expected, with increasing levels of nickel, cobalt and zinc incorporation. The only exception was NiSMM-34. It showed the trend of higher levels of tetrahedral aluminium but the hydroxyl aluminium formation was suppressed. As

this was the only catalyst with extra framework metal present, this divalent nickel cation or its oxide form could have been disrupted the formation of the hydroxy aluminium species. The remaining aluminium would then have been washed out of the catalyst during the post synthesis treatment. This resulted in a high Si/Al ratio for NiSMM-34 of 2.00 as opposed to 1.08 and 1.07 for CoSMM-33 and ZnSMM-31, respectively.

The fluorine levels of 0.3 to 1.0% for the NiSMMs found by Swift and Black (1974) were similar to those reported for NiSMM in this work of 0.6 to 1.0%. It has been postulated by Wright, *et al.* (1972) that final dehydroxylation of a fluoride-free SMM should occur more easily than for fluoride containing SMM. This was in accordance with the observations of Granquist and Kennedy (1967). Dehydroxylation of an (OH, F) pair should take place with greater difficulty since the loss of either a proton or a hydroxyl from such a pair would result in a charged species. Bercik, *et al* (1978) found little difference in the propene/butene oligomerization activity between 6 and 15% NiSMM with 0.5 and 4% fluorine, respectively. Fluorine addition (2%) by post synthesis HF deposition did, however, decrease the activity of 9.6% NiSMM for hexane hydroisomerisation to C_6 isomers from 50% to 16% (Black, *et al.*, 1976). The catalyst, containing 0.8% Pd, had been precalcined in air at 538°C for 10hr, then reduced in hydrogen at 343°C for 16hr. The variations in the levels of fluorine content found in the metal substituted catalysts in this work was not considered to be significant for their structure or activity. The fluorine was incorporated into the catalyst matrix during crystallisation and not added by post synthesis deposition.

4.1.2 Crystalline Structure

4.1.2.1 2:1 Layer Spacing

Tabulated summaries of the X-ray diffraction patterns for NiSMM have been given by Black *et al.* (1976). They have assigned indices to the peaks found, together with the peak heights and peak shape descriptions. The patterns were for NiSMM with a nickel content of 0 to 6 nickels per unit cell with the tetrahedral aluminium content constant at 1.5. The 001 basal spacing increased from 10.6Å for unsubstituted SMM to 13.6 for a fully substituted trioctahedral clay. Values of 11.3 to 11.8Å were reported for 0.125, 1 and 2 Ni/u.c. Higher spacings of 12.25 to 12.56Å were found in this work for similar

nickel loadings (0.14 to 1.48 Ni/u.c). These are characteristic of the layer spacing of 12.5Å for montmorillonite and indicate the more montmorillonite nature of the synthesised clays. The 001 peak spacings of 13.0 to 13.6Å that Black *et al.* (1976) found for 3 to 6 Ni/u.c. were attributed to the effect of intercalated acetate between the 2:1 layers. This acetate caused a basal spacing greater than that expected for even a pure montmorillonite by keeping the layers further apart. The peaks also became less well-defined and broader, indicative of a less ordered and more disrupted crystal structure. The higher nickel loaded catalysts of 2.70 and 6.00 Ni/u.c. (NiSMM-16 and -34) in this work showed a similar increased basal spacing of 13.11 and 13.45Å, respectively, with corresponding broader and less well-defined peaks. This again is attributed to the presence of acetate between the 2:1 layers. The greater levels of acetate were present at these higher nickel loadings due to the introduction of the nickel into the synthesis gel as a nickel acetate solution.

CoSMM showed a sharp drop in the 001 peak height from 0.15 to 1.04 Co/u.c. Again the peak became broader and less well-defined. The trend was not only true for the 001 basal spacing but for all structural peaks. This effect was so marked that the 001 peak for 5.85 Co/u.c. was indiscernible from the baseline. The reduction of the structural peaks was due to the increase in cobalt content in the SMM structure. The mass adsorption coefficient for cobalt is 329.4 as opposed to 49.0 and 58.6 for nickel and zinc, respectively, as shown in Appendix 10. The 06 peak height, once corrected for elemental mass absorption, showed a reflection similar in order to the other SMM catalysts. The 002 spacing of 7.12Å for CoSMM-33 (5.85 Co/u.c.) would seem to indicate a 2:1 layer spacing of above 13Å as found for the high nickel loadings for NiSMM. The presence of intercalated acetate possibly contributing to this phenomena.

The basal spacing for ZnSMM showed a reverse trend to NiSMM. It decreased from 12.89Å for ZnSMM-1 to 11.33Å for ZnSMM-7 and 10.70Å for ZnSMM-31. A more mica-like nature was evident at higher metal loadings. The 2:1 layers were pulled closer together by the highly electronegative zinc ion and were seemingly not affected by intercalated acetate.

A more crystalline mica-like structure was found for commercial SMM (SMM-F) than for the SMM synthesised in this work. This was seen by the well defined 001 peak at 11.4 for SMM-F as opposed to a more poorly defined peak at 12.1Å for SMM. The synthesis of 3hr at 300°C for the clays manufactured in this work, as opposed to 16hr at 285°C for the commercial SMM could account for the poor structural nature of the clay. The presence of the metal cations in the synthesis mixture of metal substituted SMM was seen to facilitate mica montmorillonite structural formation.

4.1.2.2 Tetrahedral Layer

The effect of aluminium substitution for silicon in the tetrahedral layer of trioctahedral (6 Ni/u.c.) NiSMM on the 001 peak spacing and shape has been given by Black *et al.* (1976). The 001 peak shifted from 9.6Å for no tetrahedral substitution to 13.6Å for 1.5 Al^{tetra}/u.c. and no peak was identified for 2.0 Al^{tetra}/u.c. The peaks were very strong and well defined for no substitution and became progressively weaker and less defined as more aluminium was incorporated in the tetrahedral layer. The 2:1 layers were shown not to be drawn closer together as would be expected for a mica-like structure as the tetrahedral charge was increased. The substitution of silicon by aluminium in this layer disrupted the order of the 2:1 layer stacking. This was an effect over and above that of intercalated acetate as the nickel content was kept constant at 6 Ni/u.c. for these clays.

For nickel, cobalt and zinc substitution in this study the amount of tetrahedral aluminium increased with increasing metal substitution as was seen in the proposed unit cell formulae for the catalysts. The effect of Al^{tetra} could not be isolated as the amount of acetate present was also increasing due to the higher metal loadings. As mentioned previously the acetate can contribute towards the increase in the 001 spacing. At the highest levels of metal substitution (6 metals/u.c.) the tetrahedral aluminium was greatest for cobalt, followed by zinc then nickel as seen in Table 3.2.

The amount of acetate present was very similar for the three metals at 6 metals/u.c. and the effect of tetrahedral aluminium substitution could thus be implied at this level of metal substitution. The expected trend as seen by Black *et al.* (1976) of Al^{tetra} disrupting the 001 peak shape was seen. The 001 peak for CoSMM-33 with the highest

degree of tetrahedral Al was absent and was less well defined for ZnSMM-31 than for NiSMM-34. Crystal structure disruption by Al^{tetra} could be the cause of the poor peak definition.

Even though SMM-F had a higher level of tetrahedral aluminium substitution of 1.17 compared to 0.57 Al^{tetra}/u.c. for SMM, a more well defined 001 peak was seen. With no acetate present, the synthesis procedure was again held accountable for the less crystalline SMM structure. This effect was more dominant than the crystal disruptions caused by Al^{tetra} substitution.

4.1.2.3 Octahedral Metal Substitution

The 1.52Å (hk:06) trioctahedral peak intensity as a function of Ni/u.c. has been given by Black *et al.* (1976). The reflection intensity, corrected for change in the mass absorption coefficient as nickel increased and aluminium content decreased was essentially a linear function of nickel from 0 to 6 Ni/u.c. This was investigated for tetrahedral aluminium contents of 0.45, 1.0 and 1.45 per unit cell. Zinc incorporation has been shown to improve the crystallinity, yielding an X-ray pattern with a better resolved 06 reflection doublet than in patterns for NiSMM (Swift, 1977).

The 06 X-ray reflections for Ni, Co and ZnSMM showed diminishing 1.50Å dioctahedral peak intensities and increasing 1.52Å trioctahedral peak intensities as increasingly more metal was incorporated in the matrix. These metals were thus seen to take up positions in the octahedral layer of the clay. Even though the proposed unit cell formula for NiSMM-34 indicated a completely substituted trioctahedral clay, a dioctahedral peak was still seen at 1.50Å. More nickel must therefore have been present as charge-balancing Ni^{2+} ionic structures than calculated for in the unit cell structure.

The 06 trioctahedral reflection intensities, once corrected for changes in the mass absorption coefficients, showed a linear relationship with the metals per unit cell for Ni, Co and ZnSMM. The relative refractivities for similar metal loadings, had the trend of Zn > Co > Ni. The would seem to indicate that the packing density of the octahedral metal increased from nickel, through cobalt, to zinc. The ease of metal incorporation into the structure would thus follow the reverse trend of Ni > Co > Zn. This was seen in

the elemental analyses of NiSMM-34, CoSMM-33 and ZnSMM-31. The percentage of metal loaded into the synthesis gel that was found in the final clay structure was 96.4% for NiSMM-34, 92.5% for CoSMM-33 and 82.2% for ZnSMM-31. The reason for this can be seen in the restriction on the divalent cation ionic radius of 0.75Å for incorporation into the octahedral position of the SMM matrix. The ionic radii are: Ni^{2+} - 0.69, Co^{2+} - 0.72, Zn^{2+} - 0.74Å (Black, *et al.*, 1976; Purcell and Kotz, 1977). The divalent metal cations thus became increasingly more difficult to include in the octahedral position with increasing ionic size. The ionic radius of Zn^{2+} is close to the maximum allowable size of 0.75Å and was therefore the most difficult of the three metal cations to incorporate and yielded the structure with the greatest packing density and most crystalline nature.

4.1.3 Metal Reducibility

Heinerman *et al.* (1983) showed that less than 4% of the nickel in 20.8% NiSMM was reduced after 24hr at 440°C. This amount was in excess of 20% at 480°C after 16hr. The higher temperature of 650°C to which the reduction was temperature programmed in this work enabled up to 100% of nickel, depending on content, to be reduced in less than 2hr.

The amounts of metal reduced at similar contents decreased Ni > Co > Zn. The standard reduction potentials for these divalent metal cations showed a similar trend. The low value of -0.76 for Zn^{2+} compared to -0.25 and -0.28 for Ni^{2+} and Co^{2+} (Dillard and Goldberg, 1978), respectively, shows the relative difficulty with which Zn^{2+} is reduced. The difficulty with which cobalt and especially zinc were reduced could also be indicative of a more tightly bound structure. The shift in the low temperature reduction peak from 260°C for NiSMM to 360°C for CoSMM showed the greater difficulty with which cobalt is reduced and again could also possibly represent a more tightly bound cobalt species. Because of the low level of zinc reduction, there were no low and high temperature reduction peaks that enabled a comparison to be made between metal included in the SMM structure and that present external to the 2:1 platelets for ZnSMM. Such peaks were seen for Ni and CoSMM which gave evidence of higher levels of extra structural metal for CoSMM than for NiSMM at similar metal

loadings. This was indicated by the size of the low temperature reduction peaks. The larger ionic radius of Co^{2+} (0.72Å) over Ni^{2+} (0.69Å) could have contributed towards the increased metal exclusion. The high temperature peak decreased from 650°C to 636°C for NiSMM-16 and to 623°C for NiSMM-34. At these higher loadings more nickel would be present at platelet edges. The greater ease of reduction of the nickel could be due to its greater accessibility and the fact that it would be less tightly bound within the SMM structure.

4.1.4 Surface Area

The surface areas on both the commercial and synthesised catalysts showed good agreement with those found in previous studies (Swift and Black, 1974). The areas of SMM-F and NiSMM7-F as measured by the above authors gave values that were within 3% of the areas found for the Harshaw-Filtrol catalysts in this work and within 8.5% of the areas measured on the clays that were synthesised in the present work.

The NiSMM surface areas reported by Swift and Black (1974) showed increased surface areas with increasing metal content (see Table 3.3). As the trend was not uniform (a drop in surface area between 21.6 and 30.5% NiSMM) another factor contributing towards catalyst surface may have been present. The NiSMM catalysts in the present work also showed a non-uniform change in surface area. The area increased up to NiSMM-10 whereafter it decreased down to NiSMM-34.

An increase in surface area of between 21% (ZnSMM-1) and 38% (NiSMM-1) over unsubstituted SMM surface area was found for the catalysts synthesised in this work. The basal spacing of SMM has been shown by Wright *et al.* (1972) using X-ray diffraction to irreversibly collapse to 9.4Å after calcination at 650°C. This means that only the platelet edges and faces would be accessible to the probe nitrogen molecule during surface area measurements. For an increase in accessible surface area to occur either the platelet height is decreased through a decrease in the number of 2:1 layers per platelet, rendering more platelet face area available, or smaller platelets result, making more platelet edge are accessible. The explanation of smaller platelets seems plausible when considered along with the observation made in catalyst wafer preparation for the

infrared study. SMM wafers could be obtained by filtration of a finely dispersed clay slurry and subsequent drying of the filter cake. NiSMM (7%) wafers could not be made in this manner due to the wafer breaking up during the drying procedure. This could have been due to the small platelets being formed for NiSMM.

It would appear that the metal incorporation immediately resulted in a smaller platelet diameter of <1000Å. More platelet edge area would therefore have contributed to the total catalyst surface area. Based on the above assumption and that the platelet density of SMM and NiSMM is the same, a platelet diameter of 184Å was calculated for NiSMM-1 using the surface area increase found (see Appendix 13). A platelet diameter decrease of 81.6% was thus needed to get a surface area increase of 38%. This is a substantial reduction in platelet diameter resulting from just a 1wt% nickel incorporation into the SMM structure. For this to be a valid explanation, the nickel in the structure would need to be the source termination of two dimensional crystal growth. Two dimensional growth refers to the platelet diameter size increase along the a and b crystal axes. NiSMM-1 contains 0.14 nickels per unit cell as given in Table 3.2. In a structure that comprised of five 2:1 layers per platelet and similar a (5.19Å), b (8.965Å) and B (99°) unit cell dimensions to SMM (Wright *et al.*, 1972), NiSMM-1 would contain 1 nickel per 65.7Å^2 of platelet face area. A platelet of 1000Å diameter (SMM, Wright *et al.*, 1972) would therefore contain over 10 000 nickel atoms or points of potential growth termination. A platelet diameter of 184Å for NiSMM-1 requires a platelet face area reduction of only 29.5 times. The nickel would not be present as single isolated atoms but would be located together in groups of at least three atoms (to charge balance replacing two aluminium ions) of which there are potentially about 3 000. There are thus over 100 times the number of such groups available in NiSMM-1 to cause the platelet diameter reduction that has been proposed. It is more likely that clusters of high nickel concentration in the platelet result in the crystal growth termination.

Platelet diameters of 255Å and 290Å would explain the increase in surface areas found for CoSMM-1 and ZnSMM-1, respectively (Appendix 13). The initial increase in surface area with metal incorporation is thus felt to be due to smaller platelets crystallising out.

The surface area increased with Ni loading until NiSMM-10, at which point it dropped at higher loadings. A similar surface area decrease was seen for Co and ZnSMM. This drop occurred at concentrations of >7% for CoSMM and >1% for ZnSMM. At this level of metal incorporation the surface area reduction could be due to an increase in the number of 2:1 layers per platelet, i.e. more than the 5 layers per platelet found for SMM by Wright *et al.* (1972). It must also be borne in mind that in conjunction with the above postulations three metal ions of higher atomic weight are substituting for two aluminium ions of lower atomic weight. The platelet density would more than likely be increasing with metal incorporation. As the surface area is measured as a function of catalyst mass, this density change must be taken into account when relating surface area changes to platelet dimension changes.

The surface areas are thus represented as area per unit cell in Table 4.1. The unit cell molar masses were calculated from the formulae given in Table 3.2. The 2:1 layer spacing as presented by the 001 X-ray diffraction peak is also shown.

Table 4.1 SMM surface areas per mole of unit cell

Catalyst	Unit Cell Molar Mass (g/mole)	Surface Area (m^2/u.c. x 10^{-3})	001 Layer Spacing (Å)
SMM	720.0	102	12.1
NiSMM-1	725.37	141	12.56
NiSMM-7	762.89	165	12.45
NiSMM-10	778.79	171	12.26
NiSMM-16	828.61	162	13.11
NiSMM-34	962.56	174	13.41
CoSMM-1	725.79	128	12.26
CoSMM-7	761.73	136	12.11
CoSMM-33	956.80	121	–
ZnSMM-1	726.97	124	12.89
ZnSMM-7	759.68	106	11.33
ZnSMM-31	951.05	94	10.70

A decrease in surface area has also been seen as increasing quantities of zinc were incorporated into SMM (Swift, 1977). The surface areas for the NiSMM catalysts increased from SMM to NiSMM-1, then further to NiSMM-10. At higher nickel loadings a slight increasing trend was seen, with the exception of NiSMM-16. The increases seen with nickel content could result through further reduction in platelet diameter. The increase in the 001 spacing for NiSMM-16 and NiSMM-34 supports a possible increase in 2:1 layer spacing at nickel loadings of >10%.

The reduction in surface area per mole of unit cell seen from ZnSMM-1 to ZnSMM-31 corresponded to a decrease in interlayer spacing from 12.89Å to 10.70Å. The 2:1 layers appeared to be pulled closer together. The 17% reduction in basal spacing for uncalcined ZnSMM does not quite match the 24% reduction seen in surface area from ZnSMM-1 to ZnSMM-31. Other factors including variations in the number of 2:1 layers per platelet with metal type and loading could contribute towards changes in the surface areas. The difficulty with which Zn^{2+} was reduced as seen in the temperature programmed reduction experiments and the high reflectivity of the ZnSMM 06 X-ray diffraction peak would support a more tightly bound structure for the ZnSMM catalysts.

The initial increase seen in surface area from SMM to CoSMM-1 and to CoSMM-7 was assigned to smaller platelets as in the case of the NiSMM catalysts. The reduction in surface area for CoSMM-33 could be caused by a reduction in 2:1 layer spacing. Although no 001 peak was observed in the X-ray diffraction pattern, the increased 06 reflection did indicate a more densely packed structure for CoSMM-33 over NiSMM-34, as discussed for ZnSMM-31.

4.1.5 Platelet Edge Charges

The possible platelet edge charges generated as a result of nickel incorporation into SMM is discussed in this section in light of the postulation made in Section 4.1.4 that nickel incorporation results in termination of two dimensional crystal growth.

The sheet structure of SMM is broken at the edges of the platelets and the crystal is terminated by OH-groups. These have been shown by White and Zelazny (1988) for

smectite layers with tetrahedral aluminium substitution and magnesium octahedral substitution. Based on these structures, the edge charges for metal substituted SMM can be determined. Nickel is used in this discussion as the octahedrally substituted cation. Two types of chains, B and A+C, are found in smectites. The development of the edge structure from pyrophyllite through SMM to NiSMM for both these chain types are shown in Figure 4.1.

B Chain

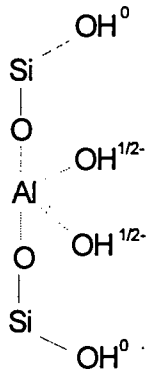

pyrophyllite

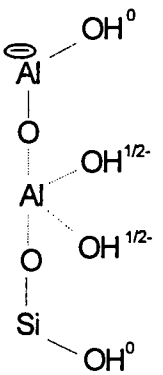

SMM

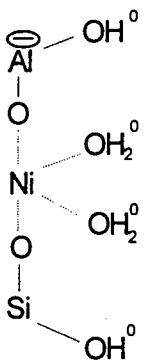

NiSMM

A and C chains

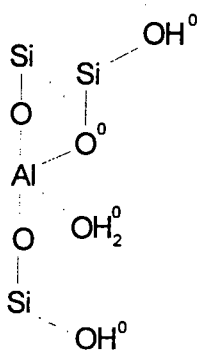

pyrophyllite

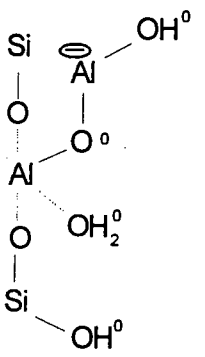

SMM

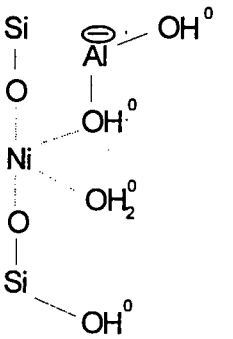

NiSMM

Figure 4.1 Edge charges for pyrophyllite, SMM and NiSMM

The charge balancing cation (NH_4^+) has not been shown. The termination of the crystal edges yields a more stable structure for NiSMM over SMM for the B type chains. The

edges are electronically neutral as opposed to charged hydroxyl end groups for the octahedrally co-ordinate aluminium for SMM. This edge stability could result in smaller platelets condensing out in NiSMM. Two dimensional sheet propagation would be more favoured by the edge structure postulated for SMM, metal substitution favouring termination.

4.2 Acidity of metal substituted SMM

The acidity of SMM after varying pre-treatment conditions has been examined by Kojima *et al.* (1986). They found the number of Lewis sites per gram of SMM after calcination at 500°C to be 2.4 x 10^{19} sites/g. This was computed using the integrated absorbence coefficients of Hughes and White (1967) in their infrared pyridine absorption study. The exact same number of sites was determined by Wright *et al.* (1972), assuming a one to one conversion between Bronsted and Lewis acidity. The calculated number of acid sites/g for calcined SMM based on the unit cell structure and inaccessibility to the interlayer space is 2.4 x 10^{20} sites/g. This is 10 times the number detected by Kojima *et al.* (1986) and Wright *et al.* (1972) through pyridine adsorption.

Kojima *et al.* (1986) found TPD and IR absorption of pyridine to be comparable analytical techniques in that they gave results that agreed very well. Acidities of 1.7 x 10^{19} sites/g and 1.8 x 10^{19} sites/g were obtained by TPD and IR, respectively. These were for catalyst samples containing only Lewis acidity, having been calcined at 650°C.

The number of acid sites detected on SMM-F (the same commercial catalyst used by Kojima *et al.* 1986) in this work were 1.02 and 3.72 x 10^{20} sites/g by NH_3 - TPD and IR pyridine absorption respectively. This was after calcination at 500°C and should be comparable with the value of 2.4 x 10^{19} sites/g obtained by both Kojima *et al* (1986) and Wright *et al.* (1972). These values were higher than expected. The number of sites of 3.72 x 10^{20} sites/g obtained by pyridine was higher than the theoretical value amount of 2.4 x 10^{20} sites/g. The experimental amount of 1.02 x 10^{20} sites/g by NH_3 - TPD was lower than that found by pyridine despite NH_3 being a smaller probe molecule and a stronger base than pyridine.

The differences in the analytical techniques used were NH_3 as opposed to pyridine as the probe molecule for TPD and wafer preparation for IR pyridine absorption. Since only external platelet acidity was being studied these two differences in analytical technique could not be expected to account for the large variations in site determination found between this work and previous investigations. The discrepancy between the results obtained for the acidities by NH_3-TPD and IR pyridine adsorption did not allow clear trends in acidity to be made with metal type and loading. The relative, rather than the absolute values for the acid sites were therefore considered in the discussion of the metal substituted SMM acidity. It could generally be said, however, that the total acidity of NiSMM as given by both NH_3-TPD and IR pyridine adsorption increased with increased metal loading (see Tables 3.5 and 3.8 for NH_3-TPD and IR pyridine adsorption acidity results). This acidity was to Lewis acidity as the Bronsted acidity characterised by IR pyridine adsorption decreased with increased nickel loading. The Lewis acidity as measured by IR pyridine adsorption was able to be related to the propene oligomerization activity of the NiSMM catalysts as is shown later in Section 4.4.4.1.

The acidity trend with increased metal content for CoSMM showed conflicting results for NH_3-TPD and IR pyridine adsorption. Although both techniques indicated an increase from the 1% to 7% cobalt levels, IR pyridine adsorption showed a decrease whereas NH_3-TPD demonstrated a continued increase in acidity for CoSMM-33. The lower result found by IR pyridine adsorption for CoSMM-33 did correspond with activity results that are discussed later in Section 4.4.4.2.

Both analytical techniques indicated low acidities for the ZnSMM catalysts. No acidity trend with zinc loading was shown. IR pyridine adsorption yielded a higher result for ZnSMM-1 than NH_3-TPD, which as for CoSMM-33, was able to be correlated to the propene oligomerization activity results that are discussed later in Section 4.4.4.2. The results obtained by both techniques did, generally, seem to indicate a decrease in catalytic acidity, NiSMM > CoSMM > ZnSMM.

The acid site strength distribution over Ni, Co and ZnSMM showed a uniform strength for all the catalysts. This was seen in both the NH_3-TPD (Figure 3.5) and IR pyridine

desorption profiles (Figure 3.8a and b). No distinction between 'weak' and 'strong' acid sites was seen by low (±200°C) and high (>400°C) temperature NH_3 desorption peaks, as was evident for the ZSM-5 catalysts (Schwarz *et al.* 1989). The infrared pyridine desorption profile in Figure 3.8(b) showed an increased number of Lewis acid sites for NiSMM-34 as opposed to NiSMM-1 and NiSMM-7 when measured at room temperature. At a desorption temperature of 100°C NiSMM-1, -7 and -34 all had a similar number of acid sites. The increased level of nickel incorporation for NiSMM-34 generated additional sites which were weak Lewis acid sites.

Based on the two types of acidity, viz. Bronsted and Lewis, that were identified through infrared detection of pyridine adsorption and the nature of these sites as proposed by Fletcher (1984) for SMM, similar sites structures are given for NiSMM in Figure 4.3 and Figure 4.4, respectively. A trioctahedral of fully nickel substituted SMM is used for this illustration. The deammoniation of NiSMM is also shown in Figure 4.2. A third type of site is also given in Figure 4.6 which shows the nickel sites at the platelet edges. Weak Lewis acidity, as seen for NiSMM-34, is attributed to this type of acid site.

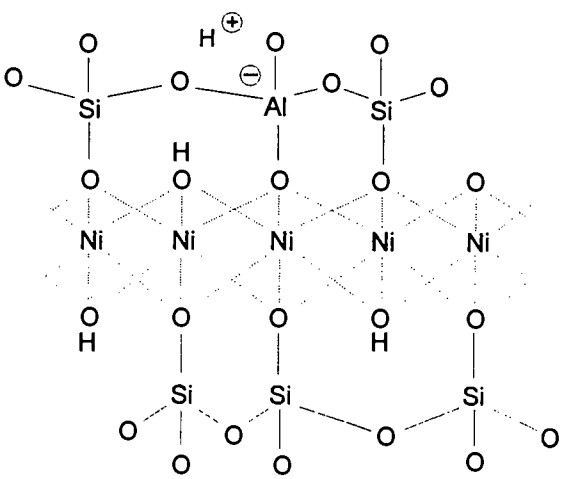

Figure 4.2 Deammoniation in NiSMM

The proton from deammoniation attaches to the oxygen forming the Si-O-Al linkage. This attachment results in the breaking of the link and the formation of a SiOH group. An association of the structural hydroxyl group and the SiOH was also postulated. This is shown in Figure 4.3.

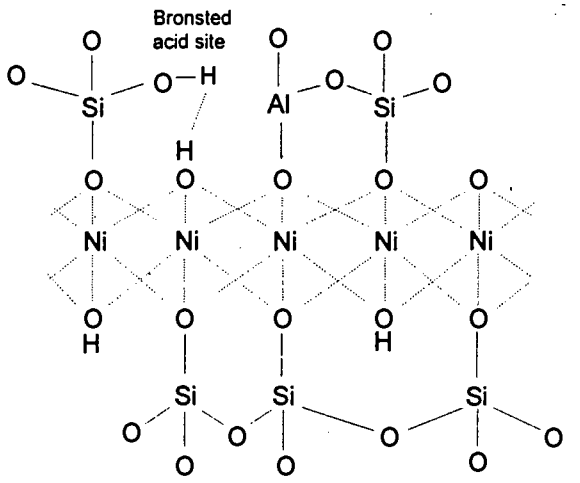

Figure 4.3 Bronsted acidity in NiSMM

A similar structure was suggested by Russel and White (1966) where they showed the proton from deammoniation to occur between the apical oxygen associated with tetrahedral aluminium and the oxygen of the structural hydroxyl group.

The further formation of Lewis acidity by dehydroxylation of the silanol OH group and the H from the structural hydroxyl group is given in Figure 4.4.

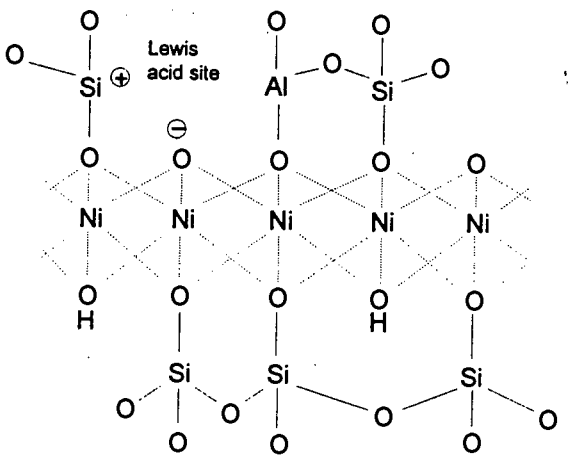

Figure 4.4 Lewis acidity in NiSMM

The Bronsted and Lewis acid sites as described are all generated on the platelet faces and arise only through aluminium substitution for silicon in the tetrahedral layer. The increase in metal loading would potentially increase the number of these sites by

making more aluminium available for substitution by replacing it in the octahedral layer. The increase in tetrahedral aluminium with increased metal loading has been shown in the postulated unit cell formulae in Table 3.2.

Acid sites will also arise from the platelet edges. These would result from octahedrally co-ordinated nickel being present at the platelet edges. The co-ordination positions of nickel are completed by one (A and C chains) or two (B chains) waters, as shown in Figure 4.5.

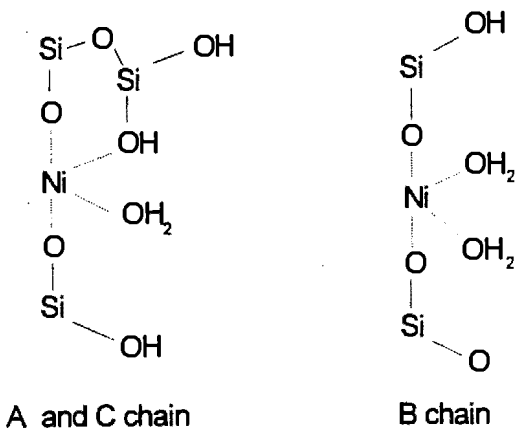

Figure 4.5 Nickel octahedral positions at platelet edges

These octahedral water ligands would be driven off under the calcination conditions of 500°C in flowing air. The exposed nickel would then exhibit weak Lewis acidity at the platelet edges. At the lower oligomerization reaction temperatures of 130°C any water present would take up the ligand position, rendering the site inactive for the oligomerization reaction. The effect of the presence of water was seen in both the atmospheric iso-butene and 5MPa propene oligomerization studies. The presence of water lowered the oligomerization activity of the catalyst in both cases.

Changes in the electron density of the nickel have been previously shown to account for the changes in ethene oligomerization activity and selectivity obtained with homogeneous nickel catalysts involving oxygen-containing chelating ligands (Keim *et al.*, 1979, and Peuckert *et al.*, 1983). Espinoza *et al.* (1987a) have found that supports

or sites which render the nickel ion more electron deficient result in more active catalysts. The stronger the acidity of the support, the more electron deficient the nickel became. The increased aluminium substitution for tetrahedral silicon as nickel loading was increased resulted in a more acidic catalyst. This would cause the octahedrally bound nickel at the platelet edges to be more electron deficient and the catalyst would become more active.

4.3 Low Pressure Olefin Adsorption and Reactivity

Simultaneous TG-DTA has been demonstrated by Gabelica *et al.* (1984) to be useful for investigating catalytic properties of zeolites. Although olefin oligomerization is carried out at much higher pressures than the 0.03MPa(abs) partial pressures used in the thermogravimetric study in this work, the object of the study was to demonstrate the ability of this technique to give insight into the interaction of the catalyst with different reacting species under different reaction conditions. It was also used to obtain comparative adsorption and reaction information of different catalyst types operating under the same conditions.

4.3.1 Olefin Adsorption

The comparative iso-butene adsorption levels for ZSM-5, NiSMM-7-F were in the ratio 4.4:2:0:1.0. These were in good agreement with their relative BET surface areas which are in the ration 4.0:1.9:1.0 (O'Connor *et al.*, 1988; Inui *et al.*, 1984) The type of isothermal adsorption used would cover both physi- and chemisorbed species and would be more indicative of surface area than of acidity.

The adsorbtion level in NiSMM-7-F was increased from 4.1 to 6.0-7.3% when water was co-fed with iso-butene. A larger proportion of weakly held species resulted, 36% as opposed to 17% in the absence of water. Due to the absence of a suitable analytical technique it was not possible to ascertain what percentage of these desorbing species were water or iso-butene. The increase in adsorption level in the presence of water could be due to both species adsorbing on separate sites, or, more likely, iso-butene adsorbing through Van der Waals forces on to polarised water on an acid site. This would require that water would preferentially adsorb on an acid site and much of the

iso-butene would desorb as weakly held species. Iso-butene adsorption on what has been termed "hydrated" surface was low in comparison to a dry surface (3.5 cf 4.1%). The amount of weakly held species on this hydrated surface was large in comparison (36 cf 17%). This would add support to the postulation that water causes iso-butene to be more weakly held to the catalyst surface.

The above discussion remains hypothetical in the light of insufficient experimental data on both physi-and chemisorbed species. In order to obtain more clarity only chemisorbed species need to be considered. Individually NiSMM-7-F chemisorbs 2.8 and 5.1 x 10^{20} molecules/g of iso-butene and water, respectively, as seen in Table 3.10. The number of acid sites available on the external platelet faces on NiSMM-7-F based on the postulated unit cell, inaccessibility of the interlayer space and an average of 5.2:1 layers per platelet should be 2.4 x 10^{20} site/g. The number of chemisorbed iso-butene molecules is close to this value. Since it is possible that some chemisorption of iso-butene would also take place on platelet edge sites the figure looks even more realistic. The higher value found for water chemisorption must be due to some form of clustering of water around the acid sites. It is possible that the rehydration at 30°C could rehydroxylate the catalyst to a small extent as has been found by Fletcher (1984) for SMM-F. This makes sense since the number of water molecules absorbed is close to double that of the number of theoretical site available: one water rehydroxylating the Lewis acid site to a Bronsted site and the second water being chemisorbed to this newly created acid site. Since Fletcher (1984) used rehydroxylation temperatures of 650°C and 4.5torr water vapour pressure, it seems unlikely that complete rehydroxylation can be expected to take place at 30°C even at 12torr water vapour pressure. The previous explanation of water clustering around an acid site seems more likely.

When iso-butene chemisorption followed water chemisorption a level of 2.2 x 10^{20} molecules/g was reached, just below that of 2.8 x 10^{20} molecules/g on a "clean" surface. This was equivalent to iso-butene adsorption on a hydrated catalyst surface. No desorption endotherm was seen during the iso-butene adsorption. indicating replacement of water by iso-butene. The iso-butene appeared to adsorb over the polarised water.

A desorption endotherm was observed by Gabelica *et al* (1984) when water replaced adsorbed ethylene on ZSM-5. Again no desorption endotherm, indicating replacement of iso-butene by water was found in this work.

Iso-butene adsorption was seen to significantly inhibit adsorption of water. Only 1.8 x 10^{20} water molecules/g are adsorbed on a surface already covered with chemisorbed iso-butene, 35% of what would have absorbed in the absence of iso-butene. Water thus requires access to acid sites for chemisorption whereas iso-butene can adsorb on an acid site or on polarised water.

Simultaneous adsorption of iso-butene and water, when both are co-fed, resulted in a mass increase of 2.7%. This was similar to the of 2.6% reached when pure iso-butene was adsorbed and it was higher than the mass increase of only 1.5% attributed to pure water adsorption. Although the relative contributions of water and iso-butene to this simultaneous adsorption was not known, it would appear to be indicative of a scenario similar to that of iso-butene preceding water adsorption. This would imply that the rate of adsoption of iso-butene on the catalyst surface is greater than that of water.

A comparison of the iso-butene chemisorption levels was done on NiSMM-7-F and SMM-F. The relative adsorption levels of 2.6 and 1.2% for NiSMM-7-F and SMM-F (Figure 3.13a) are comparable not only to their area but also to their relative atmospheric iso-butene and high pressure propene oligomerization activities.

4.3.2 Catalyst Reactivity

Indications were given that the low pressure oligomerization of iso-butene over NiSMM-7 occured between an adsorbed molecule and one in the gas phase. No evidence of reaction was seen by increasing the temperature of a catalyst with purely adsorbed reactant throughout the temperature range. This was indicative of a Langmuir-Rideal reaction mechanism. The kinetics of iso-butene oligomerization over Amberlyst-15 observed by Haag (1967) in a batch reactor at 0.5MPa and 60°C were consistent with a Langmuir-Rideal mechanism.

The positions of the TG and DTA peak maxima for the three catalysts are given in Table 4.2.

Table 4.2 Position of TG and DTA peak maxima for SMM-F, NiSMM-7-F and ZSM-5

Catalyst	Peak maximum (°C) DTA	TGA
SMM-F	64	87
NiSMM-7-F	67	89
ZSM-5	92	96

The position of the DTA peak maxima indicated the temperatures at which a rate of oligomerization reached its maximum and corresponded to the greatest rate of mass gain in the TG reaction peak. The TG peak maxima were the points at which desorption of reaction products became the dominant mass change effect.

The higher reactivity of NiSMM-7-F (56% mass gain) compared with SMM-F (36% mass gain) is in accordance with the findings of O'Connor *et al* (1988) that the high pressure propene oligomerization activity of NiSMM-7-F is almost double that of SMM-F. Although ZSM-5 had a lower extent of reaction than the clays, the shoulders on the TG and DTA reaction peaks indicate reactivity at higher temperatures. NiSMM-7-F, the most reactive of the three catalysts, also had the greatest coke build-up.

The trends in the relative reactivities of ion-exchanged SMM-F and pure SMM-F were similar to those reported by O'Connor *et al* (1988). Ion-exchanging SMM-F with 1% of the cation exchange capacity with cobalt, nickel or zinc increased its activity for propene oligomerization at 5MPa.

The iso-butene activity of SMM-F was increased substantially from a mass gain of 36% to in the region of 60% by the ion-exchange incorporation of 0.06wt% nickel, cobalt or zinc. The enhanced activity could be as a result of the interlamella divalent metal ion

catalysing the reaction. The shift in TGA peak maximum by 3°C is not considered significant and could be due to the metal catalysed reaction.

4.3.3 Water - olefin interaction during reaction

Adsorbed water and water in the flowing nitrogen stream were both seen to lower the iso-butene oligomerization activity of NiSMM-F. The extent to which the reaction was affected was dependant on water being both physi- and chemisorbed, purely chemisorbed (a hydrated surface) or present in the gas phase during reaction. Physi- and/or chemisorbed water increased the DTA reaction peak maximum from 67°C to 82°C or 83°C. The presence of water on the catalyst surface seemed to impose an additional energy barrier for the reaction. The extent to which the reaction occurred was strongly inhibited by physisorbed water as seen by the reduction in the TGA reaction peak maximum from 61.2 to 26.2%. The physisorbed water would inhibit iso-butene accessibility to the catalyst's acid sites.

The reaction was unaffected and even slightly enhanced (TGA from 56.1 to 61.2%) by a hydrated catalyst surface. It was seen in the chemisorption study that iso-butene adsorption was not greatly affected by a hydrated surface. The extent of reaction followed suit, taking place as easily on a dry as on a hydrated surface. It seems that the low pressure oligomerization of iso-butene is catalysed to a similar extent by a hydrated and a Lewis acid site. The activation energy required for reaction on a hydrated site would be higher as indicated by the higher temperature at which the oligomerization exotherm peak occurred. The higher temperatures could have been required to give the water co-ordinated at the catalyst metal edge sites to leave their ligand position, enabling the oligomerization reaction to occur at the metal acid site.

This exotherm was shifted to an even higher temperature by gaseous water during reaction, further increasing the energy requirement for reaction. The extent of reaction was reduced to a mass increase of only 15%. The water thus not only inhibited interaction of iso-butene with the acid site but also with other iso-butene molecules during reaction.

4.4 Olefin Oligomerization

4.4.1 Reaction Conditions

The reproducibilty of the propene conversion levels over NiSMM made the data sufficiently accurate to discriminate between the different reaction conditions and structural aspects of the catalysts.

The credibility of the synthesis procedure for the oligomerization activity of NiSMM has been established by the enhanced activity of NiSMM-7 over a commercially synthesized catalyst of similar metal content (Figure 3.17). The poor activity of SMM in comparison with the commercial SMM showed the unsuitability of the metal substituted SMM synthesis procedure for unsubstituted SMM. X-ray diffraction showed a more crystalline mica-like structure for commercial SMM than for the SMM synthesized in this work. The longer synthesis time used for commercial SMM synthesis (16hr as opposed to 3hr) is thought to be responsible for the poor crystal structure and hence poor oligomerization activity.

The calcination temperature that gave optimum catalyst activity (500°C, seen in Figure 3.18) was the same optimum pretreatment temperature found by Fletcher *et al.* (1986). This calcination temperature corresponded to the greatest Lewis acid site concentration found by the above authors in comparing temperatures of 400, 500 and 650°C.

The necessity of drying the propene feed prior to reaction was shown by the reduction in activity in the presence of water (Figure 3.19). The rate of deactivation found was not as marked as reported by Fletcher *et al.* (1986) for SMM-F and O'Connor *et al.* (1988) for NiSMM-7-F. The reduction in oligomerization activity by the presence of water was also seen in the iso-butene thermogravimetric study of NiSMM-7-F. This was attributed to hindrance of olefin-acid site and olefin-olefin interactions by water. A similar phenomenum could account for the reduced activity seen at 5MPa for propene oligomerization over NiSMM-7-F.

4.4.2 Synthesis pH

The synthesis pH of and silica/alumina concentration in silca-rich silica alumina gels has been found by Snel (1984) to control porous structure due to high charge densities in the hydrogels and high silica and alumina solubilities. These high pH's and reactant concentration resulted in highly porous gels. Maes *et al.* (1976) and White and Zelazny (1988) have shown that there is a pH dependent part of the CEC (cation exchange capacity) from the edge charges of smectite layers. An increase in pH resulted in an increase in the CEC of the pH dependent part of the clay particles.

A uniform increase in the BET surface area and catalyst acidity was not seen with an incease in pH in this study. An optimum in BET surface area and acidity, as measured by pyridine adsoption, was found at pH = 8.5. NiSMM-7 synthesised at a pH of 8.5 had the highest propene conversion level over synthesis pH's of 7 and 10 (Figure 3.20). This pH was used by Black *et al.* (1976) in their patented synthesis of nickel substituted SMM. It would seem that the structural crystallization was best affected at a pH of 8.5.

4.4.3 Reactant Flowrate

Espinoza *et al.* (1987b) have found that decreasing the ethene flowrate over nickel-exchanged amorphous silica alumina shifted the product spectrum towards heavier products. The result was expected since a decrease in flowrate increases the residence time of the reactant in the catalyst bed and thereby increases the chain growth probability. This was demonstrated in the product analysis. The product spectrum was measured at ethene flow rates of 0.5, 3 and $6h^{-1}$ and at very similar conversion levels of between 47.8 % and 51.8%. The C_{8+} fraction, which is equivalent to the C_{12+} fraction for propene oligomerization, decreased from 18 to 7wt% in their study by doubling the mass hourly space velocity (MHSV) from 3 to $6h^{-1}$.

Although measured at different conversion levels, the product selectivity in the present work (see Figure 3.23) showed a shift to lighter products with increased propene flow rate. At the higher WHSVs of 50 and 90g/g.hr the change in selectivity was slight. As these reactant flow rate were an order of magnitude higher than those used by Espinoza *et al.* (1987b) and the conversion levels at these two WHSVs were similar, between 8

and 12%, it did indicate a possible decrease in the effect of mass transfer on product selectivity at the higher propene flow rates. No definite effect could be isolated, however, due to the differences in conversion. It would suffice to say that the increase in selectivity to C_{12+} as a result of the increase in conversion level was as expected from a series/parallel oligomerization reaction mechanism.

The initial propene consumption rates demonstrated an almost linear increase with propene flow rate. This relationship is shown in Figure 4.6.

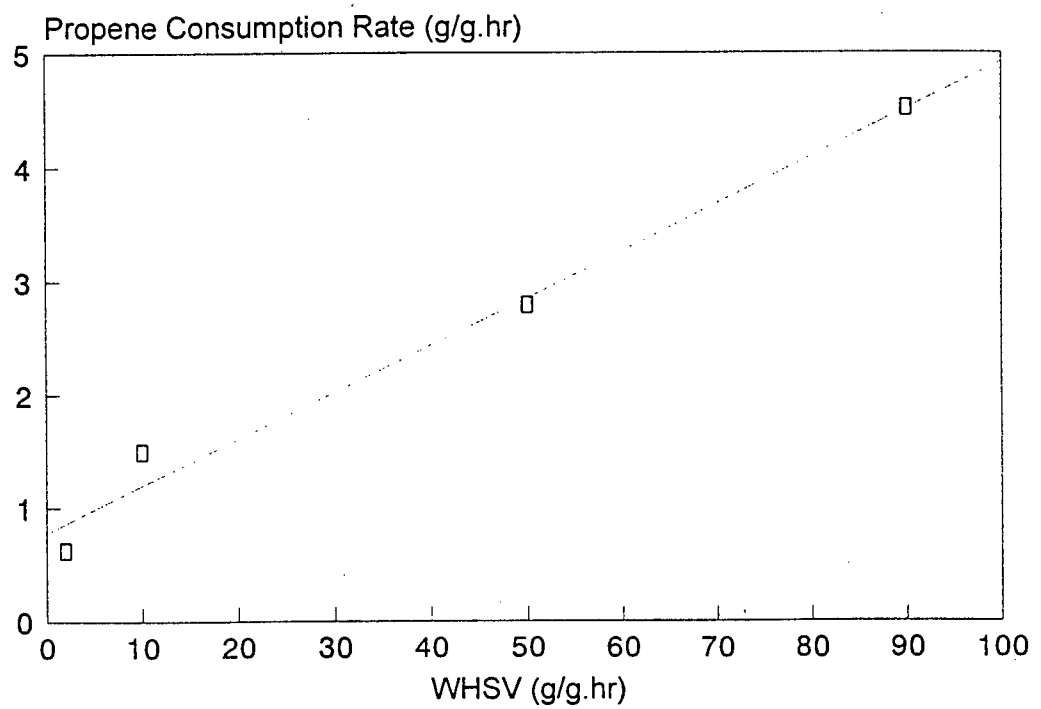

Figure 4.6 Initial propene consumption rate (@ 1hr) vs WHSV for NiSMM-1

The propene consumption rate was dependent on WHSV, showing mass transfer to be the rate determining step.

4.4.4 Metal Content

4.4.4.1 Nickel

The propene oligomerization activity of NiSMM-7-F was studied by O'Connor *et al.* (1988) as a comparison to SMM-F. This was in order to establish the effect of the incorporation of 7% nickel into the SMM structure. The activity of NiSMM-7-F was found to be double that of SMM-F at 130°C and 5MPa as was also found in this work (Figure 3.17). Nickel has also been exchanged onto silica-alumina catalysts by Espinoza *et al.* (1987a). The reaction considered was ethene oligomerization at 300°C and 1.15MPa. The product distribution was strongly dependent on the nickel concentration. Increasing the nickel concentration resulted in a marked shift to a lighter product. These comparisons were done at the same level of ethene conversion of 22.5%. The deactivation rate also increased at increased nickel content. The effects on product distribution and catalyst deactivation were attributed to the nickel being associated with sites of higher acidic strength.

The conversion level was seen to increase with increasing nickel content in NiSMM in the present work as shown in Figure 3.25. The relationship is shown in Figure 4.7.

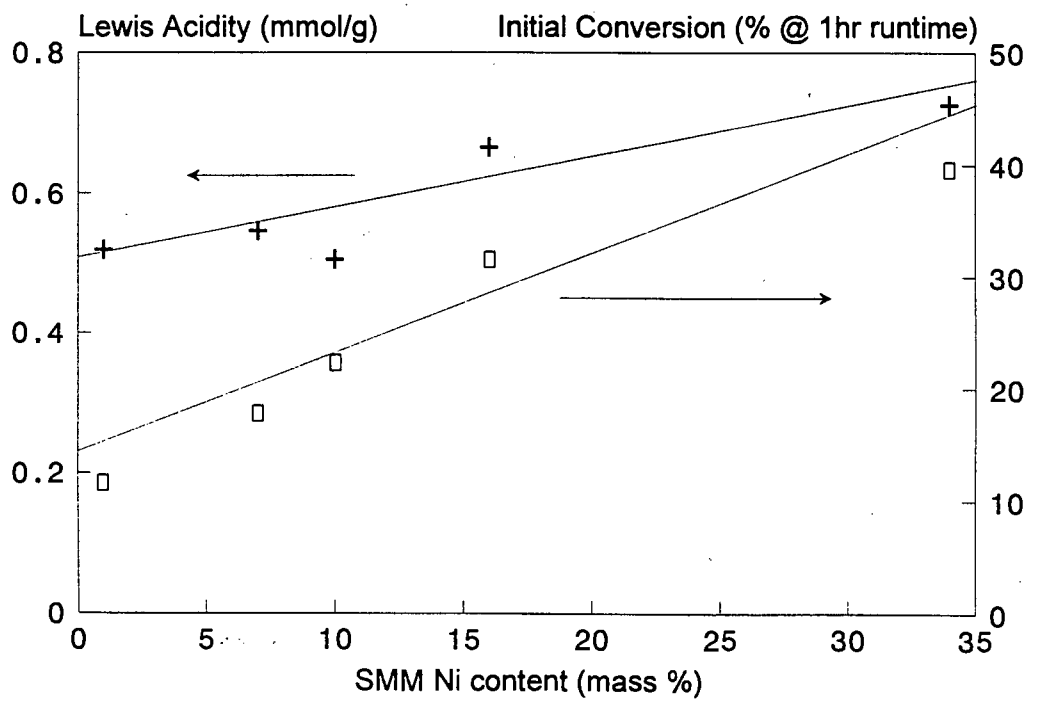

Figure 4.7 Initial propene conversion level at 90g/g.hr vs nickel content

The initial propene conversion levels were taken at a runtime of 1hr and a WHSV of 90g/g.hr for the different nickel contents. The Lewis acidity as measured in the infrared study of pyridine adsorption (LPy) is also given in Figure 4.7 as a function of nickel content in SMM. The previous discussion of Lewis acidity in the NiSMM catalysts (Section 4.2) described the increase in Lewis acidity with increased nickel content. A linear correlation between nickel content and initial conversion level can be seen. This observation agrees with Espinoza *et al.*'s (1987a) finding of a proportional dependence of ethene oligomerization on nickel content. The increased oligomerization activity was shown in Figure 4.7 to be as a result of an increase in Lewis acidity brought about by higher levels of nickel in the catalyst. The rate of deactivation was also shown to increase with increasing nickel content as was seen in Figure 3.24.

The shift to lighter products with increasing nickel content and increasing acid site strength of the metal support have previously been ascribed to electronic effects exerted on the nickel by the anionic sites present on the support (Espinoza *et al.*, 1987a). Changes in the electron density of the nickel have been shown to account for the changes in ethene oligomerization activity and selectivity obtained with homogeneous nickel catalysts involving oxygen-containing chelating ligands (Keim *et al.*, 1979 and Peuckert *et al.*, 1983).

It was seen in the present work that the selectivity was significantly affected by nickel content. At a constant conversion level the product spectrum became lighter with increased nickel content as was seen in Figure 3.25. The data for the NiSMMs also collectively showed the product spectrum to become lighter with increased conversion level. Two factors were changing to generate this trend, viz. conversion level and nickel content. In the absence of the effect of different nickel loadings the product spectrum has been shown to become heavier with increased conversion (Figure 3.23). The extent of the effect of nickel on the product spectrum was such that the decreasing trend with increasing conversion level was reversed.

It was postulated earlier (Section 4.1.4) that nickel incorporation into the SMM matrix leads to the formation of smaller platelets. This could potentially increase the

percentage contribution of platelet edges to the total platelet surface area from 6.8% for SMM to 32.1% for NiSMM-1. The nickel present in the octahedral position of the SMM structure would then be exposed on the platelet edges and would contribute to the activity of the catalyst. The possibility of nickel causing termination of two dimensional crystal propagation was also shown in Section 4.1.5. This increases the likelihood of nickel being present at platelet edges. An increase in nickel content would result in an increased number of these nickel edge sites. The increase in nickel content resulted in an increase in the number of Lewis acid sites and hence an increase in the activity.

A suggested mechanism for propene dimerization on an A or C chain on an edge nickel site in NiSMM is shown in Figure 4.8.

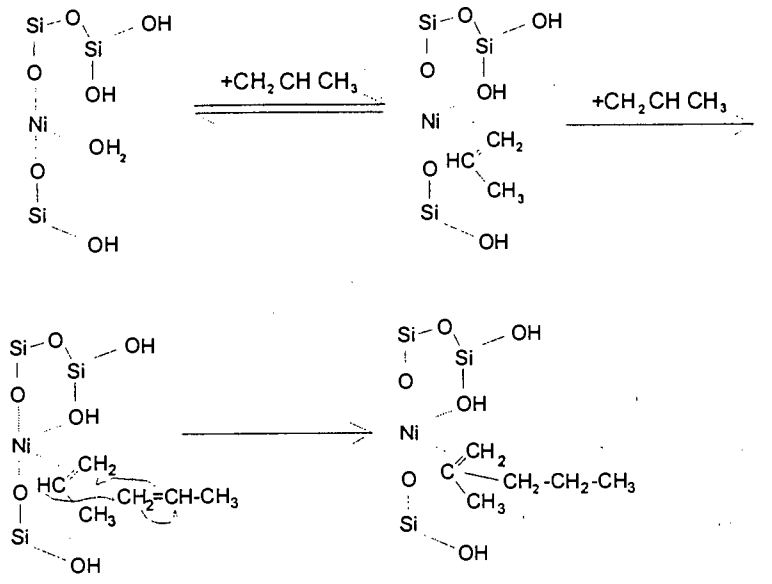

Figure 4.8 Proposed propene oligomerization mechanism by octahedral nickel edge sites in NiSMM

The water that would be present as 'non-structural' nickel ligands at the platelet edges (ligands that did not form part of the SMM matrix structure) would be driven off during the calcination process, rendering the edge nickel sites available for reaction. These nickel sites would be active as weak Lewis acidity (Hogan *et al.*, 1955). The product distribution from these sites would favour the lighter oligomers. The marked effect that

increased nickel had on the product spectrum was as a result of the contribution of the oligomerization reaction occurring on these weak Lewis acid sites.

4.4.4.2 Cobalt and Zinc

An increase in hexane hydroisomerization and hydrocracking activity was found by Swift and Black (1974) with increasing cobalt content in SMM. The increase in activity was, however, not nearly as extensive as that obtained with catalysts containing a corresponding molar amount of nickel. ZnSMM exhibited hydrocracking activities at similar metal molar contents that were an order of magnitude lower than for CoSMM. At the higher loadings (24wt%) ZnSMM was inactive.

The initial (first hour) oligomerization activities of the Co and ZnSMM catalysts is related to their Lewis acidities in Figure 4.9 as was done for the NiSMM catalysts in Figure 4.7. The Lewis acidity shown was measured by infrared analysis of pyridine adsorption.

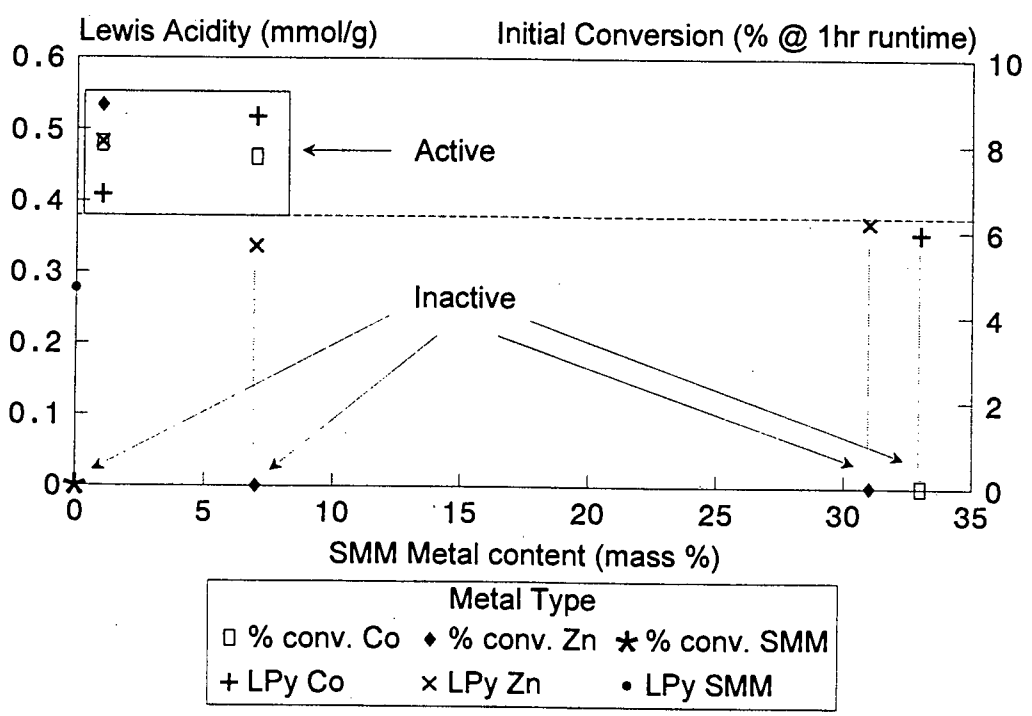

Figure 4.9 Initial conversion and Lewis acidity vs cobalt and zinc content in SMM

The propene oligomerization activity was found in this work to decrease with increasing cobalt and zinc content. This was opposite to what was found for the NiSMM catalysts, where activity increased with increasing nickel content and to the results found by Swift and Black (1974) for hexane hydroisomerisation and hydrocracking. At the higher loadings (CoSMM-33, ZnSMM-7 and ZnSMM-31), the cobalt and zinc catalysts were inactive under the reaction conditions used.

Although a clear trend for the acidity and activity as was found in the case of the NiSMM catalysts (Figure 4.7) was not be seen for CoSMM and ZnSMM. It could be very broadly said that the propene oligomerization activity decreased, NiSMM > CoSMM > ZnSMM. Figure 4.9 does show that a certain "minimum" Lewis acidity of about 0.4mmol/g was required for the catalysts to be active. The differences in catalytic activity between these three metals is not fully understood. It is possible that the relative platelet edge activities, decreasing Ni > Co > Zn, could be related to the electronic structure of the divalent metal cations. The two 4s orbital electrons are expelled during ionization leaving partially filled 3d orbitals for nickel and cobalt ($3d^7$ - Co^{2+}; $3d^8$ - Ni^{2+}) and a complete 3d orbital for zinc ($3d^{10}$ - Zn^{2+}). The filled 3d orbital for Zn^{2+} could possibly contribute to its lower activity compared to the other two metals.

4.4.5 Oligomerization Reaction Kinetics

Ethene has been oligomerized at 300 - 340°C, 1.1MPa and WHSV = $6h^{-1}$ over 0.27wt% nickel on silica-alumina by Espinoza *et al.* (1987b). The reaction rate was approximately first order. The low temperature (20°C) iso-butene (in hexane solvent) oligomerization reaction kinetics was found by Haag (1967) to obey first order kinetics at 1.03MPa over an Amberlyst 15 ion-exchange resin. However, at concentrations below 0.04mol.liter^{-1} second order behaviour was observed. Similar behaviour was found by the above author with di-isobutene. First order kinetics were seen only down to 1mol.liter^{-1} with second order behaviour being found at lower concentrations. These results were consistent with a Langmuir-Rideal reaction mechanism. The order of reaction for 1-butene oligomerization was found to be second order in this work by varying the reactant partial pressure between 1 and 4MPa. The reaction data were extrapolated to zero time to obtain the initial reaction rates. At this point the product

composition is taken as zero. In light of the bi-order nature of iso-butene oligomerization caused by reactant concentration observed by Haag (1967), it was possible that a second order reaction mechanism could be seen at low product concentrations. The 1-butene concentrations in the present work at 1.3 to 5.5mol.litre^{-1} were, however, an order of magnitude higher than those used by Haag (1967).

The rate of converison of ethene and propene were similar and that for 1-butene was half the rate for ethene (Espinoza *et al.*, 1987b). All olefins had terminal double bonds and acid catalysis would have made a significant contribution to conversion. The reaction rates were therefore not expected to be influenced by double bond position. The lower rates reported by Espinoza *et al.* (1987b) were attributed to the larger size of the 1-butene molecule.

The initial rate of 1-butene oligomerization found over NiSMM-1 at a partial pressure of 0.8 was 12.1g/g.hr at a WHSV of 50g/g.hr. This rate was double that of 6.2g/g.hr obtained for propene oligomerization over NiSMM-1 at the same WHSV at a similar reactant partial pressure of 0.86. 1-Butene is also a terminal olefin and would therefore not be expected to have reduced rates of oligomerization over ethene and propene. The greater reactivity of iso-butene over 1-butene and propene and that of these two olefins over ethene could be explained by the stability of formation of the tertiary (iso-butene), secondary (1-butene and propene) and primary (ethene) cations during acid catalysed oligomerization. The difference between 1-butene and propene was perhaps due to a slightly enhanced stability of the butyl cation over the propyl cation.

The kinetic data otained for 1-butene oligomerization was used to determine the controlling reaction mechanism. Two models were developed, viz. surface reaction between two adjacent absorbed molecules (Langmuir-Hinshelwood mechanism) and reaction between a gas phase and absorbed molecule (Langmuir-Rideal mechanism). The development of these two models is given in Appendix 14. The two models were used to predict the reaction rates at the experimetal conditions that were used. This data was then compared with the actual experimental results obtained. The comparisons are given in Table 4.3.

Both the reaction rates predicted by the two models were close to the experimental values actually obtained. It was not possible to eliminate either of the models and both are thus considered possible for olefin oligomerization.

Table 4.3 Experimental and Predicted 1-Butene Reaction Rates

Partial Pressure (MPa)	Reaction Rates (mol/g cat. hr)		
	Experimental	Langmuir-Hinshelwood	Langmuir-Rideal
1	0.015	0.016	0.018
2	0.071	0.063	0.067
3	0.13	0.14	0.13
4	0.22	0.23	0.21

Although the 1-butene kinetic study was unable to confirm or repute the evidence in the atmospheric iso-butene oligomerization work conducted over NiSMM-7-F that suggested a Langmuir-Rideal reaction mechanism, it is supported by the work done by Haag (1967).

Chapter 5

Conclusions

5. Conclusions

Metal substituted SMM was successfully synthesised. The synthesis method enabled nickel, cobalt and zinc to be incorporated into the clay structure. The divalent ions of the above mentioned metals occupied octahedral positions in the 2:1 layer structure of SMM as shown by the 06 reflection in the X-ray diffractograms. The SMM structure demonstrated a preference for these divalent metal ions over aluminium ions in the octahedral position. Relative to pure SMM, the aluminium was displaced from the octahedral layer, some being found in the tetrahedral position in the 2:1 layer. It was most likely that the remaining aluminium formed charge balancing hydroxy aluminium species. The presence of the metal cations in the synthesis mixture facilitated mica montmorillonite structural layer formation. This was shown by the poorly defined basal spacing as indicated by the 001 X-ray diffraction peak for SMM as opposed to that found for the metal substituted forms. Fluorine addition at the 1wt% levels used in this work was not seen to affect the SMM crystal structure.

The 2:1 SMM layer spacing increased and the crystalline structure became less well-defined with increased nickel and cobalt content. A montmorillonite-like structure was evident for these two metals, as indicated by basal spacings close to 12.6Å, the layer spacing for pure montmorillonite. Values for the 001 spacing of >12.6Å found for NiSMM-16 (13.1Å) and -34 (13.4Å) were attributed to the effect of intercalated acetate. Greater quantities of this material would have been present at these higher metal loadings. Zinc incorporation showed a more mica-like structure at metal loadings >1wt%. The layer spacing for ZnSMM-34 of 10.7Å was close to the pure mica basal spacing of 10.6Å. The 2:1 layers were pulled closer together by the more electronegative zinc ion, seemingly not affected by the higher levels of acetate.

The packing density of the metals in SMM, as shown by the relative 06 X-ray diffraction intensities once corrected by mass absorption coefficients, increased Ni < Co < Zn. This was due to the ionic radii of the divalent metal ions which increase similarly. The ease with which these metals were incorporated into the SMM structure at the higher loadings, or for fully trioctahedral clays, had the reverse trend, Ni > Co > Zn. This was shown by the amounts of metal charged to the synthesis gel that were found present in the final SMM catalyst. Higher levels of cobalt than nickel were excluded from the SMM structure (or extra-framework cobalt) as was shown by the size of the low temperature TPR peak. This peak was equivalent to 0.73mmol H_2 consumed/g

0.73mmol H_2 consumed/g for CoSMM-33 as opposed to 0.15mmol H_2 consumed/g for NiSMM-34. The framework nickel was more accessible at higher nickel contents. This was shown by the greater ease with which nickel was reduced at the higher loadings. A greater quantity of nickel would have been present at the platelet edges and reduced by hydrogen. No evidence of the location of zinc atoms could be found by TPR due to the low standard reduction potential of Zn^{2+}.

The catalyst surface area of SMM was increased from 141m^2/g to 195m^2/g by the addition of 1wt% nickel. This area increased up to 219m^2/g at 10wt% nickel incorporation. The SMM surface area increased to 176m^2/g and 170m^2/g by 1wt% cobalt and zinc addition, respectively. These areas were, however, reduced to 126m^2/g and 99m^2/g at the >30wt% level of inclusion of cobalt and zinc, respectively. These surface area effects were still evident when the surface area was normalised to a mole of catalyst unit cell. This operation removed the effect of platelet of unit cell density changes with increased metal incorporation. It was postulated that the increase in area by nickel addition was as a result of smaller 2:1 platelets crystallising out. The nickel in the clay was cited as possible points of crystal growth termination.

The acidity of NiSMM was increased from 0.643 to 0.756mmol pyridine adsorbed/g as nickel content increased from 1 to 34wt%. This was shown by IR pyridine adsorption to be due to Lewis acidity. The Bronsted acidity decreased from 0.124 to 0.029mmol pyridine adsorbed/g over the same nickel content range. A linear correlation between Lewis acidity and nickel content was found. The increased acidity at high nickel content (NiSMM-34) was due to weak acid sites. These sites lost adsorbed pyridine at 100°C. It was proposed that these weak acid sites generated by increased nickel content were located at the SMM platelet edges, having been sites of crystal growth termination. It could generally be concluded that the acidity of SMM decreased with metal type, NiSMM > CoSMM > ZnSMM.

It has been shown that combined TG-DTA can be used successfully to compare the olefin adsorption levels and low pressure oligomerization activity of acid catalysts. The incorporation of matrix nickel and ion-exchanging 1% nickel, cobalt and zinc into SMM increased the catalyst's low pressure iso-butene oligomerization activity. These findings were consistent with the results of the high pressure propene oligomerization conducted by O'Connor *et al.* (1988). The presence of water in the olefinic feed led to higher adsorption levels due to water adsorption

species were both water and olefin. The oligomerization activity was reduced and the temperature required for the reaction to occur was increased. It was also found that adsorbed iso-butene and iso-butene in the gas stream were necessary for low pressure oligomerization of these olefins to occur.

The NiSMM-1 synthesised in this work compared favourably for propene oligomerization at 5MPa and 130°C with an equivalent commercial catalyst. The conversion level after 1hr was 17.8% as opposed to 10.8% for the commercial catalyst at a WHSV of 90g/g.hr. The optimum calcination temperature for the reaction was 500°C, the same as found by Fletcher *et al.* (1986) for SMM. The presence of water in the reactant feed caused a reduction in the catalytic oligomerization activity. The optimum NiSMM-7 synthesis pH was 8.5, as reported by Black *et al.* (1976).

The initial propene consumption rate over NiSMM-1 for oligomerization at 5MPa and 130°C increased linearly with reactant flow rate between WHSVs of 2 and 90g/g cat.hr. As expected the oligomerization selectivity showed heavier products being formed as propene conversion increased. The C_{12+} product content increased from 28.7 to 59.7% over a conversion range of 7.5 to 81.7%. This was consistent with a series/parallel reaction mechanism. The propene conversion data, when represented as a propene consumption rate, showed no sign of reaching a plateau at the high WHSVs. Film mass transfer was thus shown as the rate determining step in this range of WHSVs.

The level of initial (1hr) propene conversion in oligomerization at 5MPa and 130°C increased from 11.6 to 39.4% with increasing structural nickel content in SMM from 1 to 34wt%. As for the relationship between nickel content and Lewis acidity, a linear correlation existed between these initial conversion levels and nickel content. The rate of deactivation also increased with increasing nickel content.

The selectivity of propene oligomerization was shifted to lighter products with increased nickel content. The C_{12+} product mass percentage increased from 12.1 to 35.7% as nickel content increased from 7 to 34wt%. This effect was seen at a constant conversion level of about 17.5%. It was proposed that the increase in acidity and hence activity, was due to nickel becoming increasingly available at the platelet edges as its content in the clay was increased. The higher

levels of acidity were characterised by IR pyridine adsorption as weak Lewis acidity and would account for the shift to lighter products with increased nickel content at fixed propene conversion.

A clear trend in propene oligomerization activity could not be found for the Co and ZnSMM catalysts. The activity trend very broadly decreased, NiSMM > CoSMM > ZnSMM. It did appear that a certain minimum acidity of about 0.4mmol/g as measured by IR pyridine adsorption was required for the catalysts to be active for propene oligomerization at 5MPa and 130°C.

The 1-butene oligomerization reaction was found to be approximately second order with a rate constant of 0.01 $litre^{1.87}.mol^{-0.87}.\ g\ cat^{-1}.\ hr^{-1}$. The order of reaction was, however, not confirmed by previous olefin oligomerization studies (Haag, 1967). The kinetic data was not able to confirm or refute the proposal of a Langmuir-Rideal reaction mechanism as suggested in the low pressure thermogravimetric study of iso-butene oligomerization and reported in previous studies (Haag, 1967).

Appendices

APPENDIX 1

Calculation of nickel acetate masses for catalyst syntheses

Synthesis mixture:

10.0g SiO_2	-	10.0g
9.6g $Al_2O_3.3H_2O$	-	6.2
0.5g $NH_4F.HF$	-	0.5
3.5ml NH_4OH	-	0.8 (@ 0.9g/ml and 25% NH_4OH)
		17.5g on a nickel, water and acetate free basis

Molecular weight of nickel is 38.7g/mol and of nickel acetate is 249g/mol, hence nickel is 58.7/249 = 0.236 weight fraction of nickel acetate.

On a water and acetate-free basis:

$$\text{Ni mass fraction} = \frac{\text{mass Ni}}{17.5 + \text{mass Ni}}$$

$$\text{Ni acetate mass (g)} = \frac{17.5\ (\text{Ni mass fraction})}{0.236\ (1 - \text{Ni mass fraction})}$$

APPENDIX 2

Conversion of nickel acetate masses to cobalt and zinc acetate masses for equimolar loadings

Ni wt %	Ni acetate (g)	Moles Ni	Mass Co acetate * (g)	Mass Zn acetate * (g)
1.0	0.75	0.0030	0.75	0.66
6.8	5.40	0.0217	5.4	4.76
12.0	10.1	0.0406	10.1	8.91
21.6	20.4	0.0819	20.4	18.0
35.7	41.2	0.1655	41.2	36.2

* Molecular weights used: (g/mol)	Ni - 58.7	Co - 58.9	Zn - 65.4
	Ni acetate - 249.0	Co acetate - 249.0	Zn acetate - 219.5

APPENDIX 3

Calculation of average molar mass of gas

A typical gas analysis obtained from the GOW MAC GC for a reaction temperature of 130°C is given below:

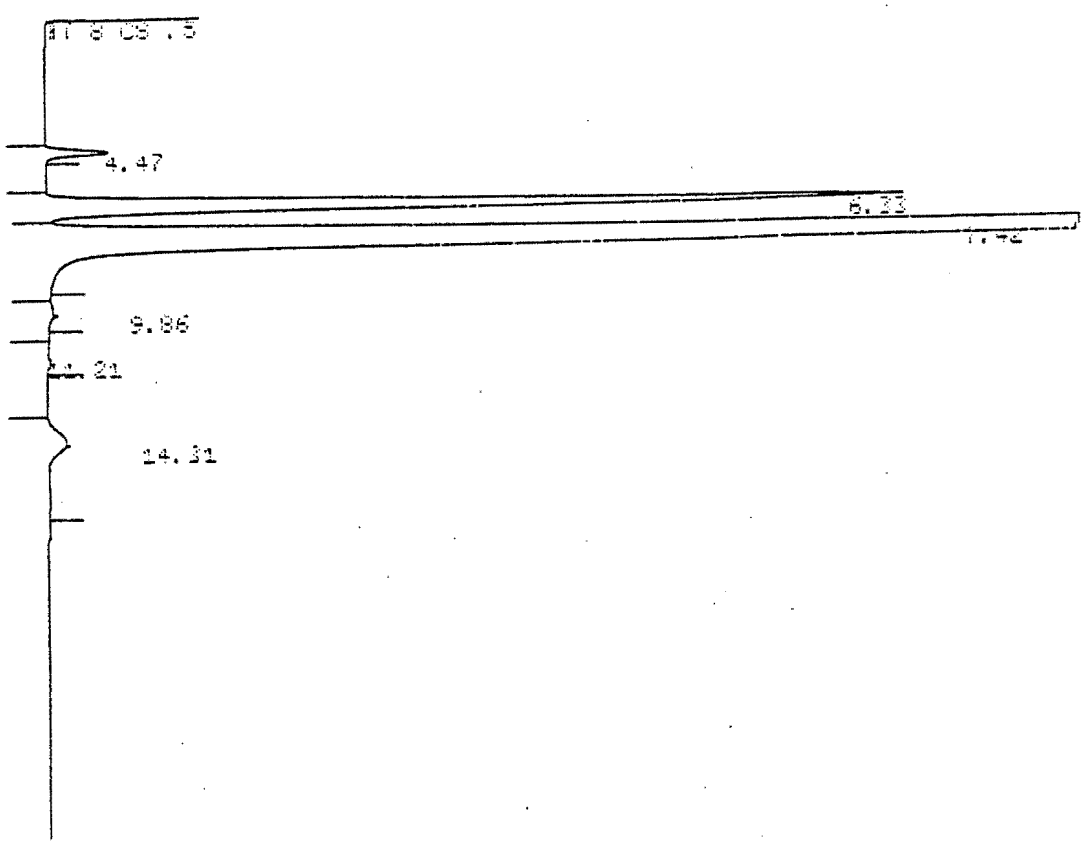

Basis: 1.0g of gas

Species	Mass fraction	Molecular weight (g/mol)	Mass fraction x Molecular weight
Ethane	0.00749	30	0.225
Propane	0.1532	44	6.741
Propene	0.82815	42	34.782
Iso-butane	0.00114	58	0.066
n-Butane	0.0004	58	0.023
n-Butene	0.00964	56	0.540

Average molar mass = 42.377

APPENDIX 4

Calculation of the feedrate, volumetric and mass flowrates of the exit gas and conversion to liquid product.

The volumetric flowrate (V) of the exit gas was calculated as:

$$V = C_f \times WGFM/t$$

V	=	flowrate (litres/hr)
C_f	=	wetgas flowmeter correction factor (See Appendix 5)
WGFM	=	difference in WGFM readings between the two time intervals
t	=	length of time interval (hr)

The compressibility factor for the effluent gas stream (25°C, 1atm) was calculated using principles of corresponding states (Smith and Van Ness, 1983) and found to be sufficiently close to unity (0.992) that it was considered to be 1.0 (i.e. an ideal gas) for the following calculation which converts the volumetric flowrate to a mass flowrate. The exit gas mass flowrate was calculated as:

$$m = [P \times V \times M / R \times (T+273) + Lg] / t$$

m	=	gas flowrate (g/hr)
P	=	atmospheric pressure
V	=	volumetric gas flowrate (litre/hr)
M	=	average molar mass
R	=	gas constant (0.082 atm. dm^3 / K)
T	=	WGFM temperature (°C)
Lg	=	mass of feed alkene and associated alkane in liquid sample
t	=	time interval (hr)

APPENDIX 4 (Continued)

The mass of the oligomerization products in the liquid sample was $L^1 = L - Lg$. The liquid production rate (LPR) was calculated as:

$$LPR = L^1 / (c \times t)$$

LPR	=	liquid production rate (g/gcat.hr)
L^1	=	mass of liquid product
c	=	catalyst mass (gcat)
t	=	time interval (hr)

The feedrate or weight hourly space velocity (WHSV) was calculated as:

$$WHSV = m/c + LPR$$

WHSV=		feedrate (g/gcat.hr)
m	=	gas flowrate (g/hr)
c	=	catalyst mass
LPR	=	liquid production rate (g/gcat.hr)

The WHSV was based on total feed (alkenes and alkanes) not just on reactant feed (alkenes).

The conversion to liquid product is given by:

$$Co = 100 \times LPR / WHSV$$

This conversion is based on total feed. To correct it to consider only the conversion of reactant feed Co is adjusted as:

$$Co^1 = 100 \times Co / (\% \text{ reactant in feed})$$

APPENDIX 4 (Continued)

A detailed example calculation of the run data is given in Appendix 6.

A mass balance was calculated for each run. This considered the total mass entering and leaving the system from run time zero until the last data point was logged.

Mass in = cylinder mass start - cylinder mass end

Mass out = $(L^1 + m \times t)$ for all time intervals

Runs for which the difference between mass in and mass out exceeded 3% were discarded.

APPENDIX 5

Calibration of the wet gas flow meter (WGFM)

The WGFM needed to be calibrated for the propene/propane hydocarbon gas mixture used in this study. The WGFM was connected to a feed cylinder by a rubber tube. The cylinder mass and WGFM reading were recorded before the gas was carefully opened to the WGFM . After a period of time (10 - 15min), the cylinder was closed and its weight and WGFM reading were noted. The ideal gas law gives the actual volume from the gas mass and the difference in the WGFM readings the apparent volume. The correction factor corrects the apparent volumetric reading to give the actual volumetric reading. This process was repeated 3 times to check the correction factor obtained. The calculations are given:

Mass of gas passing through the WGFM = Cylinder mass before - cylinder mass after

= 53.4g

From the ideal gas law:

Actual volume of gas, V = nRT/P, then for a gas of molar mass 42.38g/mol, at 1atm, 25°C and R = 0.082atm.dm^3/°K mol

$$V = (n \times 0.082 \times 298) / 1$$

$$= \frac{\text{mass of gas}}{42.38} \times 0.082 \times 298$$

$$= 30.8\text{dm}^3$$

Apparent volume of gas, V^1 = $WGFM_2$ - $WGFM_1$

= 785.8 - 754.4

= 31.4dm^3

The two volumes are related by the correction factor: $C_f = V / V^1$

= 0.981

The value of C_f was found to be reproduceable within 0.3%.

APPENDIX 6

Calculation of run data

The data below is from Run no. 86 using NiSMM-34 as the catalyst.

Data:	Reaction temperature	=	130°C
	Reaction pressure	=	5MPa
	Feed molar mass	=	42.35g/mol
	% Propene	=	86.41 mass %
	Catalyst mass (c)	=	0.50g
	C_f	=	0.981
	$WGFM_1$	=	809.9
	$WGFM_2$	=	834.2
	Gas temperature (T)	=	25°C
	Liquid sample mass (L)	=	2.01g
	Propene/propane in liquid	=	3.51 mass %
	Time (t)	=	1hr

$V = C_f \times (WGFM_2 - WGFM_1)/t$

$= 0.981 \times (834.2 - 809.9)/1$

$= 23.84 dm^3/hr$

$Mass = P(atm) \times V(dm^3.hr^{-1}) \times M(g.mol^{-1}) / [R(dm^3.atm.K^{-1}.mol^{-1}) (T(°C) + 273)]$

$= 1 \times 23.84 \times 42.35/[0.082 (25 + 273)]$

$= 41.32 g/hr$ of effluent gas

Mass of gas in liquid = 3.51/100 x L

= 0.0351 x 2.01

= 0.071g gas

Hence L^1 = 2.01 - 0.0701

= 1.94g of liquid

Activity A = $L^1/(t \times c)$

= $1.94/(1 \times 0.50)$

= 3.88g liquid/g cat. hr

WHSV = $(L/t + m)/c$

= $(2.01/1 + 41.32)/0.50$

= 86.66g/g cat.hr

Conversion based on propene feed

x = $[3.88/(86.66 \times 0.8641)] \times 100$

= 5.18%

APPENDIX 7

Chromatograms of liquid product analysis for propene and 1-butene oligomerization

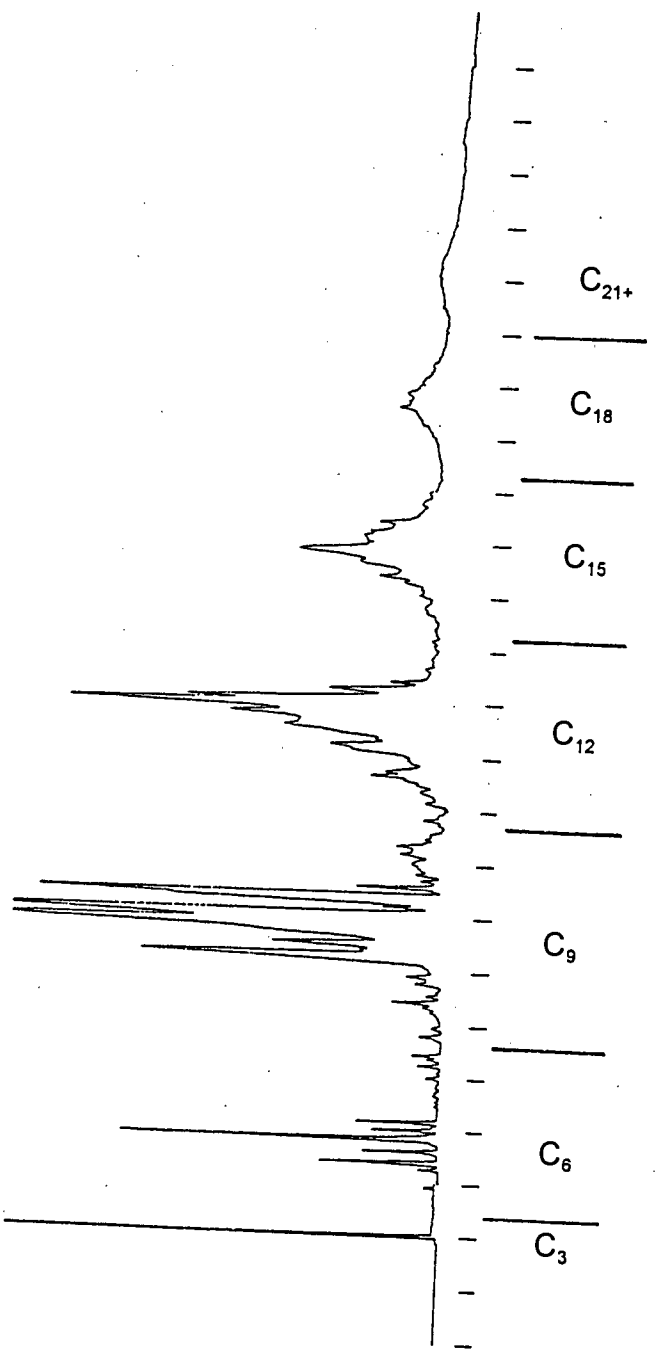

Propene

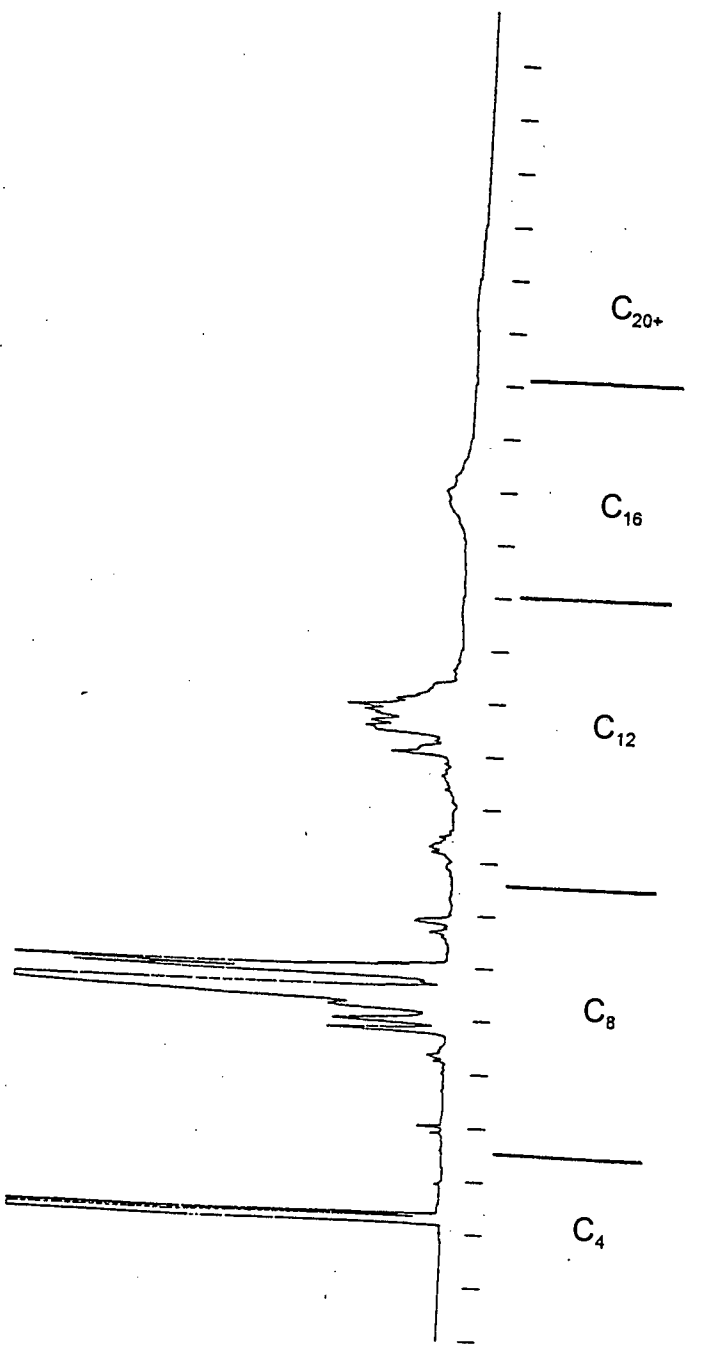

1-Butene

APPENDIX 8

Unit cell formula calculation for NiSMM-7

Chemical analysis and charge data for NiSMM-7 are given in the table below:

Component	Analysis	Cation Equiv.	Charge Equiv.	Charge per 44 Charges	Cations per unit cell
Si	20.4	0.729	2.92	25.7	6.43
Al	16.5	0.611	1.83	16.1	5.37
Ni	7.1	0.121	0.242	2.1	1.07
F	0.9	0.047	-	-	-
			4.99	43.9	

Based on the information in the table above, calculations can be made to show the distribution of cations in the tetrahedral and octahedral layers. All of the silicon is assumed to be in the tetrahedral layer and is equal to 6.43 cations per unit cell. Since there are 8 cations per unit cell in the tetrahedral layer, the number of aluminium cations per unit cell must be 1.57. There is thus a negative charge in the tetrahedral layer of 1.57.

The nickel analysis shows 1.07 cations in the octahedral layer. Since it is known that the octahedral layer has 12 charges per unit cell, it is assumed that the remaining charge of 9.89 is taken up by 3.29 aluminium cations per unit cell. The remaining 0.51 aluminiums per unit cell are ascribed to hydroxy-aluminium species, designated as $Al(OH)^{z+}_{3-z}$ which play a charge balancing role.

The number of fluorines per unit cell can be obtained by noting F/Si, expressed in terms of cation equivalents, equals that expressed as cations per unit cell, i.e.

$$\frac{F}{6.43} = \frac{0.047}{0.729}$$

$$F = 0.41$$

APPENDIX 8 (Continued)

The unit cell is thus calculated as:

$$[(Ni_{1.07}\ Al_{3.29})^{octa}\ (Si_{6.43}\ Al_{1.57})^{tetra}\ O_{20}\ (OH)_{3.54}\ F_{0.41}]\ 0.51\ Al(OH)^{z+}_{3-z}\ (1.57 - 0.51z)NH_4^+$$

APPENDIX 9

X-ray diffractograms

SMM

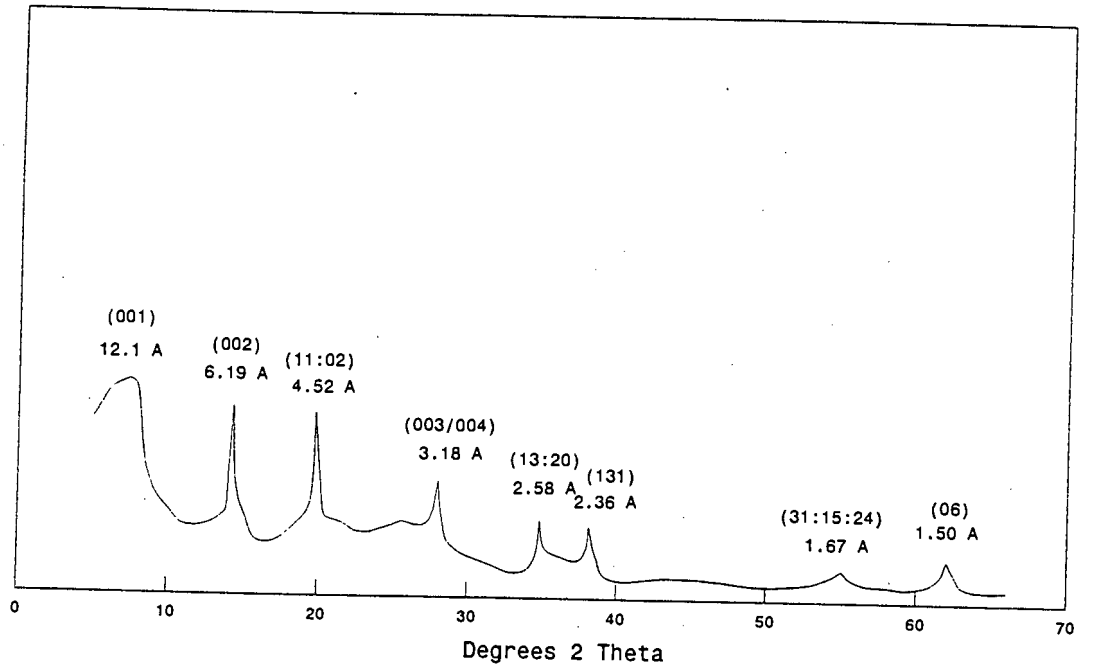

SMM-F

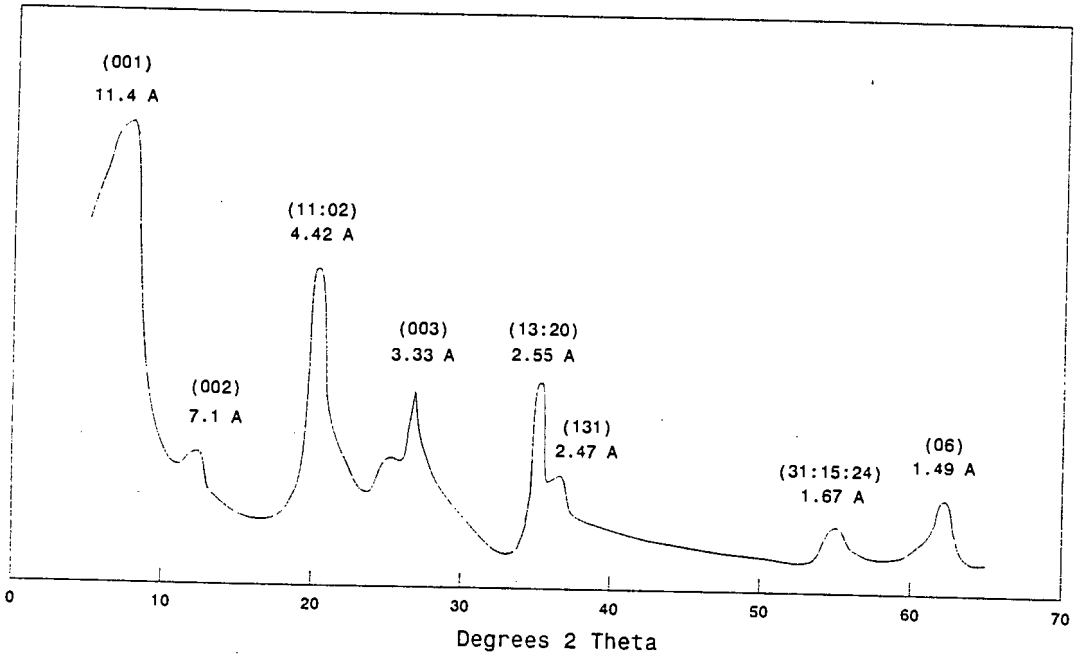

APPENDIX 9 (Continued)

NiSMM-1

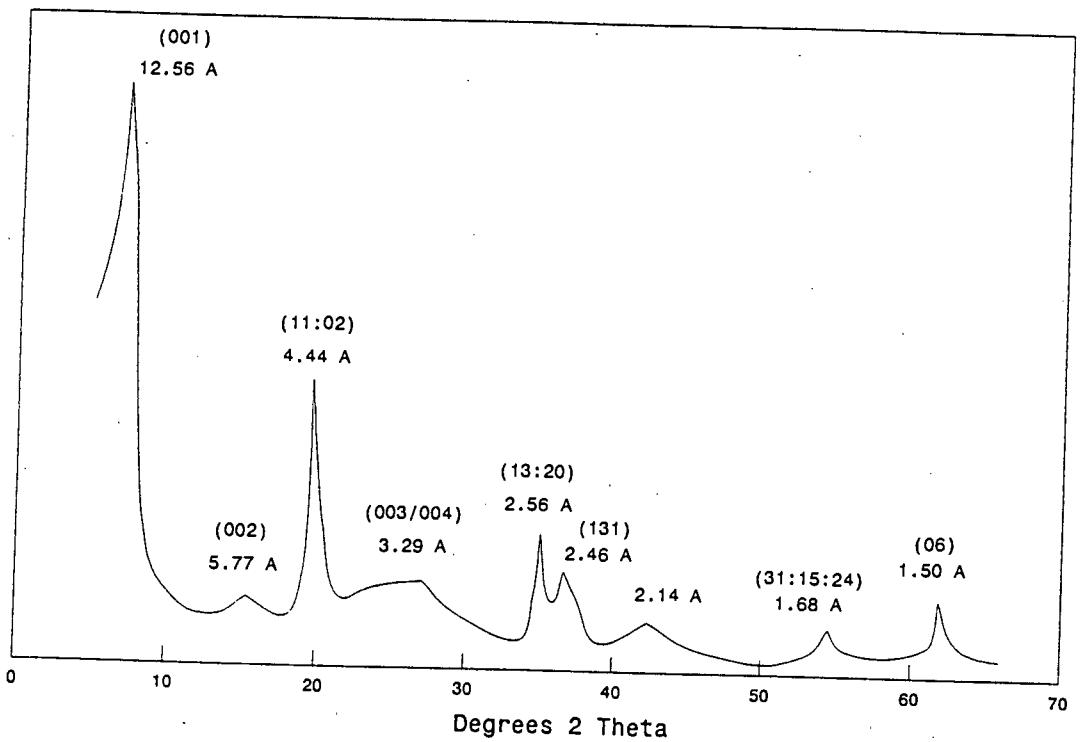

NiSMM-7

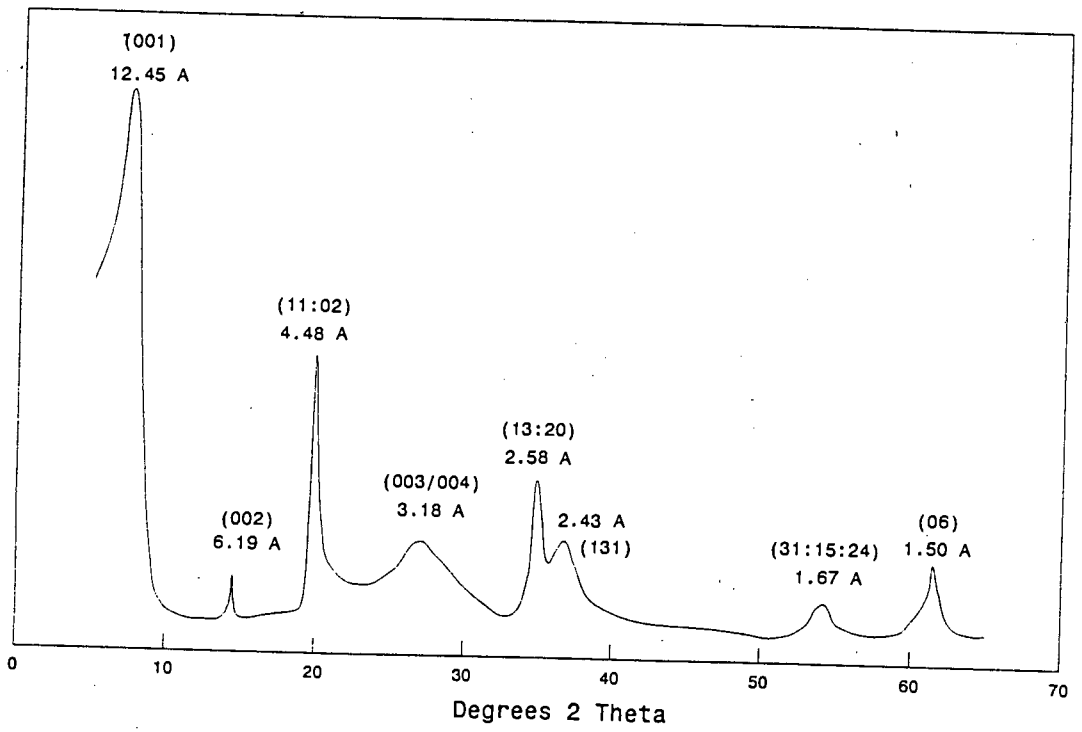

APPENDIX 9 (Continued)

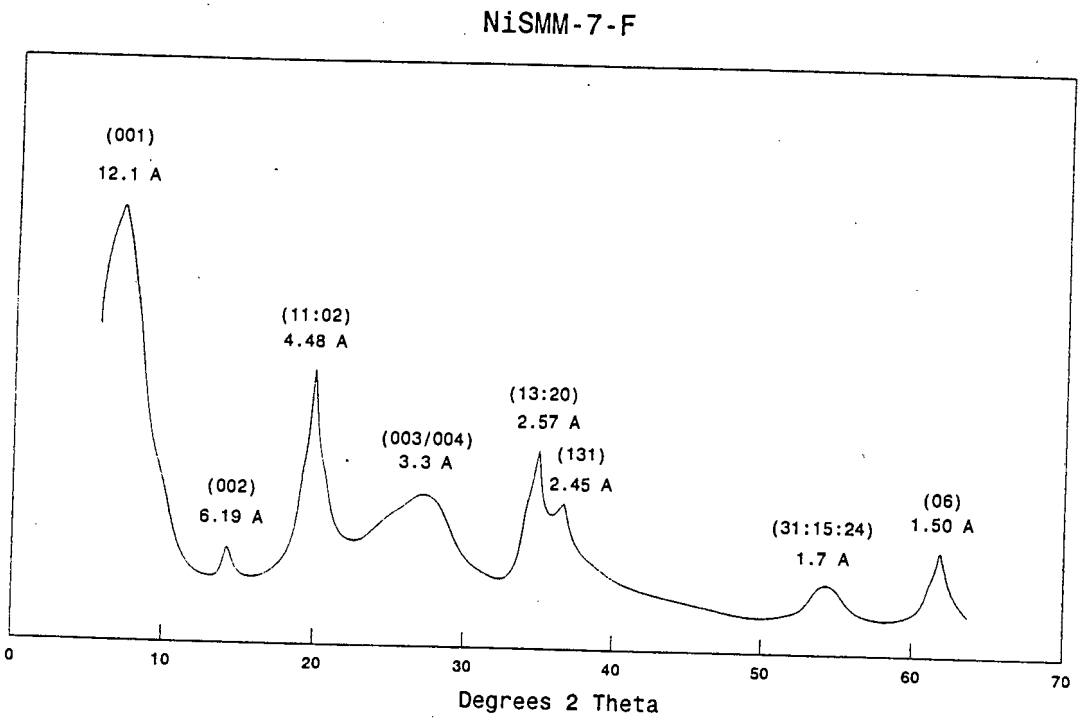

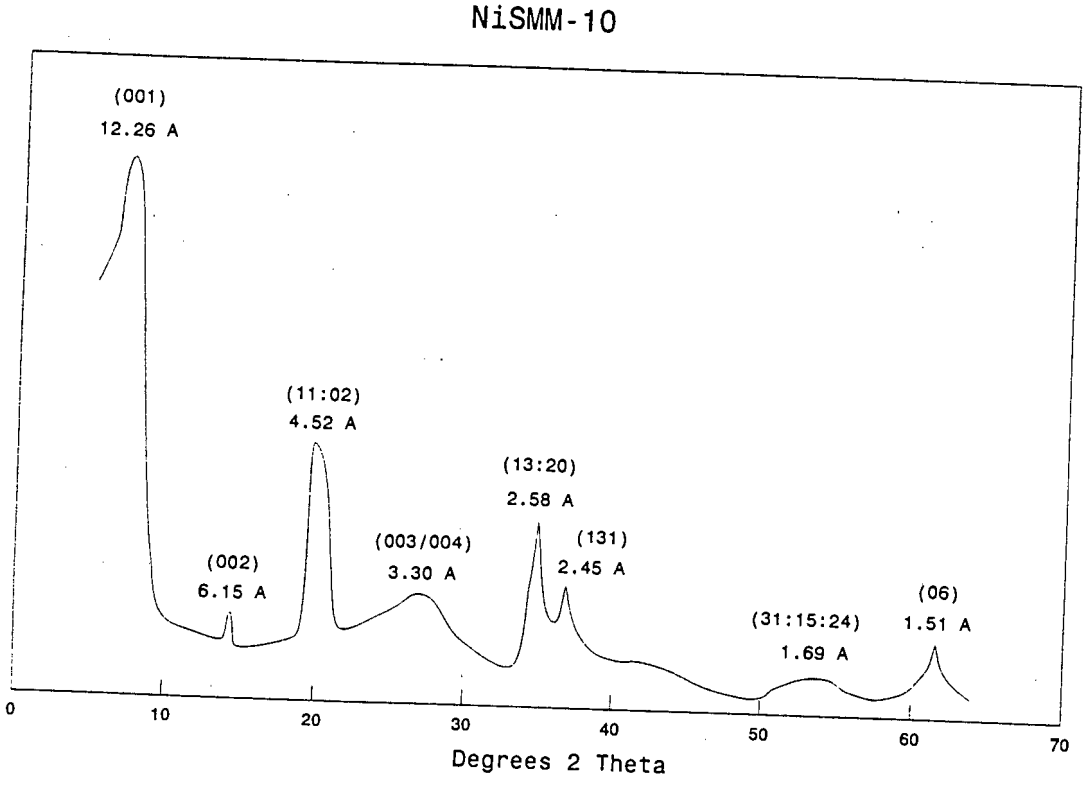

APPENDIX 9(Continued)

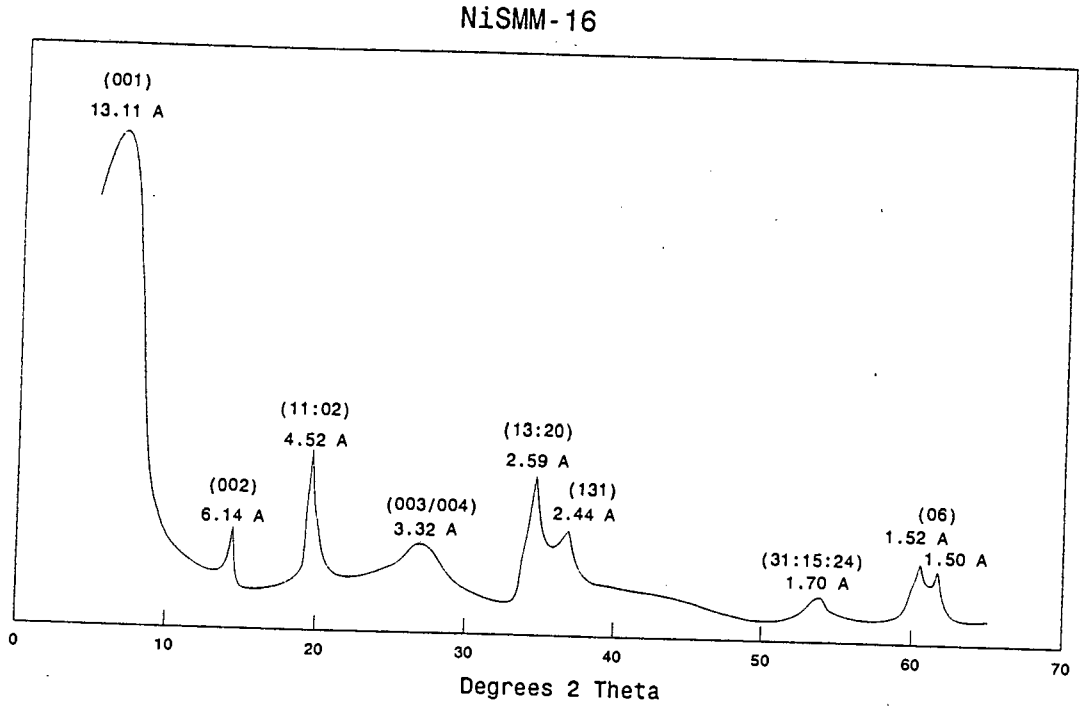

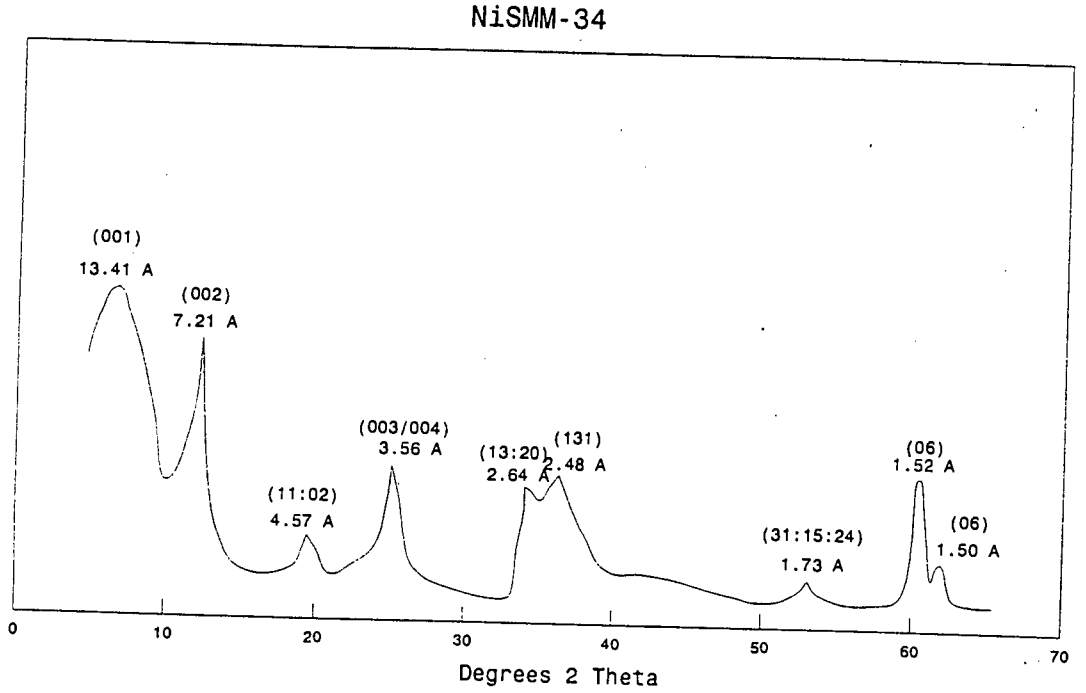

APPENDIX 9 (Continued)

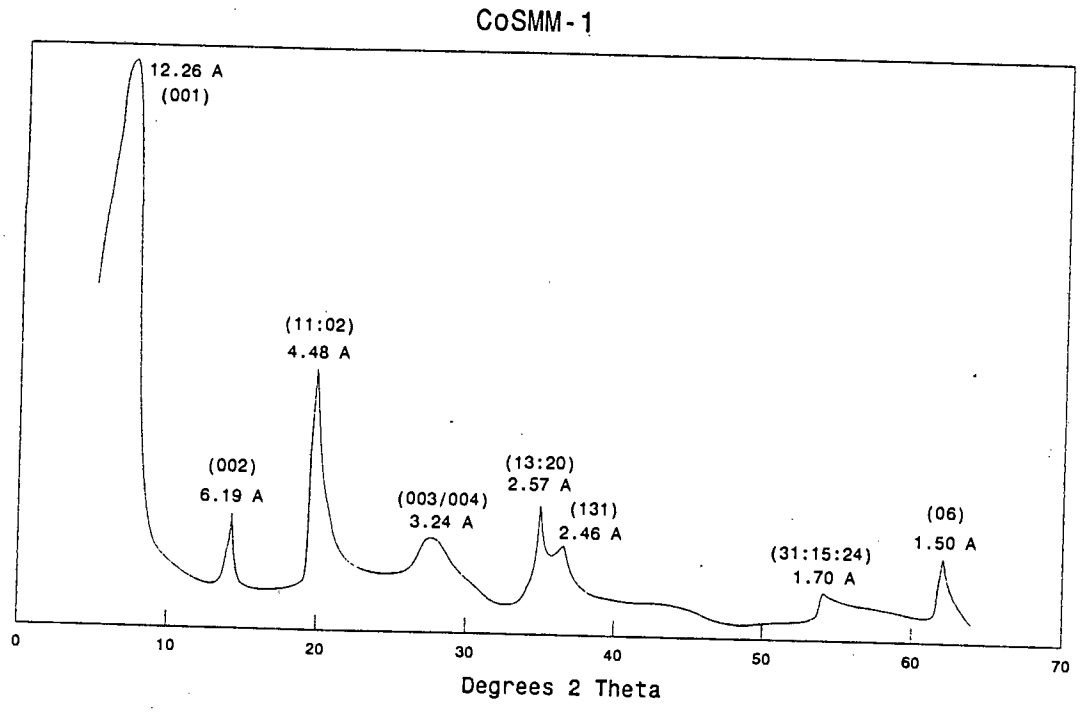

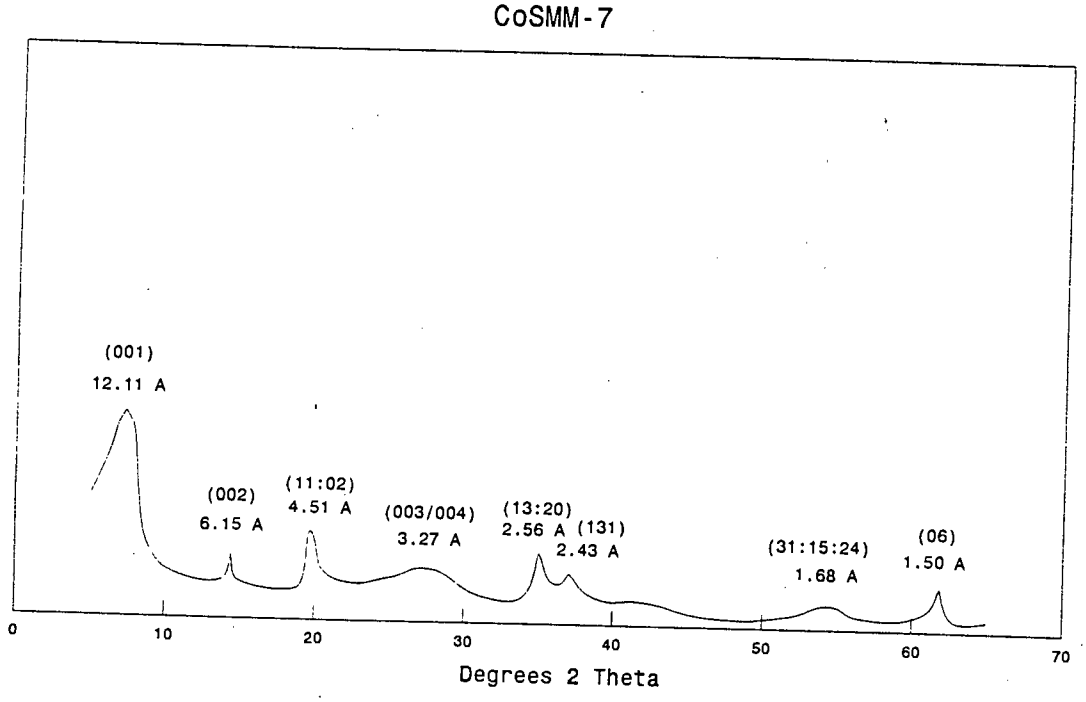

APPENDIX 9 (Continued)

CoSMM-33

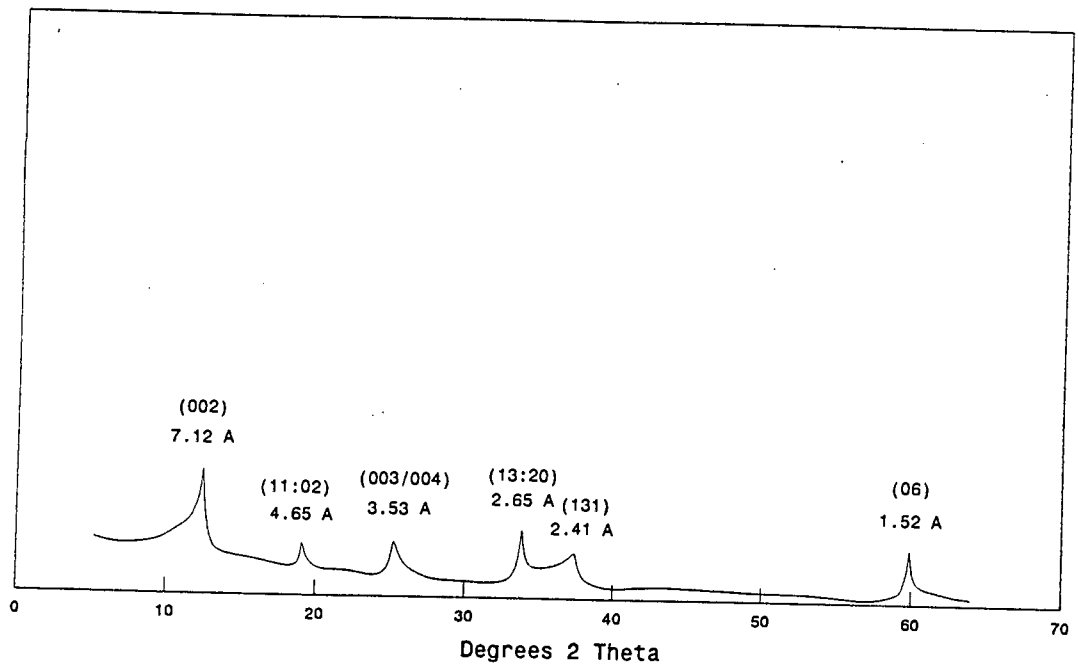

ZnSMM-1

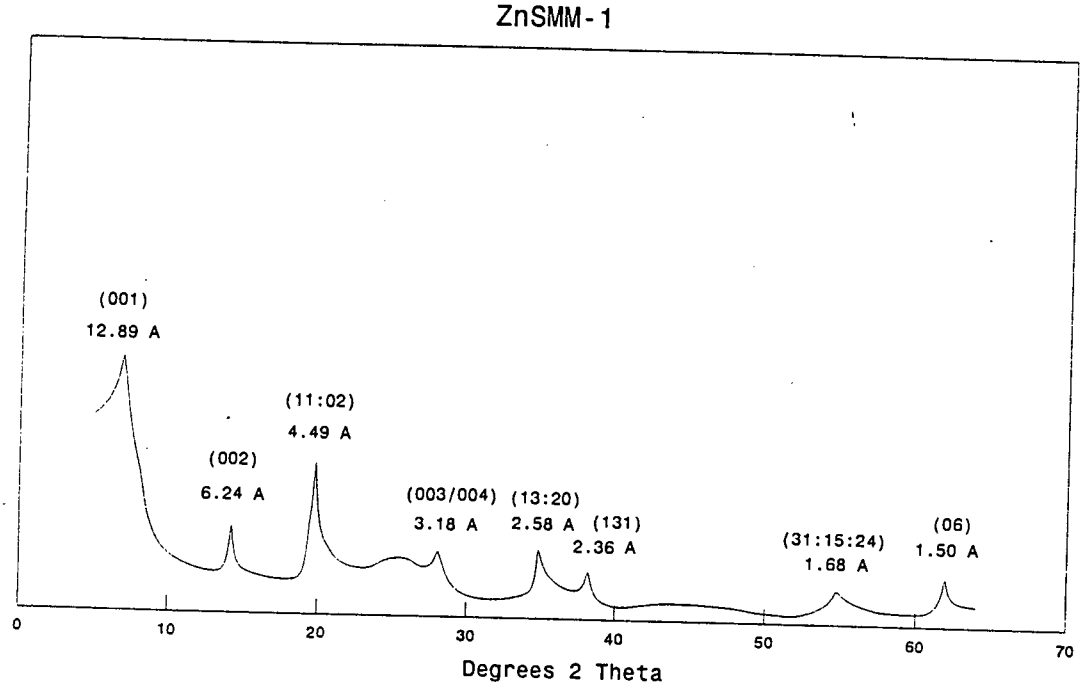

APPENDIX 9 (Continued)

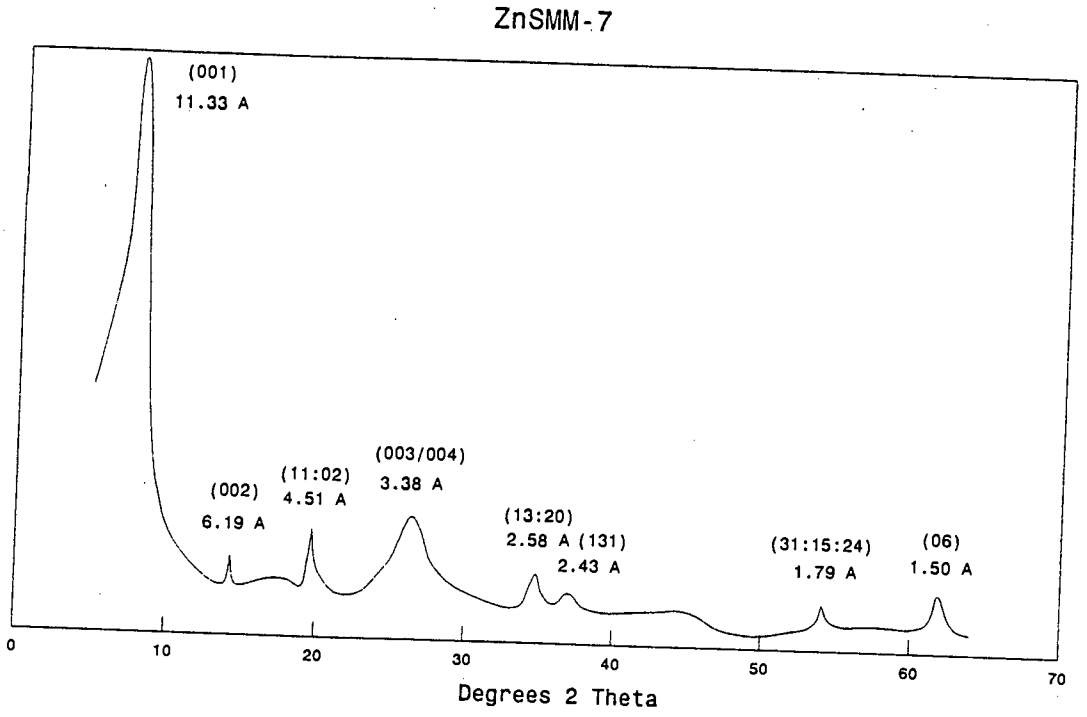

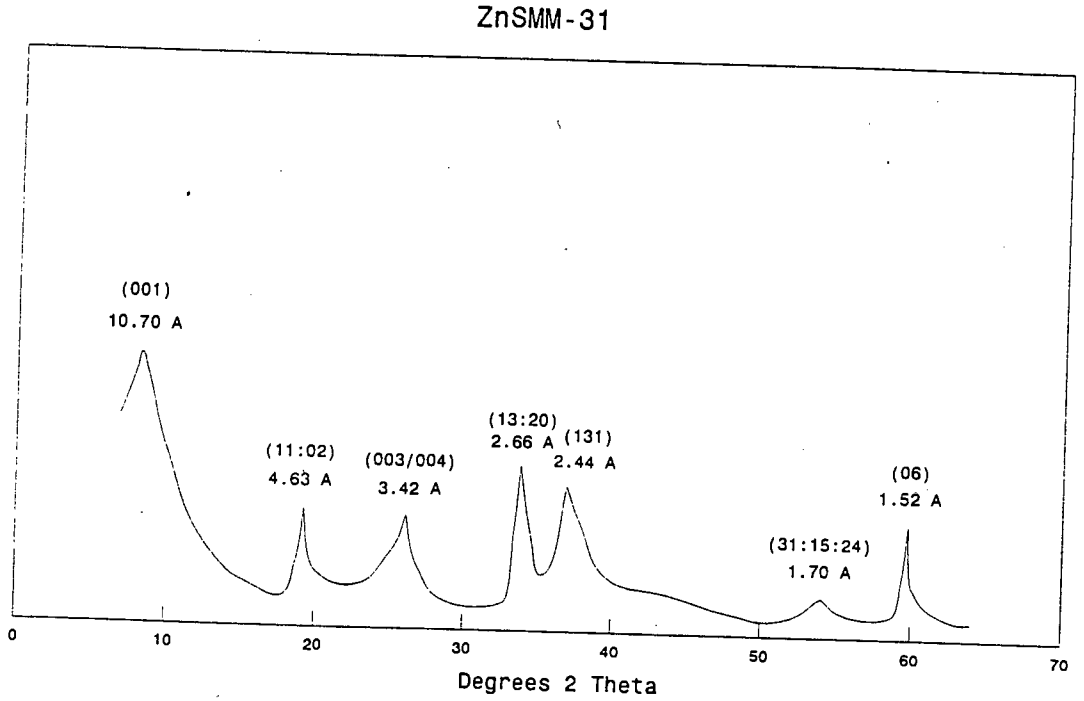

APPENDIX 10

Correction of 06 trioctahedral reflection intensities by mass absorption coefficients

The mass absorption coefficients (MAC) are calculated using the elemental analysis from Section 3.1.1. The absorption coefficient for the catalyst is the sum of the coefficients for the individual elements multiplied by their weight percentages. Si and Al are atken as their oxide forms, SiO_2 and Al_2O_3 respectively. The mass absorption coefficients used are listed below:

Element	MAC (Cu Kα)
Si	63.7
Al	49.4
O	11.2
H	0.0
F	15.5
N	49.0
Ni	49.0
Co	329.4
Zn	58.6

An example for NiSMM-1 is given:

$$MAC_1 = 0.01\,(49.0) + 0.176\,(49.4) + 0.226\,(63.7) + 0.414\,(10.2) + 0.01\,(15.5)$$
$$= 28.4$$

MAC_1 is adjusted for the contribution of an average of 10 mass % water:

$$MAC_2 = 0.9\,MAC_1 + 1.12$$
$$= 25.6 + 1.12$$
$$= 26.7$$

APPENDIX 10 (Continued)

The MAC's calculated for the catalysts, the 06 trioctahedral peak height, the corrected peak height and the number of metals per unit cell for the catalysts are listed in the following table:

Catalyst	Metals per unit cell	MAC	06 Trioctahedral peak height	Corrected height
NiSMM-1	0.14	26.7	-	-
-7	1.07	27.2	1.7	48.2
-10	1.48	28.6	2.6	74.4
-16	2.70	27.8	4.3	119.5
-34	6.00	29.7	12.5	371.3
CoSMM-1	0.15	29.4	-	-
-7	1.00	46.1	1.0	46.1
-33	5.85	114.3	3.4	388.6
ZnSMM-1	0.15	28.1	-	-
-7	0.85	28.7	1.3	37.3
-31	4.90	33.6	11.4	383.0

APPENDIX 11

Calculation of acid site concentration from infrared absorbances

From the integrated form of the Beer-Lambert law:

$$B = (cl) \int E_v^{(a)} dv \quad \text{..... (1)}$$

where B is the integrated absorbance, in cm^{-1} and (cl) is the concentration of absorbate expressed as micromoles per square centimeter of wafer cross-section.

$E_v^{(a)}$ is the apparent molar extinction coefficient at wavenumber v and $\int E_v^{(a)} dv = 0.4343$ x apparent absorption intensity.

From Hughes and White (1967),

for the Bronsted band at $1540cm^{-1}$ (pyridine ads) for zeolite Y (NH_4):

apparent integrated absorption intensity = 3.03cm/μmole

for the Lewis band at 1450cm-1 (pyridine ads) for Al-600:

apparent integrated absorption intensity = 3.26cm/μmole

hence for Bpy : $\int E_v^{(a)} dv = 0.4343 \times 3.03 = 1.32$

and for Lpy : $\int E_v^{(a)} dv = 0.4343 \times 3.26 = 1.42$

since the wafer surface area is known to be $1.327cm^2$, equation (1) can be expressed as:

APPENDIX 11 (Continued)

BPy concentration = B/wafer mass x 1.005

and LPy concentration = B/wafer mass x 0.935

where concentration is in millimoles/g catalyst and wafer mass is in mg.

An example for NiSMM-1 is given below, where B is the integrated area shown in the figure.

B (Bpy) = 0.642

B (Lpy) = 2.886

and wafer mass = 5.2mg

thus BPy = 0.124millimoles/g

and LPy = 0.519millimoles/g

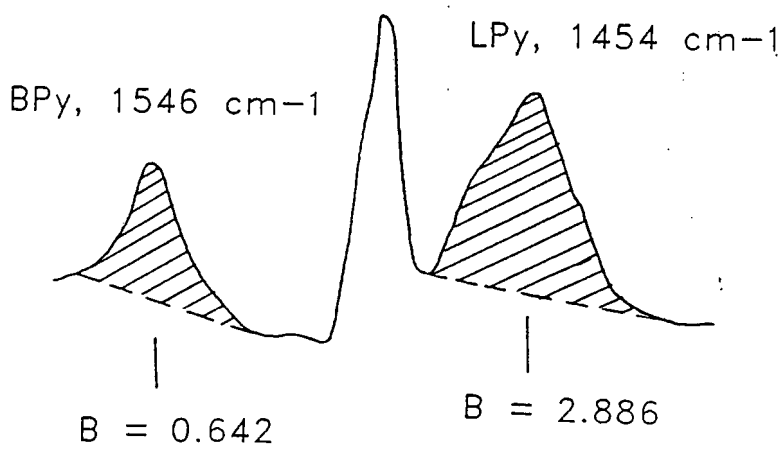

APPENDIX 12

Recalculation of propene conversion level

The propene conversion level was recalculated by correcting the $C_3^=$ content in the post-reaction gaseous stream using propane as an internal standard. The data set used was that obtained for NiSMM-34 and is presented below:

Catalyst	-	NiSMM-34
WHSV	-	88.16 g/gcat.hr
Catalyst Mass	-	0.5g
Conversion	-	6.3%
Runtime	-	4hr
Feed analysis	-	$C_3^=$ 86.41% or 38.09 g/hr
		C_3 11.76% or 5.18 g/hr
Gas rate	-	41.68 g/hr
Liquid rate	-	2.40 g/hr

The gas chromatograph used to analyse the liquid product (see Section 2.4.3.2) did not discriminate between propane and propene but gas lumped composition for both compounds. The analysis gave a value of 4.0% for the combined C_3 / $C_3^=$ liquid mass content. It was not possible to determine the split between propane and propene in the liquid product analysis. This could not be done using the gas analysis and Raoult's Law due to the error in the gas analysis. The quantity of propane in the liquid would, however, be small. The maximum amount of propane possible in the liquid would be 0.040 x 2.58 = 0.10 g.hr, which is less than 2% of the total propane in the feed and is within the 3% accuracy level required for the data. The propane liquid content was thus not used in the calculation, considering that the actual level would be even lower and would have less of an effect on the accuracy.

The propane mass in the feed was taken to be the same as the propane mass in the post reaction gas analysis. The propene mass in the post reaction gas stream was corrected by multiplying it by the propane feed mass divided by the analysed propane gas mass. This correction factor could also be applied to ethane, butane and butene gas analyses.

APPENDIX 12 (continued)

The post reaction gas mass analysis was:

	Gas Mass Analysis (%)	Analysed Mass (g.hr)	Corrected Mass (g/hr)
C_2	0.67	0.28	0.24
C_3	14.23	5.93	5.18*
$C_3^=$	83.52	34.81	30.41
C_4	0.24	0.10	0.09
$C_4^=$	1.34	0.56	0.49
	100.00	41.68	36.41

* Propane mass in feed.

The propene conversion level was calculated as:

$$x = (C_3^= \text{ in} - C_3^= \text{ out}) / C_3^= \text{ in}$$

$$= (38.09 - 30.41) / 38.09$$

$$= 20.2\%$$

APPENDIX 13

Calculation of Ni, Co and ZnSMM-1 platelet diameters

SMM has platelet dimensions:

Diameter, $D_S = 1000Å$

Height, $H_S = 37.6Å$

A platelet height of 47.0Å was used for calcined SMM considering five 2:1 layers per platelet (Wright *et al.*, 1972). The uncalcined 2:1 layer spacing of 12.5Å (platelet height = 50) collapses to 9.4Å upon calcination at 650°C (Wright, *et al.*, 1972) corresponding to the above platelet height.

Face surface area $= 2 \times 1/4 \pi D_s^2$

$= \frac{1}{2} \pi D_s^2$

Edge surface area $= \pi D_S H_S$

Total surface area $= \pi D_S (\frac{1}{2} D_S H_S)$

Platelet volume $= \frac{1}{4} \pi D_s^2 H_S$

Surface area/volume $= \dfrac{2D_S + 4H_S}{D_S H_S}$

For the following calculations it is assumed that 1% metal substituted SMM has a similar calcined 2:1 layer spacing and platelet density to SMM. The platelet height will therefore be the same. The assumption of similar platelet densities is considered valid since they have been calculated to be 720.0 and 724.5g/mol u.c. for SMM and NiSMM-1, respectively, from the unit cell formulae in Table 3.2.

APPENDIX 13 (Continued)

For metal substituted SMM,

$$\text{Surface area/volume} = \frac{2D_m + 4H_s}{D_m H_s}$$

The surface area of the platelets must increase in the same ratio as the surface areas measured for the bulk material.

Thus, if z = surface area metal SMM ÷ surface area of SMM

$$z = \frac{2D_m + 4H_s}{D_m H_s} \times \frac{D_s H_s}{2D_s + 4H_s}$$

this reduces to

$$D_m = \frac{2D_s H_s}{z(D_s + 2H_s) - D_s}$$

Using the above formula the following platelet diameters were calculated:

	z	D_m (Å)
NiSMM-1	1.38	184
CoSMM-1	1.25	255
ZnSMM-1	1.21	290

APPENDIX 14

Langmuir-Hinshelwood and Langmuir-Rideal reaction controlling mechanisms

The two reations mechanisms that were considered are surface reaction controlling (Langmuir-Hinshelwood) and reaction controlling between a gas phase and a molecule absorbed on the catalyst surface (Langmuir - Rideal).

The following reaction steps are considered:

1) $A + X = A \,.\, X$ adsorption
2) $A + A \,.\, X = B \,.\, X$ reaction
3) $B \,.\, X = B + X$ desorption

Langmuir-Hinshelwood Reaction Controlling

For surface reaction controlling of the reaction $A + B \longrightarrow C$, the rate has been given as (Smith 1981), where ^ denotes surface concentration:

$$r = k_S C_M\hat{} K_A K_B \frac{C_A C_B - (1/K) C_C}{(1 + K_A C_A + K_B C_B + K_C C_C)^2}$$

In the dimerization reaction A = B and C will be called B. The above equation then becomes,

$$r = k_S C_M\hat{} K_A^2 \frac{C_A^2 - (1/K) C_B}{(1 + 2K_A C_A + K_B C_B)^2}$$

If $k_S C_M\hat{} K_A^2 = X$, then

$$r = \frac{X [C_A^2 - (1/K) C_B]}{(1 + 2K_A C_A + K_B C_B)^2}$$

APPENDIX 14 (Continued)

If $C_B \longrightarrow 0$,

$$r = \frac{X C_A^2}{(1 + 2K_A C_A)^2}$$

linearising, $$r^{-\frac{1}{2}} = \frac{X^1 C_A}{1 + Y C_A}$$

$$1 + Y C_A = \frac{X^1 C_A}{r^{-\frac{1}{2}}}$$

$$\frac{C_A}{r^{-\frac{1}{2}}} = X^{11} + Y^1 C_A$$

$$Y^1 = \frac{\Sigma (C_A / r^{-\frac{1}{2}}) C_A - (\Sigma C_A \Sigma C_A / r^{-\frac{1}{2}}) / n}{\Sigma C_A^2 - (\Sigma C_A)^2 / n}$$

$$X^{11} = \frac{\Sigma C_A / r^{-\frac{1}{2}} - Y^1 \Sigma C_A}{n}$$

	r (mol/g cat.hr)	C_A (mol/litre)	C_A^2	$r^{-\frac{1}{2}}$	$C_A / r^{-\frac{1}{2}}$	$(C_A / r^{-\frac{1}{2}}) C_A$
	0.015	1.3	1.7	0.12	11	14
	0.071	2.7	7.3	0.27	10	27
	0.13	4.1	12	0.36	11	45
	0.22	5.5	30	0.47	12	66
Σ	0.44	13.6	55	1.22	44	152

From the data in the table above,

$$X^{11} = 10$$
$$Y^1 = 0.27$$

The rate is therefore given as,

$$r = \frac{C_A^2}{(10 + 0.27 C_A)^2}$$

APPENDIX 14 (Continued)

The rate as predicted by the surface reaction controlling model are

C_A (mol/litre)	r_{calc} (mol/g cat.hr)	r_{exp} (mol/g cat.hr)
1.3	0.016	0.015
2.7	0.063	0.071
4.1	0.14	0.13
5.5	0.23	0.22

Langmuir-Rideal Reaction Controlling

Since reaction is the rate controlling step, then the surface concentration of reactant (C_A^) would be at equilibrium:

Adsorption: $$(C_A^)_{eq} = K_A C_A C_V^ \quad \text{.....(1)}$$

Gas phase and adsorbed phase reaction:

$$r_S = k_S C_A^ C_A - k_S^{1} C_B^$$
$$= k_S (C_A^ C_A - 1/K_S C_B^) \quad \text{.....(2)}$$

Substituting (1) into (2) yields,

$$r = k_S (K_A C_A^2 C_V^ - 1/K_S K_B C_B C_V^) \quad \text{.....(3)}$$

The total number of adsorption sites (C_M^) is given by,

$$C_M^ = C_V^ + C_A^ + C_B^ \quad \text{.....(4)}$$

Since the reaction rate is controlling, the absorbed concentraions will be at equilibrium, then substituting (1) for C_A^ and for C_B^ into (4),

$$C_M^ = C_V^ + K_A C_A C_V^ + K_B C_B C_V^$$

APPENDIX 14 (continued)

$$C_V\hat{} = \frac{C_M\hat{}}{1 + K_A C_A + K_B C_B} \quad \text{.....(5)}$$

Now, substituting (5) into (3) gives,

$$r = \frac{k_S C_M\hat{} (K_A C_A^2 - 1/K_S K_B C_B)}{1 + K_A C_A + K_B C_B}$$

If $C_B \longrightarrow 0$ (rates extrapolated to time = 0), then

$$r = \frac{k_S C_M\hat{} K_A C_A^2}{1 + K_A C_A}$$

linearising,

$$r = \frac{A C_A^2}{1 + K_A C_A}$$

$$\frac{A C_A^2}{r} = 1 + K_A C_A$$

$$\frac{C_A^2}{r} = A^1 + B^1 C_A$$

$$B^1 = \frac{\Sigma (C_A^2 / r) C_A - (\Sigma C_A \Sigma C_A^2 / r) / n}{\Sigma C_A^2 - (\Sigma C_A)^2 / n}$$

$$A^1 = \frac{\Sigma C_A^2 / r - B^1 \Sigma C_A}{n}$$

APPENDIX 14 (Continued)

	r (mol/g cat.hr)	C_A (mol/litre)	C_A^2	C_A^2 / r	$(C_A^2 / r) C_A$
	0.015	1.3	1.7	110	140
	0.071	2.7	7.3	100	270
	0.13	4.1	16	120	490
	0.22	5.5	30	140	770
Σ	0.44	13.6	55	470	1700

From the data in the above table,

$$B^1 = 12$$

$$A^1 = 77$$

Hence

$$r = \frac{C_A^2}{77 + 12\,C_A}$$

The reaction rate as predicted by the Langmuir Rideal reaction model,

C_A (mol/liter)	r_{calc} (mol/g cat.hr)	r_{exp} (mol/g cat.hr)
1.3	0.018	0.015
2.7	0.067	0.071
4.1	0.13	0.13
5.5	0.21	0.22

The calculated rates obtained for both the Langmuir-Hinshelwood and Langmuir-Rideal reaction mechanisms were essentially the same as the experiment values found considering that the numbers were reported to two significant figures.

References

REFERENCES

Agrawal, C.L., and Banerjee, S.P., J. Inst. Chem. (India), **57,** *2,* 65 (1985)

Alberty , R.A., Chem. Eng. Sci., **42,** *10,* 2325 (1987)

Alberty, R.A., and Gehrig, C.A., J. Phys. Chem. Ref. Data, **14,** *3,* 803 (1985)

Annual Report, SASOL (1995)

Argauer, R.J., and Landolt, G.R., US Patent 3 702 886 (1972)

Ashley, K.D., and Innes, W.B., Ind. Eng. Chem., **42,** 866 (1952)

Austermann, R.L., Analytical Chem., **59**, 12 (1987)

Bailey, S.W., in "Crystal Structures of Clay Minerals and their X-ray Indentification", Brindley G.W., Brown, G., (Eds), Mineral Soc., London (1980)

Barrer, R.M., "Zeolites and Clay Minerals as Sorbents and Molecular Sieves", Academic Press, New York (1978)

Barrer, R.M., and Macleod, D.M., Far. Soc. Trans., **50,** 980 (1950)

Barrer, R.M., and Reay, J.S.S., J. Chem. Soc., **4,** 3824 (1958)

Bauer, R.S., Chung, H., Glockner, P.W., Keim, W., and van Zuret, H., US Patent 3 635 937 (1972)

Benedek, W.J., and Mauleon, J-L., Oil and Gas J., 77 (1980)

Benesi, H.A., and Winquist, B.H.C., Advances in Catalysis, **27** 172 (1978)

Bercik, P.G., Merzger, K.J., and Swift, H.E., Ind. Eng. Chem. Prod. Res. Dev. **17,** *3,* 214 (1978)

Bethea, S.R., and Karchmer, J.H., Ind. Eng. Chem., **48,** *3,* 370 (1956)

Black, E.R., Montagana, A., and Swift, H.E., US Patent, 3 966 642 (1976)

Bolis, V., and Vedrine, J.C., J.C.S Faraday I., **76**, 1606 (1980)

Bourne, K.H., Cummings, F.R., and Pitkethly, R.C., J. Phys. Chem., **74,** *10* 2197-2205 (1970)

Brindley, G.W., Clays and Clay Minerals, 14th Nat. Conf., 31 (1964).

Brindley, G.W., and Sempels, R., Clay Minerals, **12,** 229 (1977)

Brink, A., and Swart, J.S. de K, "The Fischer-Tropsch Synthesis as applied at Secunda with Special Reference to Product Work-up and Product Quality", International Coal Conversion Conference CSIR, South Africa (1982)

Brown, G., "The X-ray Identification and Crystal Structure of Clay Minerals", Mineralogical Society, London, (1961)

Brown, G. (Ed), "The X-ray Identification and Crystal Structures of Clay Minerals", Jarrold and Sons Ltd., Norwich (1972)

Burch, R., and Flambard, A.R., J. Catal., **85,** 16 - 24 (1984)

Capell, R.G., and Granquist, W.J., US Patent 3 252 889 (1966)

Cariati, F., Erre, L., Micera, G., Piu, P., and Gessa, C., Clays and Clay Minerals, **31,** *2,* 155 (1983)

Cavell, K.J., in "Methane Conversion", Biddy, B.M., Chang, C.D., Howe, R.F., and Yurchak, S. (Ed's) Elsevier, Amsterdam, 523 (1988)

Chu, C.T.W., and Valyocsik, E.W., US Patent 4 665 250 (1987)

Coleman, N.T., and Harward, M.E., J. Amer. Chem. Soc., **75,** 6045 (1953)

Coleman, N.T., and Mc Auliffe, C., "Clays and Clay Minerals , 3rd Nat. Conf., 282 (1954)

Csicsery, S.M., US Patent 3 617 488 (1971a)

Csicsery, S.M., US Patent 3 617 489 (1971b)

Csicsery, S.M., US Patent 3 617 490 (1971c)

Csicsery, S.M., US Patent 3 617 491 (1971d)

Csicsery, S.M., and Kittrell, J.R. , US Patent 3 632 500 (1972)

Datka, J., Turek, A.M., Jehng, J.M., and Wachs, I.E., J.Catal., **135,** 186 (1992)

Davidson, R.C., Ewing, E.J., and Shute, R.S., Natl. Pet. News., **35,** 318 (1943)

Davidtz, J.C., J. Catal., **43,** 260 (1976)

De Lange, M., and Van Steen, E., "Review: Ion Support Interaction in Catalyst Preparation and a TRP Study on the Preparation of Co/SiO_2", University of Cape Town, Republic of South Africa, (1995)

Dejaifre, P., Auroux, A., Gravelle, P.C., and Vedrine, J.C., J Catal., **70,** 123 (1981)

Derouane, E.G., Gilson, J.P., and B.Nagy, J., J. Molec. Catal., **10,** 331 - 340 (1981)

Derouane, E.G., Gilson, J.P., and B.Nagy, J., Zeolites, **2,** 42 - 46 (1982)

Dillard, C.R., and Goldberg, D.E., "Chemistry - reactions, structure and properties", 2nd Ed, Macmillan, 131 (1978)

Dry, M.E., in "Catalysis: Science and Technology1", Anderson, J.R., and Boudart, M. (Eds.) Springer Verlag, New York, 159 (1981)

Dry, M.E., "High Yield, High Quality Diesel from Fischer-Tropsch Processing", International Coal Conversion Conference, CSIR, South Africa (1982a)

Dry, M.E., Chemtech, 744 (1982b)

Dry, M.E., Catalysis Today, **6,** *3,* 183 (1990)

Elliot , D.J., and Lunsford, J.H., J. Catal., **57,** 11 (1979)

Emeis, C.A., J.Catal., **141,** 347 (1993)

Espinoza, R.L., Nicolaides, C.P., Korf, C.J., and Snel, R., Applied Catalysis, **31,** 259 - 266 (1987a)

Espinoza, R.L., Korf, C.J., Nicolaides, C.P., and Snel, R., Applied Catalysis, **29,** 175 - 184 (1987b)

Evans, A.G., and Polyani, M., J. Chem. Soc., 252 (1947)

Farmer, V.C., and Russell, J.D., Spectro-chimica. Acta, **20,** 1149-1173 (1964)

Filtrol Corporation, Clay Products Division, 3250E Washington Blvd, Los Angeles, CA 90023, USA.

Farmer, V.C., and Mortland, M.M., J. Chem. Soc. **A,** 344 (1966)

Fischer, D.C., and Giannetti, J.P., Preprints Div. Pet. Chem., **20,** *2* (1975)

Fletcher, J.C.Q., Ph D thesis, University of Cape Town, Republic of South Africa (1984)

Fletcher, J.C.Q., Kojima, M., and O'Connor, C.T., Applied Catalysis, **28,** 169 (1986)

Flory, P.J., "Principles of Polymer Chemistry", Comell University Press, Menasha, 217 (1969)

Frenkel, M., Clays and Clay Minerals, **22,** 435 (1974)

Frohning, C.D., Kölbel, M., Ralek, M., Rottig, W., Schnur, F., and Schultz, H., in "Chemical Feedstocks from Coal", Falbe, J. (Ed.), Wiley, New York (1982)

Gaaf, J., and Van Santen, R., European Patent 0 090 442 (1983)

Gabelica, Z., Nagy, J.B., Deroune, E.G., and Gilson, J P., Clay Miner., **19,** *5* 803 (1984)

Gallezot, P., and Imelik, B., J. Phys. Chem., **77,** 652 (1973)

Garwood, W.E., Caesar, P.D., and Brennan, J.A., US Patent 4 150 062 (1972)

Garwood, W.E., and Lee, W., US Patent 4 227 992 (1980)

Garwoord, W.E., in "Intrazeolite Chemistry" Chpt 23, Stucky, G.D., and Dwyer, F.G.(Eds.) ACS Symposium Series, **218,** 383 (1983)

Germain, J.E., "Catalytic Conversion of Hydrocarbons" Chpt 4, Academic Press, London (1969)

Ghosh, A.K., and Curthoys, G., J. Phys. Chem., **88,** 1130 (1984)

Gilson, J-P., Ph.D thesis, University of Naumer, Belgium (1982)

Grady, M.C., and Gorte, R.J., J. Phys. Chem., **81,** 1305 (1985)

Granquist, W.J., US Patent 3 252 757 (1966)

Granquist, W.J., US Patent 3 852 405 (1974)

Granquist, W.J., US Patent, 3 976 744 (1976)

Granquist, W.J., Hoffman, G.W., and Boteler, R.C., Clays and Clay Minerals, **20** 323 (1972)

Granquist, W.J. and Kennedy, J.V., Clays and Clay Minerals, Proc. 15th Intl. Conf., Pegaman Press, New York, 103 (1967)

Granquist, W.J., and Pollack, S.S., Am. Mineral, **52,** 212 (1967)

Grim, R.E., "Clay Mineralogy, 2nd Ed., Mc Graw-Hill, 194 (1968)

Haag, W.O., Chem. Eng. Prog. Symp. Ser., **63,** *73,* 140-147 (1967)

Hall, P.L., Clay Minerals, **15,** 321 (1985)

Harms, S.M., Kojima, M., and O'Connor, C.T., Fuel Proc. Tech., **31,** 231 (1989)

Horvarth, I., Sanko, E.S., Paukshtis, E.A., and Yurschenko, E.N., Chemicke Zvesti, **36,** *4,* 515-522 (1982)

Hattori, S.W., Milliron, D.L., and Hightower, J.W., Preprints Div. Pet. Chem., **18,** *1* (1973)

Heinerman, J.J.L., Freriks, J.L., Gaaf, J., Pott, G.T., and Coolegem, J.G., J. Catal., **80,** 145 (1983)

Hoffman, G.W., and Granquist, W.J., US Patent 3 816 343 (1974)

Hogan, J.P., Banks, R.L., Lanning, W.C., and Clark, A., Ind. Eng. Chem., **47,** *4,* 752 (1955)

Hongdu, H., Masters Thesis, Research Institute of Petroleum Processing, Beijing, China, (1981)

Hoogendoorn, J.C., "The Sasol Story", American Institute of Mechanical Engineers, 23rd Annual Meeting (1974)

Hoogendoorn, J.C., Hydrocarbon Processing, 34-E (1982)

Hughers, J.R., and White, H.M., J. Phys. Chem., **71,** 2192 (1967)

Hulthén, B., "Clay Minerals - Modern Society", Nordic Society for Clay Research in Shaikh, N.A., and Wik, N.-G., (Eds), Uppsala, 99-109 (1986)

Inui, T., Matsuda, H., and Takegami, Y., Proc. Sixth Int. Zeolite Conf., Reno, 316 - 324 (1984)

Ipatieff, V.N., Ind. Eng. Chem., 1067 (1935)

Jaffe, J., US Patent 3 652 457 (1972a)

Jaffe, J., US Patent 3 664 971 (1972b)

Jaffe, J., US Patent 3 664 972 (1972c)

Jaffe, J., US Patent 3 664 973 (1972d)

Jaffe, J., and Kittrell, J.R., US Patent 3 671 425 (1972)

Jager, B., Fischer-Tropsch Synthesis, Spring School in Coal Conversion, Rand Afrikaans University, South Africa, (1978)

Jasra, R.V., and Bhat, S.G.T., Advances in Catalysis, Science and Technology, Proc. 7th Nat. Symp. on Catalysis, 423 (1985)

Jepson, W.B., in "Clay Minerals: Their Structure, Behaviour and Use", Fowden, L., Barrer, R.M., and Tinker, P.B. (Eds), The Royal Society, London 191-212 (1984)

Johns, W.D., and Shimoyama, A., Amer. Ass. Petrol. Geol. Bull, **56,** 2160 (1972)

Jones, W., Catalysis Today, **2,** 357 (1988)

Keim, W., Hoffman, B., Lodewick, R., Peuckert, M., Schmitt, G., Fleischhauer, J., and Meier, U., J. Molec. Catal., **6,** 79 (1979)

Keim, W., Behr, A., and Kraus, G., J. Organometallic Chem., **251,** 377 (1983)

Kittrell, J.R., US Patent 3 632 501 (1972a)

Kittrell, J.R., US Patent 3 632 502 (1972b)

Kittrell, J.R., Langlois, G.E., and Scott, R., US Patent 3 625 865 (1972)

Kofke, T.J.G., and Gorte, R.J., J Catal., **115,** 223 (1989)

Kojima, M., Fletcher, J.C.Q., and O'Connor, C.T. Applied Catalysis, **28,** 169 (1986)

Kojima, M., Rautenbach, M.W., and O'Connor, C.T., Ind. Eng. Chem. Res., **27,** 248 (1988)

Kubelkova, L., Novakova, K., Tupa, M., and Tvaruzkova, Z., Acta Phys. Chem., **31,** *1-2* 649 (1985)

Maes, A., Peignew, P., and Cremers, A., in "Proc. Int. Clay Conf., Mexico City, July 16-23 1975" S.W. Bailey (Ed.), Applied Publishing, Wilmette, 319-329 (1976)

Maiden, C.J., Stud. Surf. Sci. Catal., **36,** 1 (1988)

Makarova, M.A., Karim, K., and Dwyer, J., Microporous Minerals, **4,** 243 (1995)

Malasky, B.F., US Patent 3 682 811 (1972)

Mathers, A.C., Weed, S.B., and Coleman, N.T., Clays and Clay Minerals, 3rd Nat. Conf. 403 (1954)

Matsumato, M., Bull. Chem. Soc., Japan, **57,** 1795 (1984)

Mc Mahon, J.F., Bednars, C., and Solomon, E., in "Adv. Pet. Chem. Refin. 1", Chpt 5, McKetta jr., J.J., (Ed), Interscience Publishers (1963)

McClean,D.M.M., Ph.D thesis, University of Cape Town, South Africa, (1988)

Meisel, S.L., Mc Cullough, J.P., Lechthaler, C.H., and Weisz, P.B., Chemtech, **86** (1976)

Ming-Yuan, H., Zhanghui, L., and Enze, M., Catalysis Today, **2,** 321 (1988)

Mortland, M.M., Trans., 9th Int. Congr. Soil Sci., **1,** 691 (1968)

Mortland, M.M., and Berkheiser, V., Clays and Clay Minerals, **24,** 60 (1976)

Mortland, M.M., and Raman, K.V., Clays and Clay Minerals, **16,** 393 (1968)

NL Industries (Baroid Division, Houston, Texas), US Patent 3 852 405 (1972)

O'Connor, C.T., Kojima, M., and Schumann, W.K., Appl. Catal., **16,** 193 (1985)

O'Connor, C.T., Fasol, R.E., and Foulds, G.A., Fuel Proc. Tech., **13,** 41 (1986a)

O'Connor, C.T., Fletcher, J.C.Q., and Rautenbach, M.W., J. Phy. E: Sci. Instrum., **19,** 367-368 (1986b)

O'Connor, C.T., Jacobs, L.L., and Kojima, M., Appl. Catal., **40,** 277 (1988)

Oblad, A.G., Mills, G.A., and Heinermann, H., in "Catalysis" vol. 6, Emmett, P.H.(Ed), Reinhold, New York, 341 (1958)

Ocelli, M.L., and Tindura, R.M., Clays and Clay Minerals, **31** 22 (1983)

Ocelli, M.L., Hsu, J.T., and Galya, L.G., J. Mol. Catal. **32** 377 (1985)

Ocelli, M.L., Drake, B., and Gould, S.A.C., J. Catal., **142,** 337 - 348 (1993)

Odom, I.E., in "Clay Minerals: Their Structure, Behaviour and Use", Fownden, L., Barrer, R.M., and Tinker, P.B. (Eds), The Royal Society, London 171-189 (1984)

Owen, H., Mash, S.K., and Wright, B.S., US Patent 4 456 779 (1984)

Parry, E.P., J. Catal., **2,** 371-379 (1963)

Peuckert, M., Keim, W., Strop, S., and Weber, R.S., J. Molec. Catal., **20,** 115 (1983)

Purcell, K.F., and Kotz, J.C., "Inorganic Chemistry", Holt - Saunders (1977)

Public Relations Department, SASOL, "SASOL in a nutshell" (1980)

Quann, R.J., Green, L.A., Tabak, S.A., and Krambeck, F.J., Ind. Eng. Chem. Res., **27,** 567 (1988)

Read, R.C., in "Chemical Applications of Graph theory" Chpt 4, Balaban, A.T.(Ed), Academic Press, New York (1976)

Rhodes, C.N., and Brown, D.R., Cat. Let., **24,** *4,* 285 (1994).

Robschlager, K.H.W., Emeis, C.A., and van Santen, R.A., J. Catal., **86,** 1 (1984)

Rogers, D.E., and Parker, L.M., Applic Catal., **47**, 181 (1989)

Russel, J.D., and White, J.L., Clays and Clay Minerals, Proc. 14th Conf., Pergammon Press, New York, 181 (1966)

Saus, A., and Schmidl, E., J. Catal., **94,** 187 (1985)

Schmerling, L., and Ipatieff, V.N., Adv. Catal., **2,** 21 (1950)

Schwarz., S., Ph. D thesis, University of Cape Town, Republic of South Africa (1990)

Schwarz, S., O'Connor, C.T., and Kojima, M., Applied Catalysis, **56**, 263 (1989)

Sealy, S.J., Fraser, D.M., Möller, K.P., and O'Connor, C.T., Chem. Eng. Sci.,**49**, *19*, 3307-33312 (1994)

Shabtai, J., Frydmond, N., and Lazar, R., Proc. 6th Int. Congr. Catal., **B5**, 1 (1976)

Sidorov, A.N., Optiki: Spektroskopiya, **8**, 51 (1960)

Smith, J.M., and van Ness, H.C., "Introduction to Chemical Engineering Thermodynamics", 3rd Ed., Mc Graw Hill, 270 (1983)

Snel, R., Appl. Catal., **12**, 189 (1984)

Solomon, D.H., and Rosser, M.J., J. Appl. Polymer Sci., **9,** 1261 (1965)

Solomon, D.H., Clay and Clay Minerals, **16,** 31 (1968)

Stock, T., Dombrowski, D., Hoffman, J., and Fruwert, J., Z. Phys. Chem. Leipzig, **265,** 551 (1984)

Swartzen-Allen, S.L., and Matijevic, E., Chemical Reviews, **74,** 385 (1974)

Swift, H.E., "Advances Materials in Catalysis", Academic Press, 209 (1977)

Swift, H.E., and Black, E.R., Ind. Eng. Chem. Prod. Res. Dev., **13,** *2,* 106 (1974)

Swift, H.E., and Vogel, R.F., US Patent 4 254 295 (1979)

Tabak, S.A., US Patent 4 254 295 (1981)

Tabak, S.A., Thailand - US Natural Gas Utilization Symposium, Bangkok (1984)

Tabak, S.A., US Patent 4 547 612 (1985)

Tabak, S.A., Krambeck, F.J., and Garwood, W.E., A.I. Ch. E. J., **32,** *9,* 1526 (1986)

Tabak, S.A., and Yurchak, S., Cat. Sci. and Tech., Andersen, J.R., and Boudart, M., (Eds), Springer Verlag, New York (1990).

Thomas, C.L., and Barmby, D.S., J. Catal., **12** 341 (1968)

Thomas C.L., In "Catalytic Processes and Proven Catalysts", Thomas, C.L., (Ed.), Acedemic Press, New York, 173 (1970)

Uytterhoeven, J.B., Christner, L.G., and Hall, W.K., J. Phys. Chem., **69,** 2117 (1965)

Van Olphen, H., "An Introduction to Clay Colloid Chemistry", Interscience Publishers, New York, 66 (1963)

Van Wagner, J., Chapman, J.A., and Bell, J.A., Stud. Surf. Sci. Catal., 497 (1984)

Vaughan, D.E., and Lussier, R.J., Proc. 5th Int. Conf. Zeolites, 94 (1980)

Voge, H.H., in "Catalysis 6" Chp 5, Emmet, P.H., (Ed), Reinhold Publishing Corp., Waverly Press, Baltimore (1958)

White, G.N., and Zelazny, L.W., Clays and Clay Min., **36,** 141-146 (1988)

Wright, A.C., Granquist, W.T., and Kennedy, J.V., J. Catal., **25,** 65 (1972)

Wu, Q., Gobolos, S., Grange, P., and Delamay, F., Thermochim. Acta, **81,** 281 (1984)

Yuehua, L., Internal Report of Research Institute of Petroleum Processing, Beijing, China (1985)

Zeuch, E.A., US Pat. 3 849 507 (1974)

Zhou, L., and Zang, T., Shiyou Huangong, **14**, *12,* 744 (1985)